



Endbericht  
Algorithmen zur Triebwerksansteuerung  
Fkz: 50 JR 0484

Doc.No.: INT-TAS-RP-ZAR-001  
Issue: 1.0  
Page: 1 of 20

# Endbericht

## Algorithmen zur Triebwerksansteuerung

### Fkz: 50 JR 0484

Project:	Document No.:
Thruster Actuation System	INT-TAS-RP-ZAR-001
ZARM - Center of Applied Space Technology and Microgravity	
Am Fallturm D 28359 Bremen Germany	Phone: +49-421-218-8136 Fax: +49-421-218-2521 E-Mail: bindel@zarm.uni-bremen.de

Doc. No.: INT-TAS-RP-ZAR-001

Issue: 1.0

Written:

Daniel Bindel

Approved: -

Date: 30. April 2008

Date: -

	<p>Endbericht Algorithmen zur Triebwerksansteuerung Fkz: 50 JR 0484</p>	<p>Doc.No.: INT-TAS-RP-ZAR-001 Issue: 1.0 Page: 2 of 20</p>
---	---	---

## Document Change Record

Issue	Date	Changed Pages / Changed Chapters	Remarks	Done
1.0	29.04.2008	all	Initial Version	✓

# Inhaltsverzeichnis

<b>1</b>	<b>Einleitung</b>	<b>4</b>
<b>2</b>	<b>Aufgabenstellung</b>	<b>5</b>
<b>3</b>	<b>Planung und Ablauf des Vorhabens</b>	<b>6</b>
3.1	Thematischer Aufbau . . . . .	6
3.2	Zeitlicher Ablauf . . . . .	8
3.3	Ergebnisse der Arbeiten . . . . .	8
<b>4</b>	<b>Voraussetzungen</b>	<b>9</b>
4.1	Stand der Forschung . . . . .	9
4.1.1	Eigene Vorarbeiten . . . . .	10
4.1.2	Abgrenzung des Vorhabens zu den geleisteten Vorarbeiten . . . . .	11
4.2	Fachliteratur, Informationsquellen . . . . .	12
4.3	Zusammenarbeit mit anderen Stellen . . . . .	12
<b>5</b>	<b>Verwendung der Zuwendung</b>	<b>13</b>
5.1	Angemessenheit der geleisteten Arbeiten . . . . .	13
5.2	Zusätzliche Ergebnisse des Vorhabens . . . . .	13
5.3	Fortschritt anderer Stellen während des Vorhabens . . . . .	14
<b>6</b>	<b>Erfolgskontrollbericht</b>	<b>15</b>
6.1	Wissenschaftlich-technisches Ergebnis / Erreichte Nebenergebnisse . . . . .	15
6.2	Fortschreibung des Verwertungsplans . . . . .	15
6.2.1	Erfindungen/Schutzrechtsanmeldungen . . . . .	15
6.2.2	Wirtschaftliche Erfolgsaussichten . . . . .	16
6.2.3	Wissenschaftliche oder technische Erfolgsaussichten . . . . .	16
6.2.4	Wissenschaftliche und wirtschaftliche Anschlussfähigkeit . . . . .	16
6.3	Arbeiten, die zu keiner Lösung geführt haben . . . . .	16
6.4	Präsentationsmöglichkeiten . . . . .	17
6.5	Einhaltung des Ausgaben- und Zeitplans . . . . .	17
<b>7</b>	<b>Zusammenfassung</b>	<b>18</b>
	<b>Literatur</b>	<b>19</b>
	<b>Anhang</b>	<b>20</b>

	Endbericht Algorithmen zur Triebwerksansteuerung Fkz: 50 JR 0484	Doc.No.: INT-TAS-RP-ZAR-001 Issue: 1.0 Page: 4 of 20
---	--	--

# 1 Einleitung

Dieses Dokument bildet den Endbericht des DLR Fördervorhabens 50JR0484

## **Algorithmen und Optimierungsverfahren für die Ansteuerung von $\mu$ -Propulsion-Triebwerken zur Bahn- und Lageregelung von Raumfahrzeugen**

Der Endbericht gliedert sich nach *BNBest-BMBF 98 Anlage 2* in eine kurze Darstellung zur Aufgabenstellung, den Voraussetzungen des Vorhabens, der Planung und des Ablaufes, dem vorhandenen technischen Stand und der Zusammenarbeit mit anderen Stellen.

In einem weiteren Kapitel wird die Verwendung der Zuwendung erläutert, sowie zusätzliche Ergebnisse beschrieben, die erzielt werden konnten. Der Bericht wird abgeschlossen mit einem Erfolgskontrollbericht und dem Berichtsblatt zu den wesentlichen fachlichen Inhalten des Schlussberichtes.

Im Anhang finden sich Zusammenfassungen von wissenschaftlich-technischen Ergebnissen, die während des Vorhabens erzielt wurden. Es sind außerdem zwei Veröffentlichungen beigelegt, mit denen das Thema auf internationalen Kongressen präsentiert wurde.

## 2 Aufgabenstellung

Das Ziel war es, generische Algorithmen zu entwickeln, die zu jedem Zeitpunkt in der Lage sind eine gültige Schublösung innerhalb einer festgesetzten Zeitspanne mit einer festgesetzten Anzahl von Rechenschritten zu produzieren, wobei die resultierende Schublösung die durch Triebwerkstyp und Mission gegebenen Randbedingungen erfüllt. Der Einsatz von Verbrennungs- oder Kaltgastriebwerken auf Satelliten zur Lage- und Bahnregelung wird zunehmend durch die Verwendung von elektrischen Antrieben ersetzt. Im wissenschaftlichen Bereich können sogar einige Missionen nur mit elektrischen Antrieben durchgeführt werden. Ein Beispiel dafür sind die sogenannten Drag-Free Missionen.

Die Arbeitsweise von elektrischen Antrieben unterscheidet sich jedoch grundlegend von denen der Verbrennungs- und Kaltgassystemen. Während die Entwicklung im Bereich der Lageregelung eher auf impulsive Schubstöße ausgelegt sind, werden elektrische Antriebe vor allem für einen kontinuierlichen Einsatz konstruiert. Durch ihre Arbeitsweise und ihre unterschiedlichen Eigenschaften stellt sich die Frage, ob es auch eine unterschiedliche Art und Weise der Ansteuerung geben sollte. Bisherige Erfahrungen haben außerdem gezeigt, dass es möglich ist, optimale Lösungen für die Lage- und Bahnregelungstriebwerke zu berechnen. Mit Wissen über die Eigenschaften von elektrischen Triebwerken können sich daher auch Aussagen ableiten lassen, welche Ansteuerungskommandos optimal für die Antriebe sind.

In dem Vorhaben sollte also untersucht werden, welche Anforderungen der Betrieb von elektrischen Triebwerken an die Ansteuerung stellt und wie diese aufgebaut sein kann. Eine Identifikation von Optimalitätskriterien soll helfen, Algorithmen zu entwickeln, die bestmögliche Schubkommandos für die Triebwerke berechnen. Diese Optimierungsverfahren sind zu untersuchen und eventuell weiterzuentwickeln.

### 3 Planung und Ablauf des Vorhabens

#### 3.1 Thematischer Aufbau

Das Fördervorhaben wurde in vier Hauptabschnitte AP 1000 bis AP 4000 eingeteilt.

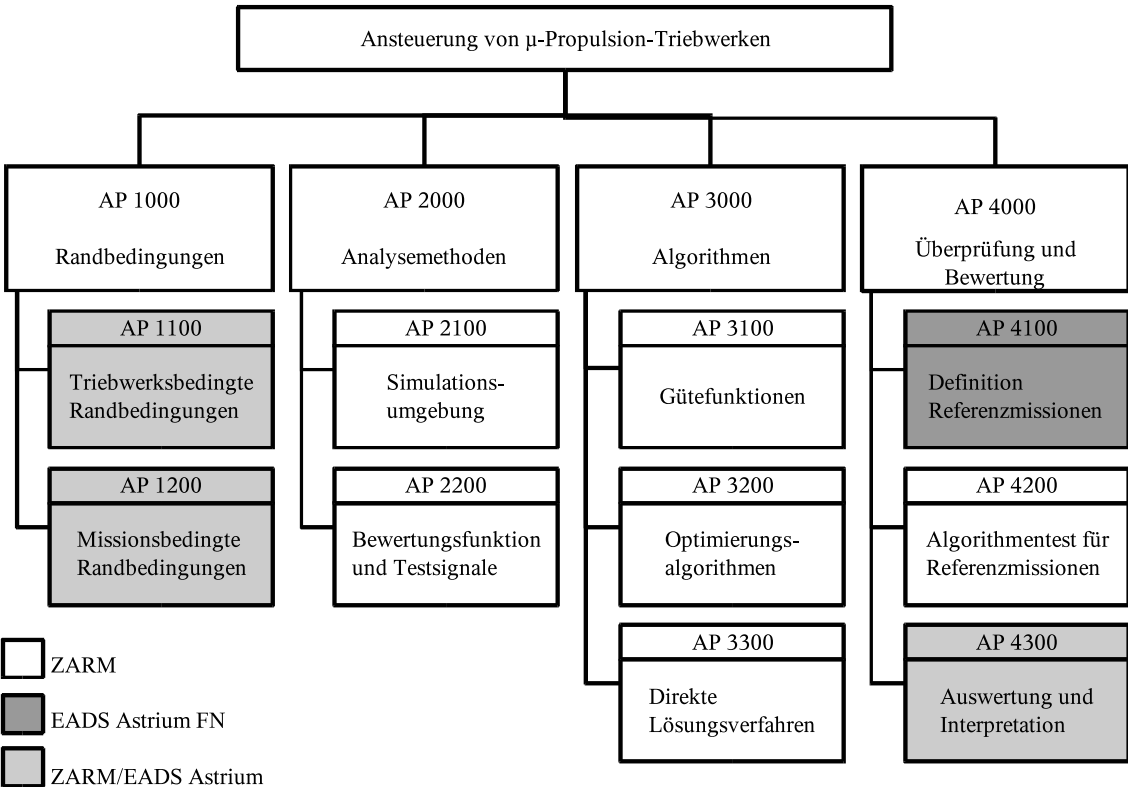


Abbildung 1: Arbeitsaufteilung des Vorhabens

Im ersten Teil AP 1000 wurden die Eigenschaften von verschiedenen elektrischen Antrieben untersucht, um Aufschlüsse über die Arbeitsweise zu gewinnen. Die Auswertung von sechs verschiedenen Antriebsarten wurde vorgenommen. Hierbei wurde auch die Technologie von Kaltgasriewerken mit berücksichtigt, da sie im Bereich der Mikroantriebe in einer gewissen Konkurrenzsituation zu den elektrischen Antrieben stehen. Bei einigen neuen Missionen könnten daher elektrische Antriebe oder auch Kaltgasysteme verwendet werden. Der Fokus des Vorhabens wurde hier aufgrund der technischen Voraussetzungen etwas erweitert.

Parallel dazu wurde auch untersucht, welche Art von Missionen die Mikroantriebe in Zukunft benutzen könnten, und welche Anforderungen von der Einsatzseite an die Triebwerke und die Ansteuerung gestellt werden könnten.

	<p>Endbericht Algorithmen zur Triebwerksansteuerung Fkz: 50 JR 0484</p>	<p>Doc.No.: INT-TAS-RP-ZAR-001 Issue: 1.0 Page: 7 of 20</p>
---	---	---

Das Ergebnis war eine Übersicht über die Eigenschaften der Triebwerke und erste Rückschlüsse, welche Bedingungen eine optimale Ansteuerung deshalb erfüllen sollte.

Im zweiten Abschnitt AP 2000 des Vorhabens wurden Werkzeuge geschaffen, mit deren Hilfe die später entwickelten Ansteuerungsalgorithmen getestet werden sollten. Dies umfasst zum einen eine Simulationsumgebung, und zum anderen eine Bewertungsmethode zum Vergleich der verschiedenen Methoden.

Die Simulationsumgebung wurde so ausgelegt, dass einige Elemente ausgetauscht werden konnten. Damit war es möglich, das Zusammenspiel unterschiedlicher Missionsprofile, Triebwerke und Raumfahrzeuge zu analysieren.

In die Entwicklung der Bewertungsfunktion flossen die Ergebnisse der Triebwerksuntersuchungen aus dem ersten Arbeitsabschnitt ein. In Verbindung mit der Simulationsumgebung ist es daher möglich, die Qualität der Ansteuerungsalgorithmen in Hinblick auf die Triebwerke zu überprüfen.

Im dritten Abschnitt AP 3000 des Vorhabens wurden dann die Algorithmen selbst recherchiert und implementiert. Dies war auch vom Arbeits- und Zeitumfang der größte Abschnitt. Im Verlauf der Arbeiten wurden sowohl Methoden implementiert, die als der aktuelle technische Stand bekannt waren, als auch neue Technologien umgesetzt, um bessere Ergebnisse zu erzielen.

Ein Teil der Arbeiten wurde außerdem dafür aufgewendet, die neuen Technologien so weit zu modifizieren, dass sie den Randbedingungen genügen, die bei einem Einsatz als On-Board Software erwartet werden. So stand die Robustheit und der benötigte Rechenaufwand an oberster Stelle bei der Verbesserung während des Vorhabens.

Obwohl entscheidende Fortschritte erzielt werden konnten, um das entwickelte Optimierungsverfahren für den Einsatz auf einer bevorstehenden, wissenschaftlichen Mission einzusetzen, sind immer noch Fragen in Bezug auf die Qualifikation und Verifikation der Software offen. Besonders die sicherheitsrelevanten Aspekte in der Raumfahrt erfordern hier leider eine intensive Analyse und Begutachtung der Algorithmen, bevor sie auch in der Planung und bei der Auslegung der zukünftigen Missionen akzeptiert und berücksichtigt werden können.

Im vierten und letzten Abschnitt AP 4000 wurden die verschiedenen untersuchten und implementierten Methoden anhand der Beispielmision LISA untersucht. Das Ergebnis aus dieser Untersuchung unterstreicht, dass die neu entwickelten Ansteuerungsalgorithmen in allen Bereichen mindestens genauso gut, und sehr oft besser abschneiden, als die bisher verwendeten Methoden.

### 3.2 Zeitlicher Ablauf

Das Vorhaben wurde auf eine Laufzeit von 36 Monaten, mit Start im Oktober 2004 und Ende im September 2007, ausgelegt. Die zeitliche Einordnung und Verteilung der Arbeitspakete ist aus Abbildung 2 ersichtlich.

<i>AP</i>	<i>2004</i>	<i>2005</i>	<i>2006</i>	<i>2007</i>
AP 1000	■			
AP 2000		■		
AP 3000		■		
AP 4000		▤		■
<i>AP 4100</i>		▤		■
<i>AP 4200</i>				■
<i>AP 4300</i>				■
KOM	●			
PM		●	●	●
FP				●

Abbildung 2: Zeitplanung des Vorhabens

### 3.3 Ergebnisse der Arbeiten

Die Ergebnisse der Arbeiten in den Abschnitten AP 1000 und AP 2000 sind als Anhänge B-E dem Endbericht beigelegt. Die Ergebnisse aus dem Abschnitt AP 3000 sind als kurze Veröffentlichung in Anhang H und I angelegt. Ein Beispiel für eine Anwendung der erstellten Methoden ist in Anhang F zu finden. Die zusätzlich erzielten Ergebnisse sind im Anhang G beschrieben.

Eine detailliertere Beschreibung der Algorithmen und deren Anwendung (AP 3000 und 4000) soll gesondert in einer Dissertation zusammengefasst und veröffentlicht werden.



## 4 Voraussetzungen

### 4.1 Stand der Forschung

Die ersten Untersuchungen zum Thema optimale Schubverteilung auf Proportionaltriebwerke für die Regelung von allen sechs Freiheitsgraden wurden bereits 1983 von Jeng-Heng Chen in seiner Dissertation [2] durchgeführt. Allerdings beschränkte er sich auf zweiseitige Triebwerke, d.h. Triebwerke, die sowohl positiven, als auch negativen Schub erzeugen können. In diesem Fall ist die Lösung des Schubverteilungsproblems trivial, da die analytische Lösung auch ohne Nullraumvektor immer gültige Lösungen produzieren würde.

Eine intensivere Untersuchung des Themas unter Berücksichtigung verschiedener Optimierungskriterien wurde dann 1992 von Peter Wiktor in seiner Dissertation [8] im Rahmen der Entwicklung von Gravity Probe B durchgeführt. Er definierte die drei grundlegenden Optimierungsprobleme, das des minimalen Treibstoffverbrauchs, der minimalen Leistung und der Minimierung des maximalen Schubs. Er leitete die Problemstellung her und testete die Implementierungen, wobei er sich in Tests auch auf zweiseitige Triebwerke beschränkte. Darüber hinaus entwickelte er den so genannten „Minimum Control Authority Plot“ ([8], [9]) als Bewertungskriterium für die verschiedenen Algorithmen. Seine Arbeit stellt die wohl umfangreichste Untersuchung dar, die bisher zu diesem Thema verfasst worden ist. Allerdings stellt die Arbeit im Wesentlichen eine theoretische Untersuchung des Themas dar. Praktische Aspekte der Implementierung wie Robustheit und Missionssicherheit werden nicht berücksichtigt. Auch die Untersuchung verschiedener Optimierungsmethoden wird nicht behandelt.

Eine Erweiterung der theoretischen Resultate von Wiktor ist in der 1996 veröffentlichten Dissertation von Haiping Jin [3] zu finden, der den Algorithmus für einen minimalen Treibstoffverbrauch auf die STEP Mission angewandt hat. Im Gegensatz zu Wiktor untersucht er in seiner Analyse einseitige Triebwerke, die ausschließlich positiven Schub erzeugen können. Auch verwendet er ein anderes Bewertungsverfahren für die Güte der Schublösung, bei der er die maximal auftretenden Störkräfte und Momente mit der „Control Authority“ des Triebwerkssystems vergleicht und so einen Sicherheitsfaktor für die Triebwerkskonfiguration und den Algorithmus definiert. Auch Jin hat keine Untersuchungen zum Thema Robustheit durchgeführt.

Neben den zumeist Drag Free geregelten Wissenschaftssatelliten wird eine kontinuierliche Regelung aller sechs Freiheitsgrade vor allem im Bereich der hochpräzisen Formationsregelung sowie im Bereich Rendezvous und Docking benötigt. Ein Beispiel aus dem Bereich Rendezvous und Docking ist das Automated Transfer Vehicle (ATV). Besonders in der letzten Phase der Annäherung an die ISS ist eine hochpräzise Regelung aller sechs Freiheitsgrade unerlässlich. Im Rahmen des ATV Programms wurde von EADS Space Transportation auch das Schubverteilungsproblem untersucht ([4], [6]). Der von EADS

verfolgte Lösungsansatz verzichtet auf eine Onboard Optimierung. Vielmehr wird bereits am Boden ein Katalog mit optimalen Schublösungen entwickelt, der dann an Bord des ATV in einem iterativen Prozess verwendet wird, um die jeweils optimale Schublösung zu finden. Darüber hinaus verwendet das ATV im Gegensatz zu den meisten zukünftigen Wissenschaftsmissionen Impulstriebwerke und keine Proportionaltriebwerke.

Im durchgeführten Vorhaben sollte der allgemeine Fall der kontinuierlichen Sechsfreiheitsgradregelung mit Proportionaltriebwerken betrachtet werden. Basierend auf den Ergebnissen von Wiktor sollten Algorithmen für die Online-Berechnung einer optimalen Schublösung entworfen werden. Dabei sollten insbesondere die Themen Robustheit, Missionssicherheit und Zeit- bzw. Operationenminimierung betrachtet werden. Im Gegensatz zu den Arbeiten von Chen, Wiktor und Jin standen hierbei also eindeutig die praktische Anwendung der Theorie im Vordergrund. Insbesondere die Untersuchung verschiedener Optimierungsmethoden im Bezug auf ihre Anwendbarkeit und Robustheit sind für fehlertolerante, robuste Algorithmen unerlässlich.

#### 4.1.1 Eigene Vorarbeiten

Die Arbeitsgruppe Raumfahrttechnologie des Zentrums für Angewandte Raumfahrttechnologie und Mikrogravitation (ZARM) der Universität Bremen hat sich in den letzten Jahren eine große Expertise auf dem Gebiet der hochgenauen Lage- und Translationsregelung und insbesondere der Drag-Free Regelung erarbeitet. Projekte wie STEP, HYPER oder LISA Pathfinder erfordern alle eine hochpräzise Regelung aller sechs Freiheitsgrade. Im Rahmen der verschiedenen Projekte ist zum Teil auch das Thema Schubverteilungsalgorithmus untersucht worden. Erste Untersuchungen dazu wurden bereits während der DIVA Studie durchgeführt.

Während der Entwicklungsphasen A und B des Astronomiesatelliten DIVA war das ZARM für die Entwicklung von Lagebestimmung und Lageregelung des Satelliten verantwortlich. Im Rahmen der Phase B wurde dann auch ein Algorithmus für das Schubverteilungsproblem entwickelt. Hauptschwierigkeit war hier die Erzeugung von kleinen, genauen Impulsen mit Lageregelungstriebwerken, deren minimaler Impuls vergleichsweise groß ist. Der Algorithmus konnte mittels Simulationen verifiziert werden ([7], [10]). Eine detaillierte Betrachtung der Robustheit und Missionssicherheit für das Triebwerkssystem wurde nicht durchgeführt.

Während der, von der ESA finanzierten, HYPER Machbarkeitsstudie, bei dem das ZARM unter anderem für die Entwicklung der Regelungsalgorithmen für das „Drag-Free and Attitude Control System“ (DFACS) verantwortlich war, wurde auch ein einfacher Algorithmus für die Verteilung der Schübe auf die einzelnen Triebwerke entwickelt. Der Algorithmus basierte auf der Pseudoinversen der Triebwerkskonfigurationsmatrix.

	<p>Endbericht Algorithmen zur Triebwerksansteuerung Fkz: 50 JR 0484</p>	<p>Doc.No.: INT-TAS-RP-ZAR-001 Issue: 1.0 Page: 11 of 20</p>
---	---	--

Die größte Erfahrung auf dem Gebiet optimale Ansteuerung von Triebwerken konnte während der Arbeit an der LISA Pathfinder Mission gesammelt werden. Neben der Entwicklung der Regelungsalgorithmen für das DFACS und die Testmassenpositionierung hat das ZARM auch den Ansteuerungsalgorithmus für das Triebwerkssystem entwickelt [5]. Der damals aktuelle Algorithmus bestand aus einer Kombination eines auf dem SIMPLEX Verfahren basierenden Algorithmus, der den Treibstoffverbrauch minimiert, und einem Backupalgorithmus, der auf der Pseudoinversen der Triebwerkskonfigurationsmatrix basiert. Das Vorhaben sollte die Erkenntnisse, die während der Arbeit am Schubverteilungsalgorithmus von LISA Pathfinder gemacht werden konnten, vertiefen und erweitern, da die Entwicklung gezeigt hat, dass die Problematik sehr komplex und vielschichtig ist. Insbesondere die Themen Robustheit und Missionssicherheit sowie die Minimierung von Rechenzeit und Rechenoperationen sollten weiter untersucht werden.

#### 4.1.2 Abgrenzung des Vorhabens zu den geleisteten Vorarbeiten

Das durchgeführte Vorhaben unterscheidet sich von bereits durchgeführten Arbeiten für LISA-Pathfinder durch folgende Punkte:

1. **Breiteres Spektrum von Randbedingungen:** Die Lösungsalgorithmen sollten für eine größere Menge von Randbedingungen entwickelt werden, die nicht nur die LISA Pathfinder Mission und die Benutzung der FEEP-Triebwerke beinhaltet. Damit wurden die Einflüsse eines breiteren Spektrums von Missionsprofilen und anderen Arten von Triebwerken auf die Schubverteilungsalgorithmen berücksichtigt.
2. **Neue Algorithmen und Lösungsverfahren:** Der Algorithmus zur Triebwerksansteuerung in der vorher untersuchten LISA Pathfinder Mission basiert auf der Kombination eines iterativen SIMPLEX-Verfahrens mit einer direkten Pseudoinvers-Methode. Diese Algorithmen waren vorher schon bekannt und wurden bereits bei anderen Missionen als Lösung implementiert. In dem durchgeführten Vorhaben sollten hingegen neben den bereits verwendeten Optimierungsverfahren auch andere Algorithmen auf ihre Eignung hin recherchiert und untersucht werden. Weiterhin wurde nach besseren Alternativen zur bestehenden direkten Lösungsmethode gesucht.
3. **Bewertung der Algorithmen (Bench-Marking):** Mit der Entwicklung von verschiedenen Lösungsverfahren für unterschiedliche Missionsprofile war eine Bewertung notwendig, die eine Aussage über geeignete Kombinationen von Algorithmen und bestimmten Missionstypen zulässt. Hierzu war es zum einen notwendig, Bewertungsfunktionen zum Vergleich zu entwickeln. Zum anderen war ein spezieller

	Endbericht Algorithmen zur Triebwerksansteuerung Fkz: 50 JR 0484	Doc.No.: INT-TAS-RP-ZAR-001 Issue: 1.0 Page: 12 of 20
---	--	---

Simulator zu entwickeln, mit dem die unterschiedlichen Kombinationsmöglichkeiten getestet werden konnten.

## 4.2 Fachliteratur, Informationsquellen

Die hauptsächliche Quelle der Literatur stellte das Journal of Guidance and Control der AIAA dar, da dort die aktuellen Ergebnisse der Forschung im Bereich der Raumfahrt-Regelungstechnik publiziert werden. Die dort angegebenen Referenzen verweisen jedoch auch auf Doktorarbeiten und Bücher, die im Rahmen von früheren Missionen und Projekten veröffentlicht wurden.

Für die Weiterentwicklung des SIMPELX Verfahrens konnte auf einschlägige Literatur zur linearen Optimierung zurückgegriffen werden, da dieser Algorithmus zu den Standardverfahren in der Mathematik gehört.

## 4.3 Zusammenarbeit mit anderen Stellen

Während der Arbeiten an der HYPER Studie sowie während der Arbeiten an LISA Pathfinder hat die Arbeitsgruppe Raumfahrttechnologie des ZARM mit der EADS Astrium GmbH in Friedrichshafen zusammengearbeitet. Der Hauptpartner bei der Durchführung des Vorhabens war daher die EADS Astrium GmbH. Es wurden zwei Arbeitspakete innerhalb des Vorhabens übernommen und durchgeführt. Den größten Einfluss hatte EADS Astrium durch die reiche Erfahrung bei der Planung und dem Bau von wissenschaftlichen Raumfahrzeugen. Dadurch konnten viele Impulse für die Entwicklung der Algorithmen gegeben werden, und es stand für ein weiteres Arbeitspaket eine beratende Funktion zur Verfügung.

	<p>Endbericht Algorithmen zur Triebwerksansteuerung Fkz: 50 JR 0484</p>	<p>Doc.No.: INT-TAS-RP-ZAR-001 Issue: 1.0 Page: 13 of 20</p>
---	---	--

## 5 Verwendung der Zuwendung

Die zu Beginn des Vorhabens gestellten Ziele konnten im Rahmen der Arbeiten vollständig erreicht werden. Eine grobe Übersicht über die Verwendung der Zuwendung bietet folgende Liste. Eine detaillierte Übersicht über die Abrechnung der einzelnen Positionen wird unabhängig von diesem Bericht mit der Abrechnung des Vorhabens geliefert.

- Aus der Zuwendung wurde über den Zeitraum von 36 Monaten ein wissenschaftlicher Mitarbeiter (Gehaltsstufe BAT IIa) bezahlt.
- Der Mitarbeiter wurde während seiner Arbeit von studentischen Hilfskräften unterstützt.
- Eine weitere finanzielle Position des Vorhabens war die Beauftragung der EADS Astrium GmbH zur Durchführung von zwei Arbeitspaketen.
- Die Ergebnisse des Vorhabens wurden auf mehreren Konferenzen präsentiert, für deren Besuch Reisekosten in Anspruch genommen wurden.
- Aus den Reisemitteln wurden außerdem die Teilnahme an den geplanten Progress-Meetings bestritten, die während des Vorhabens in Friedrichshafen und Bonn durchgeführt wurden.

### 5.1 Angemessenheit der geleisteten Arbeiten

Die zu Beginn eingeplanten Zeiträume entsprachen dem zu leistenden Arbeitsumfang in vollem Umfang. Den größten Anteil stellte dabei die Entwicklung der neuen Ansteuerungsalgorithmen dar, da sie der Kernpunkt des Vorhabens waren. Der lange Zeitraum von über zwei Jahren, der für die Durchführung dieses Abschnittes benötigt wurde, spiegelt die Komplexität und die Herausforderungen wieder, auf die während der Arbeiten gestoßen wurde.

Das Themengebiet verbindet Problematiken aus der Raumfahrttechnologie mit komplexen Zusammenhängen aus der höheren Mathematik, die eine gewisse Einarbeitungsphase benötigen. Außerdem konnte bei der Erarbeitung von völlig neuartigen Methoden und Ansätzen nicht immer Know-How aus vorhandenen Arbeiten benutzt werden. Dadurch ist der Zeitrahmen für die Lösungsfindung, Implementierung und Verifikation höher anzusetzen, als bei reiner Auftragsarbeit, die sich aus einem bekannten Wissensstand bedienen kann.

### 5.2 Zusätzliche Ergebnisse des Vorhabens

Im Zuge der Entwicklung der Simulationsumgebung aus dem zweiten Abschnitt des Vorhabens wurde noch ein weiteres Software-Werkzeug, das Control Authority Analy-

	<p>Endbericht Algorithmen zur Triebwerksansteuerung Fkz: 50 JR 0484</p>	<p>Doc.No.: INT-TAS-RP-ZAR-001 Issue: 1.0 Page: 14 of 20</p>
---	---	--

sis Tool (CAAT), entwickelt, das die Anordnung von Triebwerken auf einem Satelliten vereinfachen und erleichtern soll.

Bisher wurde es aufgrund einer nur geringen Nachfrage nicht über einen groben Prototypen-Status hinaus entwickelt und weiter vermarktet.

### 5.3 Fortschritt anderer Stellen während des Vorhabens

Im Verlauf des Vorhabens wurde außerdem noch eine Arbeit [1] der D3Group veröffentlicht, die sich mit dem Thema der Triebwerksansteuerung auf dem Autonomous Transfer Vehicle (ATV) beschäftigt. Nach einer Analyse der verwendeten Methoden und Voraussetzungen wurde jedoch deutlich, dass der vorgeschlagene Algorithmus nicht direkt für die Ansteuerung von elektrischen Triebwerken eingesetzt werden kann. Der Hauptgrund ist hier die Unmöglichkeit, Randbedingungen der Triebwerke zu implementieren. Das Verfahren der D3Group wurde für impulsiv betriebene Antriebe entwickelt, und gelangt bei kontinuierlichen Triebwerken an seine methodischen Grenzen.

	Endbericht Algorithmen zur Triebwerksansteuerung Fkz: 50 JR 0484	Doc.No.: INT-TAS-RP-ZAR-001 Issue: 1.0 Page: 15 of 20
---	--	---

## 6 Erfolgskontrollbericht

### 6.1 Wissenschaftlich-technisches Ergebnis / Erreichte Nebenergebnisse

Im Rahmen des Projektes *Algorithmen und Optimierungsverfahren für die Ansteuerung von  $\mu$ -Propulsion-Triebwerken zur Bahn- und Lageregelung von Raumfahrzeugen* wurden Mikrotriebwerke untersucht, und ein Algorithmus entwickelt, der sie in Hinblick auf ihre Eigenschaften optimal ansteuert. Die wesentlichen wissenschaftlich-technischen Ergebnisse kann man wie folgt zusammenfassen:

- Die operationellen Eigenschaften von Mikroantrieben wurden in einer Untersuchung identifiziert.
- Aus den Eigenschaften der Antriebe wurde abgeleitet, welche Eigenschaften eine optimale Ansteuerung aufweisen muss.
- Es wurde eine Simulationsumgebung erstellt, in der überprüft werden kann, inwieweit ein implementierter Algorithmus eine optimale Ansteuerung für die Mikrotriebwerke berechnet.
- Mehrere Steuerungsalgorithmen wurden in der Simulationsumgebung implementiert, um ihre Arbeitsweise zu analysieren.
- Die SIMPLEX Methode wurde als aussichtsreichster Kandidat für eine Weiterentwicklung identifiziert.
- Die Robustheit des Optimierungsverfahren konnte durch Erweiterung der ursprünglichen Programmierung deutlich erhöht werden.
- Genaue Analysen der SIMPLEX-Arbeitsweise haben Verbesserungen im Bereich der Geschwindigkeit und der numerischen Stabilität des Verfahrens erbracht.
- Die Funktionsfähigkeit des fertigen Algorithmus konnte anhand einer Testmission verifiziert werden.
- Zusätzlich zum anfangs definierten Arbeitsplan wurde eine Erweiterung der Simulationsumgebung entwickelt, die es erlauben soll, die Auslegung des Antriebssystems von Kleinsatelliten zu vereinfachen.

### 6.2 Fortschreibung des Verwertungsplans

#### 6.2.1 Erfindungen/Schutzrechtsanmeldungen

Es wurden keine Schutzrechtsanmeldungen vorgenommen oder in Anspruch genommen.



	<p>Endbericht Algorithmen zur Triebwerksansteuerung Fkz: 50 JR 0484</p>	<p>Doc.No.: INT-TAS-RP-ZAR-001 Issue: 1.0 Page: 16 of 20</p>
---	---	--

### 6.2.2 Wirtschaftliche Erfolgsaussichten

Mit der erfolgreichen Entwicklung einer modernen Ansteuerungsmethode von Triebwerken für zukünftige Wissenschaftsmissionen ist das ZARM in der Lage, sich aktiv in diese Projekte einzubringen. Die in der Vergangenheit aufgebaute Kompetenz in Bereich der Drag-Free Lageregelung wird dadurch auch auf der Seite der Algorithmik erweitert.

### 6.2.3 Wissenschaftliche oder technische Erfolgsaussichten

Die neu entwickelten Algorithmen erlauben einen Missionsbetrieb, der weniger Treibstoff verbraucht, als ursprüngliche Technologien. Es konnten außerdem Möglichkeiten aufgezeigt und implementiert werden, um die Alterung von elektrischen Triebwerken zu reduzieren, und damit technischen Ausfällen vorzubeugen. Das Ergebnis des Fördervorhabens wird also dazu beitragen können, die Lebensdauer zukünftiger wissenschaftlicher Missionen zu verlängern.

### 6.2.4 Wissenschaftliche und wirtschaftliche Anschlussfähigkeit

Aufgrund der neu entwickelten Technologien, die sich grundlegend von den bisher benutzten Methoden auf dem Gebiet der Triebwerksansteuerung unterscheiden, ist es schwierig, die Algorithmen in einer neuen Mission zu implementieren. Hierzu ist eine weitere Phase im Anschluss notwendig, die eine gründliche Qualifikation der Algorithmen durchführt. Die ersten Resultate, die im Rahmen des Vorhabens erzielt wurden, sind sehr optimistisch, doch die Akzeptanz der Technologie ist aufgrund des jungen Entwicklungsstadiums noch nicht zweifelsfrei gegeben.

## 6.3 Arbeiten, die zu keiner Lösung geführt haben

Das Vorhaben wurde strukturiert durchgeführt, so dass kaum Arbeiten durchgeführt wurden, die zu keiner Lösung führten. Lediglich bei der Erarbeitung von technischen und mathematischen Lösungen für aufgetretene Probleme wurden teilweise mehrere Lösungsmöglichkeiten untersucht, von denen sich einige als nicht erfolgsversprechend herausstellten.

Als Beispiel ist hier der Versuch zu nennen, einen Algorithmus für das vorliegende Problem zu implementieren, der sich an den Methoden der D3Group orientiert [1]. Die Gründe für die Erfolglosigkeit lagen in der Struktur des Algorithmus der D3Group, der prinzipiell einen Null-Schub als untere Grenze für ein Triebwerk vorsieht. Leider erfüllen gerade die Mikroantriebe diese Anforderung nicht, so dass der D3Group Algorithmus nicht erfolgreich implementiert werden konnte.



	Endbericht Algorithmen zur Triebwerksansteuerung Fkz: 50 JR 0484	Doc.No.: INT-TAS-RP-ZAR-001 Issue: 1.0 Page: 17 of 20
---	--	---

## 6.4 Präsentationsmöglichkeiten

Die Ergebnisse des Vorhabens sollen als Dissertation veröffentlicht werden, um sie einem großen Anwenderkreis zugänglich zu machen. Außerdem wurde das Thema auf Fachkongressen bereits vorgestellt und in Publikationen behandelt (siehe Anhang). Es ist geplant, die letzten Ergebnisse des Vorhabens auf dem Deutschen Luft- und Raumfahrtkongress des DGLR im September 2008 vorzustellen.

## 6.5 Einhaltung des Ausgaben- und Zeitplans

Die im Projekt *Algorithmen und Optimierungsverfahren für die Ansteuerung von  $\mu$ -Propulsion-Triebwerken zur Bahn- und Lageregelung von Raumfahrzeugen* eingeplanten Ausgaben wurden wie vorgesehen verwendet. Zu Beginn des Vorhabens gab es Verzögerungen bei der Durchführung der Arbeiten am ersten Projektabschnitt. Diese wurden allerdings durch Vorziehen von Projektarbeiten kompensiert, die erst später stattfinden sollten. Dadurch konnte der Ausgaben- und Zeitplan eingehalten werden.

	<p>Endbericht Algorithmen zur Triebwerksansteuerung Fkz: 50 JR 0484</p>	<p>Doc.No.: INT-TAS-RP-ZAR-001 Issue: 1.0 Page: 18 of 20</p>
---	---	--

## 7 Zusammenfassung

Im DLR Fördervorhabens 50JR0484 *Algorithmen und Optimierungsverfahren für die Ansteuerung von  $\mu$ -Propulsion-Triebwerken zur Bahn- und Lageregelung von Raumfahrzeugen* konnten erfolgreich neue Methoden entwickelt werden, die es erlauben, Mikroantriebe effektiver auf wissenschaftlichen Missionen einzusetzen.

Nach einer Analyse der verfügbaren Technologien im Bereich der elektrischen und Kaltgas-Antriebe wurden Kriterien abgeleitet, unter denen eine Ansteuerung optimal auf die Eigenschaften der Triebwerke ausgelegt ist. Zur Überprüfung, in wie weit die vorhandenen oder neu zu entwickelnden Algorithmen diesen Optimalitätskriterien entsprechen, wurde eine Simulationsumgebung erstellt.

Im Hauptteil des Vorhabens konnte aufbauend auf eine vorhandene Basistechnologie eine neuartige Ansteuerungsmethode entwickelt werden, die den allgemeinen Anforderungen einer Raumfahrtmission entspricht. In Hinblick auf die Robustheit, Optimalität und Geschwindigkeit wurden einzigartige Ergebnisse erzielt. Die Anwendbarkeit der Resultate ist im Rahmen von zukünftigen Wissenschaftsmissionen grundsätzlich gegeben. Durch die Neuartigkeit der entwickelten Algorithmen ist jedoch noch der Nachweis der fehlerfreien Funktionalität (Verifikation) zu erbringen, bevor eine breite Verwendung möglich ist.

Das Vorhaben konnte innerhalb des geplanten Zeit- und Finanzrahmens durchgeführt werden.

	<p>Endbericht Algorithmen zur Triebwerksansteuerung Fkz: 50 JR 0484</p>	<p>Doc.No.: INT-TAS-RP-ZAR-001 Issue: 1.0 Page: 19 of 20</p>
---	---	--

## Literatur

- [1] F. Ankersen, S. Wu, A. Aleshin, A. Vankov, and V. Volochinov. Optimization of spacecraft thruster management function. *Journal of Guidance, Control and Dynamics*, 28(6):1283–1290, 2005.
- [2] Jeng-Heng Chen. *Helium Thruster Propulsion System for Precise Attitude Control and Drag Compensation of the Gravity Probe-B Satellite*. PhD thesis, Department of Aeronautics and Astronautics, Stanford University, December 1983.
- [3] HaiPing Jin. *Translation and Attitude Control for the QUICK-STEP Satellite*. PhD thesis, Department of Aeronautics and Astronautics of Stanford University, August 1996.
- [4] F. Martel. Optimal Simultaneous 6 Axis Command of a Space Vehicle with a Precomputed Thruster Selection Catalogue Table. In *Proceedings of the AAS/AIAA Astrodynamics Specialist Conference Meeting, Big Sky, Montana, USA, August 2003*.
- [5] A. Schleicher. Thruster actuation algorithm design and analysis. Technical Report S2-ZAR-TN-2001, ZARM, July 2004.
- [6] N. Silva, A. Ducarouge, and P. Delpy. Three DOF Optimal Thruster Selection and Modulation for Space Vehicles. In *Proceedings of the 16th IFAC Symposium on Automatic Control, St.Petersburg, Russia, June 2004*.
- [7] S. Theil, S. Scheithauer, S. Winkler, and H. J. Rath. Attitude Control and Post-Mission Attitude Reconstruction for the DIVA Mission. In *52nd International Astronautical Congress, Toulouse, France, October 2001*.
- [8] Peter J. Wiktor. *The Design of a Propulsion System Using Vent Gas from a Liquid Helium Cryogenic System*. PhD thesis, Department of Aeronautics and Astronautics of Stanford University, June 1992.
- [9] Peter J. Wiktor. Minimum Control Authority Plot: A Tool for Designing Thruster Systems. *AIAA Journal of Guidance, Control and Dynamics*, 17(5):998 – 1006, September 1994.
- [10] S. Winkler, S. Theil, and H. Rath. High Accuracy Attitude Determination and Control of the Astronomy Satellite DIVA. In *AIAA/AAS Astrodynamics Specialist Conference, Monterey, California, August 2002*.

	<p>Endbericht Algorithmen zur Triebwerksansteuerung Fkz: 50 JR 0484</p>	<p>Doc.No.: INT-TAS-RP-ZAR-001 Issue: 1.0 Page: 20 of 20</p>
---	---	--

## Anhang

Der Anhang zu diesem Endbericht besteht aus folgenden Dokumenten:

- **Anhang A**, Berichtsblatt, Kurzfassung des wesentlichen fachlichen Inhaltes des Schlussberichtes
- **Anhang B**, Technical Note zu den Ergebnissen des Arbeitspakets AP 1100
- **Anhang C**, Technical Note zu den Ergebnissen des Arbeitspakets AP 1200
- **Anhang D**, Technical Note zu den Ergebnissen des Arbeitspakets AP 2100
- **Anhang E**, Technical Note zu den Ergebnissen des Arbeitspakets AP 2200
- **Anhang F**, Untersuchung einer Beispielmision MICROSCOPE mit Hilfe der in dem Vorhaben entwickelten Methoden
- **Anhang G**, Kurze Beschreibung zu einem zusätzlich entwickelten Werkzeug zur Auslegung des Triebwerkssystems auf Satelliten (CAAT)
- **Anhang H**, Veröffentlichung vorläufiger Ergebnisse des Vorhabens auf dem *56th International Astronautical Congress of the International Astronautical Federation* im Jahr 2005
- **Anhang I**, Veröffentlichung fortgeschrittener Ergebnisse des Vorhabens auf dem *30th ANNUAL AAS GUIDANCE AND CONTROL CONFERENCE* im Jahr 2007

	<p>Endbericht Algorithmen zur Triebwerksansteuerung Fkz: 50 JR 0484</p>	<p>Doc.No.: INT-TAS-RP-ZAR-001 Issue: 1.0 Page: 21 of 20</p>
---	---	--

## Anhang A

Berichtsblatt, Kurzfassung des wesentlichen fachlichen Inhaltes des Schlussberichtes

## Berichtsblatt

1. ISBN oder ISSN <b>geplant</b>	2. Berichtsart (Schlussbericht oder Veröffentlichung) <b>Veröffentlichung</b>
3. Titel <b>Algorithmen und Optimierungsverfahren für die Ansteuerung von <math>\mu</math>-Propulsion-Triebwerken zur Bahn- und Lageregelung von Raumfahrzeugen</b>	
4. Autor(en) [Name(n), Vorname(n)] <b>Bindel, Daniel</b>	5. Abschlussdatum des Vorhabens <b>September 2007</b>
6. Veröffentlichungsdatum <b>geplant</b>	
7. Form der Publikation <b>Buch</b>	
8. Durchführende Institution(en) (Name, Adresse) <b>Zentrum für angewandte Raumfahrttechnologie und Mikrogravitation (ZARM)          Universität Bremen          Am Fallturm          28359 Bremen</b>	9. Ber. Nr. Durchführende Institution  
10. Förderkennzeichen *) <b>50JR0484</b>	
11. Seitenzahl ca. 150	
13. Fördernde Institution (Name, Adresse) <b>Bundesministerium für          Bildung und Forschung (BMBF)          53170 Bonn</b>	12. Literaturangaben  
14. Tabellen  	
15. Abbildungen  	
16. Zusätzliche Angaben  	
17. Vorgelegt bei (Titel, Ort, Datum) <b>Deutscher Luft- und Raumfahrtkongress 2008. Darmstadt, 23.-15. September 2008</b>	
18. Kurzfassung <ol style="list-style-type: none"> <li>1. Momentan werden statische, pseudoinverse Matrizen zur Berechnung der notwendigen Schubkommandos für die Triebwerke benutzt. Sehr einfaches Verfahren, mit geringer Komplexität und Rechenaufwand. Wird als Standardverfahren zur Lösung von unterbestimmten Systemen verwendet (mehr als eine Lösung möglich).</li> <li>2. Momentan gibt es keine Möglichkeit, echte dynamische Randbedingungen der aktuellen Triebwerkszustände zu berücksichtigen. Dies ist aber für elektrische Triebwerke notwendig, aufgrund ihrer Dynamik-Eigenschaften. Ansteuerung kann keine Kommandos berechnen, die optimal für die Eigenschaften der (elektrischen) Triebwerke sind. Hauptproblem ist hier vor allem die Lebensdauer der Triebwerke, die auch durch die Art der Ansteuerkommandos beeinflussbar ist. Daher wurde ein Optimierungsalgorithmus entwickelt, der für die Eigenschaften von elektrischen Triebwerken geeignet ist, vor allem für den Einsatz bei aktuellen und zukünftigen, wissenschaftlichen Drag-Free Missionen. Ein weiteres Entwicklungsziel war auch eine hohe Robustheit des Algorithmus in der Lauffähigkeit, sowie ein möglichst geringer Verbrauch von Speicher- und Rechenzeit-Verbrauch.</li> <li>3. Beginn des Vorhabens mit Analyse der Arbeitsweise von elektrischen und Kaltgas Mikroantrieben und Identifikation von Eigenschaften einer optimalen Schublösung für solche Triebwerke, sowie notwendiger Anforderungen an die allgemeine Schublösung. Anschließend Untersuchung der existierenden Ansteuerungsalgorithmen und Überprüfung, in wieweit sie den festgestellten Anforderungen genügen können. Selektion der Linearen Optimierung zur Weiterentwicklung. Umsetzen der physikalisch optimalen Eigenschaften einer optimalen Schublösung in mathematische Optimierungsziele. Verbesserung der Rechengeschwindigkeit durch Analyse der Algorithmen-Arbeitsweise und der Randbedingungen des Einsatzszenarios.</li> <li>4. Es konnte ein Optimierungsverfahren entwickelt werden, dass sowohl die Eigenschaften von elektrischen Antrieben berücksichtigt, als auch die Anforderungen eines Echtzeitsystems an Bord eines Raumfahrzeuges (Robustheit, Geschwindigkeit).</li> <li>5. Anwendung der Technologie bei Drag-Free Missionen möglich und angestrebt. Allerdings noch zusätzliche Qualifikation notwendig, da die Technologie sehr neu ist und noch nicht eingesetzt wurde.</li> </ol>	
19. Schlagwörter <b>elektrische Antriebe, Ansteuerung, Algorithmen, Optimierung, Linear Programming</b>	
20. Verlag  	21. Preis  

	<p>Endbericht Algorithmen zur Triebwerksansteuerung Fkz: 50 JR 0484</p>	<p>Doc.No.: INT-TAS-RP-ZAR-001 Issue: 1.0 Page: 22 of 20</p>
---	---	--

## Anhang B

Technical Note zu den Ergebnissen des Arbeitspakets AP 1100



# Compilation of $\mu$ -Propulsion Thrusters for Attitude and Orbit Control of Spacecraft

Project:	Document No.:
Thruster Actuation System	INT-TAS-TN-ZAR-001
ZARM - Center of Applied Space Technology and Microgravity	
Am Fallturm	Phone: +49-421-218-8939
D 28359 Bremen	Fax: +49-421-218-4356
Germany	E-Mail: schlotterer@zarm.uni-bremen.de

Doc. No.: INT-TAS-TN-ZAR-001

Issue: 1.1

Written: 

Markus Schlotterer

Date: 2nd May 2006



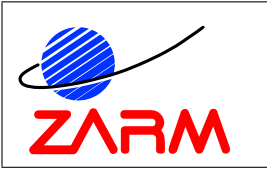
Daniel Bindel

Approved: 

Stephan Theil

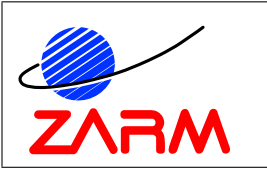
Date: -





## Document Change Record

Issue	Date	Changed Pages / Changed Chapters	Remarks	Done
1.0	26.09.2005	all	Initial Version	✓
1.1	02.05.2006	4.1	updated thrust range and time delay	✓



# Contents

- 1 Introduction 4**
- 2 Overview of Thruster-Technologies 4**
- 3 FEEP - Field Emission Electric Propulsion 7**
  - 3.1 ALTA S.p.A., Italy . . . . . 8
  - 3.2 Austrian Research Centers in Seibersdorf, Austria . . . . . 9
- 4 Colloid Thruster 10**
  - 4.1 Busek Co. Inc., USA . . . . . 11
  - 4.2 RAL, UK . . . . . 12
- 5 PPT - Pulsed Plasma Thruster 13**
  - 5.1 IRS University Stuttgart . . . . . 14
- 6 HEMP - High Efficiency Multistage Plasma 15**
  - 6.1 Thales Electron Devices GmbH . . . . . 16
- 7 RIT - Radio frequency Ion Thruster 17**
  - 7.1 I.PI Uni-Gießen / EADS Astrium . . . . . 18
- 8 Cold-gas/Resistojet Thruster 19**
  - 8.1 Marotta U.K. Ltd., Cheltenham, Great Britain . . . . . 20
  - 8.2 Bradford Engineering B.V., Heerle, Netherlands . . . . . 21
  - 8.3 Ångström Space Technology Centre, Uppsala, Sweden . . . . . 22
  - 8.4 ILR TU-Berlin . . . . . 22
  - 8.5 Moog . . . . . 23
- 9 Selection of suitable Thrusters 24**
- 10 Boundary Conditions and Optimization Criteria 26**
  - 10.1 Boundary Conditions . . . . . 26
  - 10.2 Optimization Criteria . . . . . 26

## 1 Introduction

This document contains the investigation results for the work package 1100 of the research project

### **Algorithmen und Optimierungsverfahren für die Ansteuerung von $\mu$ -Propulsion-Triebwerken zur Bahn- und Lageregelung von Raumfahrzeugen**

There will be an overview of the currently available thruster-technologies. Therefore the different engine-families and specific examples are presented together with their functional principle. Furthermore a justified selection of thrusters is presented, that can be used in further investigations of the research project.

## 2 Overview of Thruster-Technologies

The compilation of the reviewed thrusters is looking for the engine's ability to provide a controlled thrust in a range of about a micro-Newton up to a few milli-Newton. This thrust-range is called *Micro-Propulsion*, though it is not always possible for the thrusters to offer a controllability across the whole bandwidth of three orders of magnitude.

This limitation is originated by the mechanical construction of the engines and the appropriate control electronic for electrical thrusters. For some electrical thruster concepts like FEEP, colloid or PPT, the power conditioning unit is one of the major system driver for the realization of the requirements. In this case, the ability to change high voltages very fast or to charge capacitors rapidly are crucial for the achievable dynamic of the thruster.

Today available technologies, that offer the feature of micro-propulsion, can be divided into following technology-families:

- FEEP - Field Emission Electric Propulsion
- Colloid Thruster
- PPT - Pulsed Plasma Thruster
- HEMP - High Efficiency Multistage Plasma
- RIT - Radio frequency Ion Thruster
- Cold-gas/Resistojet Thruster

These engine concepts are in the state of production readiness or in an advanced development state. Although there also exist other approaches that reached so far a very early phase of research:



- Pyrocluster
- Micro-Catalyst  $H_2O_2$  Thruster

Before a selection of the thrusters for this research project is done, a description of every technology will give an impression of the engines and shall help to follow the selection. As far as the functional principle and the documentation of the engines are able to provide information, following attributes are collected to characterize the thrusters:

$T_{min}$  and  $T_{max}$  represent the lower and upper boundary of the thrust range, covered by the engine. Most thrusters can not lower their thrust in a controlled way to 0 Newton, but have a gap between a complete shut-off and their lowest thrust. Small residual thrust due to leakage in the fuel flow control shall not be considered here. Some of the engines are limited at the upper boundary by decreasing efficiency and higher degradation of the system. The electronics can also be a limiting factor when a controllable thrust shall be produced across some orders of magnitude. Cold-gas thrusters may also have mechanical limits of the actuators for the fuel mass flow rate.


$T_{step}$  indicates the available accuracy for the desired thrust. Although the physical principles of the engines would provide a continuous control, most of the Power Conditioning Units (PCU) have a digital interface. The bit width of the command signal and the resulting resolution are one element that has an influence to  $T_{step}$ . Another effect is the stability of the thruster, to hold a desired thrust. For this requirement, electronic and a closed-loop controller are necessary. In combination with sensors for the thrust measurement, the system can reach only a finite accuracy.

The value  $time_{delay}$  defines the maximum reaction time that a thruster needs, to realize an alternation of the command signal with a change of the thrust. This attribute is influenced by the idleness of the actuators in a cold-gas system or rather the limited power of the driver electronics for electrical engines.

The specific impulse ( $Isp$ ) indicates how mass efficient the thruster system works. The higher this value is, the fewer fuel is consumed to create a certain thrust. Chemical engines have values up to 450 seconds, while electrical thrusters can reach several thousand seconds. The unit seconds is originated from the calculation  $Isp = thrust / (massflowrate \cdot g_0)$ . There is also the advantage, that the time is equal in all unit-systems, so comparisons with non-metric literature are simplified.

The electrical energy that is needed for the operation of the thruster is characterized by  $P_{electr}$ .

Real engines produce a thrust that is affected by small noise due to stochastic effects.

	Compilation of $\mu$ -Propulsion Thrusters for Attitude and Orbit Control of Spacecraft	Doc.No.: INT-TAS-TN-ZAR-001 Issue: 1.1 Page: 6 of 29
---	---	--

With the help of a Power Spectral Density ( $PSD_{noise}$ ) analysis, a statement can be made about the magnitude of these disturbances with respect to different frequencies.

The total impulse of a thruster characterizes the integral impulse, that can be delivered throughout the lifetime. The important factors for this item are the failure probability, the system degradation and the amount of fuel.

### 3 FEED - Field Emission Electric Propulsion

Field Emission Electric Propulsion (FEED) thrusters emit single ions or small droplets of ions directly out of a liquid metal surface. The metal has a positive charge while the acceleration electrode in exhaust direction is negatively charged. The liquid metal propellant is drawn from the tank to the ion-extraction point by capillary forces. The materials that are used as fuel are Indium and Cesium because they have a high atomic mass, a low ionization potential and low melting temperatures. The tank of a FEED thruster is heated to melt the solid fuel before it can be emitted.

It shall be noted that the usage of metallic propellant can raise the problem of contamination of optical surfaces. So it must be paid attention to the mounting points and orientation of the thrusters at the circumference of the satellite. Also formation flying of satellites should not be neglected, because the exhausted ion jet of an engine may hit the other satellite. So the thruster configuration should be optimized for at least the nominal satellite formation.

The FEED effect is generated by needle or slit emitters that are able to bring the fuel to a surface with a high curvature in a very small area. The radius of curvature is in the range of  $1 \mu m$ . Due to the balance of the electrostatic forces of the electric field (approx.  $10^9 V/m$ ) and the surface tension, the surface is further stretched until a so called Taylor cone is formed. The ions leave the liquid metal directly at the very end of the cone-tip. Due to the fact that the electric field is used both for ionization and acceleration, the electric losses are very small (electr. efficiency approx. 95%). The thrust range of a needle emitter system can be varied by the number of needle tips. For slit emitters the length of the slit is the appropriate constructive detail to predetermine the thrust power.

For the operation of a needle emitter it should be noted, that the thrust for each needle shall not exceed  $10 \mu N$  otherwise the erosion of the emitter tip would increase noticeable. This leads for long term operations to a subsidence of the  $Isp$ . But a high thrust is also immediately accompanied by a lower mass efficiency because there are more droplets emitted than single ions. The dependency of the  $Isp$  from the commanded thrust is provided in the specifications of the engines.

Two different configurations are developed in Europe in different countries. The Austrian Research Centers in Seibersdorf/Austria (ARCS) uses needle emitters while Alta S.p.A. in Pisa/Italy develops a slit emitter thruster.

The ion beam has a positive charge, so an additional neutralizer is needed to neutralize the satellite with respect to the ambient space by the disposal of electrons.

For the conclusion it should be annotated that at the moment the FEED thrusters have some problems with lifetime and stability. But they represent a very advanced state of the technology and combine good micro propulsion properties with a low fuel consumption, so they are an option for the choice of a suitable thruster.

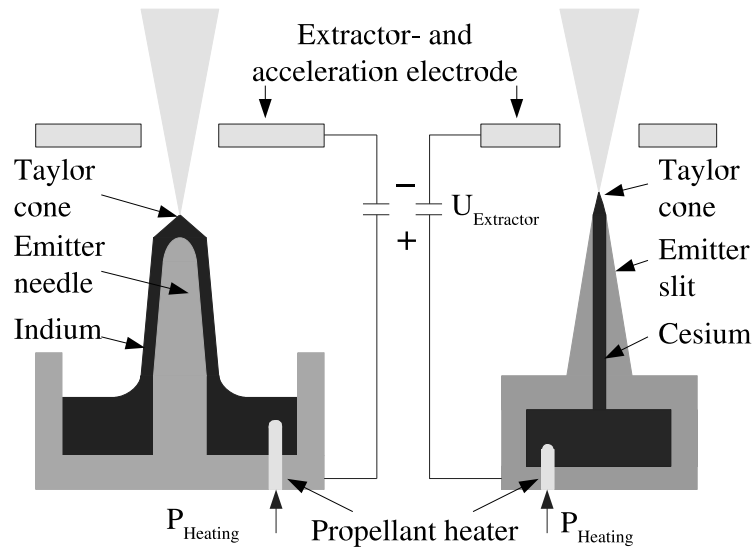


Figure 1: Principle design of FEEP engines

### 3.1 ALTA S.p.A., Italy

Manufacturer:	ALTA S.p.A., Pisa, Italy [1]
Emitter-Configuration:	Slit-Emitter
Fuel:	Cesium
Control mode:	continuous
State of development:	in testing, 1000 h duration tests solved
Utilization examples:	planned for Microscope, optional for LISA Pathfinder, LISA
Contact:	Fabio Ceccanti (f.ceccanti@alta-space.com)

$T_{min}$ :	$0.1 \mu\text{N}$
$T_{max}$ :	$150 \mu\text{N}$
$T_{step}$ :	$0.1 \mu\text{N}$
$time_{delay}$ :	$< 100\text{ms}$
$I_{sp}$ :	$> 6000\text{s}$
$P_{electr}$ :	$< 60 \text{ W/mN}$
$PSD_{noise}$ :	$0.1 \frac{\mu\text{N}}{\sqrt{\text{Hz}}}$ für $> 0.1 \text{ Hz}$
Disturbances:	no, needs neutralizer for satellite decharging
Degradation:	no data
Total impulse:	$> 4500\text{Ns}$ at 75g fuel storage
Lifetime:	Endurance tests up to 1000 hours

### 3.2 Austrian Research Centers in Seibersdorf, Austria

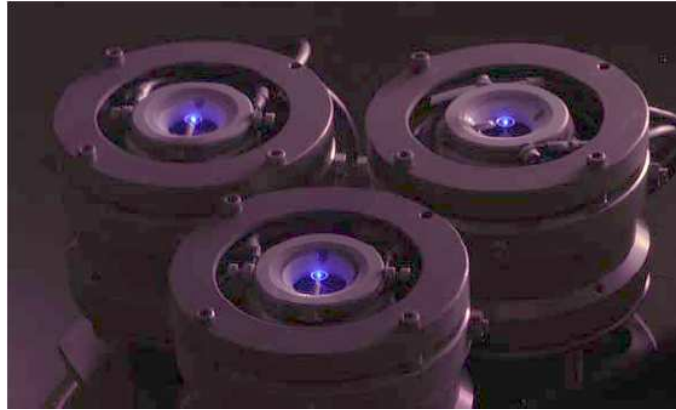


Figure 2: Indium FEEP thruster (image by ARCS)

Manufacturer:	ARCS Austrian Research Centers Seibersdorf [4] [12]
Emitter-Configuration:	Indium-FEEP, tungsten needle emitter
Fuel:	Indium
Control mode:	continuous
State of development:	advanced development, 2000 h duration tests solved
Utilization examples:	predecessor of thruster was already in space as neutralizer; In-FEEP-technology demonstrated in space
Contact:	Angelo Genovese (Angelo.Genovese@arcs.ac.at) Martin Tajmar (Martin.Tajmar@arcs.ac.at)
$T_{min}$ :	0.1 $\mu$ N
$T_{max}$ :	100 $\mu$ N
$T_{step}$ :	0.1 $\mu$ N
$time_{delay}$ :	no data
$Isp$ :	1600-8000s, $Isp \approx 30(T[N])^{-0.42}$ , $Isp \approx 8000s$ for $T < 1.7$ $\mu$ N
$P_{electr}$ :	approx. 45-84 W/mN, 13W for housekeeping
$PSD_{noise}$ :	0.1 $\frac{\mu N}{\sqrt{Hz}}$ for 1 mHz to 20 mHz 0.02 $\frac{\mu N}{\sqrt{Hz}}$ for > 20 mHz
Disturbances:	no, needs neutralizer for satellite decharging
Degradation:	for thrust < 10 $\mu$ N neglectable for higher thrust the $Isp$ is declining
Total impulse:	approx. 600 Ns at 30g fuel storage
Lifetime:	Endurance tests up to 2000 hours, accumulated up to 4000 hours per thruster



## 4 Colloid Thruster

Colloid engines work in a similar way like FEEP thrusters, because they extract ionized particles directly from a liquid surface and accelerate them. But they do not use liquid metal, but very conductive, organic fluids that are composed of glycerol or formamide and sodium iodide or lithium chloride. New developments [13] use a fuel called 'ionic fluid' or EMI-Im ( $C_8H_{11}F_6N_3O_4S_2$ ). This fluid has the advantage, to be relatively resistant against radiation.

Another difference is the size of the accelerated particles. While FEEP thrusters are extracting more or less single ions, the electro spray of colloid engines is formed by small droplets. This leads to a considerably smaller specific impulse. But the benefit is the usage of two separate electrodes for the extraction and acceleration of the electro spray. Thus lower voltages are needed and the variation of the acceleration potential increases the controllable thrust range.

The emitter configuration from the company Busek, that have been developed to maturity phase, uses a hollow micro-needle to transport the fuel to the extraction point. Here is also a Taylor cone formed from where the charged particles are extracted. In comparison to FEEP engines an active pumping is necessary for the fuel supply. Though this allow for a more sophisticated control of the thrust, because the fuel flow rate applies for a rough and the accelerating voltage for an accurate adjustment. To select the thrust range even in the design phase of the engine, a number of emitter needles can be combined to one thruster.

In the UK the Rutherford Appleton Laboratory (RAL) is working on a colloid technology. But this research is not in the same development state as the Busek engine. Furthermore the designated utilization is an engine for small satellites. So their requirements are not so sophisticated in terms of thrust range and continuous proportional control. That seems to be the reason for the engine design of discrete thrust levels. The selection of the thrust range is done by the activation of a specific amount of emitters. For example the current thruster head from RAL consists of a matrix of multiple emitters and is divided into three areas that can provide 10, 40 and 50  $\mu$ N thrust. Hence this results in 6 different thrusts from 10 to 100  $\mu$ N. Unfortunately the single emitters can only be activated in a discrete way, so a continuous proportional control is not feasible.

There is also the possibility to modulate the thrust by the electrode voltage. Indeed the specifications [11] claim a very narrow dynamic range. The thrust variation by the use of mass flow control was not yet implemented by RAL. This could increase the achievable, proportional thrust range.

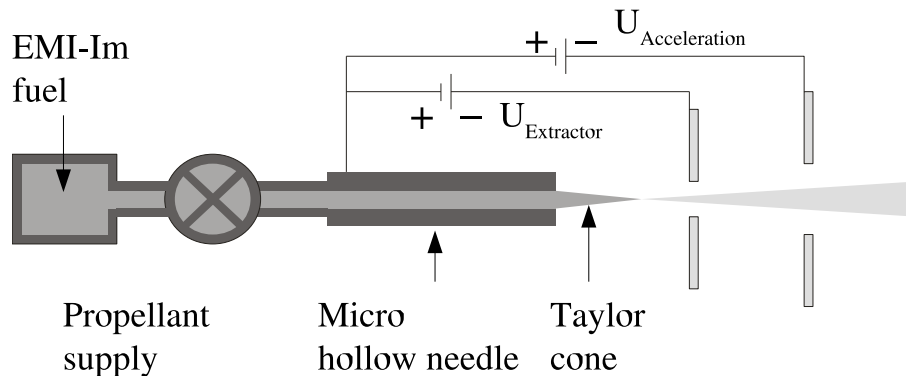


Figure 3: Principle design of a colloid thruster

#### 4.1 Busek Co. Inc., USA

Manufacturer: Busek Co. Inc., Natick MA, USA [9] [14]  
 Emitter configuration: Micro hollow needle  
 Fuel: EMI-Im ( $C_8H_{11}F_6N_3O_4S_2$ )  
 Control mode: continuous  
 State of development: advanced, development of EM, single engines accumulated up to 3000 hours tests  
 Contact: www.busek.com

$T_{min}$ :  $5.0 \mu N$   
 $T_{max}$ :  $30.0 \mu N$  (at the moment verified thrust range, broader bandwidth possible with more emitters [3],  $0.1 \mu N$  to  $3 \mu N$  per emitter are normal [14])  
 $T_{step}$ :  $0.06 \mu N$   
 $time_{delay}$ : 100ms for steps  $< 20\%$  of current thrust, 100s for large steps  
 $I_{sp}$ : 500-1500s  
 $P_{electr}$ : ca  $50 W/mN$   
 $PSD_{noise}$ :  $< 0.1 \frac{\mu N}{\sqrt{Hz}}$  for 7 mHz to 1Hz  
 Disturbances: no, needs neutralizer for spacecraft discharge  
 Degradation: no data  
 Total Impulse: no data  
 Lifetime: no data



Figure 4: Colloid thruster with propellant storage and neutralizer (Busek Co. Inc.)

## 4.2 RAL, UK

Manufacturer:	Rutherford Appleton Laboratory, Oxfordshire, Great Britain [10]
Emitter configuration:	Matrix of MEMS-emitters within one thruster head
Fuel:	1-Butyl-3- methylimidazolium tetrafluoroborate ( <i>BmimBF<sub>4</sub></i> ) [5]
Control mode:	continuous, switch between different thrust ranges necessary
State of development:	first prototypes build for utilization on small satellites, no research planned for a proportional micro-thruster
Contact:	Barry J. Kent (B.J.Kent@rl.ac.uk)
$T_{min}$ :	0.05 $\mu$ N per emitter
$T_{max}$ :	100 $\mu$ N per thruster head (multiple emitters)
$T_{step}$ :	approx 10 $\mu$ N rough stepping by emitter switching, precise adjustment by voltage (between 0.05 and 0.1 $\mu$ N per emitter)
$time_{delay}$ :	no data
$I_{sp}$ :	ca 400s
$P_{electr}$ :	ca 20 W/mN
$PSD_{noise}$ :	no data
Disturbances:	none known, neutralizer needed
Degradation:	no data
Total impulse:	no data
Lifetime:	no data

## 5 PPT - Pulsed Plasma Thruster

A Pulsed Plasma Thruster (PPT) is based on the combination of an electrical field, charge carriers in a plasma and a self induced magnetic field. There can be two different PPT technologies identified depending on the type of propellant, solid or gaseous. Here the function principle of PPT working with solid ablative propellant is outlined.

The configuration of such an engine is displayed in fig. 5. Between two electrodes is a block of PTFE (Teflon) located that is pressed against a stopper by a spring.

To start an ignition in the thruster, a charged capacitor is connected to the electrodes. Directly in front of the propellant block are some charged particles released, that produce an arc by their current. The radiated heat from this arc releases even more electrons and ions from the ablative surface. The particles are accelerated in the electrical field accordingly to their charge. Due to this high current, a magnetic field is induced that lies parallel to the PTFE-surface and the electrodes (points in fig. 5 into the plane). The movement of the charged particles is now influenced by the Lorentz force in a way, that they accelerate on their way to the electrodes towards the exit of the engine (fig. 5 right). The exhaust of a PPT is a neutral plasma cloud.

The duration of the discharge is in the range of some microseconds, because the charge of the capacitor is rapidly consumed by the high current in the arc. The advantages of the PPT are the relative low voltage (a few hundred volts) for their operation, the good adjustment and repeatability of the thrust impulses and the easy propellant maintenance. A drawback is the possible contamination of areas that lie directly in the exhaust direction of the thruster by carbon from the PTFE propellant. Furthermore the control strategy must be adapted to the pulsed operation of the thruster to avoid negative effects of the single impulse bits. A variation of the thrust can be achieved by a change of the capacitor voltage and the pulse frequency of the engine.

The Institute of Space Systems at the University of Stuttgart is developing small satellites since 2002, to build and operate a moon orbiter. For some phases of the mission a PPT engine is planned and developed at the institute. But this are only first studies to become familiar with the technology of PPT engines (they are called I-MPD, instationary pulsed MPD thrusters, at the ISS).

The following specifications are therefore collected for an engine, that have not been developed directly as a micro propulsion thruster. Additionally the early state of development leads to a more rudimentary amount of documentation.

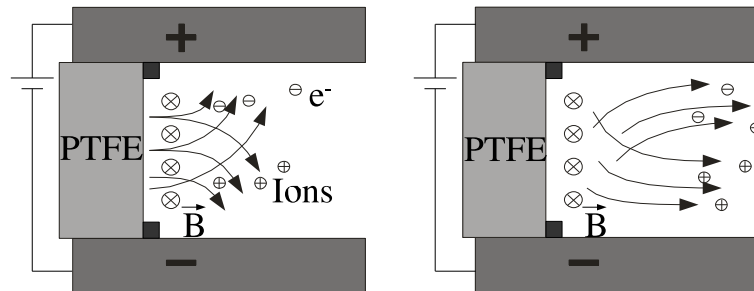


Figure 5: Self-induction of magnetic field and acceleration of Ions in PPT



Figure 6: PPT study model (image by IRS Uni Stuttgart)

## 5.1 IRS University Stuttgart

Manufacturer:	Institute of Space Systems, University of Stuttgart [8]
Configuration:	Ablative PPT, solid propellant with back-feed
Fuel:	solid PTFE
Control mode:	thrust pulses
State of development:	Study models, no optimization known
Contact:	Anuscheh Nawaz (nawaz@irs.uni-stuttgart.de)

$T$ :	ca 1,5 mN nominal
$T_{step}$ :	no data
$time_{delay}$ :	Pulse freq. approx. 1-2 Hz, Pulse length approx. 4 $\mu$ sec
$I_{sp}$ :	500-1000s
$P_{electr}$ :	no data
Disturbances:	contamination by carbon possible, can perhaps be avoided by better design
Degradation:	Degradation of ignition electrodes for the starting arc
Total impulse:	depends on fuel storage
Lifetime:	no data

## 6 HEMP - High Efficiency Multistage Plasma

A High Efficiency Multistage Plasma (HEMP) thruster is an electrical engine that offer a high ionization efficiency and low wall losses. The specific feature of the HEMP is based on the Periodic Permanent Magnet (PPM) focus of the generated plasma along the centerline of the thruster. The field of multiple subsequent magnets forces the plasma electrons to closed Hall current loops.

The positive charged anode is located at the fuel inlet and attracts the electrons, that are released during the ionization in the chamber. This electrons also collide with the entering fuel that is still neutral. The negative electrode of the electric acceleration field is the neutralizer and is located outside the ionization chamber (fig. 7).

The released ions accelerate into the direction of the chamber exit but they are affected by the magnetic focus and are forced to follow the magnetic flux lines in circular trajectories. This leads to a high number of collisions with the neutral gas. These impacts are concentrated at the intersections where the fields of two magnets are merged and compressed. This way, a very high rate of ionization can be achieved along the centerline towards the exit of the chamber. The electrons that are released during the ionization are also streaming back into the chamber to the anode and contribute to even more collisions with the plasma or neutral fuel.

A neutralizer is necessary for the ignition of the system and for the neutralization of the ion stream. For the upkeep of the plasma is no more dispersion of electrons by the neutralizer needed, because the back streaming electrons from the ionization are maintaining the plasma production. But the exhausted positive ion beam demands a neutralizer, so a negative charge of the satellite can be omitted.

The magnetic focus has not only the positive property of a good ionization rate, but also ensures that the hot plasma has nearly no contact with the wall. So the erosion of the wall material is very low.

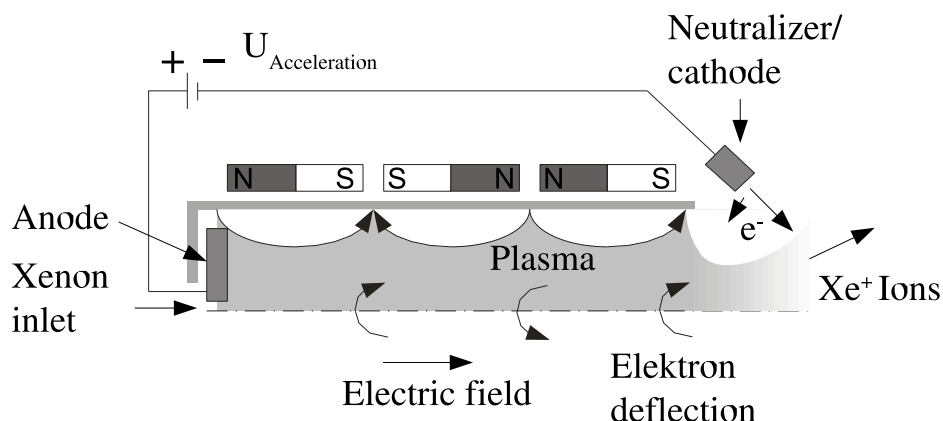


Figure 7: Function principle of a HEMP-thruster

## 6.1 Thales Electron Devices GmbH

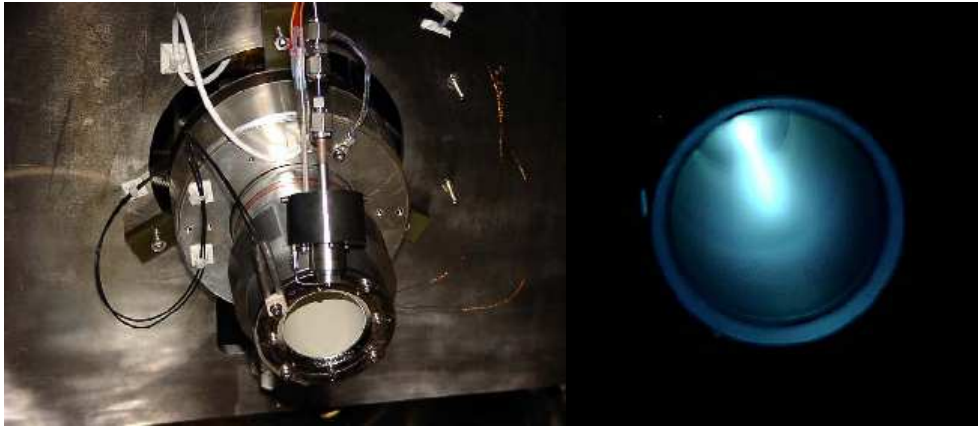


Figure 8: HEMP thruster(image by Thales Electron Devices GmbH)

Manufacturer:	Thales Electron Devices GmbH, Ulm, Germany [6]
Configuration:	HEMP 3050 DM7
Fuel:	Xenon
Control mode:	continuous
State of development:	studies of a HEMP system, bigger HEMP models developed to EM state, Micro-HEMP not yet available for tests
Contact:	Dr. Günter Kornfeld (guenter.kornfeld@de.thales-ElectronDevices.com)
$T_{min}$ :	5mN
$T_{max}$ :	150mN
$T_{step}$ :	no data
$time_{delay}$ :	no data
$I_{sp}$ :	500s - 3600s
$P_{electr}$ :	75W - 6kW
	10 - 25 W/mN ideal
	20 - 35 W/mN normal
$PSD_{noise}$ :	no data
Disturbances:	permanent magnetic field around the thruster, strength not specified
Degradation:	estimated very low, because plasma has nearly no contact with thruster
Total impulse:	no data
Lifetime:	no data



## 7 RIT - Radio frequency Ion Thruster

Radio frequency ion thrusters use a static electric field to accelerate ions. This field is generated by grid-electrodes that are passed through by the ions.

For this thruster type the ion production is very interesting. Electrically neutral propellant is inserted into an ionization chamber, that resides behind the grid electrodes. Around the chamber is a high frequency coil located, that produces an electromagnetic field of about 1 MHz. In this field charged particles are influenced by the Lorentz force. The number of collisions between the particles is increasing. The effect is boosted by the alternating electromagnetic field because this leads to an alternation of the deflection direction. By this way, inside the ionization chamber a constant amount of plasma can be held. A low and constant stream of neutral propellant is fed into the thruster, so there is always small thrust by exiting neutral gas, regardless of the acceleration voltage. The modulation of the thrust can be done by three different parameters. The mass flow rate of the propellant determines the lowest possible thrust. Even if the engine is not extracting and accelerating ions, the neutral gas produces a thrust. Unfortunately the exact control of the propellant mass flow in such small ranges is a delicate issue. So the current thrusters use a constant and low mass flow.

The second influence to the thrust is the amount of plasma in the ionization chamber. It is possible to put different amounts of electrical power into the radio frequency coil. By this way the amount available plasma can be controlled.

The most intuitive way to control the thrust is the acceleration voltage. After some ions have been extracted from the storage in the ionization chamber, the acceleration is done by two electrodes. Today a combination of RF-power and acceleration voltage is used to control the thrust of a RIT engine.

The configuration of the grid electrodes (fig. 9) can consist of two or three elements. Beside the necessary shield and acceleration electrode, that are used to establish the static electric field, also a deceleration electrode can be added. This prevents the back streaming of ions. For the operation of a RIT is a neutralizer required.

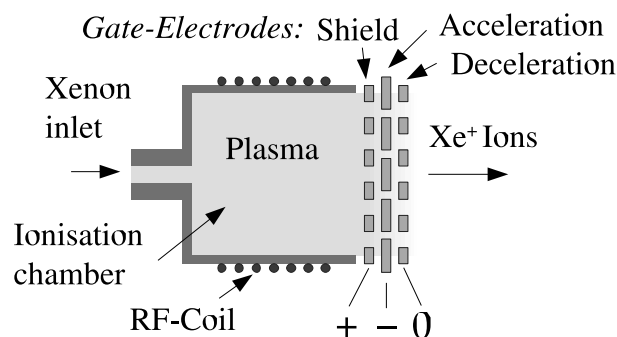


Figure 9: Principle design of a Radio frequency Ion Thruster



## 7.1 I.PI Uni-Gießen / EADS Astrium

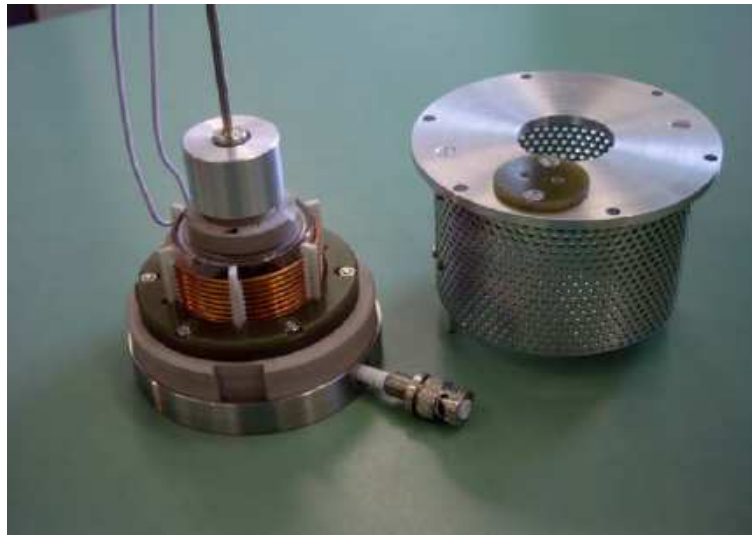


Figure 10: RIT 4 (image by I.PI Uni-Gießen)

Manufacturer:	1. Physical Institute of JLU-Gießen / Astrium, Germany [7], [2]
Configuration:	RIT 4
Fuel:	Xenon
Control mode:	continuous
State of development:	RIT 1 and RIT 2 still in prototype state, bigger RIT already in production
Utilization examples:	RIT 10 flown on EURECA and Artemis
Contact:	Dr. Feili Davar (davar.feili@expl.physik.uni-giessen.de)
$T_{min}$ :	$20\mu\text{N}$
$T_{max}$ :	$350\mu\text{N}$
$T_{step}$ :	$0.5\mu\text{N}$
$time_{delay}$ :	approx. 10-50ms
$I_{sp}$ :	2000s
$P_{electr}$ :	approx. 80W
$PSD_{noise}$ :	no data
Disturbances:	RF-coil emits high frequency field outside the thruster
Degradation:	expected at the grid electrodes
Total impulse:	no data
Lifetime:	more than 25000 accumulated hours proven for used RIT technology

## 8 Cold-gas/Resistojet Thruster

The technology of cold-gas thrusters is well understood and utilized in space flight since decades. The function principle is based on the expansion of pressurized stored gas by a valve and a subsequent nozzle to the ambient space. The range of possible fuel covers several gases like nitrogen, helium or xenon. The achievable thrust depends among other things from the mass flow rate and the temperature of the expanding gas. The high storage pressure is typically decreased to a working pressure of a few bar, before a valve is adjusting the desired mass flow rate.

While solenoid valves are sufficient for established thrusters to maintain the mass flow rate, the  $\mu$ N thrusters require more precise mechanisms. Almost all engines that have been investigated for this project use piezo actuators for a highly accurate control of the valves. A possible configuration of this technology can be seen in figure 11. Another interesting approach to create the minimal valve motions is a paraffin actuator. A heater coil takes advantage of the high expansion coefficient of the material to produce a change of the volume. For one of the engines this method was utilized with an MEMS-architecture (Micro Electro Mechanical System).

Many thrusters add thermal energy to the gas between the valve and the nozzle to increase the exit velocity and therefore the specific impulse.

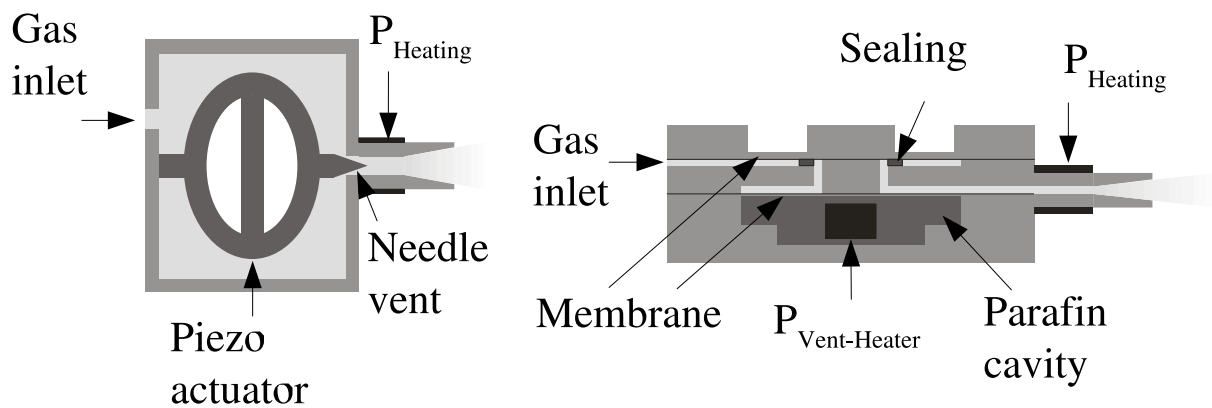


Figure 11: Piezo-valve (left) and paraffin-valve in MEMS-design (right)



Figure 12: VP03 Thruster (image by Marotta U.K. Ltd.)

## 8.1 Marotta U.K. Ltd., Cheltenham, Great Britain

Manufacturer:	Marotta U.K. Ltd. (Polyflex)
Configuration:	VP03 - Piezo-element presses valve needle in nozzle-throat
Fuel:	helium, nitrogen, xenon
Control mode:	continuous
State of development:	advanced development, prototypes exist
Utilization examples:	...
Contact:	Roland McLellan (rmclellan@marotta.co.uk)

$T_{min}$ :	$0.6\mu\text{N}$
$T_{max}$ :	$1000\mu\text{N}$
$T_{step}$ :	$0,8\mu\text{N}$ für $0-25\mu\text{N}$ $2.5\mu\text{N}$ für $25-100\mu\text{N}$
$time_{delay}$ :	5ms (90% of thrust change)
$I_{sp}$ :	ca 60s (approx 80s heated)
$P_{electr}$ :	2W heater power
$PSD_{noise}$ :	$\leq 0.1 \frac{\mu\text{N}}{\sqrt{\text{Hz}}}$ , 0.1 mHz to 1 Hz, $\leq 25\mu\text{N}$ $\leq 1 \frac{\mu\text{N}}{\sqrt{\text{Hz}}}$ , 0.1 mHz to 1 Hz, $25-100\mu\text{N}$
Disturbances:	no
Fuel consumption:	0-2 mg/s, for GN2 and 1 bar inlet pressure $\dot{m} \approx 1.27(T[N])[g/s]$
Degradation:	no information
Total impulse:	depends on gas reservoir
Lifetime:	no information

## 8.2 Bradford Engineering B.V., Heerle, Netherlands



Figure 13: Micro Thruster Assembly (image by Bradford Engineering)

Manufacturer:	Bradford Engineering B.V.
Configuration:	Micro Thruster Assembly, valve needle is pressed by Piezo-element in nozzle-throat
Fuel:	gaseous nitrogen, helium, xenon
Control mode:	continuous
State of development:	advanced development, prototypes exist
Utilization examples:	qualified for PLEIADE, DEMETER, GOCE
Contact:	Patrick van Put (P.vanput@bradford-space.com)

$T_{min}$ :	$0\mu\text{N}$
$T_{max}$ :	$1200\mu\text{N}$
$T_{step}$ :	$0.1\mu\text{N}$ für $0-50\mu\text{N}$ $1\mu\text{N}$ für $50-1200\mu\text{N}$
$time_{delay}$ :	$<10\text{ms}$
$I_{sp}$ :	$>60\text{s}$ (no heating)
$P_{electr}$ :	no heating
$PSD_{noise}$ :	no data
Disturbances:	no
Fuel consumption:	$\dot{m} \approx 1.7(T[N])[g/s]$
Degradation:	no data
Total impulse:	depends on gas reservoir
Lifetime:	no information

### 8.3 Ångström Space Technology Centre, Uppsala, Sweden

Manufacturer:	Ångström Space Technology Centre
Configuration:	MEMS-technology, valve control by paraffin-expansion
Fuel:	gaseous nitrogen
Control mode:	continuous
State of development:	prototypes, not yet flown, studies, test results expected in a few months
Utilization examples:	intended engine for ÅSTC nanosatellite
Contact:	Lars Stenmark (Lars.Stenmark@Angstrom.uu.se) Anders Eriksson (anders.eriksson@angstrom.uu.se)

$T_{min}$ :	ca $5\mu\text{N}$
$T_{max}$ :	ca $5\text{mN}$
$T_{step}$ :	no data
$time_{delay}$ :	approx 100ms expected
$Isp$ :	60s (120s heated)
$P_{electr}$ :	no data
Disturbances:	no
Fuel consumption:	$\dot{m} \approx 0.85(T[N])[g/s]$
Degradation:	no data
Total impulse:	depends on gas reservoir
Lifetime:	no information

### 8.4 ILR TU-Berlin

Manufacturer:	Institut für Luft- und Raumfahrttechnik, TU-Berlin, Germany
Configuration:	Resitojet
Fuel:	water, water vapor
Control mode:	continuous or pulse-modulation
State of development:	studies started, hardware/prototypes to be expected in a few months/years
Utilization examples:	utilization for small satellites, no $\mu\text{N}$ application planned
Contact:	Harry Adirim (030-314-22826)
$T$ :	ca $100\mu\text{N}$ nominal thrust
$Isp$ :	70-150s, heated
Addition:	No development for micro-propulsion planned, stated by Mr. Adirim



## 8.5 Moog

Manufacturer: Moog GmbH Böblingen / Moog Inc.

Configuration: nozzle with solenoid valve

Fuel: nitrogen?

Control mode: continuous

Contact: jdrew@moog.com

$T$ : ca 4 mN nominal thrust

Addition: Since January no response on requests

## 9 Selection of suitable Thrusters

This research project analyzes thruster actuation methods for highly accurate satellite missions. Based on the expected requirements for the controlling of the thrusters, a preliminary selection of suitable engines out of the presented models can be made. An important issue is the thrust range. Because there are missions with highly accurate control requirements investigated, the thrusters must also be able to provide low and precise thrust. Another important item are the available information about an engine. So thrusters with a complete set of documentation are preferred, because they are more accurate to simulate. To allow a comparison between different technologies, models from different engine-families have been selected.

For the further analyses the following thrusters have been selected:

- FEEP, Austrian Research Centers Seibersdorf
- Colloid Thruster, Busek Co. Inc.
- $\mu$ -HEMP
- RIT 1, University Gießen
- VP03 Cold Gas Micro Thruster Assembly, Marotta U.K. Ltd.


The HEMP technology is very promising. The high dynamic range, the low degradation and the high efficiency are very positive attributes of this technology and should be observed for future developments. At the moment there is a  $\mu N$  HEMP engine announced, that could be parametrized by using the data from existing models. The implementation of this engine will be updated, as soon as more precise information are available.

The PPT of the University of Stuttgart is a special category of the investigated engines because it is used in a pulsed mode. But the development is not very advanced, so there are just a few test results. On the other hand, the nominal thrust with  $750 \mu N$  for each pulse is much higher than the demanded level.

In the FEEP category, the ARCS model from Austria have been selected, because for this engine some rudimentary information about degradation have been published. Otherwise the engine from Alta/Italy seems to be equal competitive.


The colloid thruster of the Rutherford Appleton Laboratories had to be withdrawn, because the information were only rudimentary and the presented dynamic range was very small.

The family of cold gas engines offer a wide variety of solutions and examples. The Marotta thruster was chosen for further investigations because it provides a detailed documentation and was proposed as alternative propulsion system for LISA Pathfinder. On the other hand the system from Bradford Engineering was classified as equally good. The small amount of data and the early state of development of the MEMS engine from

	Compilation of $\mu$ -Propulsion Thrusters for Attitude and Orbit Control of Spacecraft	Doc.No.: INT-TAS-TN-ZAR-001 Issue: 1.1 Page: 25 of 29
---	---	---

the Ångström Space Technology Centre was the reason to not select this technology. The water vapor thruster from the ILR TU-Berlin has a thrust range that is far to high for the destined utilization. About the thruster from the Moog Inc. almost no data could be gathered.



	<p style="text-align: center;">Compilation of <math>\mu</math>-Propulsion Thrusters for Attitude and Orbit Control of Spacecraft</p>	<p>Doc.No.: INT-TAS-TN-ZAR-001 Issue: 1.1 Page: 26 of 29</p>
---	--	--

## 10 Boundary Conditions and Optimization Criteria

### 10.1 Boundary Conditions

For the design of the thruster actuation algorithm it is necessary to express the boundary conditions of the thruster operation in a mathematical manner.

The easiest constraint is given for the elements of the solution vector  $T$  by the condition:

$$T_{min} \leq T \leq T_{max} \quad (1)$$

It should be noted that the minimal thrust is not inevitable zero newton. Most engines need at least a low value for a controlled thrust.

Another restriction can be a limited fuel mass flow rate. Some thrusters need a precisely controlled fuel flow. The valves for this task have a limited maximum flow rate. On the other hand also the satellite can have a boundary condition for the fuel supply. This may be imposed by pressure vents at the tank or due to the storage of the fuel. Cryogenic missions like Gravity Probe B for example must slowly vaporize the stored helium to feed the thrusters and cool the experiment. In this case the thruster actuation system have to drive the thrusters in such a way, that exactly the same amount of helium is consumed as it is vaporized. This fact is expressed by the 1-norm. This is the sum of all absolute values of the solution vector  $T$ :

$$\|T\|_1 = \sum |T_i|, \|T\|_1 \leq \dot{m}_{max} \quad (2)$$

Furthermore the dynamic of the thruster can play an important role. It may be necessary to avoid large steps in the commanded thrust for the single thrusters:

$$|\Delta T_i| \leq \Delta T_{max} \quad (3)$$

### 10.2 Optimization Criteria

Beside clear boundary conditions, the thruster actuation algorithm also needs criteria for the optimization. Because the thrust distribution problem is under-determined, an optimal solution vector  $T$  can be selected from a band of solutions.

There are different targets for the optimization that are connected to different technical attributes of the thrusters. For example it is important for the cold gas thrusters, to use as few propellant as possible. The  $I_{sp}$  of these engines is very low so the fuel consumption is enormous in comparison to electrical thrusters.

Therefore the 1-norm of the thrust vector  $T$  ( $n$  thrusters) must be minimized to minimize the overall fuel consumption:

$$\min_T \|T\|_1 = \min_T \left( \sum_{i=1}^n |T_i| \right) \quad (4)$$

If information about the degradation of the thrusters are available, it is possible to create models for the changing of the thruster efficiency. Due to erosion of electrodes or symptoms of abrasion there may be a degradation of the specific impulse  $I_{sp}$ , a higher power consumption or a higher failure risk.

A possible reduction of the degradation is a low usage of the thrusters. This can be done by the minimizing the  $\infty$ -norm of the solution vector. The  $\infty$ -norm is the greatest absolute value of each vector element:

$$\begin{aligned} \|T\|_\infty &= \max(|T_i|), \text{ so that} \\ \min_T (\|T\|_\infty) &= \min_T (\max(|T_i|)) \end{aligned}$$

Another procedure can be the minimization of the cumulative wear  $W$  of the thruster during its lifetime. For this task the thrust distribution algorithm should integrate the impulse of every single thruster. The result can be used to redistribute the thrust to other engines if one thruster has been wear down more then the others.

$$W_i = \int_{t_0}^t T_i dt \quad (5)$$

$W_i$  can now be used as factor for optimizing the  $\infty$ -norm:

$$\min_T (\|T(W)\|_\infty) = \min_T (\max(|W_i \cdot T_i|)) \quad (6)$$

This optimization criterion is especially important for the FEEP and colloid thrusters, because here the thrust is generated by very sharp needles or edges. An erosion of this surface leads to a considerably degradation of the engine. But also the gate electrodes and the ionization chamber of RIT engines are affected by erosion due to high thrust.

## References

- [1] M. Andrenucci, F. Ceccanti, and L. Serafini. FEEP micropropulsion system for the Microscope Mission. In *Workshop on Micro Propulsion for Spacecraft*, November 2004. Centre de Competence Technique Propulsion Toulouse.
- [2] D. Feili, W. Loeb, K.H. Schartner, St. Weis, D. Kirmse, Meyer B.K., R. Kilinger, and H. Mueller. Testing of new microN-RITs at Giessen. July 2005.
- [3] M. Gamero-Castano, V. Hruby, D. Spance, N. Demmons, R. McCormick, Gasdaska C., and P. Falkos. Micro Newton Colloid Thruster for St7-DRS Mission. In *39th AIAA/ASME/SAE/ASEE Joint Propulsion Conference and Exhibit*, July 2003. AIAA 2003-4543.
- [4] A. Genovese, M. Tajmar, N. Buldrini, M. Scheerer, E. Semerad, and W. Steiger. Indium FEEP Multiemitter Development and Test Results. In *40th AIAA/ASME/SAE/ASEE Joint Propulsion Conference and Exhibit*, July 2004. AIAA-2004-3620.
- [5] Barry Kent, John Stark, Bob Stevens, Matt Alexander, Adam Baker, Dave Gibbon, and Douglas Liddle. A MEMS Based Experimental Colloid Thruster Package for Nano satellites. In *18th AIAA/USU Conference on Small Satellites*, August 2004. AIAA SSC04-X1-3.
- [6] Günther Kornfeld, N. Koch, and G. Coustou. The highly efficient multistage plasma (HEMP) thruster, a new electric propulsion concept derived from tube technology. In *4th IEEE International Conference on Vacuum Electronics*, May 2003.
- [7] Hans J. Leiter, Rainer Killinger, Helmut Bassner, Johann Müller, Ralf Kukies, and Thomas Fröhlich. Evaluation of the Performance of the advanced 200mN Radio Frequency Ion Thruster RIT\_XT. In *38th AIAA/ASME/SAE/ASEE Joint Propulsion Conference and Exhibit*, July 2002. AIAA 2002-3836.
- [8] A. Nawaz, M. Auweter-Kurtz, H. Kurtz, and H. P. Wagner. Pulsed Plasma Thrusters for Primary Propulsion and Attitude Control of a Small All Electrical Satellite. In *ESA SP-555: 4th International Spacecraft Propulsion Conference*, October 2004.
- [9] Jeffrey G. Reichbach, Sedwick Raymond J., and Manuel Martinez-Sanchez. Micropropulsion System Selection for Precision Formation Flying Satellites. Master's thesis, Department of Aeronautics and Astronautics, Massachusetts Institute of Technology, January 2001.



- [10] John Stark, Barry Kent, Matt Alexander, Bob Stevens, Dave Gibbon, and Douglas Liddle. An Experimental Colloid Thruster Package for Nano Satellites. In *39th AIAA/ASME/SAE/ASEE Joint Propulsion Conference and Exhibit*, July 2004. AIAA-2004-3594.
- [11] John Stark, Barry Kent, Bob Stevens, Michael Sandford, Mathew Alexander, Kate Smith, and Mark Paine. Colloid Propulsion - A Re-Evaluation, With An Integrated Design. In *39th AIAA/ASME/SAE/ASEE Joint Propulsion Conference and Exhibit*, July 2003. AIAA 2003-4851.
- [12] M. Tajmar, A. Genovese, and W. Steiger. Indium Field Emission Electric Propulsion Microthruster Experimental Characterization. *Journal of Propulsion and Power* 2004, 20(2):219–227, 2004.
- [13] John K. Ziemer, Colleen M. Marrese-Reading, Mark Anderson, Gary Plett, and James Polk. Colloid Thruster Propellant Stability after Radiation Exposure. In *39th AIAA/ASME/SAE/ASEE Joint Propulsion Conference and Exhibit*, July 2003. AIAA 2003-4853.
- [14] John K. Ziemer and Stephen M. Merkowitz. Microthrust Propulsion for the LISA Mission. In *40th AIAA/ASME/SAE/ASEE Joint Propulsion Conference and Exhibit*, July 2004. AIAA 2004-3439.

	<p>Endbericht Algorithmen zur Triebwerksansteuerung Fkz: 50 JR 0484</p>	<p>Doc.No.: INT-TAS-RP-ZAR-001 Issue: 1.0 Page: 23 of 20</p>
---	---	--

## Anhang C

Technical Note zu den Ergebnissen des Arbeitspakets AP 1200

Title: **Mission Descriptions**

DRD No.: MPA-ASD-TN-1201

Prepared by: Bernd Schürenberg Date: 13/08/2007

\_\_\_\_\_  
\_\_\_\_\_  
\_\_\_\_\_

Checked by: \_\_\_\_\_

Approved by: Peter Gath \_\_\_\_\_

\_\_\_\_\_

DLR contract No. 50 JR 0484

Copying of this document, and giving it to others and the use or communication of the contents thereof, are forbidden without express authority. Offenders are liable to the payment of damages. All rights are reserved in the event of the grant of a patent or the registration of a utility model or design.

## Change Record

Issue	Date	Section	Description of Change	Release
N/A	15/12/05	N/A	Subsequent release of individual mission descriptions to ZARM until December 2005	
0.1	31/07/07	all	Assembly of all mission descriptions in on report; internal review	
1.0	13/08/07	all	First issue	1

Table of Contents

**1 INTRODUCTION.....4**

**2 DOCUMENTS.....5**

2.1 APPLICABLE DOCUMENTS .....5

2.2 REFERENCE DOCUMENTS .....5

**3 MISSION OVERVIEW.....6**

3.1 MISSION CLASSES.....6

3.2 MICRO-PROPULSION TECHNOLOGIES .....7

3.3 MICRO PROPULSION SYSTEMS SUITED FOR THE DIFFERENT MISSIONS.....8

**4 DETAILED DESCRIPTIONS OF VARIOUS MISSIONS .....10**

4.1 MICROSCOPE .....10

4.2 LISA PATHFINDER .....13

4.3 LISA .....18

4.4 FUNDAMENTAL PHYSICS EXPLORER (FPE; ODYSSEY) .....23

4.5 HYPER.....24

4.6 METEOSAT THIRD GENERATION.....28

4.7 GAIA .....34

4.8 XEUS .....43

4.9 GOCE.....60

4.10 LASER DOPPLER INTERFEROMETER (LDI) .....65

4.11 PRISMA .....71

4.12 PROBA 3.....75

4.13 DARWIN .....75

4.14 LUNAR MISSION BW 1.....87

**5 OTHER MISSIONS.....95**

5.1 DON QUIJOTE.....95

**6 CONCLUSIONS .....101**



## 1 INTRODUCTION

A number of new missions are emerging or are already under development, which depend on the availability of micro-propulsion.

Descriptions of these missions have been compiled and are given to some detail in chapter 3.

In chapter 2, the more generic aspects of these missions are outlined, such as:

- Mission classes
- Suitable micro-propulsion technologies

Potential reference missions for the purpose of this study are also addressed in chapter 2.

## 2 DOCUMENTS

### 2.1 Applicable Documents

AD	Doc. No.	Title
01		

### 2.2 Reference Documents

RD	Doc. No.	Title
01	HOPAS-TN-01	High Precision Attitude Control on Earth Observation Satellites (HOPAS), DLR contract No. 50 JR 0649  Part I: Design and analysis of HEMP thrusters based propulsion systems for geostationary satellites  27. November 2006

## 3 Mission Overview

### 3.1 Mission Classes

The following missions are described in detail in chapter 3, in order to permit a good understanding of the individual missions.

The following missions will employ Electric Propulsion or other propulsion technologies capable of very low thrust of less than 1 mN:

(a) drag-free missions

- Microscope
- LISA Pathfinder
- LISA
- Fundamental Physics Explorers (FPE)
- HYPER

(b) precision pointing missions

- Meteosat Third Generation (MTG)
- GAIA
- XEUS
- HYPER

(c) new gravity field mission

- GOCE
- Laser Doppler Interferometer (LDI)

(d) Formation Flying (FF) missions

- PRISMA
- Radar tandem mission
- PROBA-3
- DARWIN
- XEUS
- LDI

(e) Interplanetary missions (these missions operate in the mN range, and are only included, because they will provide valuable experience in electric propulsion)

- SMART-1
- BW-1 (university mission to the Moon)
- Don Quijote
- BepiColombo

(f) Precursor missions, test beds, technology missions:

- Microscope
- PRISMA

- LISA Pathfinder
- PROBA-3

It must be noted, that there are several overlaps of the different mission classes.

### 3.2 Micro-Propulsion Technologies

The available micro-propulsion technologies are far from being “established” technologies, with the exception of the Pulsed-Plasma Thrusters (PPT). The following candidates are emerging and in development:

#### (a) FEEP

- For the most demanding applications (optimal commandability, high resolution, very high Isp, and low thrust noise)
- Enabling technology, but still struggling with development problems
- Two alternatives still in competition: single-slit FEEP and arrays of needle emitter FEEPs
- Currently, limited to approx. 150  $\mu\text{N}$
- Wide ion beam; plume impingement must be avoided (sputtering or surface contamination)
- Cs as propellant is highly reactive and must be kept in a sealed tank and the slit emitter must be protected in a container with tight lid. No ground testing is possible, and thus risk of failure.
- Indium as propellant does not need such protective measures. Due to higher melting temperature, special effort for thermal control is necessary.
- 1<sup>st</sup> flight will be on MICROSCOPE in 2009.

#### (b) Colloid thrusters systems

- development in USA (BUSEK for LISA Pathfinder and LISA)
- development of micro-machined colloid thrusters arrays planned in UK
- considerably lower Isp, probably higher thrust noise
- thrust range lower
- physics of these thrusters well-understood from technology development for medical / analytical applications

#### (d) Cold-Gas micro-propulsion systems

- various developments are on-going at:
  - MAROTTA (UK)
  - Bradford (NL)
  - Moog (USA)
  - NanoSpace (Sweden)
- First applications
  - Gradiometer Calibration Device on-board GOCE
  - MEMS micro-propulsion system (silicone-bases) on-board PRISMA
- GAIA probably has to rely on cold-gas micro-propulsion, because FEEP technology is not yet mature enough.
- Performance aspects:
  - very low ISP compared to electric micro-propulsion
  - slower commandability of proportional thrusters
  - common propellant supply

- discretely built system or integrated MEMS solutions
- in MEMS solutions, propellant heating could increase ISP.

### (e) Pulse width modulated (PWM) Ion Engines

- suitable thrusters could be RIT 4
- PWM allows to operate down to micro-N level (1 – 10 kHz pulse frequency)
- This control concept requires further assessment w.r.t. experiment requirements.
- Good commandability / fine thrust adjustment achievable
- Thrust noise due to neutral Xenon flow

### (f) Micro-HEMPT

- Existing HEMP thrusters were shown to operate down to < 100  $\mu$ N. Scaled down engines conceivable.
- Some feasibility assessments were performed by the supplier.
- New development. Tests on micro-balance not available. Commandability to be investigated.
- At low thrust levels, there is no plasma-wall interaction.
- Promising engine at  $\mu$ N to mN thrust range.

### (g) Pulsed Plasma Thrusters (PPT)

- Existing hardware in USA and Russia.
- Pulse repetition rate up to 2 Hz.
- Poor man's solution used in nano- and micro-satellites. But also attractive for attitude control of medium-sized satellites!
- Contamination issues appear controllable / avoidable.
- No neutraliser needed, because electrons and ions are ejected.

The current situation can be summarised as follows:

- FEEPs are the best performers, but this technology is not yet mature, and thus a major risk factor.
- Cold-gas MPS are the current solution, but still associated with development needs.
- Micro-RITs with PWM are promising, but have not yet sufficiently studied within system performance simulations.
- PPTs are existing systems (USA, Russia) and can be used for some applications.
- Colloid thrusters are the backup for FEEPs, although inferior w.r.t. performance.

### 3.3 Micro propulsion Systems suited for the different missions

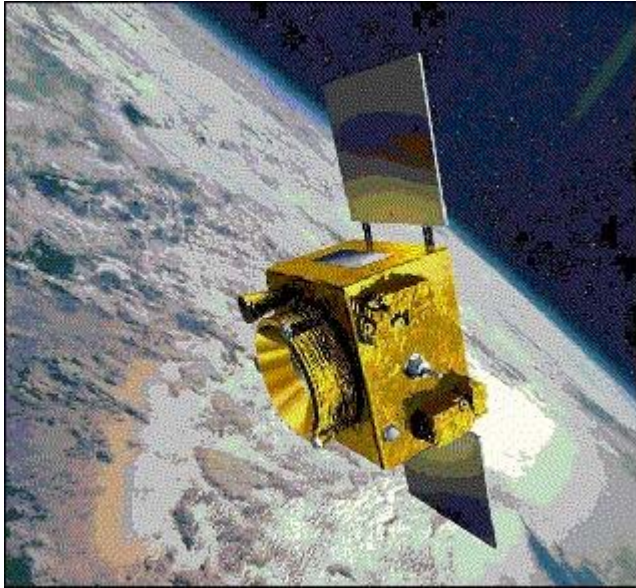
In the following table, the possible micro-propulsion technologies are identified for the different missions:

**Table 3.3-1:** *Potential technologies for the different missions*

	FEEP	Colloid	Cold-Gas	Micro-RIT	PPT
Microscope	X	x		1	1
LISA Pathfinder	X	X	X		
LISA	X	X			
FPE	X	X	X	X	X
HYPER	X				
Meteosat 3 <sup>rd</sup> Gen.				X	X
Gaia	X		X	X	
XEUS MSC			X		
XEUS DSC			X	X	
GOCE			x		
LDI			x	x	x
PRISMA			x		
Radarsat Tandem			x	x	x
PROBA-3	x			x	
DARWIM	x				
BW-1					x

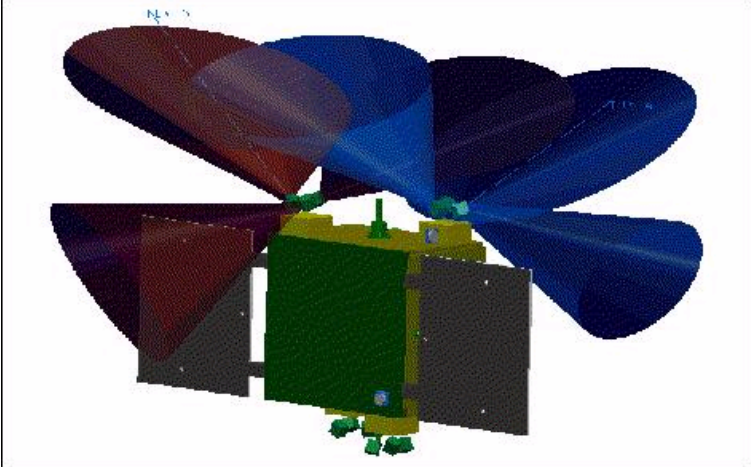
## 4 Detailed descriptions of various missions

### 4.1 Microscope

Mission type:	Micro-Satellite for fundamental physics (test of Equivalence Principle)
Mission class	Approved CNES / ESA / ONERA program (in 2004);  launch in March 2009
Launcher, Orbit	DNEPR launch, as secondary payload  Orbit: sun-synchronous dawn-dusk orbit (h = 730 km , i= 98°)
S/C configuration	Myriade series spacecraft bus  
Mission objectives	<ul style="list-style-type: none"> <li>• Test of Equivalence Principle (general theory of relativity)</li> <li>• DFACS technology demonstrator (precursor for LISA; GAIA, etc.)</li> <li>• Measurement of the thermosphere at h = 730 km</li> </ul>
Experiment:	Free fall of 2 quasi-cylindrical proof masses of different materials (Pt and Ti)

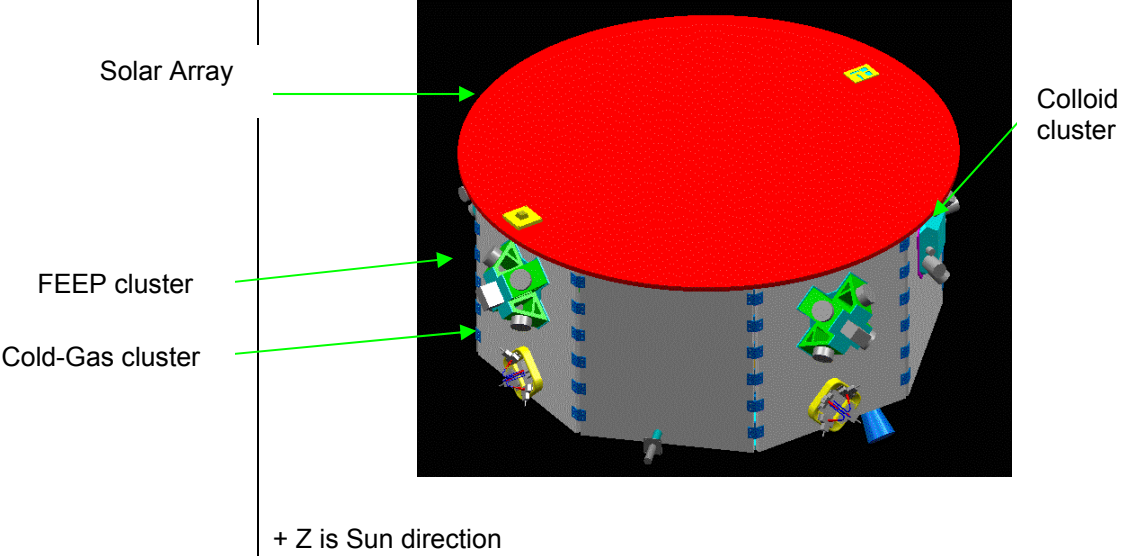
	<p>Masses are concentric, share the same CoG, and are designed for the same gravity-gradient effects</p> <p>By means of DFACS, the satellite isolates the experiment from disturbances (atmospheric drag, radiation pressure, magnetic torques).</p> <p>DFACS is 6-DOF actuator and measurement system of the S/C external disturbances</p>
<p>DFACS dynamic range and stability</p>	<p>Angular velocity: <math>1 \times 10E-06 \text{ rad/s}</math>, resp. <math>1 \times 10E-06 \text{ rad/s}/\sqrt{\text{Hz}}</math></p> <p>Angular acceler.: <math>2 \times 10E-06 \text{ rad/s}^2</math>, resp. <math>2 \times 10E-06 \text{ rad/s}^2/\sqrt{\text{Hz}}</math></p> <p>Linear acceleration: <math>3 \times 10E-08 \text{ m/s}^2</math>, resp. <math>1 \times 10E-10 \text{ m/s}^2/\sqrt{\text{Hz}}</math></p>
<p>On-board Propulsion</p>	<p>FEEP based Micro-Propulsion System:</p> <ul style="list-style-type: none"> <li>• 12 thrusters (4 pods with 3 thrusters, each)</li> <li>• thrust range: up to 150 microN, each</li> <li>• controllable in 1 microN steps</li> <li>• total mass (FEEP, electronics, propellant): 40 kg</li> <li>• power: <span style="float: right;">80 W (8 FEEP ON)</span> <span style="float: right;">120 W (12 FEEP ON)</span></li> <li>• part of experiment; provided by ESA</li> <li>• contractor for MPS: ALTA S.p.A./ Pisa / Italy</li> </ul>
<p>Thruster arrangement</p>	<p>4 pods with 3 FEEP thrusters, each</p> <p>on crossed diagonals</p> <p>large beam width, as shown below</p>

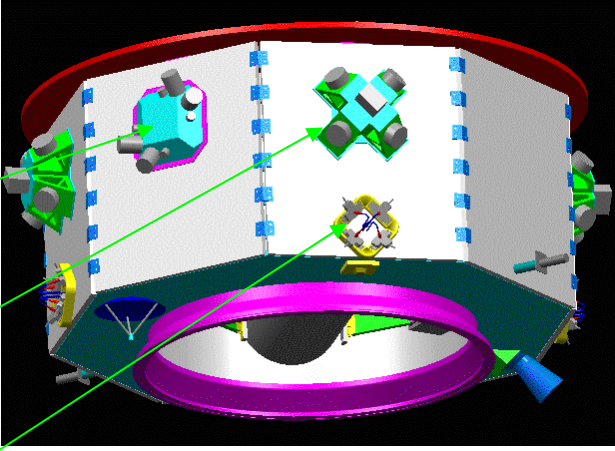


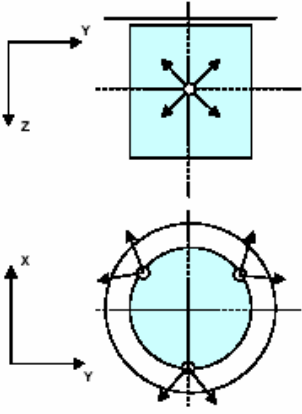
	
Mission duration	Nominally 1 year in orbit
S/C mass, power, and dimensions	<ul style="list-style-type: none"> <li>• mass: 200 kg</li> <li>• dimensions of S/C body: 1,300 x 900 x 900 mm</li> <li>• Total power: 200 W</li> </ul>
References	<p>[1] Microscope  <a href="http://directory.eoportal.org/pres_Microscope.html">http://directory.eoportal.org/pres_Microscope.html</a></p> <p>[2] P. Touboul, M. Rodrigues: The microscope Space Mission, Classical and Quantum Gravity 18 (2001) 2487 – 2498</p> <p>[3] Space Science News 3 (Dec. 2002)  <a href="http://www.rssd.esa.int/sys/TOP/docs/SSD3/Contents3.html">http://www.rssd.esa.int/sys/TOP/docs/SSD3/Contents3.html</a></p> <p>[4] The Microscope project begins          PR38-2004, dated June 25, 2004  <a href="http://www.cnes.fr/html/_455_465_2424_.php">http://www.cnes.fr/html/_455_465_2424_.php</a></p> <p>[5] Microscope Mission Support Request (dated Dec 14, 2005)  <a href="http://ilrs.gsfc.nasa.gov/satellite-missions/list-of-satellites/microscope/">http://ilrs.gsfc.nasa.gov/satellite-missions/list-of-satellites/microscope/</a></p>

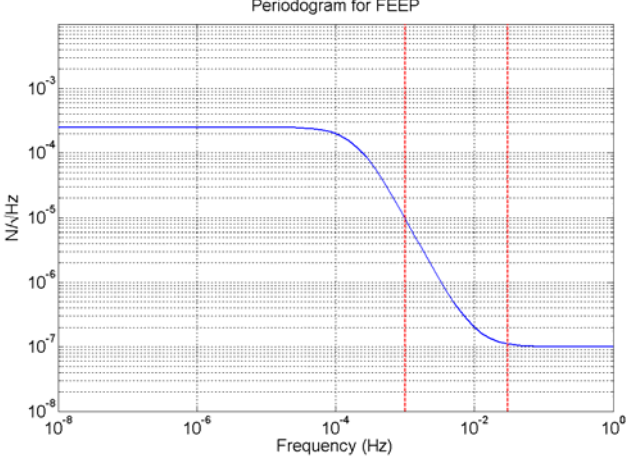
### 4.2 LISA Pathfinder

Mission type:	Fundamental Physics
Mission class	Technology Demonstration Mission for LISA and also for other micro-propulsion missions; currently in Phase B
Launcher, Orbit	<ul style="list-style-type: none"> <li>• launch in 2009</li> <li>• separable Bi-Propellant Transfer Stage ("Propulsion module") to reach L1, stable solar illumination, no eclipses</li> </ul>
Payload and mission objective	<p>Satellite carries:</p> <ul style="list-style-type: none"> <li>• LISA Technology Package (LTP), consisting of: <ul style="list-style-type: none"> <li>- 2 electrostatically suspended proof masses</li> <li>- laser interferometers</li> </ul> </li> <li>• DRS - equivalent package by NASA-JPL</li> <li>• FEED Micro-Propulsion System, associated with LTP</li> <li>• Cold-Gas Micro-Propulsion System, associated with LTP</li> <li>• Colloid Micro-Propulsion System, , associated with DRS</li> </ul> <p>Demonstration mission for LTP and for the Disturbance Reduction System (DRS) of JPL, but also for other missions using:</p> <ul style="list-style-type: none"> <li>• in-orbit performance verification of micro-propulsion systems (FEED, colloid, cold gas)</li> <li>• DFACS (drag-free and attitude control system)</li> </ul> <p>Top science requirement: DFACS shall reduce disturbances, in order to achieve LTP measurement accuracies of <math>3 \times 10^{-14} \text{ m/s}^2 / \sqrt{\text{Hz}}</math> in the Measurement Bandwidth (MBW) of 1 mHz - 30 mHz in the science</p>

	measurement / sensitive axis.								
Mission duration	12 months (3 months cruise + commissioning; 3 months for LTP; 3 months joint LTP + DRS; 3 months DRS)								
S/C configuration:	 <p>+ Z is Sun direction</p>								
S/C dimensions and mass	<table> <tr> <td>Solar Array diameter:</td> <td>~ 1,600 mm</td> </tr> <tr> <td>S/C overall height:</td> <td>~ 950 mm</td> </tr> <tr> <td>Box shape:</td> <td>octagonal</td> </tr> <tr> <td>Mass after separation:</td> <td>450 - 500 kg</td> </tr> </table>	Solar Array diameter:	~ 1,600 mm	S/C overall height:	~ 950 mm	Box shape:	octagonal	Mass after separation:	450 - 500 kg
Solar Array diameter:	~ 1,600 mm								
S/C overall height:	~ 950 mm								
Box shape:	octagonal								
Mass after separation:	450 - 500 kg								
Conditions for DFACS initialisation	<ul style="list-style-type: none"> <li>accuracy of inertial attitude: &lt; 15 arcmin, each axis</li> <li>residual rates: &lt; <math>1 \times 10^{-6}</math> rad/s, each axis</li> <li>residual accelerations: &lt; <math>1 \times 10^{-7}</math> m/s<sup>2</sup>, each axis</li> </ul>								
On-board Propulsion	<p>(a) FEEP Micro-Propulsion System with 3 clusters of 4 thrusters, each.</p> <p>(b) Cold Gas Micro-Propulsion System with 3 x 4 micro-thrusters arranged similar to the FEEP System. Back-up for</p>								

	<p>FEEP MPS.</p> <p>(c) JPL supplied Colloid Micro-Propulsion System (part of DRS) with 2 x 4 colloid thrusters</p> <p>The Micro-Propulsion Systems are used for:</p> <ul style="list-style-type: none"> <li>• attitude acquisition after separation from transfer stage</li> <li>• Orbit maintenance once every 3 months</li> <li>• Science Mode (6 DOF drag-free control, with 1 sensitive axis)</li> <li>• Acquisition and Safe Mode</li> </ul>
<p>Micro-Propulsion thruster arrangements</p> <p>2 Colloid clusters at 180°</p> <p>3 FEEP clusters at 120°</p> <p>3 Cold-Gas clusters at 120°</p>	

<p>FEEP thruster arrangement</p>	
<p>FEEP performance requirements</p>	<ul style="list-style-type: none"> <li>• total impulse per thruster: <span style="float: right;">~ 2,500 Ns</span></li> <li>(propellant reservoir sized for <span style="float: right;">4,000 Ns</span>)</li> <li>• overall 4.4 kg of liquid metal propellant <span style="float: right;">(Isp &gt; 4,000 s)</span></li> <li>• max thrust: <span style="float: right;">30 μN (nominal), resp. 100 μN (failure cases)</span></li> <li>• min thrust: <span style="float: right;">1.0 μN (required)</span></li> <li>• rate of change: <span style="float: right;">≤ 30 μN/s (tbc)</span></li> <li>• command update rate: <span style="float: right;">10 Hz</span></li> <li>• (absolute) thrust stabilisation loop at <span style="float: right;">approx. 100 Hz</span></li> <li>• thrust response: <span style="float: right;">&lt; 100 ms for 95 % of commanded step</span></li> <li>• bias + linearity error: <span style="float: right;">0.5 μN +/- (1-5%)</span></li> <li>• repeatability of thrust profile: <span style="float: right;">0.5 μN +/- 0.5 % (TBC)</span></li> <li>• thrust vector alignment error <span style="float: right;">&lt; 5 ° half-cone</span></li> <li>• thrust vector stability: <span style="float: right;">0.5 ° half-cone over life</span></li> </ul>

<p>Thruster noise</p>	<div style="text-align: center;">  <p>Periodogram for FEEP</p> </div> <p>measurement bandwidth: 1 mHz - 30 mHz</p>
<p>FEEP MPS mass</p>	<ul style="list-style-type: none"> <li>• 3 x FEEP PCU &lt; 4.0 kg, each</li> <li>• 3 x FEEP cluster &lt; 4.5 kg, each</li> </ul>
<p>FEEP MPS failure tolerance</p>	<p>only single-failure tolerance required</p>
<p>Cold-Gas Micro-Propulsion System</p>	<p>Performance requirements equivalent to FEEP MPS</p> <p>Higher maximum thrust: up to 1,000 <math>\mu</math>N (non-DFACS)</p>
<p>Magnetic cleanliness</p>	<p>Proof masses sensitive to AC and DC magnetic:</p> <ul style="list-style-type: none"> <li>• FEEP PCU &lt; 0.5 A m<sup>2</sup>, each</li> <li>• FEEP cluster &lt; 0.1 A m<sup>2</sup>, each</li> </ul>
<p>Chemical cleanliness (FEEP)</p>	<ul style="list-style-type: none"> <li>• Cs FEEPs are extremely sensitive to O<sub>2</sub>, H<sub>2</sub>O, etc.</li> <li>• effect of liquid metal on surfaces and optical apertures</li> <li>• large beam divergence of FEEP thrusters</li> </ul>
<p><u>References:</u></p>	<p>RD-1: Requirements Specification FEEP Micro-Propulsion</p>

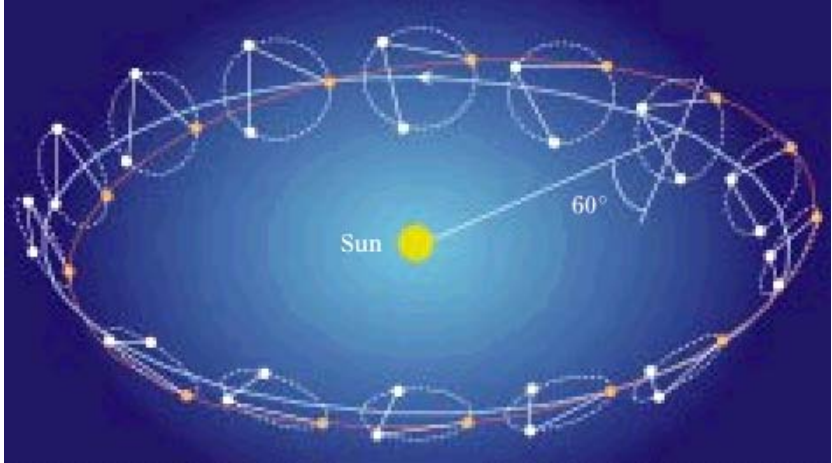
	<p>System, S2.ASU.RS.2002, issue 2, September 2004</p> <p>RD-2: Requirements Specification Cold Gas Micro-Thrusters, S2.ASU.RS.2003, issue 2, September 2004</p> <p>RD-3: System Definition Synthesis Report, S2.ASU.RP.2003, issue 3, March 2005</p>
--	---

### Abbreviations:

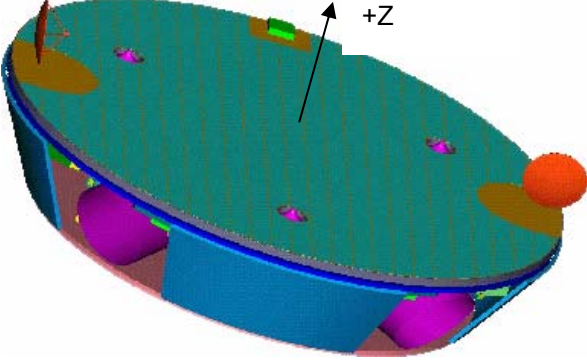
DFACS	Drag-Free and Attitude Control System
DOF	Degree of Freedom
DRS	Drag Reduction System
FEEP	Field Emission Electric Propulsion
FPCA	FEEP Cluster Assembly
IRS	Inertial Reference Sensor (synonym: GRS - Gravity Reference System)
LTP	LISA Technology Package
MBW	Measurement Bandwidth
MPA	Micro-Propulsion Assembly (1 TCA + dedicated PCU)
MPS	Micro-Propulsion System (all MPA's + flight diagnostic package)
PCU	Power Control Unit (for the FEEP thrusters)
PM	Proof Mass
TCA	(FEEP) Thruster Cluster Assembly

### 4.3 LISA

Mission type:	Science (Astrophysics)
Mission class	<p>NASA-JPL + ESA (cornerstone) mission</p> <p>Phase A+ (Mission Formulation Phase) starting in Jan 2005, duration 2 years</p> <p>Followed by Mission Definition Phase (duration 2 years)</p> <p>Then Phase B / C / D.</p>
Launcher, Orbit	<ul style="list-style-type: none"> <li>• 3 satellites launched in 2013 / 2014 with one Delta-4</li> <li>• Bi-prop Transfer Stage to reach heliocentric orbit</li> </ul>

	<p>(Earth trailing, 20 deg from Earth, 50,000,000 km distance to Earth)</p> <ul style="list-style-type: none"> <li>rotating triangle 60° inclined to ecliptic;</li> </ul> <p>each leg 5,000,000 km</p> 
<p>Payload and mission objective</p>	<p>Satellites consist of:</p> <ul style="list-style-type: none"> <li>Science Craft (SC)</li> <li>Propulsion Module (with Bi-propellant System; Propulsion Module will be separated from Sciencecraft after orbit acquisition)</li> </ul> <p>Each Sciencecraft (satellite) carries:</p> <ul style="list-style-type: none"> <li>2 Laser interferometers (2 legs, baseline 5 Mio km, each)</li> <li>2 freely floating proof masses per SC, acting as Inertial Reference Systems (IRS) and as reference mirrors for the interferometer</li> <li>laser interferometers measure distance between the 2 Proof Masses of 2 adjacent S/C, each Proof Mass acting as reference mirror</li> <li>2 Telescopes with Pointing Acquisition and Tracking Systems</li> </ul>



	<p>(PAT)</p> <ul style="list-style-type: none"> <li>• Micro-Propulsion System (e.g. FEEP or colloid engines)</li> <li>• DFACS and PAT Control Electronics</li> </ul> <p>Mission objectives:</p> <ul style="list-style-type: none"> <li>• detection of Gravity Waves in the measurement bandwidth (MBW) of <math>10^{-4}</math> Hz - <math>10^{-1}</math> Hz by monitoring baseline distance changes with an accuracy of 40 picometers/<math>\sqrt{\text{Hz}}</math>.</li> <li>• 2 sensitive axes per SC</li> </ul>
<p>Mission duration</p>	<p>1.5 years for transfer + commissioning</p> <p>5 years for science (+ 5 years extended science)</p>
<p>Science Craft (SC) configuration:</p>	 <p>+ Z is Sun direction</p>
<p>SC dimensions and mass: (TBC)</p>	<p>Solar Array / SC diameter: 2,700 mm</p> <p>SC height: will increase to TBD mm</p> <p>Mass: ~ 400 - 500 kg (Science Craft) + ~ 250 kg (Propulsion Module)</p>
<p>Operational envelope for Laser interferometry:</p>	<p>to be provided by:</p> <p>(a) 6 DOF DFACS to isolate Proof Masses from external</p>

	<p>disturbances and control induced disturbances;</p> <ul style="list-style-type: none"> <li>- removes accelerations and rotations to better than <math>3 \times 10^{-15} \text{ m/s}^2 / \sqrt{\text{Hz}}</math> in the 2 sensitive axes</li> <li>- position jitter of Proof Mass in 1 sensitive axis of each Proof Mass: <math>2.5 \text{ nanometer} / \sqrt{\text{Hz}}</math> relative to Proof Mass housing.</li> </ul> <p>(b) PAT (laser pointing acquisition and tracking system)</p> <p>Pointing jitter: <span style="float: right;"><math>8 \text{ nrad} / \sqrt{\text{Hz}}</math></span></p>
<p>On-board Propulsion (Science Craft):</p>	<p>Micro-Propulsion System with 3 clusters of 4 thrusters, each SC (TBC) + reserve set (TBD).</p> <p>Micro-Propulsion is used for:</p> <ul style="list-style-type: none"> <li>• Formation acquisition at BOL</li> <li>• Science Mode (DFACS)</li> <li>• Acquisition and Safe Mode</li> </ul>
<p>Micro-Propulsion thruster arrangement:</p>	<p>Thrusters must be arranged on the circumference of the Science Craft. Preliminary definition of the thruster needs and arrangement is expected in May 2005;</p> <p>Assumptions:</p> <ul style="list-style-type: none"> <li>• 1-failure tolerant</li> <li>• life-time requirement will probably require a second set of micro-thrusters (total ON-time: 90,000 h)</li> <li>• severe constraints on thruster positions must be observed / resolved: <ul style="list-style-type: none"> <li>- no contamination of Telescopes + parallel STRs, and of</li> </ul> </li> </ul>

	<p>Solar Array</p> <ul style="list-style-type: none"> <li>- thermal input (modulation due to sun - no sun on thruster clusters to be avoided)</li> <li>• 1st torque and force profiles by simulation in mid-2005, in order to confirm thrust level requirements</li> <li>• freeze of LISA thruster configuration expected in 3 - 4 years</li> </ul>
Micro-Propulsion performance requirements	<p>LISA must employ "existing technology", which must have been demonstrated on LISA Pathfinder.</p> <ul style="list-style-type: none"> <li>• total impulse per thruster (over 10 years): ~ 4,500 Ns</li> <li>• Specific impulse: high</li> <li>• max thrust: &lt; 100 <math>\mu</math>N (30 <math>\mu</math>N probably sufficient)</li> <li>• min thrust: 0.3 <math>\mu</math>N (required), 0.1 <math>\mu</math>N (target)</li> <li>• command update rate: 10 Hz</li> <li>• resolution: 0.1 <math>\mu</math>N</li> <li>• rate of change: <math>\leq</math> 10 <math>\mu</math>N/step</li> <li>• thrust response: &lt; 100 ms for 95 % of commanded step</li> </ul>
Thruster noise:	<p>See LISA Pathfinder;</p> <p>drives controller bandwidth, respectively command update rate</p>
Thruster redundancy concept:	<p>to be commensurate with up to 10 years of in-orbit operation!</p>
Magnetic cleanliness	<ul style="list-style-type: none"> <li>• DC, each Micro-Prop PCU &lt; 10 <math>\mu</math>Tesla at Proof Mass</li> <li>• DC, each thruster cluster &lt; 10 <math>\mu</math>Tesla at Proof Mass</li> <li>• AC, total &lt; 650 nTesla <math>\sqrt{\text{Hz}}</math> at Proof Mass</li> </ul>
Chemical cleanliness	<ul style="list-style-type: none"> <li>• effect of liquid metal (if FEEP) on surfaces and optical apertures</li> </ul>

	<p>severely constrains the possible thruster positions on the SCs.</p> <ul style="list-style-type: none"> <li>• large beam divergence of some <math>\mu\text{N}</math>-thrusters to be taken into account</li> </ul>
--	--

### Abbreviations:

DFACS	Drag-Free and Attitude Control System
DOF	Degree of Freedom
FEEP	Field Emission Electric Propulsion
IRS	Inertial Reference Sensor (synonym: GRS - Gravity Reference System)
MBW	Measurement Bandwidth
PAT	Pointing Acquisition and Tracking System
PCU	Power Control Unit (for the micro-prop thrusters)
PM	Proof Mass
SC	Science Craft
STR	Star Tracker

### References:

RD-1:	LISA Mission Requirements Document, issue 1, dated 18-08-2004
RD-2:	LISA Final Technical Report, LI-RP-DS-009, April 2000
RD-3:	LISA System and Technology Study Report, ESA-SCI (2000) 11, July 2000

## 4.4 Fundamental Physics Explorer (FPE; Odyssey)

Mission type:	Small Fundamental Physics missions in LEO and GTO
Mission class	<p>Explorer mission for ESA Cosmic Vision 2020-2025</p> <ul style="list-style-type: none"> <li>• mission proposals in spring 2006</li> <li>• industrial studies expected to start at end 2006</li> </ul>
Mission and mission objectives	<ul style="list-style-type: none"> <li>• 3 standardised small satellites launched into LEO or GTO</li> <li>• each platform provides drag-free environment</li> <li>• Typical experiments are: <ul style="list-style-type: none"> <li>- atomic interferometry</li> <li>- precision atomic clock</li> <li>- experiments on general relativity (velocity of light in different gravity)</li> </ul> </li> </ul>

Satellite mass	<ul style="list-style-type: none"> <li>approx. 450 kg, total (incl. payload instruments)</li> </ul>
Mission duration	<ul style="list-style-type: none"> <li>short (TBD months)</li> </ul>
Propulsion system(s)	<ul style="list-style-type: none"> <li>yet TBD</li> <li>short mission time permits usage of cold-gas micro-propulsion</li> </ul>
Micro-Propulsion thruster arrangement:	<ul style="list-style-type: none"> <li>yet TBD</li> </ul>
Micro-Propulsion performance requirements	<ul style="list-style-type: none"> <li>"existing technology" to be employed</li> <li>performance yet TBD</li> </ul>
Heritage	<ul style="list-style-type: none"> <li>Microscope</li> <li>HYPER</li> <li>LISA Pathfinder</li> <li>GOCE</li> </ul>

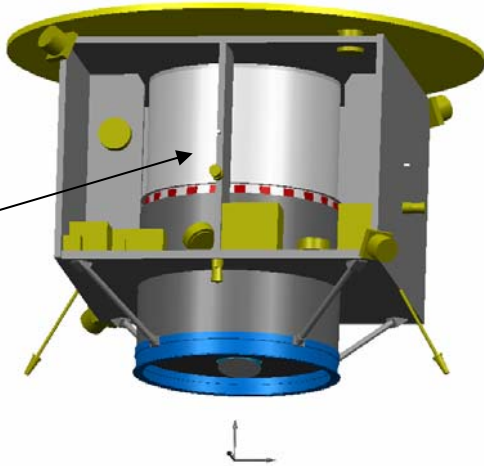
Abbreviations:

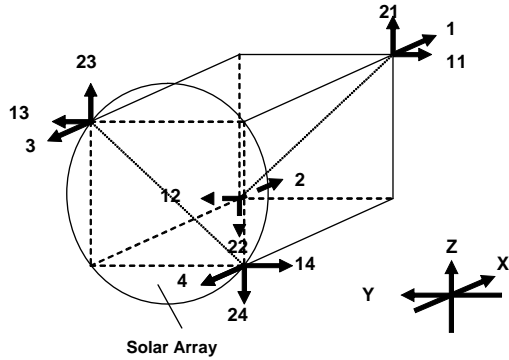
DFACS  
FEED  
GTO  
LEO

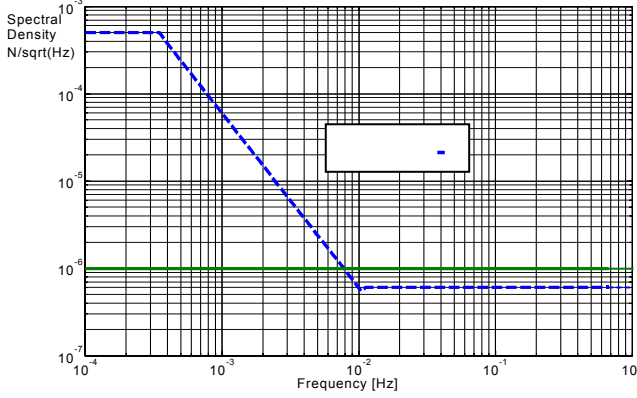
Drag-Free and Attitude Control System  
Field Emission Electric Propulsion  
Geostationary Transfer Orbit  
Low Earth Orbit

### 4.5 HYPER

Mission type:	Fundamental Physics
Mission class	Flexi mission; recommended by FPAG as Technology Reference Mission in 10 - 20 years
Launcher, Orbit	<ul style="list-style-type: none"> <li>Rokot</li> <li>sun-synchronous dawn-dusk orbit at ~ 1,000 km altitude</li> </ul>
Payload and mission	Satellite carries Optical Bench equipped with:

<p>objective</p>	<ul style="list-style-type: none"> <li>• 2 cold atom interferometers (Atomic Sagnac Units ASU) acting as hyper-sensitive gyros and accelerometers (resolution: <math>2.4 \times 10^{-12}</math> <math>\mu\text{rad} / \text{s}</math>, resp. <math>4.8 \times 10^{-13}</math> <math>\text{m/s}^2</math>)</li> <li>• 1 Precision Star Telescope for fine pointing in - X direction (resolution: <math>2 \times 10^{-2}</math> arcsec; FOV: 25 arcsec)</li> <li>• 2 Drag-free Sensors (Proof Masses)</li> <li>• 2 Star Trackers</li> </ul> <p>Scientific measurements and observations comprise an outstanding discovery potential:</p> <ul style="list-style-type: none"> <li>• macroscopic Bose-Einstein Condensates up to meter size</li> <li>• entanglement of Bose-Einstein Condensates</li> <li>• quantum de-coherence due to zero energy and fundamental interactions</li> <li>• quantum sensors for gravity accelerations and rotations (Lense-Thirring effect; quantum test of Equivalence Principle), etc.</li> </ul>
<p>Mission duration</p>	<p>2 years in Inertial Pointing Mode (IPM) / Science Mode</p>
<p>S/C configuration:</p> <p>Solar Array</p> <p>Payload cylinder</p>	 <p>The diagram shows a 3D cutaway view of the satellite. At the top is a large yellow solar array. Below it is a central payload cylinder containing various instruments. The satellite has a cylindrical body with a blue base and four legs extending downwards. A coordinate system is shown at the bottom center.</p>

	+ X in anti-Sun direction
S/C dimensions and mass	<p>Solar Array diameter: 2,200 mm (~ 710 Watt)</p> <p>S/C overall height: 1,620 mm</p> <p>Cross-section box: 1,600 x 1,600 mm</p> <p>Mass after separation: ~ 1,060 kg</p>
On-board Propulsion	<p>(a) Cold Gas RCS (8 x 40 mN thrusters, only 3.2 kg GN2) for initial rate damping and attitude acquisition, and later-on for emergency operations (TBC)</p> <p>(b) FEEP Micro-Propulsion System, used for</p> <ul style="list-style-type: none"> <li>• orbit insertion correction, if needed</li> <li>• slews to next Guide Star (once per month, &lt; 2 days per slew)</li> <li>• Inertial Pointing Mode</li> <li>• 6 DOF drag-free &amp; fine pointing control (Science Mode)</li> <li>• de-orbiting (TBC; duration &gt; 3 years of continuous firing at max thrust)</li> </ul>
FEEP thruster arrangement:  (total of 16 FEEP thrusters; different clustering is possible)	 <p>The diagram illustrates the arrangement of 16 FEEP thrusters on a spacecraft. A central cube is shown with a sphere inside, labeled 'Solar Array'. Thrusters are numbered 1 through 14, with arrows indicating their orientation. A coordinate system with X, Y, and Z axes is also shown.</p>

	<p>plus 4 x 1 FEFP for redundancy (at skewed angle; not shown)</p>
<p>Task of Drag-Free Control</p>	<p>Maintain ASUs within their operational envelope:</p> <ul style="list-style-type: none"> <li>• residual rotation over 3 sec: <math>&lt; 4.3 \times 10^{-8}</math> rad/sec about Y and Z</li> <li>• residual rotation over 3 sec: <math>&lt; 1 \times 10^{-6}</math> rad/sec about X</li> <li>• residual acceleration over 3 sec: <math>&lt; 1.2 \times 10^{-8}</math> m/s<sup>2</sup> about Y</li> </ul>
<p>FEFP performance requirements</p>	<ul style="list-style-type: none"> <li>• total impulse per thrust direction ~ 20,000 Ns (with reserve)</li> <li>• overall 4.4 kg of liquid metal propellant (Isp ~ 7,000 s)</li> <li>• max thrust: 100 <math>\mu</math>N (nominal), resp. 150 <math>\mu</math>N (peak)</li> <li>• min thrust: 0.5 <math>\mu</math>N (requirement TBC)</li> <li>• rate of change: <math>\leq 10</math> <math>\mu</math>N/s; command update rate: 10 Hz</li> <li>• thrust response: <math>&lt; 100</math> ms for 95 % of commanded step</li> <li>• resolution of commanded thrust <math>&lt; 0.1</math> <math>\mu</math>N (requirement TBC)</li> <li>• thrust vector stability over thrust range: <math>0.5^\circ</math> (<math>3\sigma</math>), and <math>0.5^\circ</math> (<math>3\sigma</math>) over life</li> </ul>
<p>Thruster noise</p>	



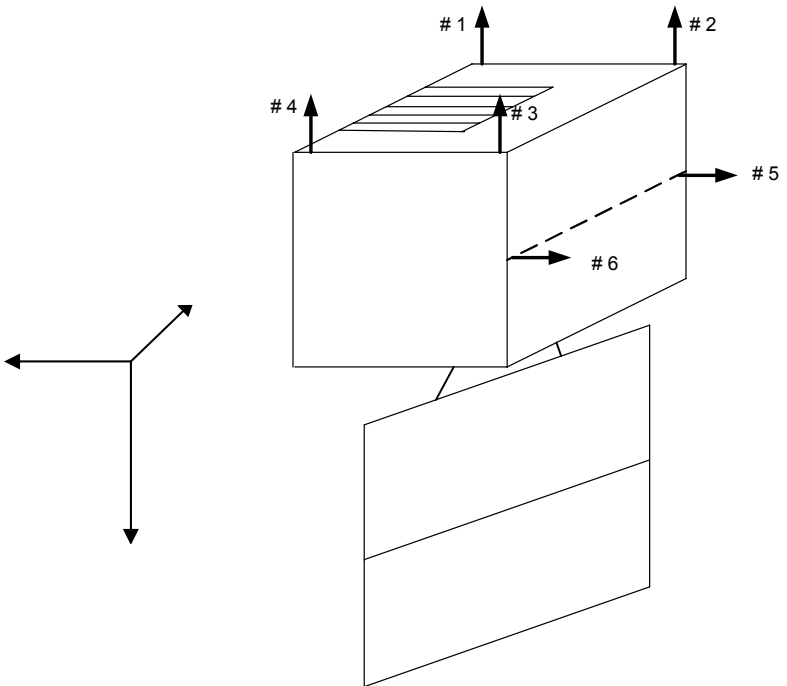
Thrust range	<p>Determined by:</p> <ul style="list-style-type: none"> <li>air drag</li> <li>gravity gradient (radial and transverse effect)</li> <li>solar pressure</li> <li>interaction of S/C magnetic moment with Earth B-field</li> </ul> <p>(assumed total magnetic moment of <math>\leq 1 \text{ A m}^2</math> is a driver for the S/C)</p>
Magnetic cleanliness requirements	<ul style="list-style-type: none"> <li>ASU very sensitive to B-fields, therefore with 2 <math>\mu</math>-metal shields</li> <li>DC field outside <math>\mu</math>-metal shield: <math>&lt; 0.1 \text{ Gauss}</math></li> <li>AC field at 0.3 Hz and at double orbit frequency <math>&lt; 100 \mu\text{Gauss}</math></li> </ul>
Chemical cleanliness	Liquid metal (Cs or In) deposition on surfaces and reactions with surface materials -- to be investigated in next study phase
References:	Hyper Industrial Feasibility Study (2003)

### 4.6 Meteosat Third Generation

Mission type:	Meteorological Satellite on Geostationary Orbit
Mission class	<p>commercial mission;</p> <p>first European imaging mission from GEO</p> <p>Currently in Pre-Phase A</p>
Launcher, Orbit	<ul style="list-style-type: none"> <li>launch in 2015</li> <li>geostationary orbit</li> </ul>
Payload and mission objective	Dominant payload is the large Imager Instrument (2-axis scanning instrument)



On-board Propulsion	<p>(a) Bipropellant Chemical Propulsion System (CPS) for:</p> <ul style="list-style-type: none"> <li>• orbit transfer from GTO</li> <li>• station acquisition and re-locations</li> <li>• orbit maintenance (NSSK and EWSK), if not by EPS</li> <li>• Reaction Wheel off-loading, if not by EPS</li> </ul> <p>(b) Electric Propulsion System (EPS), <b>if selected</b>, either for:</p> <ul style="list-style-type: none"> <li>• momentum management or</li> <li>• NSSK and momentum management</li> </ul>
Momentum management with EPS	<p>(a) Configuration Single-Wing Solar Array</p> <ul style="list-style-type: none"> <li>• without disturbance torque compensation, the following angular momentum will build-up within 24 h: <ul style="list-style-type: none"> <li>- about roll / yaw <span style="float: right;">~ 22.0 Nms</span></li> <li>- about pitch <span style="float: right;">~ 1.4 Nms</span></li> </ul> </li> <li>• disturbance torques due to solar radiation pressure (SRP): <ul style="list-style-type: none"> <li>- about roll / yaw <span style="float: right;">0.2 mN m</span></li> <li>- about pitch <span style="float: right;">0.02 mN m</span></li> </ul> </li> </ul> <p>Instead of Reaction Wheel off-loading, continuous disturbance torque compensation is possible with micro-engines. This allows to maintain the stored angular momentum in the RWs within narrow bounds.</p> <p>(a) Configuration Body-Mounted Solar Array</p> <ul style="list-style-type: none"> <li>• without disturbance torque compensation, the following angular momentum will build-up within 24 h: <ul style="list-style-type: none"> <li>- about roll / yaw <span style="float: right;">&lt; 2.0 Nms</span></li> </ul> </li> </ul>

	<p>- about pitch <span style="float: right;">&lt; 1.0 Nms</span></p> <ul style="list-style-type: none"> <li>disturbance torques due to solar radiation pressure (SRP):</li> </ul> <p>- about roll / yaw <span style="float: right;">0.02 mN m</span></p> <p>- about pitch <span style="float: right;">0.01 mN m</span></p> <p>At these very low disturbance levels, micro-engines can be operated over suitable intervals, rather continuously.</p> <p><u>Note:</u> In the following, only the Single-Wing configuration is used as reference.</p>
<p>Possible arrangement of the micro-engines</p>	 <p>EPS thrusters # 1 to # 4: for NSSK and / or roll / yaw momentum management</p> <p>EPS thrusters # 5 and # 6: for pitch momentum management</p> <p>Note: Redundancies are not shown.</p>

<p>Micro-engine usage:</p>	<p>(a) momentum management only:</p> <ul style="list-style-type: none"> <li>• roll /yaw; continuous operation of #1 to #4 in a commutating manner</li> <li>• pitch: engines # 5 or # 6 over suitable intervals</li> </ul> <p>(b) NSSK + momentum management</p> <ul style="list-style-type: none"> <li>• engines #1 - #4 continuously ON over approx. 8 h per orbit for NSSK; forces for roll / yaw wheel off-loading superimposed</li> <li>• engines #5 or # 6, as above</li> </ul>
<p>Micro-engine performance requirements</p>	<ul style="list-style-type: none"> <li>• thrust arms <span style="float: right;">approx. 1.0 m, each</span></li> <li>• thrust level (MM, only) <span style="float: right;">200 <math>\mu</math>N, each</span></li> <li>• thrust level (NSSK + MM) <span style="float: right;">2,000 <math>\mu</math>N, each</span></li> <li>• total impulse for MM, only <span style="float: right;">18,200 Ns, each</span></li> <li>• total impulse for NSSK + MM <span style="float: right;">196,000 Ns, each</span></li> <li>• number of micro-engine ON / OFF cycles <span style="float: right;">~ 4,500, each</span></li> <li>• benign commandability requirements</li> </ul>
<p>EPS propellant demand</p>	<ul style="list-style-type: none"> <li>• Momentum Management, only <span style="float: right;">3.6 kg</span></li> <li>• NSSK + Momentum Management <span style="float: right;">45 - 50 kg</span></li> </ul> <p><u>Note:</u> Isp = 2,000 s assumed.</p> <p><u>Note:</u> To be added: neutral gas loss, leakage, neutraliser gas flow, required margins</p>
<p>Suitable micro-engine technologies</p>	<ul style="list-style-type: none"> <li>• <b>FEEP:</b></li> <li>- edge-of-technology performance not needed for this crude application</li> </ul>

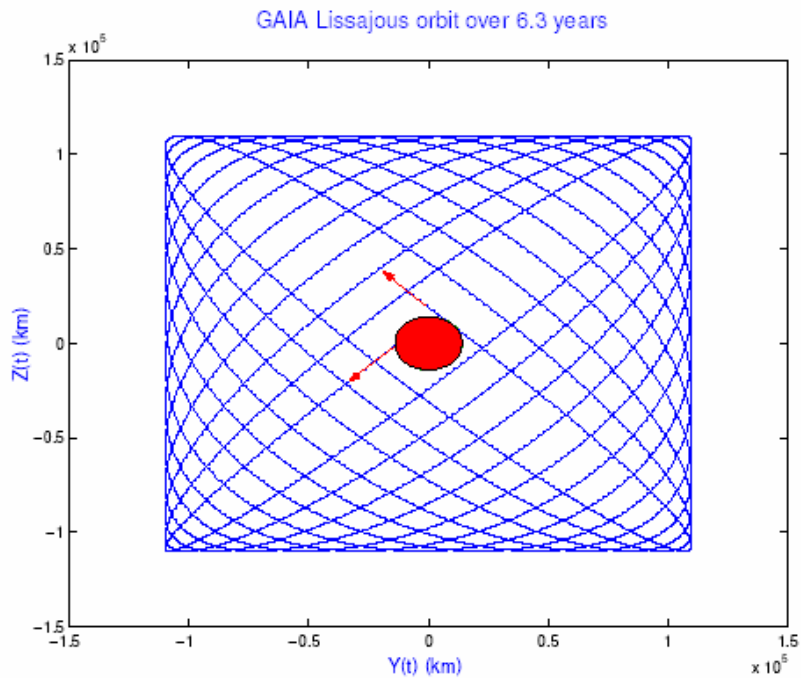
	<ul style="list-style-type: none"> <li>- limited-life item</li> <li>- liquid metal back-scatter can contaminate optical and other surfaces</li> <li>• <b>Micro-RIT:</b> <ul style="list-style-type: none"> <li>- promising lab demonstration / first performance tests</li> <li>- limited life item, but OK for momentum management, only</li> <li>- NSSK total impulse requirements possibly too demanding</li> </ul> </li> <li>• <b>Mini-HEMPT:</b> <ul style="list-style-type: none"> <li>- promising lab demonstration / first performance tests</li> <li>- long-life by design principle.</li> <li>- NSSK total impulse requirements can be met (TBC)</li> </ul> </li> </ul>
Micro-EPS failure tolerance	only single-failure tolerance needed
<u>References:</u>	RD-1: Pre-Phase A Study, 2005 (still on-going)

### Abbreviations:

AOCS	Attitude and Orbit Control System
CPS	Chemical Propulsion System
EPS	Electric Propulsion System
EWSK	East West Station Keeping
FEEP	Field Emission Electric Propulsion
GEO	Geostationary orbit
GTO	Geostationary Transfer Orbit
HEMPT	High-Efficiency Multi-Stage Plasma Thruster
MM	Momentum Management
MTG	Meteosat Third Generation
NSSK	North-South Station Keeping
PCU	Power Control Unit
RFG	RF Generator (for RIT)
RIT	RF Ion Thruster
RW	Reaction Wheel
S/C	Spacecraft
SRP	Solar Radiation Pressure

## 4.7 GAIA

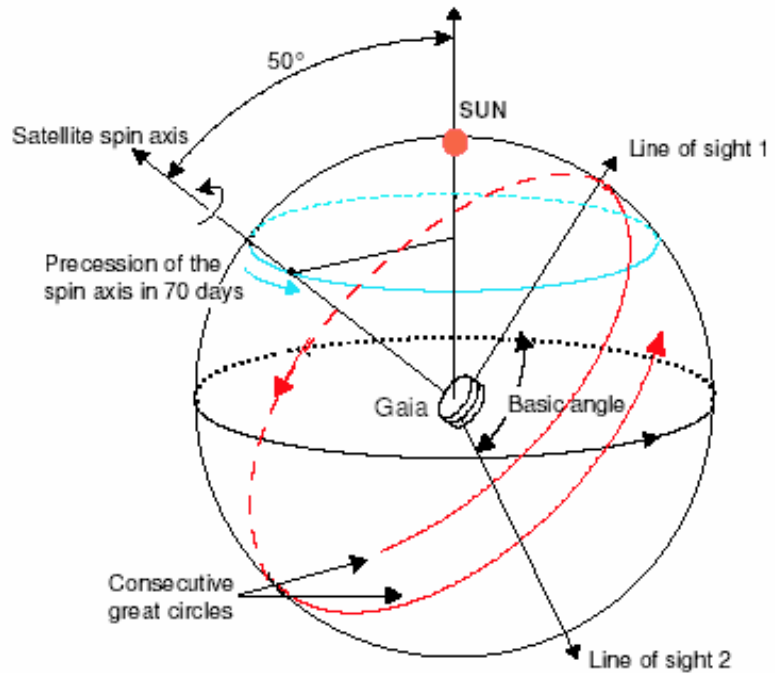
Mission type:	Astronomy and Astrometry Mission
Mission class	approved ESA cornerstone mission no. 6 (Horizon 2000)
Status	<ul style="list-style-type: none"> <li>Phase A (extended) completed in 2005-05-24</li> <li>ITT for Phase B/C/D expected in mid-2005</li> </ul>
Launcher, Orbit	<ul style="list-style-type: none"> <li>launch in 2012 with Soyuz-Fregat from Kourou</li> <li>Fregat Upper Stage injects into Transfer Orbit towards L2</li> <li>Acquisition of Lissajous orbit around L2 with the on-board bi-propellant system (required <math>\Delta V \sim 200</math> m/s)</li> <li>half-cone angle of Lissajous orbit <math>\sim 5^\circ</math>, viewed from Earth</li> <li>period of Lissajous orbit: 70 days</li> <li>orbit phased such that 6.3 years are free of eclipse</li> </ul>



<p>Mission objective</p>	<ul style="list-style-type: none"> <li>• Repeated global scans to catalogue the sky to a magnitude completeness limit of <math>V = 20.0</math> mag</li> <li>• Measurement of 3D-motion and of photometric and spectrometric characteristics to investigate the origin and evolution of our Galaxy, the Milky Way</li> <li>• huge number of new discoveries: planets, asteroids, comets, failed and dead stars, quasars, etc.</li> <li>• new tests of general relativity</li> </ul>
<p>Scientific Instruments</p>	<p>Satellite carries two large instruments:</p> <ul style="list-style-type: none"> <li>• 2 ASTRO telescopes + focal plane CCD, basic angle of astrometry = <math>106^\circ</math> between lines-of-sight, FOV of each ASTRO telescope: <math>0.65^\circ \times 0.65^\circ</math></li> <li>• SPECTRO telescope + focal plane instruments</li> </ul> <p>Governing requirements are:</p> <ul style="list-style-type: none"> <li>• star position accuracy of 7 micro-arcsec for star magnitude <math>V = 15</math> (accuracy to be achieved from repeated scans over the mission)</li> <li>• 1 billion of stars to be measured</li> </ul>
<p>Mission duration</p>	<ul style="list-style-type: none"> <li>• Transfer Orbit + Commissioning Phase: 6 months</li> <li>• Nominal Observation Phase: 5 years</li> <li>• Observation Phase extension: + 1 year</li> </ul>



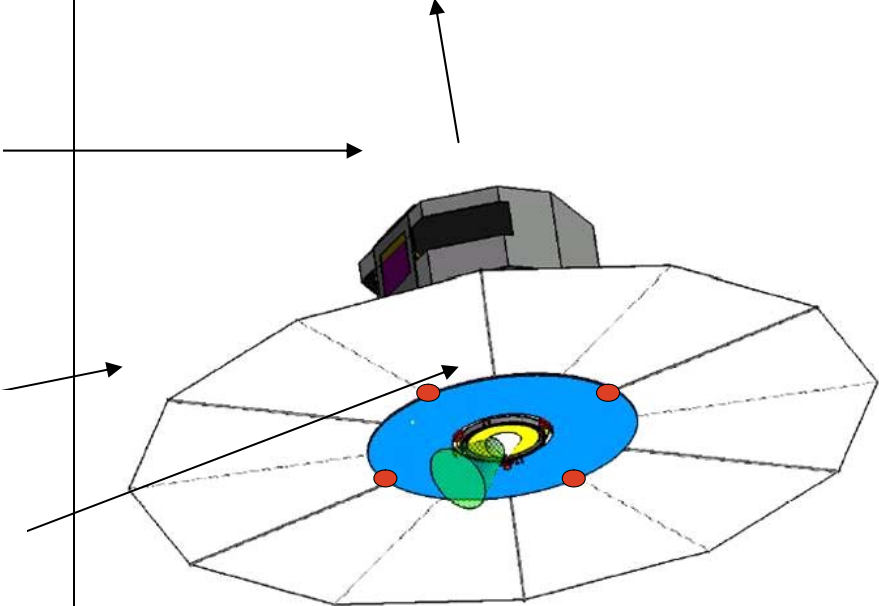
Revolving Scanning Law for  
Gaia



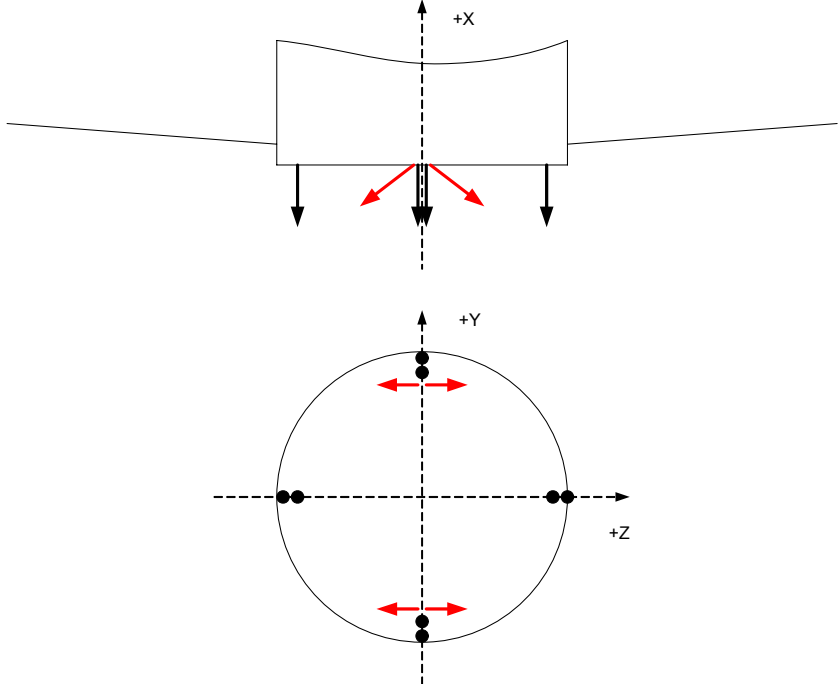
- continuous scientific observation over full mission time  
(availability  $\geq 98\%$ )
- Basic angle for astrometry:  $106^\circ$  (between LOS 1 and LOS 2)
- fixed solar aspect angle of  $50^\circ$

Revolving scanning law:

- rotation (scan) rate about X-axis precisely controlled to  
 $60 \text{ arcsec / sec}$
- forced precession of rotation axis over  $70 \text{ days}$

<p>S/C configuration:</p> <p>Telescope apertures</p> <p>Sun Shield + Solar Array</p> <p>Phased Array Antenna</p>	 <p>view on sun-exposed side of S/C</p>										
<p>S/C dimensions and mass (TBC)</p>	<table border="0"> <tr> <td>Sun Shield / Solar Array diameter:</td> <td>10,850 mm</td> </tr> <tr> <td>S/C diameter:</td> <td>3,800 mm</td> </tr> <tr> <td>S/C overall height:</td> <td>4,000 mm</td> </tr> <tr> <td>S/C wet mass after separation:</td> <td>1,700 kg</td> </tr> <tr> <td>Propellant mass</td> <td>200 kg</td> </tr> </table>	Sun Shield / Solar Array diameter:	10,850 mm	S/C diameter:	3,800 mm	S/C overall height:	4,000 mm	S/C wet mass after separation:	1,700 kg	Propellant mass	200 kg
Sun Shield / Solar Array diameter:	10,850 mm										
S/C diameter:	3,800 mm										
S/C overall height:	4,000 mm										
S/C wet mass after separation:	1,700 kg										
Propellant mass	200 kg										
<p>Solar Array power</p>	<p>~ 2,200 W</p>										
<p>On-board propulsion systems</p>	<p>Gaia is injected into the transfer orbit towards L2 by the Upper Stage of Soyuz-Fregat, which is separated after this manoeuvre.</p> <p>Two on-board propulsion systems are available:</p> <p><b>(a) Bi-propellant system</b> (using 10 N thrusters) for:</p> <ul style="list-style-type: none"> <li>attitude control during Transfer Phase</li> </ul>										

	<ul style="list-style-type: none"> <li>• trajectory correction(s) towards L2</li> <li>• large orbit insertion manoeuvres at L2 (<math>\Delta V \sim 200</math> m/s)</li> <li>• station keeping (orbit maintenance) manoeuvres around L2, approx. once per month</li> </ul> <p><b>(b) Micro-propulsion system for Observation Mode:</b></p> <ul style="list-style-type: none"> <li>• rotation rate fine control</li> <li>• attitude fine control (forced precession, disturbance compensation)</li> <li>• fine control acquisition after each station-keeping manoeuvre</li> <li>• Commands derived from the telescope instruments</li> </ul>
<p>Potential Micro-Propulsion Systems</p>	<ul style="list-style-type: none"> <li>• FEEP Micro-propulsion system (lacking development status / heritage may prohibit their usage for Gaia)</li> <li>• Proportional Cold-Gas Micro-propulsion system (on-going development effort for Gaia)</li> <li>• Micro-Ion propulsion system (interesting alternative; new control concept using Pulse Width Modulation at <math>\sim 1</math> kHz)</li> <li>• Micro-HEMPT propulsion system (potential technology)</li> </ul> <p>The final selection must yet be made in Phase B.</p>

<p>Arrangement of Micro-Propulsion Thrusters (preliminary schematic - TBC)</p>	 <ul style="list-style-type: none"> <li>• micro-N thrusters for attitude and rate control on the bottom of the Service Module (SVM)</li> <li>• 2 x 4 pitch / yaw thrusters (shown in black)</li> <li>• 2 x 2 roll thrusters (for precise rate control; shown in red); thrusters are tilted in order to minimise plume interaction</li> <li>• parasitic forces and torques due to thruster action are tolerable, respectively can be compensated</li> <li>• fully redundant set of 2 x 6 = 12 micro-thrusters</li> <li>• in particular the roll thrusters must produce very small control forces. This may require to produce such small forces by opposing thrusters (differential mode)</li> </ul>
<p>System Performance requirements</p>	<ul style="list-style-type: none"> <li>• detailed performance requirements on AOCS and micro-propulsion must yet be derived from the system pointing and rate error requirements, see below.</li> </ul>

	<p>Attitude Measurement Error AME &lt; 20 arcsec (<math>3\sigma</math>)</p> <p>Rate Measurement Error (along scan) &lt; 0.9 mas / sec (<math>3\sigma</math>)</p> <p>Rate Measurement Error (across scan) &lt; 2.7 mas / sec (<math>3\sigma</math>)</p> <p>Absolute Pointing Error APE &lt; 60 arcsec (<math>3\sigma</math>)</p> <p>Relative Pointing Error RPE (along scan) &lt; 2 mas (<math>3\sigma</math>)</p> <p>Relative Pointing Error RPE (across scan) &lt; 10 mas (<math>3\sigma</math>)</p> <p>Mean Rate Error MRE (along scan) &lt; 2 mas / sec (<math>3\sigma</math>)</p> <p>Mean Rate Error MRE (across scan) &lt; 10 mas / sec (<math>3\sigma</math>)</p> <p><u>Note:</u></p> <p>RPE specified over single detector (CCD) integration time,</p> <p>MRE specified over the time of an object crossing the ASTRO focal plane.</p>
<p>Performance requirements on micro-thrusters</p>	<ul style="list-style-type: none"> <li>• SRP disturbance torques to be continuously compensated in a commutating manner by the pitch / yaw thrusters &lt; 150 <math>\mu</math>N</li> <li>• thrust reserve for fine control re-acquisition after station-keeping manoeuvres TBD <math>\mu</math>N</li> </ul> <p>The following requirements are based on FEEP thrusters and need to be reviewed:</p> <ul style="list-style-type: none"> <li>• total impulse per thruster <math>\leq</math> 15,000 Ns</li> <li>• min thrust: &lt; 1.0 <math>\mu</math>N</li> <li>• resolution: &lt; 0.3 <math>\mu</math>N</li> <li>• thrust stability over life: &lt; 0.5 % (<math>3\sigma</math>)</li> </ul>

	<ul style="list-style-type: none"> <li>thrust vector accuracy: &lt;math&gt;&lt; 3^\circ&lt;/math&gt; half-cone</li> <li>maximum command rate: 10 Hz</li> <li>thrust response: &lt;math&gt;&lt; 100&lt;/math&gt; ms for 90 % of commanded step</li> </ul>
Micro-Thruster noise (to be reviewed and confirmed)	<ul style="list-style-type: none"> <li>&lt;math&gt;&lt; 5 \times 10^{-7}&lt;/math&gt; N / <math>\sqrt{\text{Hz}}</math> for <math>f &lt; 10</math> Hz</li> <li>transverse thrust noise &lt;math&gt;&lt; 1 \times 10^{-7}&lt;/math&gt; N / <math>\sqrt{\text{Hz}}</math> for <math>f &gt; 0.05</math> Hz, per axis</li> </ul>
Station-Keeping (SK) Manoeuvres during Observation Phase	<ul style="list-style-type: none"> <li>approx. once per month a small manoeuvre is needed to maintain the Lissajous orbit around L2 (<math>\Delta V \sim \text{TBD}</math> m/s)</li> <li>SK performed with bi-propellant thrusters, if no affordable alternative is found</li> <li>Gaia continues with the nominal scan motion</li> <li>re-acquisition of fine control and settling of flexible / slosh modes may take up to 1 day</li> </ul>
Moving parts / liquid slosh / flexible modes	<ul style="list-style-type: none"> <li>moving parts are strictly prohibited on-board GAIA</li> <li>slosh and flexible modes to be minimised and to be controlled by micro-propulsion</li> </ul>
Micro-Propulsion usage	<ul style="list-style-type: none"> <li>The Micro-Propulsion System shall be used for fine attitude control in Observation Mode.</li> <li>Dominant disturbance torques are those induced by the solar pressure on the very large Sun Shield. The spin axis is at <math>50^\circ</math> to Sun direction, and a well-predictable thrust profile for each thruster results per spin period (6 hours):</li> </ul>
Chemical cleanliness	<ul style="list-style-type: none"> <li>micro-propulsion thrusters shall not suffer damage from the bi-propellant system</li> </ul>

	<ul style="list-style-type: none"> <li>contamination of solar array, MLI and other surfaces, and of the Digital Sun Sensor e.g. by liquid metal from FEEP thrusters must be avoided</li> </ul>
Magnetic cleanliness	<ul style="list-style-type: none"> <li>no requirement at L2; no sensitive units</li> </ul>
EMC	<ul style="list-style-type: none"> <li>The micro-propulsion systems shall not interfere with the phased array antenna</li> </ul>
References:	<p>RD-1: ESA homepage</p> <p>RD-2: Gaia Mission Requirements Document, Draft, dated 10.032005 (update in mid-2005 with ITT)</p>

### Abbreviations:

AME	Attitude Measurement Error
AOCS	Attitude and orbit Control System
APE	Absolute Pointing Error
CCD	Charge Coupled Device
COG	Centre of Gravity
DSA	Deployable Sun Shield Assembly
FEEP	Field Emission Electric Propulsion
FOV	Field-of-View
ITT	Invitation to Tender
L2	2nd Lagrange Point of the Earth / Moon - Sun System
LOS	Line-of-Sight
mas	milli-arcsec
µas	micro-arcsec
MRE	Mean Rate Error
NOM	Nominal Observation Mode
OCM	Orbit Control Mode
PLM	Payload Module
RME	Rate Measurement Error
RPE	Relative Pointing Error
RVS	Radial Velocity Spectrometry
SAA	Solar Aspect Angle
SVM	Service Module

### 4.8 XEUS

Mission type:	Large X-ray Observatory for Astrophysics (approx. 200 x improved sensitivity compared to XMM-Newton)
Mission class	<ul style="list-style-type: none"> <li>• Potential cornerstone mission of ESA Cosmic Vision</li> <li>• various technology studies still on-going and / or planned</li> <li>• XEUS Mission Assessment Study: starts in January 2006</li> <li>• expected co-operation with JAXA (Japan) and NASA (Detector S/C)</li> <li>• XEUS could serve as a precursor for Darwin with respect to Formation Flying (relaxed requirements compared to Darwin)</li> </ul>
Potential XEUS precursors	<ul style="list-style-type: none"> <li>• eRosita mission with a reduced number of seven mirror modules is under discussion in Germany</li> <li>• CNES is pursuing Simbol-X (mainly as a technology precursor)</li> </ul>
XEUS as precursor for DARWIN	<ul style="list-style-type: none"> <li>• XEUS will be the first step towards precise Formation Flying (FF), although DARWIN will require a FF precision several orders of magnitude more precise.</li> <li>• XEUS as precursor for DARWIN formation flying may influence technology to be selected for the FF Metrology System (FMS)</li> </ul>
Launcher, Orbit	<ul style="list-style-type: none"> <li>• launch in 2015 - 2020 with 2 separate Soyuz-Fregat launches from Kourou (current baseline TBC)</li> <li>• halo orbit about L2 i.e. benign gravity and thermal environment (no eclipses)</li> <li>• 30° halo orbit requires a minimum of orbit maintenance <math>\Delta V</math> (&lt; 10 mm/s every 30 days)</li> <li>• Formation flying (FF) with the Detector S/C as active part</li> </ul>
Science objectives	<ul style="list-style-type: none"> <li>• study the evolution of the hot baryons in the Universe</li> </ul>



	<ul style="list-style-type: none"> <li>• detect massive black holes und the earliest Active Galactic Nuclei (AGNs) and estimate their mass, spin and red-shift</li> <li>• study the formation of the first gravitationally bound, dark matter dominated, groups of galaxies</li> <li>• trace their evolution into today's massive clusters</li> <li>• study the evolution of metal synthesis to the present epoch</li> <li>• plus a large number of important secondary science objectives</li> </ul>
Mission lifetime	<p>MSC: 15 years at L2</p> <p>DSC: 5 years at L2; scheduled DSC replacement every 5 years</p>
Benefits of L2 halo orbit	<ul style="list-style-type: none"> <li>• dramatically reduced gravity environment (minimal disturbance torques; dramatically reduced forces and total impulse for formation flying and orbit control)</li> <li>• 30° halo orbit requires very low <math>\Delta V</math> for orbit maintenance (approx. 1 - 10 mm/s every 30 days)</li> <li>• no Earth and Moon stray-light problems</li> <li>• solar aspect angle of <math>90 \pm 15^\circ</math> permits observations on a great circle, 30° wide on the celestial sphere</li> <li>• constant thermal environment (in particular no eclipses)</li> </ul>
Required instrumentation	<p>to achieve the primary science objectives, the following X-ray telescope and detectors are proposed and need to be developed:</p> <p><b>(a) X-ray telescope on Mirror S/C (MSC):</b></p> <ul style="list-style-type: none"> <li>• enabling, novel light-weight technology (Micro-Pore Optics MPO)</li> <li>• collecting area at 1 keV: <span style="float: right;">10 m<sup>2</sup>,</span></li> <li style="padding-left: 20px;">resp. at 30 keV: <span style="float: right;">3 m<sup>2</sup></span></li> </ul>

	<ul style="list-style-type: none"> <li>• size: approx. 5m x 5m</li> <li>• number of mirror petals 6 x 6</li> <li>• alignment mechanisms per mirror petal 3</li> <li>• spatial resolution: &lt; 5 arcsec HEW (required) &lt; 2 arcsec HEW (target)</li> <li>• field-of-view: approx. 5 x 5 arcmin (flat point spread function over approx. 10 x 10 arcmin)</li> <li>• focal length: 50 m</li> <li>• telescope baffles at mirror petal or sub-petal level</li> </ul> <p><b>(b) Instruments on Detector S/C (DSC) - descriptions see below:</b></p> <ul style="list-style-type: none"> <li>• WFI (Wide Field Imaging Detector)</li> <li>• NFI (Narrow Field Instrument)</li> <li>• Ancillary instruments</li> </ul>
<p>XEUS in-orbit configuration (artist's view)</p> <p><b>5m x 5m X-ray Telescope</b></p> <p><b>Sun direction</b></p>	<p>Mirror S/C</p> <p>Detector S/C</p>

	<u>Note:</u> Telescope will only see cold space and will be very cold
Payload (instruments on DSC)	<p><b>(a) WFI (Wide Field Imaging Detector):</b></p> <ul style="list-style-type: none"> <li>• efficient FOV coverage, modest broad-band spectral resolution over full energy band</li> <li>• used for extremely deep surveys (up to 10E6 seconds = 12 days per observation)</li> <li>• FOV: <span style="float: right;">5 arcmin x 5 arcmin</span></li> <li>• number of pixels: <span style="float: right;">1024 x 1024</span></li> <li>• pixel size: <span style="float: right;">75 x 75 <math>\mu\text{m}^2</math></span></li> <li>• read-out time:             <ul style="list-style-type: none"> <li>window mode (128 x 128 pixels): <span style="float: right;">0.16 msec</span></li> <li>total field: <span style="float: right;">1.25 msec</span></li> </ul> </li> <li>• physical size of detector surface: <span style="float: right;">77 x 77 <math>\text{mm}^2</math></span></li> </ul> <p><b>(b) NFI (Narrow Field Instrument)</b></p> <ul style="list-style-type: none"> <li>• restricted field, adequately efficient, high spectroscopic resolution up to 7 keV (poorer resolution up to 15 keV)</li> <li>• used as follow-up spectrometers on specific sources found by WFI</li> <li>• two instruments with cryogenic detectors (one cooled to 350 mK, the other to 30 mK). Cooling achieved with Adiabatic Demagnetisation Refrigerator (ADR), sorption pump, and Joule Thomson/Stirling cooler combination.</li> <li>• NFI 1 data:             <ul style="list-style-type: none"> <li>field of view: <span style="float: right;">0.5 x 0.5 arcmin</span></li> </ul> </li> </ul>

	<p>pixel size 150 x 150 <math>\mu\text{m}</math></p> <p>time resolution 5 <math>\mu\text{s}</math></p> <p>physical size of detector element approx. 7 x 7 mm</p> <ul style="list-style-type: none"> <li>NFI 2 data:</li> </ul> <p>field of view: 0.5 x 0.5 arcmin</p> <p>pixel size 240 x 240 <math>\mu\text{m}</math></p> <p>number of pixels 32 x 32</p> <p>time resolution 100 <math>\mu\text{s}</math></p> <p>physical size of detector element approx. 7 x 7 mm</p> <p><b>(c) Ancillary instruments:</b></p> <ul style="list-style-type: none"> <li>fast timing instrument (Mega-counts / s)</li> <li>Hard X-ray detector</li> <li>WFI with increased FOV (requires large baffle length!)</li> <li>polarisation sensitive detector.</li> </ul>
<p>Lateral placement of the instruments at the focal plane point</p>	<ul style="list-style-type: none"> <li>lateral translation to the focal plane point will be achieved by translation of the whole DSC, using the Formation Flying metrology system + propulsion system</li> </ul>
<p>Formation Flying (FF)</p>	<p>[1] <b>absolute navigation</b> (rendez-vous) to 10 km relative distance</p> <p>[2] <b>autonomous approach</b> with RF relative navigation starting from 200m x 200m x 0.1m (at 10 km distance) to 2m x 2m x 0.01m relative navigation accuracy (at 120m distance)</p> <p>[3] <b>autonomous laser relative navigation</b> to focal point with laser range-finder and lateral sensor(s)</p> <p>- for <b>observations</b> with an accuracy of several 10<math>\mu\text{m}</math> laterally</p>

	<p>and several 100µm longitudinally</p> <ul style="list-style-type: none"> <li>- with reduced accuracy during <b>Reaction Wheel off-loading</b> (MSC and DSC)</li> <li>- with reduced accuracy during <b>orbit maintenance maneuvers</b> (approx. every 30 days)</li> <li>- during <b>slews to new targets</b>, FF shall be maintained with reduced accuracy (TBC)</li> </ul>
<p>Attitude Control and Formation Flying (FF)</p>	<ul style="list-style-type: none"> <li>• dramatically reduced delta-V requirements for formation flying compared to a LEO XEUS mission</li> <li>• MSC remains passive partner in FF; maintains the telescope pointing <span style="float: right;">APE &lt; 10 arcsec</span> <u>Note:</u> FF metrology system (FMS) may require high-precision Star Tracker onboard MSC (1 - 2 arcsec class), subject of FMS concept selection.</li> <li>• DSC is the active part in FF and shall be locked at focal point within a ~ 1mm cube (absolute error)</li> <li>• Laser Rangefinder and Formation Flying Metrology System shall support a laser relative navigation with an accuracy of: <ul style="list-style-type: none"> <li>- lateral: <span style="float: right;">tens of µm</span></li> <li>- on-axis (longitudinal): <span style="float: right;">hundreds of µm</span></li> </ul> <p><b><u>Note:</u> This requirement must be understood as a stability requirement.</b></p> </li> <li>• high-precision Star Tracker onboard DSC (1 - 2 arcsec class) <u>Note:</u></li> </ul>

	probably also needed on MSC (TBC)
Relative Navigation / Formation Flying (FF)	<ul style="list-style-type: none"> <li>• RF system for relative navigation during approach</li> <li>• laser rangefinders to determine along-axis distance and camera to determine lateral position (intermediate precision needed for approach to focal point, for FF hold during orbit maintenance manoeuvres, RW off-loading and slews to new targets)</li> <li>• concept of the FF Metrology System, which is needed to achieve the ultimate performance in lateral directions, is not yet defined / selected. Figure below outlines a possible concept (laser range finder and interferometer, as described in RD-2 and RD-5.</li> <li>• other FFMS instrumentation conceivable, e.g. LR plus CCD camera(s) -- see RD-6 e.g. usage of the WFI as image navigation camera with fast update rate of the lateral position (also addressed in RD-2)</li> </ul> <div style="text-align: center; margin-top: 20px;"> <p style="margin-left: 10%; margin-right: 10%;">DSC</p> <p style="margin-left: 10%; margin-right: 10%;">MSC</p> <p style="margin-left: 10%; margin-right: 10%;">lasers and/or cameras</p> <p style="margin-left: 10%; margin-right: 10%;">retro-reflectors or LEDs</p> </div>

	<p><u>Note:</u> With respect to Formation Flying (FF), XEUS to a certain extent will serve as a precursor for DARWIN FF. However, the FF precision required by DARWIN will exceed XEUS requirements by orders of magnitude.</p>						
<p>MSC configuration</p>	<div data-bbox="582 667 1420 1254" data-label="Image"> </div> <ul style="list-style-type: none"> <li>• Launched with mirror panels stowed inside Canister.</li> <li>• Canister, sun shields and X-ray Mirror deployed at L2, as shown above</li> <li>• 3 actuators and launch locks on each mirror petal allow fine adjustment after deployment</li> <li>• The solar aspect angle (SAA) constraint allows the MSC to be pointed within the following limits:             <table style="margin-left: 40px; border: none;"> <tr> <td>- rotation about X:</td> <td style="text-align: right;">no limitation</td> </tr> <tr> <td>- rotation about Y:</td> <td style="text-align: right;"><math>\pm 15^\circ</math></td> </tr> <tr> <td>- rotation about Z</td> <td style="text-align: right;"><math>\pm 0^\circ</math></td> </tr> </table> </li> </ul>	- rotation about X:	no limitation	- rotation about Y:	$\pm 15^\circ$	- rotation about Z	$\pm 0^\circ$
- rotation about X:	no limitation						
- rotation about Y:	$\pm 15^\circ$						
- rotation about Z	$\pm 0^\circ$						

<p>MSC dimensions and mass</p>	<ul style="list-style-type: none"> <li>• S/C height: ~ 5,500 mm</li> <li>• S/C diameter: ~ 3,000 mm</li> <li>• Launch mass (wet) 2050 kg</li> <li>• Propellant mass (TBC) 54 kg</li> </ul>
<p>MSC AOCS Elements and On-board Propulsion</p>	<p><b>AOCS elements:</b></p> <ul style="list-style-type: none"> <li>• high-precision Star Tracker (mounting location: TBD)</li> <li>• Reaction Wheels (approx. 20 Nms, TBC)</li> </ul> <p><b>On-board Propulsion Systems:</b></p> <p><b>[1] Monopropellant System:</b></p> <ul style="list-style-type: none"> <li>• used for launch dispersion correction (prior to mirror deployment)</li> <li>• complete subsystem accommodated in one half-cylinder of the Canister</li> <li>• thrusters on -Y side of the closed MSC canister; thruster arrangement similar to that of TerraSAR and Kompsat-2; delta-V only in 1 direction.</li> </ul> <p><b>[2] Cold Gas Propulsion Systems (CGPS):</b></p> <ul style="list-style-type: none"> <li>• used for: <ul style="list-style-type: none"> <li>- Reaction Wheel off-loading</li> <li>- small orbit maintenance delta-V</li> <li>- slews to new observation targets (up to +/- 180°)</li> </ul> </li> <li>• because the two Canister halves will be folded out, two CGPS are needed, one in each Canister half-cylinder !!</li> <li>• thruster arrangement has to provide 6 DOF capability for MSC</li> </ul>



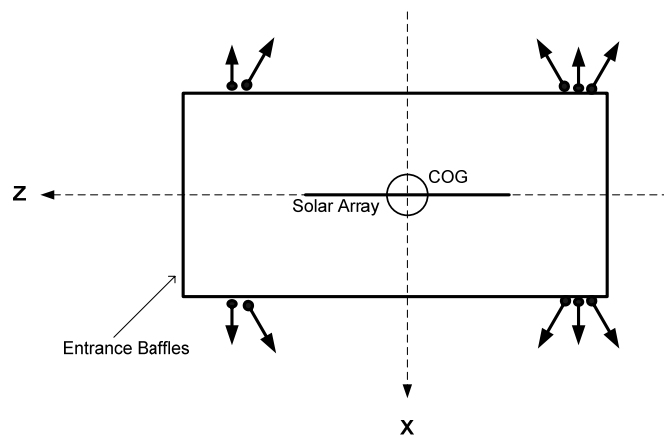
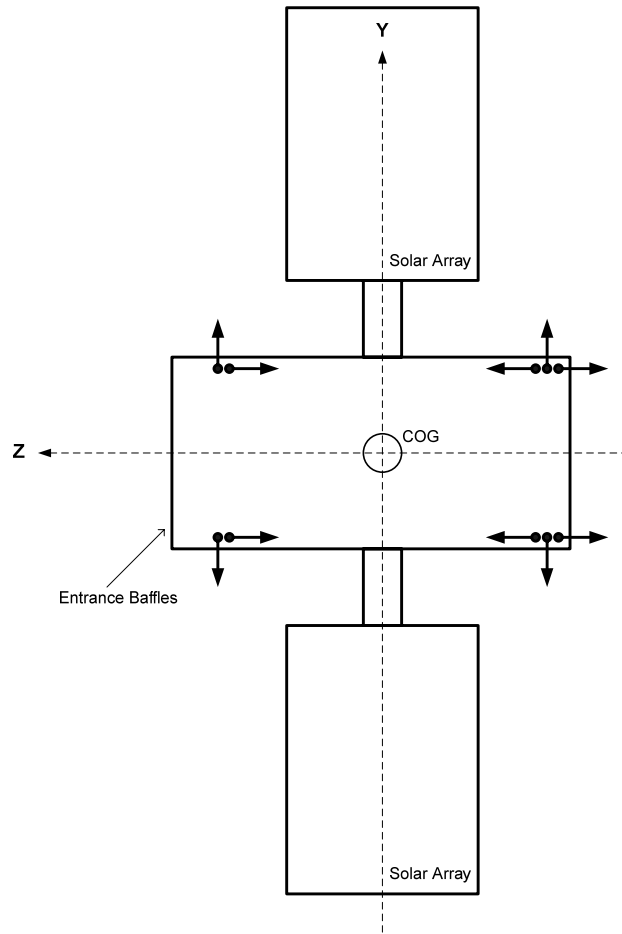
<p>Tentative arrangement of the CGPS thrusters on MSC</p>	<ul style="list-style-type: none"> <li>• total of 20 thrusters</li> <li>• no thrust vector close to X-ray Mirror</li> <li>• 3 rotational DOF's by balanced pairs</li> <li>• translations require either balance quadruples (in +/- X) or balanced thruster pairs through COG direction, plus compensation of the parasitic delta-V in -X direction</li> <li>• considerable geometric losses for all delta-V manoeuvres (30 - 50 %)</li> <li>• other thruster arrangements conceivable.</li> </ul>
<p>MSC thruster arrangement (preliminary)</p>	<p>The diagram illustrates the preliminary thruster arrangement on the MSC. It shows a central Center of Gravity (COG) and the X-Ray Mirror System extending to the right. A Sun Shield is positioned to the left of the COG. Thrusters are arranged as follows:     <ul style="list-style-type: none"> <li>4 tilted thrusters on both ends of the Canister (top and bottom).</li> <li>4 tilted thrusters on both ends of the Canister (top and bottom).</li> <li>Thruster pair at mid-height.</li> </ul>     The X-axis is labeled X<sub>MSC</sub> and the Z-axis is labeled Z<sub>MSC</sub>. The Sun Shield is shown as a curved structure on the left side of the diagram.</p>

	<p>redundancy included</p>								
<p>DSC configuration</p>	<ul style="list-style-type: none"> <li>• see artist's view on page 2</li> <li>• instrument baffle length of approx. 1.5 m, accommodated within DSC dimensions</li> <li>• Solar Arrays deploy to fixed position</li> <li>• Solar Array size has significantly decreased, because large Ion Engines with several kW power demand are no longer needed for the mission at L2.</li> </ul>								
<p>DSC dimensions and mass</p>	<table border="0"> <tr> <td>S/C shape</td> <td>box-shaped, see figure on p.2</td> </tr> <tr> <td>S/C height:</td> <td>TBD mm</td> </tr> <tr> <td>S/C width:</td> <td>TBD mm</td> </tr> <tr> <td>Launch mass (wet)</td> <td>~ 1,500 kg</td> </tr> </table>	S/C shape	box-shaped, see figure on p.2	S/C height:	TBD mm	S/C width:	TBD mm	Launch mass (wet)	~ 1,500 kg
S/C shape	box-shaped, see figure on p.2								
S/C height:	TBD mm								
S/C width:	TBD mm								
Launch mass (wet)	~ 1,500 kg								

	<p>Propellant mass (TBC) <span style="float: right;">~ 205 kg</span></p> <p><u>Note:</u> The storage of 205 kg of nitrogen at 280 bar requires a total tank volume of 745 ltr, which is not easy / not possible (?) to accommodated inside DSC.</p>
<p>Propulsion On-board</p> <p>DSC</p>	<p><b>Manoeuvre requirements:</b></p> <ul style="list-style-type: none"> <li>• attitude acquisition after separation from transfer stage</li> <li>• Orbit insertion correction manoeuvres</li> <li>• Rendez-vous manoeuvres</li> <li>• autonomous approach manoeuvres</li> <li>• Formation acquisition and hold</li> <li>• high-accuracy Formation Flying (Observation Mode)</li> <li>• scheduled orbit maintenance manoeuvres of MSC and DSC</li> <li>• slews to new targets: DSC on arc of 50m radius (formation hold)</li> <li>• Momentum dumping manoeuvres at scheduled times (Both, MSC and DSC)</li> </ul> <p><b>On-board Propulsion Systems:</b></p> <p><b>[1] Mono-propellant System:</b></p> <ul style="list-style-type: none"> <li>• used for launch dispersion correction, and rendez-vous with MSC (TBC). Then the subsystem is shut-down and isolated, before instrument aperture are opened, in order to avoid contamination.</li> <li>• propellant demand to be calculated (TBD).</li> </ul> <p><b>[2] Cold Gas Propulsion Systems (CGPS) using GN2:</b></p>

	<ul style="list-style-type: none"><li>• used for:<ul style="list-style-type: none"><li>- formation flying</li><li>- Reaction Wheel off-loading</li><li>- small orbit maintenance delta-V</li><li>- compensation of differential solar pressure induced drift (different ballistic coefficients of MSC and DSC)</li><li>- slews to new observation targets</li></ul></li><li>• thruster arrangement has to provide 6 DOF capability for DSC</li><li>• thruster arrangement has to provide 6 DOF capability for DSC. The largest total momentum must be provided by the thrusters in +/- Y (direction of the slew motion). Thrust losses (geometric loss, manoeuvre efficiency) for these manoeuvres must be minimised.</li></ul>
--	---

DSC thruster arrangement  
(preliminary concept  
requiring further  
optimisation)



without redundancy, 20 thrusters are needed.

CGPS Propellant Budget	<ul style="list-style-type: none"> <li>• approach from 10 km to 0.1 km <span style="float: right;">~ 1 kg</span></li> <li>• compensation of different ballistic coefficients (over 5 years) <span style="float: right;">~ 27 kg</span></li> <li>• Solar radiation pressure induced torques (i.e. Reaction Wheel off-loading over 5 years) <span style="float: right;">~ 10 kg</span></li> <li>• halo orbit maintenance (over 5 years) <span style="float: right;">~ 1 kg</span></li> <li>• Telescope re-targeting (slews to targets over 5 years) <span style="float: right;">~ 52 kg</span></li> </ul> <p style="margin-top: 10px;"><b>Total propellant demand <span style="float: right;">91 kg</span></b></p> <p><b>with loss factors and margins included <span style="float: right;">~ 200 kg</span></b></p>
Cold-Gas Propulsion System of DSC	<ul style="list-style-type: none"> <li>• RD-2 assumes a proportional cold-gas thruster system (using nitrogen) in miniaturised semiconductor technology. <ul style="list-style-type: none"> <li>- development status and life-time performance questionable</li> <li>- FF also possible with 10 mN cold gas thrusters in pulse mode</li> </ul> </li> <li>• Required tank volume: 200 kg of nitrogen require a huge storage volume (~ 740 ltr at 280 bar), which most likely conflicts with the dimensional and accommodation constraints on DSC. The maximum volume available for the Nitrogen Tanks may defeat a pure CGPS concept!</li> <li>• Alternatives could be: <ul style="list-style-type: none"> <li>- usage of high Isp hot gas thrusters (resistojets) for the re-targeting (slew) manoeuvres which consume most of the propellant</li> <li>- usage of electrical thrusters, such as mini-RITs or mini-HEMPTs for the most propellant consuming manoeuvres.</li> </ul> </li> </ul>



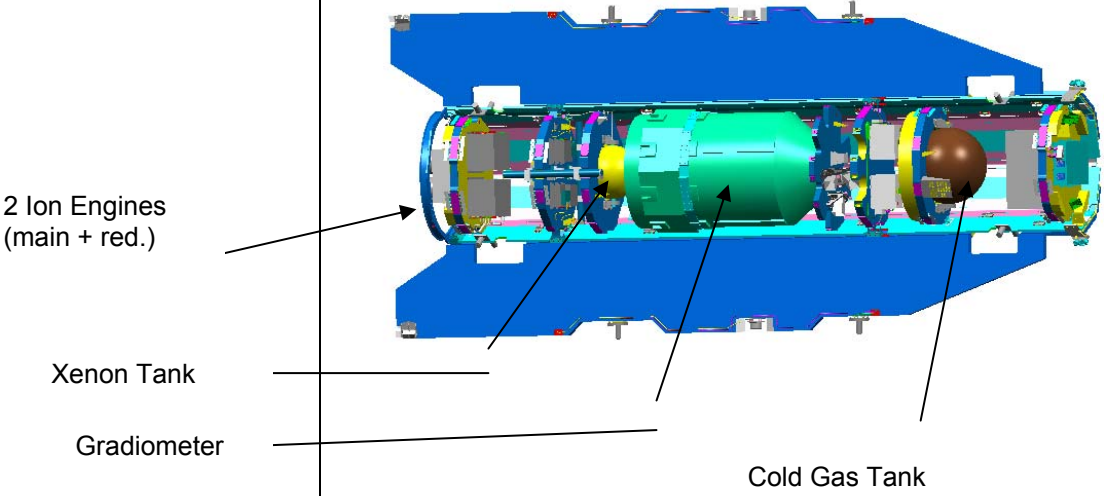
	above); no plume toward entrance baffle
<u>References:</u>	<p>RD-1: Science with XEUS - X-ray Evolving Universe Spectroscopy Mission, 2004/SCI-SA/053</p> <p>RD-2: XEUS Mission Reference Design, 2004/SCI-A/012</p> <p>RD-3: XEUS Mission - Detector Spacecraft Instrumentation package, 2004/SCI-A/013</p> <p>RD-4: Status of the X-ray Optics Development for the XEUS Mission, 2004/SCI-A/010</p> <p>RD-5: ESA CDF Report on new XEUS concept; will be issued in mid.2005</p> <p>RR-6: Optical Sensors for AOCS IX-DSS-TN-0004-03, dated 28.09.1999</p>

Abbreviations:

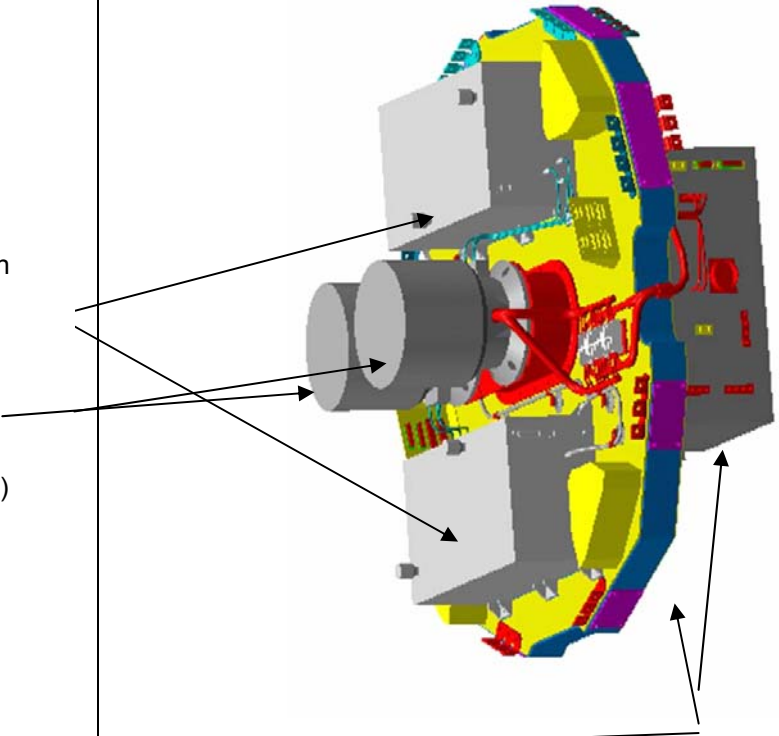
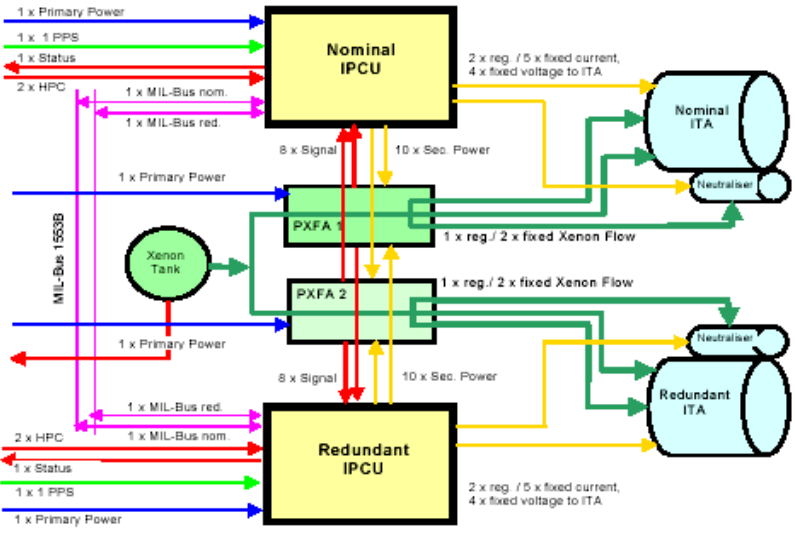
CGPS	Cold Gas Propulsion System
DOF	Degree of Freedom
DSC	Detector Spacecraft
FF	Formation Flying
FMS	Formation Flying Metrology System
HEMPT	High-Efficiency Multi-stage Plasma Thruster
HEW	Half-Energy Width
LEO	Low Earth Orbit
LR	Laser Rangefinder
MPO	Micro Pore Optics
MSC	Mirror Spacecraft
NFI	Narrow Field Instrument
PSF	Point Spread Function
RIT	RF Ion Thruster
SAA	Solar Aspect Angle
TBC	to be confirmed
TBD	to be defined
WFI	Wide Field Imaging Detector
XEUS	X-ray Evolving Universe Spectroscopy Mission



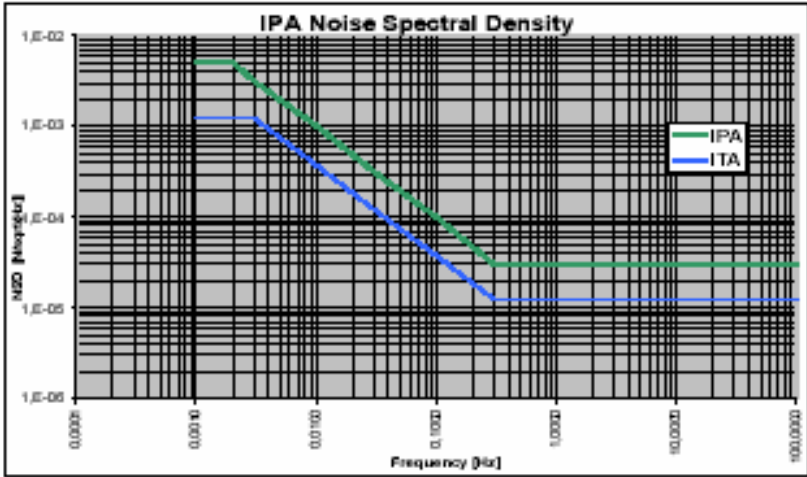
## 4.9 GOCE

Mission type:	Gravity Gradiometer mission on very low Earth orbit
Mission class	ESA explorer mission  Currently in Phase C/D
Launcher, Orbit	<ul style="list-style-type: none"> <li>• launch in 2006 with Rokot from Plestsk / Russia</li> <li>• LEO (circular sun-synchronous dawn-dusk orbit, h = 240 - 270 km, i = 96.5°)</li> </ul>
Payload and mission objective	<p>Satellite carries:</p> <ul style="list-style-type: none"> <li>• Gradiometer (3 sensitive axes)</li> <li>• GPS</li> </ul> <p>Objectives are:</p> <ul style="list-style-type: none"> <li>• measurement of the gravity tensor with high spatial resolution (&lt; 100 km)</li> <li>• measurement of anomalies with <math>10^{-5} \text{ m/s}^2</math> accuracy</li> </ul>
Mission duration	20 months in-orbit (required); resources for 30 months in orbit
S/C configuration:	 <p>2 Ion Engines (main + red.)</p> <p>Xenon Tank</p> <p>Gradiometer</p> <p>Cold Gas Tank</p>

S/C dimensions and mass	<table> <tr> <td>S/C length:</td> <td>5,300 mm</td> </tr> <tr> <td>S/C width:</td> <td>2,360 mm</td> </tr> <tr> <td>Body diameter:</td> <td>1,000 mm</td> </tr> <tr> <td>Wet Mass:</td> <td>1,120 kg</td> </tr> <tr> <td>Propellant mass (Xenon):</td> <td>40 kg</td> </tr> <tr> <td>(Nitrogen):</td> <td>~ 20 kg</td> </tr> </table>	S/C length:	5,300 mm	S/C width:	2,360 mm	Body diameter:	1,000 mm	Wet Mass:	1,120 kg	Propellant mass (Xenon):	40 kg	(Nitrogen):	~ 20 kg
S/C length:	5,300 mm												
S/C width:	2,360 mm												
Body diameter:	1,000 mm												
Wet Mass:	1,120 kg												
Propellant mass (Xenon):	40 kg												
(Nitrogen):	~ 20 kg												
On-board Ion Propulsion System	<ul style="list-style-type: none"> <li>• 2 Gridded Ion Engines (T5 from QinetiQ); 1 main + 1 red.</li> <li>• first usage of Ion Engines for Drag-free Control with commandable thrust between 1 mN to 20 mN, each engine</li> </ul> <p>The Ion-Propulsion Systems is used for:</p> <ul style="list-style-type: none"> <li>• air drag compensation</li> <li>• Orbit raising</li> <li>• Gradiometer calibration (sine profile in flight direction)</li> </ul>												

<p>Ion Propulsion Module</p>   <p>Proportional Xenon Flow Assemblies (PXFA)</p>  <p>Ion Thruster Assemblies (ITA)</p>   <p>Ion Propulsion Power Control Units (IPCU)</p>	 <p>arranged on the -X panel (diameter: 1,000 mm)</p>
<p>Ion Propulsion Assembly Schematic</p>	
<p>Ion Propulsion Mass Budget:</p>	<p>Total mass of the redundant Ion Propulsion System:</p>

	<ul style="list-style-type: none"> <li>• dry mass: <span style="float: right;">64 kg</span></li> <li>• Xenon mass: <span style="float: right;">41 kg</span></li> </ul>						
<p>Ion Engine performance requirements</p>	<p>The GOCE mission requires the edge-of-performance achievable with engine + IPCU and PXFA, in terms of commandability and noise.</p> <p>Two closed loops to achieve the required commandability:</p> <ul style="list-style-type: none"> <li>• 100 Hz loop for anode voltage and magnet current</li> <li>• 10 Hz loop for Xenon mass flow.</li> </ul> <p>Performance requirements:</p> <ul style="list-style-type: none"> <li>• total impulse per engine: <span style="float: right;">795,500 Ns</span></li> <li>• variable thrust: <span style="float: right;">1 mN - 20 mN</span></li> <li>• Isp = 3,000 s at 20 mN Isp = 2,300 s at 8.3 mN Isp = 500 s at 1 mN</li> <li>• command rate: <span style="float: right;">10 Hz</span></li> <li>• thrust increments: <span style="float: right;">12 - 250 µN</span></li> <li>• thrust variation capability: <table style="margin-left: 20px; border: none;"> <tr> <td style="padding-right: 20px;">100 ms</td> <td style="padding-right: 20px;">0.25 mN</td> </tr> <tr> <td style="padding-right: 20px;">1,000 ms</td> <td style="padding-right: 20px;">0.64 mN</td> </tr> <tr> <td style="padding-right: 20px;">10,000 ms</td> <td style="padding-right: 20px;">1.80 mN</td> </tr> </table> </li> <li>• thrust response: 60 ms for 95 % of commanded step</li> <li>• thrust vector stability over life and range: <span style="float: right;">0.2 ° half-cone</span></li> </ul>	100 ms	0.25 mN	1,000 ms	0.64 mN	10,000 ms	1.80 mN
100 ms	0.25 mN						
1,000 ms	0.64 mN						
10,000 ms	1.80 mN						

<p>Ion Engine noise</p>	 <p>ITA = Ion Thruster Assembly</p> <p>IPA = overall Ion Propulsion Assembly (incl. IPCU, PXFA, ITA)</p>
<p>Control of transverse axes and attitude control:</p>	<p>Initial intention was to use FEEPs. Due to their non-availability for GOCE, no drag-free control in these axes. Air coils are use for attitude control also during Science Mode. For calibration purposes, the GCA replaced the FEEPs, see below.</p>
<p>Gradiometer Calibration Assembly (GCA)</p>	<p>Cold Gas Propulsion System for Gradiometer calibration in the two lateral axes with trapezoidal thrust profiles of 600 <math>\mu\text{N}</math> plateau</p> <ul style="list-style-type: none"> <li>• tankage: 75 ltr at 185 bar</li> <li>• 8 cold-gas micro-thrusters</li> </ul>
<p>Magnetic cleanliness</p>	<p>overall magnetic moment: <math>&lt; 4 \text{ A m}^2</math></p> <p>gradiometer is shielded</p>
<p>Chemical cleanliness</p>	<p>no issue</p>
<p>Heritage:</p>	<ul style="list-style-type: none"> <li>• ONERA Gradiometer (derived from GRACE)</li> </ul>

	<ul style="list-style-type: none"> <li>• ARTEMIS Ion Propulsion</li> </ul> <p>GOCE itself will provide heritage for:</p> <ul style="list-style-type: none"> <li>• future applications of Gridded Ion Engines</li> <li>• Proportional Xenon Flow Assembly, which is at the currently achievable limit of response and flow control accuracy</li> </ul>
References	<p>[1] GOCE Ion Propulsion Assembly / Gradiometer Calibration Assembly Design Description</p> <p>GO-DD-ASG-0002, issue 1, dated Feb 2004</p>

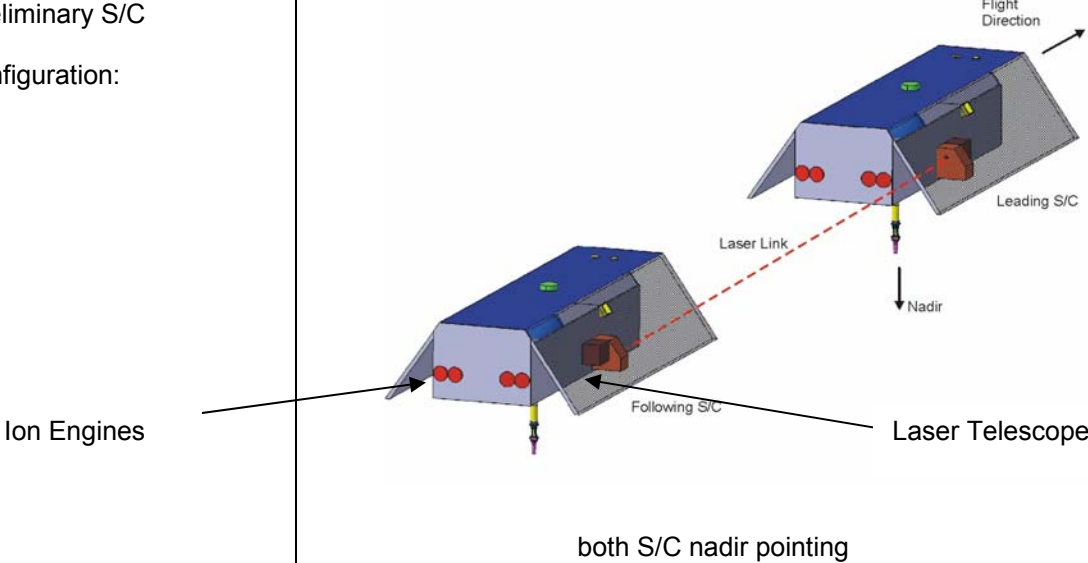
Bernd Schuerenberg, May 2005

### Abbreviations:

GCA	Gradiometer Calibration Assembly
GPS	Global Positioning System
IPA	Ion Propulsion Assembly
IPCU	Ion Propulsion Control Unit (synonym: Power Supply and Control Unit)
ITA	Ion Thruster Assembly
LEO	Low Earth Orbit
PXFA	Proportional Xenon Flow Assembly
S/C	spacecraft

### 4.10 Laser Doppler Interferometer (LDI)

Mission type:	Solid Earth mission employing satellite-satellite tracking with laser interferometer
Mission class	<p>anticipated next Solid Earth mission (Post-GRACE mission);</p> <p>proposal for Mission Definition Study submitted in April 2004;</p> <p>Mission Definition Study by Alenia ongoing till mid-2005;</p> <p>Technology Development Activities starting in 2006;</p>

	Phase A in 2009 / 2010
Launcher, Orbit	<ul style="list-style-type: none"> <li>• dual-launch in 2016 with ROKOT (or DNEPR) from Plesetsk</li> <li>• 2 satellites on polar LEO (~ 400 km altitude, <math>i = 90^\circ</math>), separated approx. 100 km</li> <li>• satellite configuration similar to the GRACE satellites</li> </ul>
Preliminary S/C configuration:	 <p style="text-align: center;">both S/C nadir pointing</p>
Payload and mission objective	<p>Gravity gradient along line-of-sight between the 2 satellites shall be measured with an accuracy 10 x better than GRACE. The separation of the two satellites (~ 100 km) is the gradiometer baseline.</p> <p>The satellites carry:</p> <ul style="list-style-type: none"> <li>• Accelerometer with free-floating Proof Mass (PM), each; (accelerometer must be close to CoM / on the pitch axis; else a forced orbit must be flown)</li> <li>• Laser Doppler Interferometer for PM-to-PM metrology</li> <li>• Drag-Free and Attitude Control System (DFACS) employing             <ul style="list-style-type: none"> <li>(a) Ion Engines (along track control)</li> <li>(b) FEEP or Cold-Gas Micro-Propulsion System (for cross-</li> </ul> </li> </ul>

	<p style="text-align: center;">track, fine attitude control, and for gradiometer calibration)</p> <p>Objectives are:</p> <ul style="list-style-type: none"> <li>determination of spherical harmonics up to degree 180 - 240</li> </ul>
Measurement accuracies and DFACS requirements	<p>Measurement accuracies:</p> <ul style="list-style-type: none"> <li>distance measurement accuracy: 10 nm (rms over 10 s) (<math>3 \times 10^{-7}</math> m /<math>\sqrt{\text{Hz}}</math> over MBW)</li> <li>acceleration measurement accuracy : <math>10^{-10}</math> - <math>10^{-9}</math> m/s<sup>2</sup>; measurement bandwidth (MBW) <math>10^{-4}</math> Hz - <math>10^{-1}</math> Hz (<math>4 \times 10^{-11}</math> m/s<sup>2</sup> /<math>\sqrt{\text{Hz}}</math> over MBW)</li> </ul> <p>Requirements on DFACS:</p> <ul style="list-style-type: none"> <li>DFACS shall reduce the accelerations at the Accelerometer to less than <math>5 \times 10^{-9}</math> m/s<sup>2</sup> (TBC)</li> </ul> <p><b>Note:</b> wide MBW !</p>
Laser Telescope Pointing Actuator (PAT)	<p><b>Note:</b> Each laser telescope is provided with a Pointing Actuator (PAT), because the AOCS with Star Trackers and Differential GPS (attitude and rate of baseline) is not sufficient to align the laser beams.</p> <ul style="list-style-type: none"> <li>fine pointing of laser telescopes: <ul style="list-style-type: none"> <li>- absolute pointing error: ~ 10 microrad</li> <li>- stability: 0.6 microrad /<math>\sqrt{\text{Hz}}</math> over <math>10^{-4}</math> Hz - <math>10^{-1}</math> Hz</li> </ul> </li> </ul>
Mission duration	up to 10 years in LEO
S/C dimensions and mass	<p>S/C dimensions:</p> <p style="text-align: right;">3,700 mm length</p> <p style="text-align: right;">2,000 mm width</p> <p style="text-align: right;">800 mm height</p>



	<p>Cross-section to air drag: <span style="float: right;">1.3 m<sup>2</sup></span></p> <p>Launch mass: <span style="float: right;">650 kg, each</span></p> <p>Propellant mass (Xenon) <span style="float: right;">22 kg</span></p>
<p>On-board Propulsion</p>	<p>Two Propulsion Systems shall be flown on-board each satellite:</p> <p>(a) Gridded Ion Engines (2 x 2 per satellite)</p> <ul style="list-style-type: none"> <li>• initial formation acquisition, after separation from launcher</li> <li>• drag-free control along X axis (1 DOF): <ul style="list-style-type: none"> <li>- air drag compensation</li> <li>- radial gravity gradient effect (forced orbit, if Accelerometer cannot be located at CoM)</li> </ul> </li> <li>• formation maintenance: <ul style="list-style-type: none"> <li>- remove effect of Accelerometer bias error; <ul style="list-style-type: none"> <li>10<sup>-6</sup> m/s<sup>2</sup> accelerometer bias causes a separation change of approx. 15 km/day (strategy not yet determined)</li> </ul> </li> </ul> </li> <li>• formation changes (different separation up to 1,000 km - TBC)</li> <li>• orbit maintenance manoeuvres (infrequent)</li> </ul> <p>(b) Micro-Propulsion System (FEEP thrusters assumed):</p> <ul style="list-style-type: none"> <li>• drag-free control in 2 cross-track axis <ul style="list-style-type: none"> <li>- transverse gravity gradient effect (forced orbit, if Accelerometer cannot be located at CoM)</li> <li>- compensation of solar pressure and high-altitude gust effects</li> </ul> </li> <li>• fine attitude control (3 DOF)</li> </ul>
<p>Ion Engine arrangement:</p>	<p>See figure, above</p>

<p>Ion Engine performance requirements</p>	<ul style="list-style-type: none"> <li>• total impulse capability of each engine: ~ 400,000 Ns</li> <li>• specific impulse: Isp ~ 3,700 s</li> <li>• min. / max. thrust: GOCE thrust range (1 - 20 mN) or lower, if suitable engines are available</li> <li>• use GOCE requirements as preliminary reference (= performance limits of current Ion Propulsion Systems for DFACS)</li> </ul>
<p>FEEP thruster arrangement:</p>	<p>not yet defined; must support 5 DOF; probably 12 FEEP thrusters, total; including redundancy; FEEP arrangement must avoid coupling into flight / anti-flight direction</p>
<p>FEEP performance requirements</p>	<p>Requirements generated for HYPER and / or LISA Pathfinder are used as reference:</p> <ul style="list-style-type: none"> <li>• total impulse per thruster: ~ 20,000 Ns</li> <li>• overall ~ 4 kg of liquid metal propellant (Isp ~ 7,000 s)</li> <li>• max thrust: 100 <math>\mu</math>N</li> <li>• min thrust: 1.0 <math>\mu</math>N</li> <li>• rate of change: <math>\leq 10 \mu</math>N/s; command update rate: 10 Hz</li> <li>• resolution of commanded thrust &lt; 0.1 <math>\mu</math>N (requirement TBC)</li> <li>• thrust response: &lt; 100 ms for 95 % of commanded step</li> </ul>

<p>Ion Thruster noise</p>	<p>Ion Engines (as achievable with Gridded Ion Engines, including Flow Control and IPCU; information from GOCE specification)</p> <div data-bbox="587 510 1374 969" data-label="Figure"> <p>The graph, titled "IPA Noise Spectral Density", is a log-log plot. The y-axis represents PSD [N/m²/√Hz] ranging from 1.E-06 to 1.E-02. The x-axis represents Frequency [Hz] ranging from 0.0001 to 100.0000. Two curves are shown: a green line for IPA and a blue line for ITA. Both curves show a decreasing trend with frequency, with the ITA curve being consistently lower than the IPA curve. The ITA curve starts at approximately 1.E-03 at 0.001 Hz and drops to about 1.E-05 at 10 Hz. The IPA curve starts at approximately 5.E-03 at 0.001 Hz and drops to about 2.E-05 at 10 Hz.</p> </div> <p>ITA = Ion Thruster Assembly          IPA = overall Ion Propulsion Assembly (incl. IPCU, PXFA, ITA)</p>
<p>FEEP thruster noise</p>	<p>FEEP thrusters (as achievable with FEEP thrusters + PCU)</p> <div data-bbox="550 1279 1193 1675" data-label="Figure"> <p>The graph, titled "FEEP", is a log-log plot. The y-axis represents Spectral Density N/sqrt(Hz) ranging from 10<sup>-7</sup> to 10<sup>-3</sup>. The x-axis represents Frequency [Hz] ranging from 10<sup>-4</sup> to 10<sup>0</sup>. A blue curve shows the spectral density, which is constant at approximately 10<sup>-3</sup> N/sqrt(Hz) up to about 10<sup>-3</sup> Hz, then decreases to about 10<sup>-6</sup> N/sqrt(Hz) at 10<sup>-2</sup> Hz, and remains constant thereafter. A green horizontal line is drawn at approximately 10<sup>-6</sup> N/sqrt(Hz).</p> </div>
<p>Magnetic cleanliness</p>	<p>affects Accelerometers, and produces disturbance torques on LEO, which must be compensated by DFACS</p>
<p>Chemical cleanliness</p>	<p>only an issue with FEEP thrusters; constraint for FEEP thruster arrangement!</p>

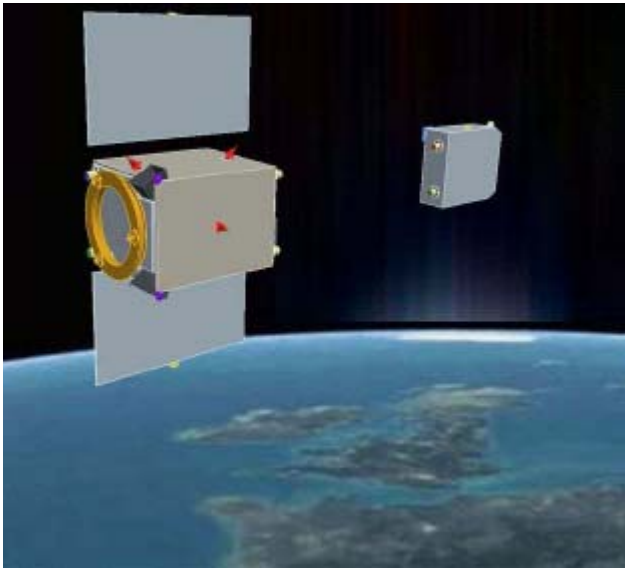
Heritage	<p>GOCE: Ion Engines and DFACS on LEO</p> <p>LISA Pathfinder: FEEP micro-propulsion and DFACS</p> <p>LISA: Laser Doppler Interferometry</p>
References	<p>[1] Enabling Observation Techniques for Future Solid Earth Missions; ESA contract no. 16668/02/NL/MM; Final Report, July 2004</p> <p>[2] LDI Proposal for Mission Definition Phase in response to ESA ITT No. AO/1-4435/04/NL/CP, submitted in April 2004</p> <p>[3] Executive Summary of the Mission Definition Study, Alenia, available in 2nd half of 2005</p>

Abbreviations:

AOCS	Attitude and Orbit Control Subsystem
CoM	centre of mass
DFACS	drag-free and attitude control system
DOF	degree-of-freedom
FEEP	Field Emission Electric Propulsion
LEO	Low Earth Orbit
MBW	Measurement Bandwidth
PAT	Pointing Actuator
PM	Proof Mass

### 4.11 PRISMA

Mission type:	demonstrator mission for autonomous formation flying and rendezvous technology
Mission class	<p>Swedish national program consisting of two micro-satellites;</p> <p>low-cost program (&lt; 25 MEuro for development, launch and operations), plus in-kind contributions from D, DK and F</p> <p>Prime contractor is Swedish Space Corporation</p>

	<p>kick-off at end of 2004; PDR at end of 2005;</p> <p>anticipated launch in 2<sup>nd</sup> half of 2008</p>
<p>Launcher, Orbit</p>	<ul style="list-style-type: none"> <li>• Dual-launch with ROKOT (together with PICARD of CNES)</li> <li>• Sun synchronous orbit (SSO), altitude: approx. 700 km / dawn-dusk orbit</li> </ul>
<p>Preliminary S/C configuration:</p>	<div data-bbox="671 669 1299 1234" data-label="Image">  </div> <p>Two cube-shaped micro-satellites:</p> <p>MAIN satellite is fully manoeuvrable; m = 140 kg</p> <p>TARGET sub-satellite is not manoeuvrable; m = 40 kg</p>
<p>Mission objectives</p>	<p>PRISMA is up to now the only demonstrator available for autonomous and precise formation flying (FF) and rendezvous (RV) sensor technologies, which are needed for a number of future missions:</p> <ul style="list-style-type: none"> <li>• DARWIN coarse FF and collision avoidance</li> <li>• LEO radar missions using formation flight</li> <li>• In-orbit servicing, e.g. ConeXpress</li> </ul>
<p>Payload / Experiments</p>	<p>PRISMA has two mission objectives:</p>

	<p>(a) validation of sensors and actuators related to formation flying:</p> <ul style="list-style-type: none"> <li>• Vision Based Sensor (VBS) based on star tracker technology (by Danish Technical University and SSC)</li> </ul>
<p>Payload / experiments (cont.)</p>	<ul style="list-style-type: none"> <li>• GPS based navigation experiment for automatic formation flying (High-grade single-frequency Phoenix GPS receiver: code tracking accuracy &lt; 0.5 m carrier-phase accuracy &lt; 1 mm mass 50 g power demand 0.8 W)</li> <li>• formation flying RF (FFRF) metrology package provided by ALCATEL and CNES</li> <li>• High-Performance Green Propellant (HPGP) system by ECAPS (SSC + Volvo Aero) to replace hydrazine thrusters</li> </ul> <p>(b) demonstration of experiments for the in-flight validation of guidance / navigation strategies for spacecraft formation flying and rendezvous. PRISMA is a precursor / test bed for critical technologies needed for</p> <ul style="list-style-type: none"> <li>• advanced formation flying (e.g. DARWIN)</li> <li>• in-orbit servicing</li> <li>• close-range proximity operations.</li> </ul> <p>(c) secondary mission objectives:</p> <ul style="list-style-type: none"> <li>• test of the silicone-based MEMS cold-gas microthruster system of</li> </ul>

	<p>NanoSpace AB (owned by SSC and Lars Stenmark)</p> <hr/> <p>DLR involvement in these experiments:</p> <ul style="list-style-type: none"> <li>• GPS based navigation system for absolute and relative navigation. Each satellite carries 2 independent GPS receivers (for redundancy and coverage reasons); inter-satellite link between MAIN and TARGET satellite.</li> <li>• Space-borne Autonomous Formation Flying Experiment (SAFE): autonomous, robust and precise formation flying at distances of 100 m to 2,000 m. Precursor for future radar missions in close formation flight.</li> </ul>
Mission duration	8 months in LEO
S/C mass	<p>Launch mass of Main Satellite: 140 kg</p> <p>Launch mass of Sub-Satellite: 40 kg</p>
Green Propulsion System of MAIN satellite	<ul style="list-style-type: none"> <li>• uses storable ammonium dinitramite (ADN) + additives</li> <li>• Rhenium catalyst; Isp comparable to hydrazine</li> <li>• 6 1N thrusters pointing through CoG (torque-free manoeuvres)</li> <li>• thrusters arrangement: see figure (indicated red)</li> </ul>
Micro-Propulsion System (MPS)	<p>MEMS nitrogen cold gas system delivering continuous, throttleable thrust</p> <p>Thrust level: 10<math>\mu</math>N to 1 mN</p> <p>Produced by NanoSpace AB / Sweden. Experiment only, because technology not yet mature. Possibly included in some closed loop tests.</p> <p>MPS comprises two pods with 4 thrusters, each</p>

Thruster arrangements:	<ul style="list-style-type: none"> <li>Green CPS: thrusters point through COG, suited for manoeuvres in 3D</li> <li>MPS: in 4 orthogonal directions, each pod</li> </ul>
MPS performance requirements	No information yet.
References	<p>[1] IAC-05-B5.6.B.07: S. Persson, B. Jacobsson, E. Gillnabing Observation Techniques for Future Solid Earth Missions; ESA contract no. 16668/02/NL/MM; Final Report, July 2004</p>

### 4.12 PROBA 3

Mission type:	Technology demonstration mission for DARWIN
Mission objective:	<p>In-orbit test-bed for Formation Flying and interferometry:</p> <ul style="list-style-type: none"> <li>guidance, navigation and control strategies</li> <li>metrology between satellites</li> <li>etc.</li> </ul>
Status:	<p>Necessary mission, but not yet defined.</p> <p>Will fly suitable Micro-Propulsion Systems, as needed for DARWIN.</p>

### 4.13 DARWIN

Mission type:	Astronomy: Search for Earth-like Exo-Planets
Mission class	<p>Candidate cornerstone mission;</p> <p>On-going TRP activities;</p>



	System Assessment Study starting in 2nd half of 2005
Launcher, Orbit	<ul style="list-style-type: none"> <li>• launch in 2015 +</li> <li>• shared launch with two Soyuz-Fregat launches</li> <li>• direct injection from HEO into cruise trajectories towards halo orbits around L2 with one Bi-propellant Propulsion Module (PM) for each satellite launch pair</li> <li>• 100 - 200 days of coast to L2, where the 4 satellites are precisely positioned for formation flying</li> </ul>
Payload and mission objective	<p>New baseline of DARWIN comprises 4 satellites:</p> <ul style="list-style-type: none"> <li>• 3 Telescope Spacecraft (TS)</li> <li>• 1 central hub &amp; master satellite, which collects and combines the light from the 3 telescopes, and which is used for the communication Earth ↔ flotilla (Beam Combiner Spacecraft (BCS))</li> </ul> <p>Scientific objectives are:</p> <ul style="list-style-type: none"> <li>• multi-axial nulling interferometry to search for exo-planets around close, sun-like target stars</li> <li>• spectroscopy of exo-planets for life traces</li> <li>• imaging interferometry for general astronomy</li> </ul>
Formation Flying and Observation conditions:	<ul style="list-style-type: none"> <li>• radius of formation: (10) 25 -250 m</li> <li>• relative positioning accuracy ~ 1 mm, each axis (with RF and laser metrology)</li> <li>• Optical Path Difference stability &lt; 15 nm</li> </ul>

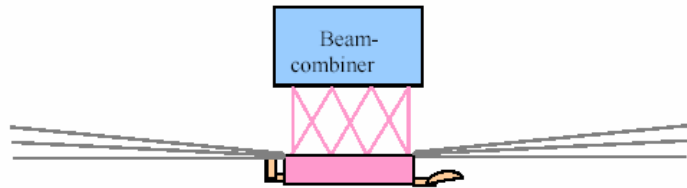
	<ul style="list-style-type: none"> <li>GNC control accuracy better than 5 nm rms</li> <li>Integration time 20 hours and longer</li> <li>Triangular formation rotates about LOS, if needed ~ 180° per day (forced formation flying ⇒ continuous FEEP thrusting)</li> </ul>
Mission duration	<ul style="list-style-type: none"> <li>approx. 100 days of cruise towards L2</li> <li>≤ 3 months of commissioning at L2</li> <li>5 years around L2 (nominal mission lifetime)</li> <li>5 years of mission extension (goal)</li> </ul>
Mission Phases and Operation Modes:	<ul style="list-style-type: none"> <li>LEOP (launch of launch pair; insertion into escape orbit; formation deployment with all S/C deployed and sun pointing)</li> <li>Cruise Phase to L2 (including checkout of metrology sub-systems and of formation flying)</li> </ul>
	<ul style="list-style-type: none"> <li>Science Operations Phase (70 % for science observations; 30 % for formation reconfigurations and fringe acquisition)</li> </ul>
Constellations:  (a) triangular configuration (TS's equilateral from BCS)	

<p>(b) linear configuration (requires long Optical Delay Lines on BCS, in order to equalise the optical path lengths)</p>	
<p>Orbit and instantaneous access to sky</p>	<ul style="list-style-type: none"> <li>• injection into halo orbit without extra delta-v results in a large orbit amplitude around L2</li> <li>• off-set pointing from sun direction: up to 45° half-cone (i.e instantaneous access of 15 % of the sky)</li> </ul>
<p>Telescope S/C configuration and dimensions:</p>	<p>Spacecraft mass ~ 900 kg</p> <p>Telescope diameter: 3,1500 mm</p> <p>Telescope height (mounting plate to entrance plane: ~ 5,200 mm</p> <p>Sun Shield + Solar Array diameter (similar to GAIA) ~ 10 m</p>

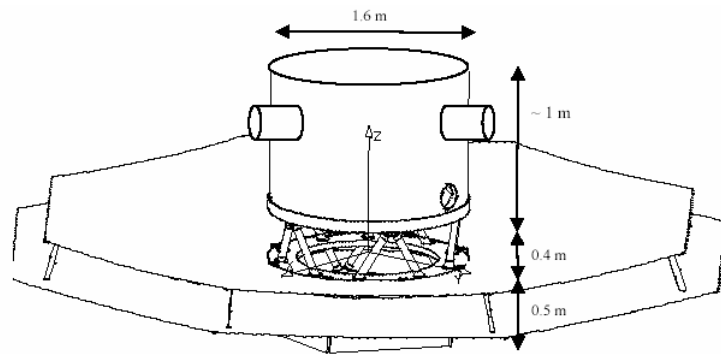


Beam Combiner Spacecraft  
configuration:

(a) schematic



(b) preliminary configuration



<p>Modes of Operation:</p> <p>green: milli-N propulsion</p> <p>pink: micro-N propulsion</p> <p>yellow: transitional</p>	<p>Delivered onto Escape Orbit by PM</p> <pre> graph TD     Start[Delivered onto Escape Orbit by PM] --&gt; FD[Formation Deployment]     FD --&gt; CM[Cruise Mode]     CM --&gt; OC[Orbit Correction Mode]     OC --&gt; CM     CM --&gt; CF[Coarse Formation]     CF --&gt; BCM[Baseline Control Mode]     BCM --&gt; FAM[Fringe Acquisition Mode]     FAM --&gt; BCM     FAM --&gt; NOM[Normal Observation Mode]     NOM --&gt; FAM     NOM --&gt; RM[Reconfiguration Mode]     RM --&gt; BCM     </pre>
<p>Metrology Systems</p>	<p>measure attitude and relative positions, as needed by the APCS in order to deploy and to control the formation in the different modes, chain of metrology systems allows to refine measurement accuracy from coarse metrology to high accuracy, as needed to start Fringe Acquisition Mode (FAM)</p>

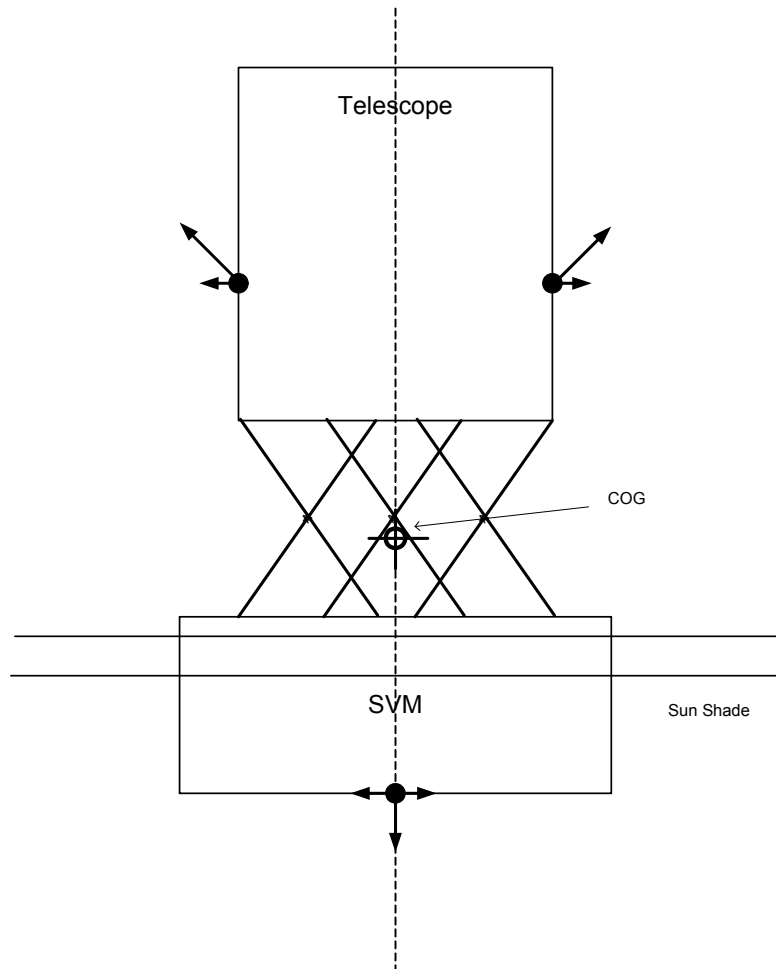
	<p><b>(a) Pointing Metrology</b></p> <p>(a.1) Wide-Field Camera (WFC) = high-performance star tracker on each Telescope S/C 1024 x 1024 pixel CCD at 40°K accuracy: ~ 0.1 arcsec (<math>1\sigma</math>) at 10 Hz, normal to LOS ~ 30 arcsec (<math>1\sigma</math>) at 10 Hz, about LOS</p> <p>(a.2) Star Tracker on Beam Combiner S/C (BCS): accuracy: ~ 1 arcsec (<math>1\sigma</math>) at 10 Hz, normal to LOS ~ 100 arcsec (<math>1\sigma</math>) at 10 Hz, about LOS</p> <p>(a.3) Co-Alignment Metrology System laser beams from BCS are imaged onto the WFC of each TS (= high-precision co-alignment)</p> <p><b>(b) Position Metrology</b></p> <p>(b.1) RF metrology operating up to 6 km range coarse position determination: 0.2 cm in range at 25 - 250 m distance; &lt; 0.1° attitude</p> <p>(b.2) Coarse lateral metrology He-Ne Laser (1° full angle) from BCS onto the corner cubes on the TS's accuracy: ~ 1 mm at 10 Hz, lateral directions operating range: 2 cm</p> <p>(b.3) Fine lateral metrology</p>
--	--

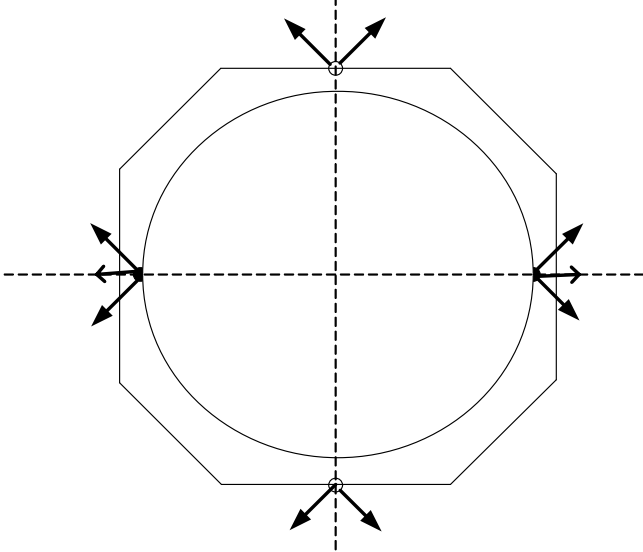
	<p>collimated laser beam from BCS onto dedicated CCD detector on each TS</p> <p>accuracy: ~ 32 <math>\mu\text{m}</math> rms at 10 Hz, lateral directions</p> <p>(b.4) Fine longitudinal metrology</p> <p>Nd-Yag lasers + send / receive optics on BCS, and retro-reflector on each TS</p> <p>accuracy of absolute distance: ~ 32 <math>\mu\text{m}</math> rms at 10 Hz</p> <p><b>(c) Fringe Sensor</b></p> <p>measures relative phase of the 3 beams. Error signal is used for optical path length stabilisation with the Optical Delay Lines.</p>
On-board Propulsion:	<p>(a) milli-N Propulsion System for satellite coarse GNC (orbit acquisition, orbit maintenance, coarse control)</p> <p>(b) micro-N Propulsion System (for science mode)</p>
Milli-N Propulsion System	<p>Technology not yet selected. In RD-1, small ion engines are recommended.</p> <p>Small HEMP thrusters are also conceivable.</p> <p>Cold Gas Micro-thruster Isp is too low.</p>
Micro-N Propulsion System	<p>Technology not yet selected. In RD-1, FEEP engines are recommended.</p> <p>Also conceivable are micro-ion engines - to be investigated in System Assessment Study.</p>
Thruster configurations:	<p>both, the milli-N Propulsion System and the micro-N Propulsion System must support 6 DOF control.</p>



(a) possible arrangement of the micro-N thrusters

- 12 mN thrusters + TBD redundancy
- 12  $\mu$ N thrusters + TBD redundancy



	 <p>In RD-1, 4 clusters of 3 micro-engines each are assumed; 2 on the SVM and 2 on the PLM.</p> <p>Redundancy concept needs yet to be established.</p>
<p>Milli-N thruster performance requirements:</p>	<p>Muß noch erarbeitet werden</p>
<p>Milli-N thruster life-time requirements:</p>	<p>TBD</p>
<p>Micro-N thruster performance requirements:</p>	<p>Muß noch erarbeitet werden</p>
<p>Micro-N thruster life-time requirements:</p>	<p>TBD</p>
<p>Comparison of micro-ion</p>	<p>Muß noch erarbeitet werden</p>

engine and FEEP performance requirements:	(es sieht so aus, als wären die FEEPs besser, als für DARWIN benötigt, d.h. micro-Ion Engines mit Pulse Width Modulation kämen wahrscheinlich auch in Frage - TBD)
Contamination aspects:	The PLM of the Telescope S/C and of the Beam Combiner S/C are at cryogenic temperatures !!! FEEP engines should be avoided, because they use liquid metal for propellant and have a very large beam width (40 - 60° half-cone)
Heritage:	LISA Pathfinder: FEEP Micro-Propulsion, if used on DARWIN  PROBA-3 or SMART-3: Formation Flying, technology for interferometry (not mandatory)
Reference Documents:	RD-1: DARWIN / TTN+ Mission Design Assessment,  ESA SCI-A/2004/187/DARWIN/DMS, issue 1.2,  December 2004

### Abbreviations:

APCS	Attitude and Position Control System
BCS	Beam Combiner Spacecraft
CGMT	Cold-Gas Micro-Thrusters
FAM	Fringe Acquisition Mode
FEEP	Field-Emission Electric Propulsion
GNC	Guidance, Navigation, and Control
HEO	Highly-Eccentric Orbit
L2	Second Earth-Sun libration point
LEOP	Launch and Early Orbit Phase
LOS	Line-of-Sight
MS	Metrology Sensor
NOM	Nominal Observation Mode
OCM	Orbit Correction Mode
ODL	Optical Delay Line
OPD	Optical Path Difference
OPL	Optical Path Length
PLM	Payload Module
PM	Propulsion Module for injection into HEO and escape orbit
RMT	Radio-Frequency with Magnetic Field Ion Thruster
S/C	Spacecraft
SVM	Service Module
TS	Telescope Spacecraft
WFC	Wide-Field Camera

### 4.14 Lunar Mission BW 1

Mission type:	Lunar mission with university small satellite
Mission class	<ul style="list-style-type: none"> <li>part of "Stuttgart Small Satellite Program" (3 small satellite missions by Institute of Space Systems / University of Stuttgart; technology demonstration, and lunar + cislunar science)</li> <li>Development Phase on-going; launch date: 2009, or later</li> </ul>
Launch, Mission Phases, and orbits	<ul style="list-style-type: none"> <li>launch as piggyback into GTO with GSLV</li> <li>Ascent Phase: ascent beyond van Allen belt</li> <li>Cruise Phase: Orbit extension up to Moon</li> <li>Capture Phase: insertion into highly elliptical lunar orbit</li> <li>Descent Phase: transfer to a circular polar orbit (h ~ 100 km)</li> <li>Science Phase: remote sensing of lunar surface; satellite +Z nadir oriented</li> <li>Impact Phase: controlled impact onto lunar surface.</li> </ul>
Mission duration	<ul style="list-style-type: none"> <li>flight to Moon: ~ 2 years (Ascent, Cruise, Capture, Descent)</li> <li>Science Phase on polar lunar orbit: ~ 6 months</li> </ul>
Payload and mission objective	<p>Objectives are:</p> <p>(a) technology test bed for:</p> <ul style="list-style-type: none"> <li>Solar Electric Propulsion (2 thermal Arcjets + 1 Pulsed Plasma Propulsion Subsystem for orbit transfer and attitude control)</li> </ul>

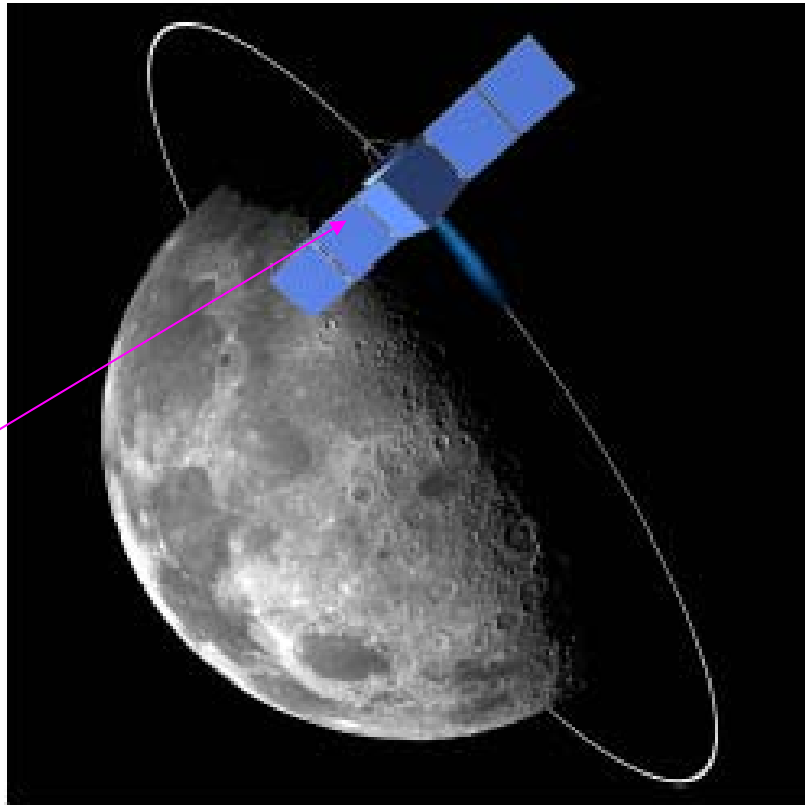
	<ul style="list-style-type: none"> <li>• IR imagers (visible/near IR and thermal IR) for smallsats</li> <li>• broad-band communication in Ka-band</li> <li>• new advanced computer architectures for enhanced on-board processing</li> <li>• complex mission operations from a University run "mission control centre"</li> </ul> <p>(b) Science:</p> <ul style="list-style-type: none"> <li>• remote sensing from low polar orbit:             <ul style="list-style-type: none"> <li>- high-resolution multi-spectral observation (IR imagers)</li> <li>- radar sounding</li> </ul> </li> <li>• cislunar science during Cruise (e.g. observation of near Earth objects)</li> </ul>
S/C dimensions and mass	<ul style="list-style-type: none"> <li>• launch mass <span style="float: right;">approx. 200 kg</span></li> <li>• Satellite (cube shaped) <span style="float: right;">1m x 1m x 1m</span></li> <li>• Solar Array (GaAs triple junction) <span style="float: right;">~ 6 m<sup>2</sup>, total</span> consisting of 2 body-mounted panels + 4 deployable panels in fixed positions</li> <li>• Available Solar Array power <span style="float: right;">~ 1,200 W max, EOL</span></li> <li>• Li-ion battery <span style="float: right;">100 Ah</span></li> </ul>

Preliminary S/C

configuration:

(a) deployed satellite on  
Lunar orbit during lunar  
orbit capture)

1m Ø Ka-band HGA



Artist's view of BW1 on Lunar orbit (from ref. [1])

orbit period: approx. 2 hours

<p>(b) Preliminary Schematic of the Thruster Arrangement on-board BW1</p>	<p>→ possible thruster arrangement (<b>still under optimisation</b>)</p> <p>→ instrument cameras view in + X direction</p>
<p>AOCS</p>	<ul style="list-style-type: none"> <li>• Fixed SA requires between target pointing and SA pointing attitude</li> <li>• 4 Reaction Wheels provide the needed agility for slews and target pointing acquisition</li> <li>• Onboard sensors: TBD</li> <li>• Pointing performance requirements: TBD (10 m resolution from Lunar orbit)</li> </ul>
<p>On-board Propulsion Subsystems and their usage</p>	<p>Two Propulsion Systems will be flown on-board BW1:</p> <p>(a) Thermal Arcjet for "fast" delta-V manoeuvres</p> <ul style="list-style-type: none"> <li>• orbit raising beyond van Allen belts</li> <li>• Lunar orbit capture</li> </ul>

	<ul style="list-style-type: none"> <li>controlled impact at EOL (if not with Cold Gas Thruster)</li> </ul> <p>(b) Pulsed Plasma Propulsion Subsystem (PPPS):</p> <ul style="list-style-type: none"> <li>comprising only 6 PPTs, due to mass limitations</li> <li>for attitude control, orbit transfer, and orbit control at Moon ("slow" low-thrust manoeuvres)</li> <li>attitude control tasks are RW off-loading and / or disturbance torque compensation</li> </ul>
Arcjet arrangement:	<ul style="list-style-type: none"> <li>number of Arcjets <span style="float: right;">1 main + 1 redundant</span></li> <li>both thrust vectors point through satellite CoM</li> </ul>
Arcjet characteristics and performance requirements	<ul style="list-style-type: none"> <li>Propellant: <span style="float: right;">ammonia</span></li> <li>total impulse capability: <span style="float: right;">&gt; 300,000 N s</span></li> <li>specific impulse: <span style="float: right;">Isp ~ 500 - 600 s</span></li> <li>nominal thrust: <span style="float: right;">100 mN (each)</span></li> <li>on-board propellant mass <span style="float: right;">≥ 50 litres</span></li> <li>power demand during thrust periods <span style="float: right;">~ 1 kWatt</span> (requires battery support)</li> </ul>
PPT performance requirements	<ul style="list-style-type: none"> <li>Solid propellant <span style="float: right;">pure PTFE (Teflon®)</span></li> <li>total impulse per thruster (I<sub>total</sub>): <span style="float: right;">~ 100 (tbd) N s</span></li> <li>Impulse bit per thruster (I<sub>bit</sub>): <span style="float: right;">1.5 mN s</span></li> <li>pulse rate: <span style="float: right;">1 - 2 Hz</span></li> <li>average thrust (4 PPTs at 1 Hz): <span style="float: right;">6 mN</span></li> <li>specific impulse: <span style="float: right;">Isp ≥ 1,200 s</span></li> <li>thruster efficiency: <span style="float: right;">η ~ 22%</span></li> </ul>



	<ul style="list-style-type: none"> <li>• total number of pulses per PPT <span style="float: right;">26 x 10E6</span></li> <li>• PPT throttling capability: <span style="float: right; color: red;">TBD</span></li> <li>• energy storage of each discharge capacitor: <span style="float: right;">80 J</span></li> <li>• power demand of PPS (4 PPT at <span style="color: red;">TBD</span> Hz): <span style="float: right;">~ 250 W</span></li> <li>• propellant mass per PPT <span style="float: right;">PTFE rods of 750 mm length, each</span></li> </ul>																											
PPT usage and thruster arrangement	<ul style="list-style-type: none"> <li>• attitude control (3 DOF) and delta-V (1 DOF, in +X only)</li> <li>• attitude control requires disturbance torque compensation, respectively RW off-loading</li> <li>• during orbit transfer, continuous thrust profile with 4 PPTs</li> </ul> <p>The PPT arrangement (position and thrust vector) shown in figure, above, is still under optimisation.</p>																											
PPPS elements and mass budget	<table border="1" style="width: 100%; border-collapse: collapse; text-align: center;"> <thead> <tr> <th style="text-align: left;">Component</th> <th>QTY</th> <th>Mass (kg)</th> </tr> </thead> <tbody> <tr> <td>PPU: EMI Filter</td> <td>1</td> <td>tbd</td> </tr> <tr> <td>PPU: Charge Converter</td> <td>1</td> <td>tbd</td> </tr> <tr> <td>PPU: HV Switches</td> <td>4</td> <td>tbd</td> </tr> <tr> <td>PPU: Housing</td> <td>1</td> <td>tbd</td> </tr> <tr> <td>DI Circuits</td> <td>8</td> <td>tbd</td> </tr> <tr> <td>Capacitors</td> <td>4</td> <td>tbd</td> </tr> <tr> <td>Capacitor + DI housing</td> <td>1</td> <td>tbd</td> </tr> <tr> <td>PPT dry (w/o Teflon bars)</td> <td>8</td> <td>tbd</td> </tr> </tbody> </table>	Component	QTY	Mass (kg)	PPU: EMI Filter	1	tbd	PPU: Charge Converter	1	tbd	PPU: HV Switches	4	tbd	PPU: Housing	1	tbd	DI Circuits	8	tbd	Capacitors	4	tbd	Capacitor + DI housing	1	tbd	PPT dry (w/o Teflon bars)	8	tbd
Component	QTY	Mass (kg)																										
PPU: EMI Filter	1	tbd																										
PPU: Charge Converter	1	tbd																										
PPU: HV Switches	4	tbd																										
PPU: Housing	1	tbd																										
DI Circuits	8	tbd																										
Capacitors	4	tbd																										
Capacitor + DI housing	1	tbd																										
PPT dry (w/o Teflon bars)	8	tbd																										

	Teflon bars	8	tbd	
	<b>Total</b>		<b>xxx</b>	
Cleanliness	<ul style="list-style-type: none"> <li>chemical cleanliness affecting Solar Array</li> <li>instruments well-separated from PPTs and Arcjets.</li> </ul>			
Heritage	<ul style="list-style-type: none"> <li>FLYING LAPTOP and DESIRE / CERMIT are precursor missions to BW1 with respect to technical subsystems (→ not propulsion)</li> <li>SPACE ANGEL = test mission to verify EP technology (with one Arcjet + one PPT)</li> <li>PPT technology is established in USA, Russia, Japan</li> <li>long-life discharge igniters from Unison (California) are qualified for 25 million pulses</li> <li>AMSAT-P3D (OSCAR) 750 W Arcjet</li> </ul>			
References	<p>[1] R. Laufer, M. Auwetter-Kurtz, M. Lengowski, A. Nawaz, H-P. Roeser, M. von Schoenermark, H. Wagner: An All-Electrical Small Satellite for a Technology Demonstration and Science Mission to the Moon, IAC-04-IAF-Q.2.b.05</p> <p>[2] A. Nawaz, M. Auwetter-Kurtz, G. Herdrich, H. Kurtz: Experimental Setup of a Pulsed MPD Thruster at IRS; paper prepared for European Conference for Aerospace Sciences (EUCASS) in Moscow, July 2005</p>			

Abbreviations:

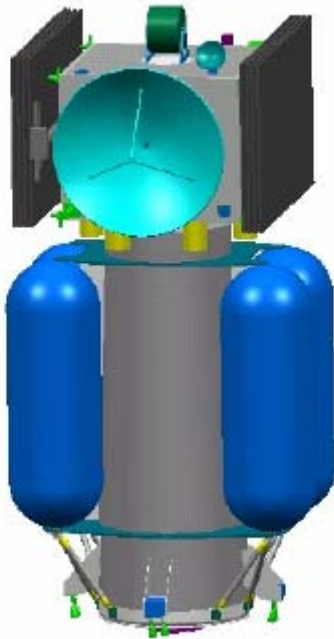
AOCS Attitude and Orbit Control Subsystem

BW1	"Baden-Wuerttemberg 1" lunar mission
Cap	Discharge capacitor / capacitor bench
CoM	centre of mass
DI	Discharge Igniter
DOF	degree-of-freedom
EOL	End-of Life
EP	Electric Propulsion
GTO	Geostationary Transfer Orbit
HGA	High-Gain Antenna
Ibit	impulse bit
Isp	specific impulse
Itotal	total impulse
IRS	Institut für Raumfahrt Stuttgart
PPPS	Pulsed Plasma Propulsion Subsystem
PPT	Pulsed Plasma Thruster
PPU	Power Processing Unit
SA	Solar Array

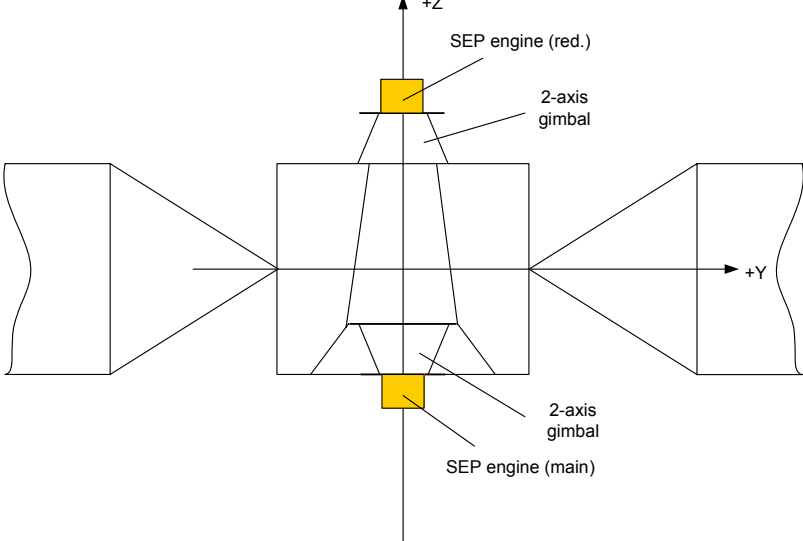
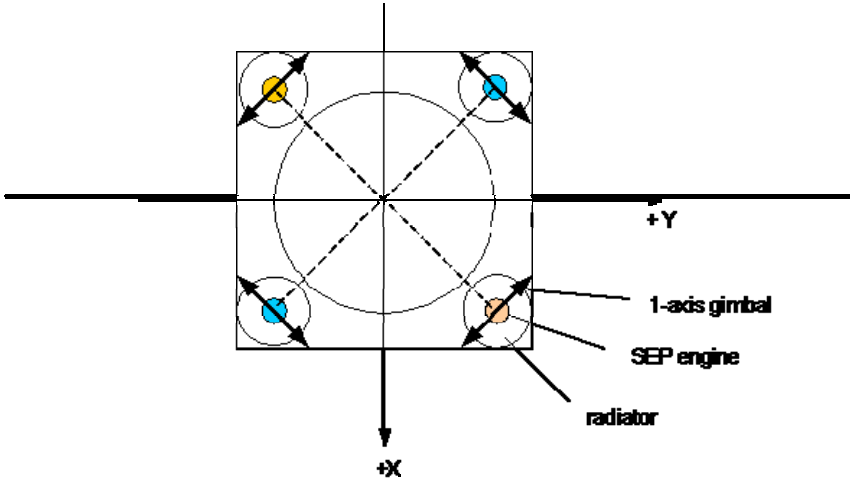
## 5 Other Missions

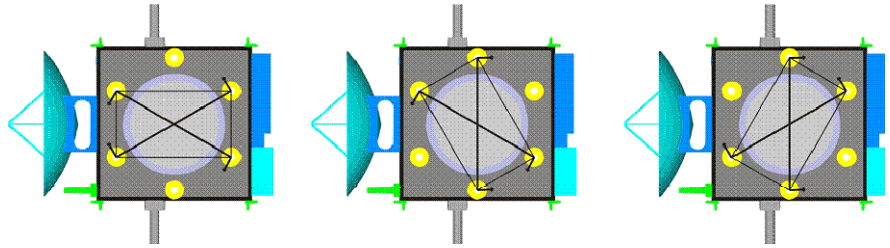
### 5.1 Don Quijote

Mission type:	Exploration of asteroid properties & technology demonstrator for planetary defense strategies
Mission class	Optional program selected by the Near-Earth Object Advisory Panel  National commitments yet open  Phase A starts at begin of 2006
Launcher, Orbit	2 satellites, which are launched separately: <ul style="list-style-type: none"> <li>• Orbiter to rendezvous and explore the asteroid</li> <li>• Impactor</li> </ul> Orbiter launched with: <ul style="list-style-type: none"> <li>• Small launcher + Propulsion Module for Earth escape</li> <li>• Electric Propulsion System for cruise to asteroid orbit</li> </ul> Impactor launched with: <ul style="list-style-type: none"> <li>• DNEPR (TBC)</li> <li>• Collision orbit acquisition with on-board bi-propellant system</li> </ul>

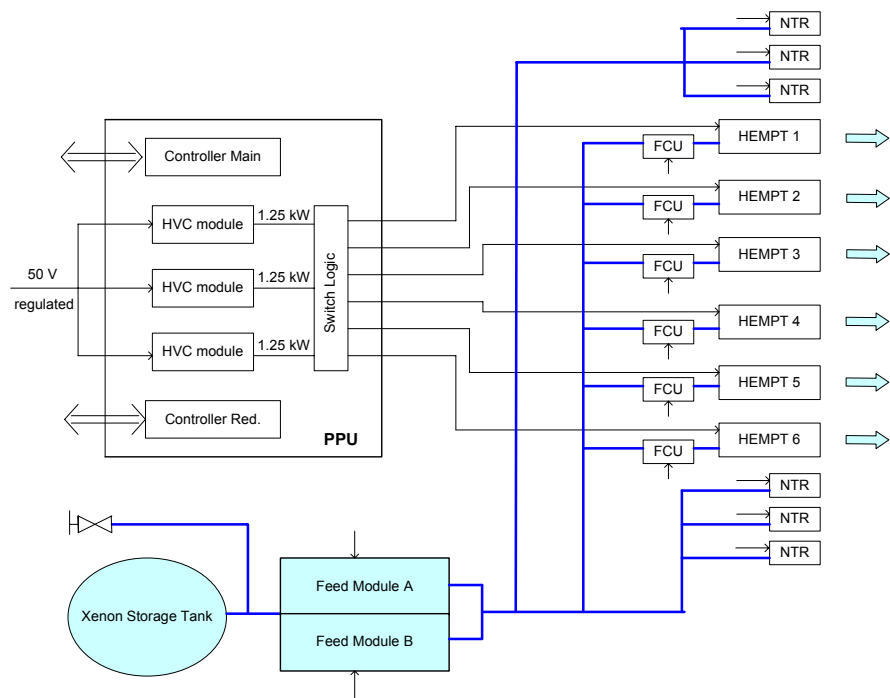
<p>Preliminary S/C configuration of Orbiter + Propulsion Module:</p>	
<p>Mission objectives</p>	<p>Orbiter:</p> <ul style="list-style-type: none"> <li>• Asteroid characterisation (mass, size, shape, gravity field)</li> <li>• precise orbit determination of asteroid (ephemerides) 6 months prior to impact and 6 months after impact</li> <li>• impact imaging from safe distance</li> </ul> <p>Impactor:</p> <ul style="list-style-type: none"> <li>• autonomous terminal navigation and impact to deflect asteroid (semi-major axis to change &gt; 100 m).</li> </ul> <p>Secondary mission objective:</p> <ul style="list-style-type: none"> <li>• Orbiter to deploy Autonomous Surface Package (ASP) after completion of primary mission</li> </ul> <p>Expected need for planetary defense:</p> <ul style="list-style-type: none"> <li>• Pre-2029 deflection of asteroid 99942 Apophys</li> </ul>

<p>Propulsion on-board Orbiter</p>	<p>(1) small hydrazine system with up to 22 x 1N thrusters:</p> <ul style="list-style-type: none"> <li>• for attitude control outside powered flight</li> <li>• for manoeuvres around asteroid, when not enough power is available for EPS</li> <li>• backup for EPS during proximity operations</li> </ul> <p>(2) Electric Propulsion System (EPS):</p> <ul style="list-style-type: none"> <li>• for thrust arcs to reach asteroid orbit (total delta-V ~ 3,000 m/s</li> <li>• sizable part of the manoeuvres during on asteroid orbit period</li> </ul>
<p>Propulsion onboard Impactor</p>	<p>Bi-propellant system integrated into the satellite and used for:</p> <ul style="list-style-type: none"> <li>• Earth escape</li> <li>• Terminal navigation</li> </ul>
<p>EPS concept for Orbiter</p>	<p>Total thrust throtttable form 100 mN down to 20 mN (TBC)</p> <p>Isp ~ 3,000 s</p> <p>Mission total impulse = 2,000,000 Ns</p> <p>Options to be traded in Phase A:</p> <p>(A) 2 Gridded ion Engines (T6 or RIT 22) on 2-axis gimbal, each (main and redudndant)</p>

	
<p>EPS concept for Orbiter (cont.)</p>	<p>(B) 4 engines (e.g. HEMP 3050) on 1-axis gimbal, each (main and redundant pair)</p>  <p>(C) 6 hard-mounted engines (HEMP 3050) (any 2 balanced pairs out of 3 balanced pairs)</p>

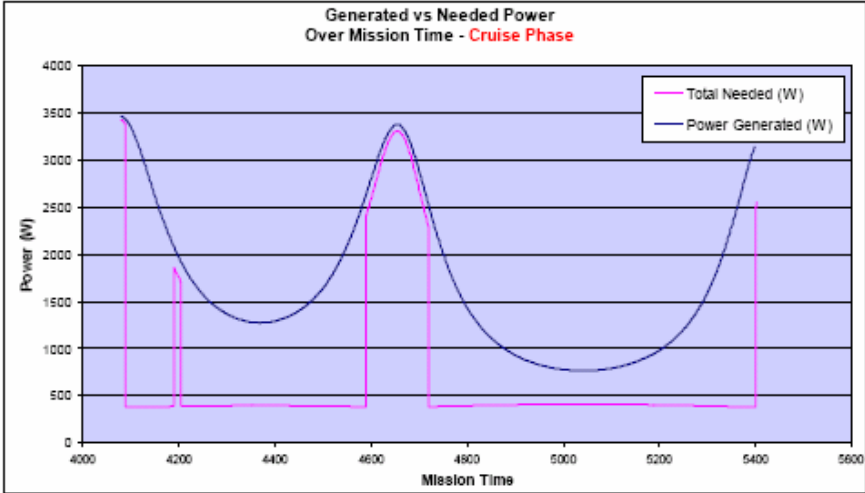


Flow schematic of EPS (resources sharing):



Orbiter Mission duration	Up to 8 years after Earth escape	
S/C mass	<ul style="list-style-type: none"> <li>• Orbiter dry mass (incl. 20% margin): 568 kg</li> <li>• Hydrazine fuel: ~ 12 kg</li> <li>• Xenon fuel for EPS: 67 kg</li> </ul>	
Orbiter power (EPS thrust arcs near perihelion shown in red):		



	<div data-bbox="549 322 1417 813" data-label="Figure">  </div> <p data-bbox="571 875 1235 969">shown is the cruise phase. On asteroid orbit, the power availability is even lower during apohelion.</p> <ul data-bbox="539 1084 1305 1187" style="list-style-type: none"> <li>• Impactor dry mass (incl. 20 % margin) ~ 940 kg</li> <li>• Bi-propellant mass ~ 2,630 kg</li> </ul>
References	<p data-bbox="539 1310 963 1462">[1] Technical Proposal Don Quijote Proposal No. A.2005-4483-0-1 November 2005</p>

## 6 Conclusions

The individual missions described above are very specific in their corresponding mission requirements. It is therefore recommended to use LISA Pathfinder and LISA as a reference scenario. However, it should be noted that the algorithm that is being developed in the framework of this study is a very general method that could also be applied to other mission, not necessarily being constrained to micro-propulsion applications.

The development status of the different thruster technologies is not yet satisfactory. FEEP and Colloid thrusters are currently being developed as flight models for the LISA Pathfinder mission, but both technologies are still bothered by technical problems. A selection between two different FEEP technologies which are currently being developed in parallel (needle vs. slit) is expected by the end of 2007.

The  $\mu$ RIT technology is currently based on laboratory models and a real system development for space applications has not yet started. However, this technology is interesting since the thrust level can easily be adjusted by applying modulation techniques.

The HEMPT technology can potentially be down-scaled to applications in the sub-milli-Newton range. This has been analyzed in more detail in [RD-01].

Pulsed Plasma Thrusters (PPT) are a low-cost niche that are interesting for university satellite projects (micro-satellites). They are sufficient for the usual station keeping and orbit manveuer requirements and potentially attitude control applications, but they are not able to meet the tight requirements of scientific micro-propulsion missions.

Up to now, virtually all micro-propulsion missions have finally selected a cold-gas system as a fall-back solution since the more advanced technologies were not ready in time. However, it must be noted in this context that the future scientific missions, such as Microscope and LISA, rely on the availability of an electrical micro-propulsion system and cannot use a cold-gas system anymore due to the very low ISP and concerns as far as the noise behaviour of a cold-gas system is concerned. Therefore, it is mandatory that a working and reliable micro-propulsion technology becomes readily available.

	<p>Endbericht Algorithmen zur Triebwerksansteuerung Fkz: 50 JR 0484</p>	<p>Doc.No.: INT-TAS-RP-ZAR-001 Issue: 1.0 Page: 24 of 20</p>
---	---	--

## Anhang D

Technical Note zu den Ergebnissen des Arbeitspakets AP 2100



# Simulationsumgebung zur Untersuchung von Algorithmen für das Thruster Actuation System

Project:	Document No.:
Thruster Actuation System	INT-TAS-TN-ZAR-002
ZARM - Center of Applied Space Technology and Microgravity	
Am Fallturm D 28359 Bremen Germany	Phone: +49-421-218-8136 Fax: +49-421-218-2521 E-Mail: bindel@zarm.uni-bremen.de

Doc. No.: INT-TAS-TN-ZAR-002

Issue: 1.0

Written:


Daniel Bindel

Date: 26. September 2006

Approved:

Stephan Theil

Date: -

	<p style="text-align: center;">Simulationsumgebung zur Untersuchung von Algorithmen für das Thruster Actuation System</p>	<p>Doc.No.: INT-TAS-TN-ZAR-002 Issue: 1.0 Page: 2 of 25</p>
---	---	---

## Document Change Record

Issue	Date	Changed Pages / Changed Chapters	Remarks	Done
1.0	25.09.2006	all	Initial Version	✓



## Inhaltsverzeichnis

<b>1</b>	<b>Einleitung</b>	<b>4</b>
1.1	Abkürzungen . . . . .	4
<b>2</b>	<b>Konzept</b>	<b>5</b>
<b>3</b>	<b>Module und Schnittstellen</b>	<b>7</b>
3.1	FT-Profil . . . . .	8
3.2	Thruster Actuation System . . . . .	10
3.3	Triebwerke . . . . .	12
3.3.1	Schubmodellierung . . . . .	12
3.3.2	Zustandsmodellierung . . . . .	15
3.3.3	Initialisierung . . . . .	18
3.4	Triebwerks-Konfiguration . . . . .	19
<b>4</b>	<b>Automatische Konfiguration</b>	<b>22</b>



# 1 Einleitung

Dieser Bericht beschreibt das Arbeitspaket 2100 des DLR Fördervorhabens 50JR0484

## **Algorithmen und Optimierungsverfahren für die Ansteuerung von $\mu$ -Propulsion-Triebwerken zur Bahn- und Lageregelung von Raumfahrzeugen**

Der Inhalt dieses Arbeitspaketes ist die Erstellung einer Simulationsumgebung. In ihr sollen die verschiedenen Algorithmen zur Triebwerksansteuerung getestet und überprüft werden.

Es sollen physikalische Modelle der Triebwerke simuliert werden, um eine Überprüfung der Leistungsfähigkeit der Algorithmen unter realistischen Bedingungen zu ermöglichen. Eine weitere Anforderung ist die Definition von geeigneten Schnittstellen für die Triebwerksansteuerung. Für eine gleichzeitige oder spätere Analyse müssen Ein- und Ausgabedaten sowie Modellzustände speicherbar sein.

Der Betrieb der Simulationsumgebung soll sowohl mit zufälligen als auch mit missions-typischen Testsignalen möglich sein.

Für die Umsetzung der Ziele in AP 2100 wurden Ergebnisse aus dem Arbeitspaket 1100 benutzt, um das Verhalten der Triebwerke möglichst realistisch zu modellieren.

Aus den Anforderungen, unterschiedliche Algorithmen, Triebwerkstypen, Triebwerksanordnungen und Testsignale zu untersuchen, ergab sich die Bedingung, die Simulation modular aufzubauen. Für die Konfiguration der Simulation wurde zusätzlich eine grafische Oberfläche entwickelt, um die Bedienung zu erleichtern.

### 1.1 Abkürzungen

TAS	Thruster Actuation System
FT	Force/Torque
AP	Arbeitspaket
KOS	Koordinatensystem
LPF	LISA Pathfinder

## 2 Konzept

Das Grundkonzept der Simulationsumgebung (siehe Abb. 1) besteht aus mehreren aufeinander folgenden Elementen. Als Eingang in die Simulation wird ein Signal eingespeist, dass eine Kraft- und Momentenanforderung eines Reglers darstellt. Dieses Signal besteht aus sechs Komponenten, jeweils drei für die Kräfte und drei für die Momente, und wird in den Schubverteilungsalgorithmus (TAS) geleitet.

Dieser berechnet eine entsprechende Schublösung für die Triebwerke, damit dieser Kommandovektor des Reglers realisiert werden kann. Die Anzahl der Komponenten in der Schublösung ist gleich der Anzahl der vorhandenen Triebwerke.

Eine wichtige Funktion übernehmen die Triebwerksmodelle. Sie haben als Eingang das geforderte Schubkommando und als Ausgang den tatsächlich realisierten Schub sowie den Status von einigen simulierten, internen Zuständen. Dies sind zum Beispiel die benötigte Spannung, der gerade verbrauchte Treibstoffmassenstrom oder der momentane Grad der Abnutzung (Wear). Der Schub wird als 3-dimensionaler Vektor ausgegeben, um kleine Schwankungen in der Axialität des Triebwerksstrahls simulieren zu können. Ein wesentlicher Bestandteil der Triebwerksmodelle ist die Nachbildung des dynamischen Verhaltens (Antwort auf Kommandosprünge) sowie der internen physikalischen Zustände. Dies ist für die spätere Gütebewertung des Schubverteilungsalgorithmus von entscheidender Bedeutung.

Die Informationen über den produzierten Schub werden im Koordinatensystem jedes einzelnen Triebwerkes ausgegeben. Eine nachfolgende Transformation rechnet sie wieder auf das Koordinatensystem des Raumfahrzeuges zurück. Hierbei werden auch die gesamten erzeugten Kräfte und Momente zusammengefasst.

Im Anschluss wird dieses Ergebnis noch mit dem am Anfang kommandierten Kraft- und Momentenvektor verglichen und die Differenz ausgewertet.

Neben diesem Hauptstrang existieren noch andere Elemente in der Simulationsumgebung, die sich mit der Analyse der Hauptelemente beschäftigen. Dies ist vor allem für die Beobachtung der Triebwerke eingebaut worden. In diesem Block werden die Informationen über die Triebwerkszustände aufgearbeitet und Kennwerte für die Bewertung des Schubverteilungsalgorithmus zur Verfügung gestellt.

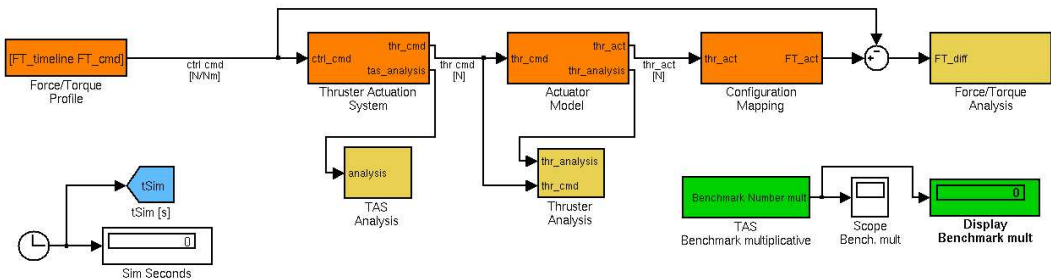



Abbildung 1: Aufbau der Simulationsumgebung



	Simulationsumgebung zur Untersuchung von Algorithmen für das Thruster Actuation System	Doc.No.: INT-TAS-TN-ZAR-002 Issue: 1.0 Page: 6 of 25
---	--	--

Die Simulationsumgebung wurde mit dem Programmpaket MATLAB Simulink implementiert. Es ermöglicht sowohl einfache und übersichtliche Strukturen zur Anordnung der verschiedenen Submodule, als auch freie Programmierbarkeit, um z.B. die Schubverteilungsalgorithmen zu integrieren.

### 3 Module und Schnittstellen

Die Simulationsumgebung wurde modular konzipiert. Dadurch ist es möglich, verschiedene Elemente auszuwechseln. Dies ist nötig, um unterschiedliche Schubverteilungsalgorithmen zu testen, andere Triebwerkstypen zu verwenden oder verschiedene Raumfahrzeuge und Konfigurationen auszuprobieren.

Die Modularität bringt allerdings auch zwei neue Systemanforderungen mit sich. Zum einen müssen die Schnittstellen normiert sein und zum anderen müssen die austauschbaren Elemente so flexibel sein, dass sie mit unterschiedlichen Bedingungen zurechtkommen. Die Schubverteilung sollte zum Beispiel mit einer unterschiedlichen Anzahl von Triebwerken umgehen können. Sollte es nicht möglich sein, die Module entsprechend flexibel anzulegen, muss für jede Variation eine entsprechende Vorlage abgespeichert sein.

Das Platzieren der richtigen Elemente in die vorgesehenen Plätze wird in einem Konfigurationsskript vorgenommen. Für dessen Steuerung wurde eine grafische Oberfläche erarbeitet (siehe Kapitel 4).

Für den Betrieb der Modul-Elemente werden auch noch Initialisierungsdaten und Arbeitsparameter benötigt. Diese werden in normierten Strukturen (z.B. *TAS\_params* oder *Thr\_params*) abgelegt und während der Simulation von den Modulen ausgelesen.

Die Module, die durch unterschiedliche Elemente ausgefüllt werden können sind folgende:

- FT-Profil als Eingang der Simulation
- TAS Algorithmus
- Triebwerkstyp mit entsprechendem Modell
- Konfiguration (Anzahl und Anordnung) der Triebwerke

Zwischen diesen Modulen existieren folgende Schnittstellen:

Verbindung zwischen Modulen	Einheit	Dimension
FT-Profil – TAS	N & Nm	6
TAS – Triebwerke	N	Anzahl Triebwerke
Triebwerke – FT-Transformation	N	3 * Anzahl Triebwerke

Tabelle 1: Schnittstellendefinition zwischen den Modulen

### 3.1 FT-Profil

Das Force/Torque-Profil ist eine Abfolge von Kommandos des Lage/Bahn-Reglers an das Antriebssystem. Es liefert für diskrete Zeitpunkte die geforderten Kräfte und Momente im Koordinatensystem des Raumfahrzeuges. Für die Simulationsumgebung wurde die Abtastrate für diese Daten vorläufig auf 10Hz festgelegt.

Innerhalb der Simulationsumgebung ist das FT-Profil unter der Variablenbezeichnung *FT\_cmd* gespeichert. Da in der aktuellen Version des Simulators diese Kommandowerte aus einer Datei eingelesen werden, hat das FT-Profil auch eine endliche Länge. Während der Initialisierung der Simulation wird die Anzahl der Datensätze ermittelt und daraus die maximal möglich Länge der Simulationszeit *tEnd* berechnet.

Zu der Variable *FT\_cmd* gehört noch eine Variable *FT\_timeline*, die für jeden Datensatz den dazugehörigen Zeitpunkt in Sekunden angibt.

Als Ursprung für die FT-Profile konnten folgende Quellen identifiziert werden:

- direkt gemessen während einer echten Mission
- Daten aus einer simulierten Mission (siehe Abb. 2)
- analytische Abschätzung mit Kenntnis über Störkräfte im Zielorbit einer Mission
- künstlich erzeugte Signale ohne Bezug zu einer Mission (siehe Abb. 3)

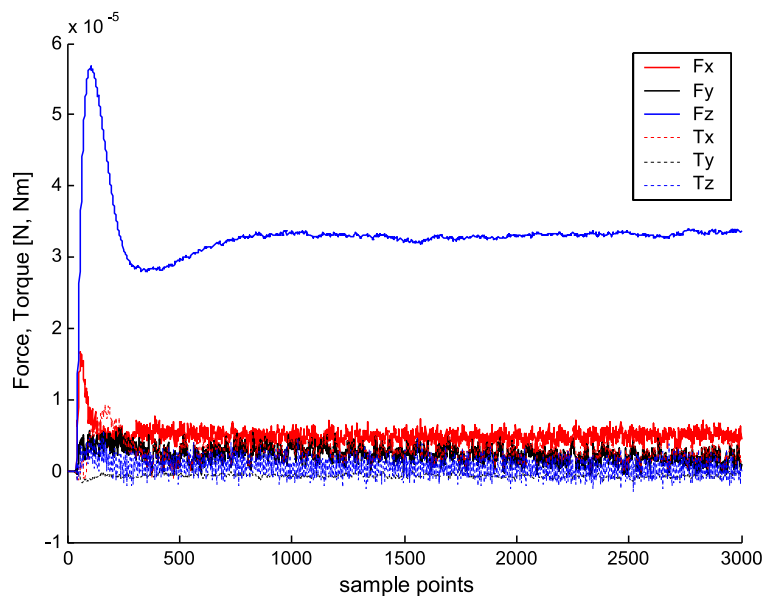


Abbildung 2: Simuliertes FT-Profil der LISA Pathfinder Mission

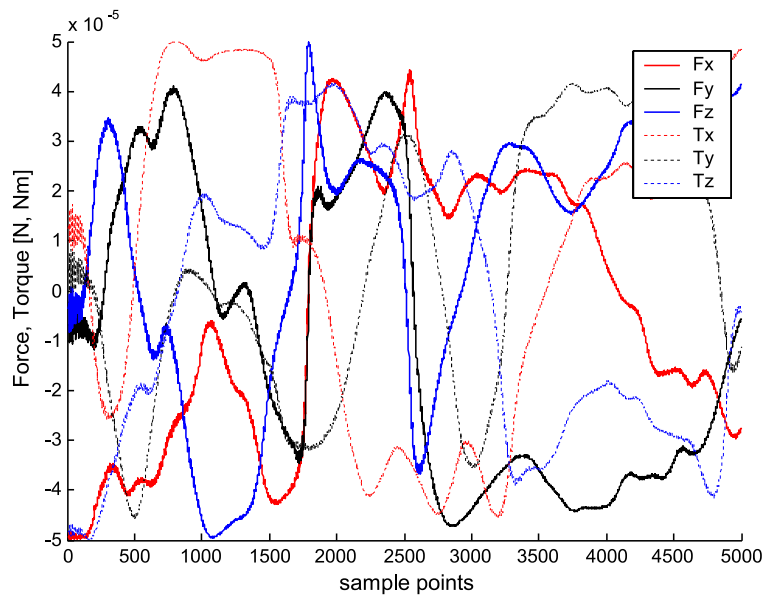


Abbildung 3: Künstliches FT-Profil (Random-Walk)

Während der Arbeit an der Simulationsumgebung wurden bisher Daten von einer simulierten Mission sowie von einem Zufallsgenerator eingesetzt.

Die Herstellung von analytisch abgeschätzten FT-Profilen wurde bisher noch nicht in Angriff genommen. Hierfür ist eine Aufarbeitung der vorgeschlagenen Missionen aus dem Arbeitspaket 1200 notwendig, die sich besonders auf die angestrebten Zielorbits, und die dort zu erwartenden Störkräfte und -momente, konzentriert.

Für die Simulationsumgebung können verschiedene FT-Profile vorbereitet werden. Die Namen dieser Dateien enden auf *\_FT\_cmd.mat*, damit sie vom automatischen Konfigurationsprogramm geladen werden können. In den Dateien sind die oben erwähnten Variablen bereits gespeichert.

Eine genauere Beschreibung dieser Signale, die zum Testen der Schubverteilungsalgorithmen eingesetzt werden, ist im Bericht zu Arbeitspaket 2200 zu finden.

## 3.2 Thruster Actuation System

Dieses Element übernimmt die Aufgabe, die vorhandenen Triebwerke so anzusteuern, dass die geforderten Kräfte und Momente realisiert werden können. In der Simulationsumgebung wurde eine einheitliche Schnittstelle für dieses Modul definiert.

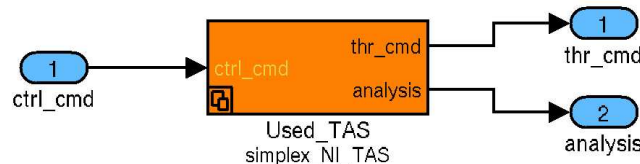


Abbildung 4: Beispiel eines TAS-Moduls

Das Element (siehe Abb. 4) verfügt über einen Eingang *ctrl\_cmd* und zwei Ausgänge *thr\_cmd* und *analysis*. Der innere Aufbau des Moduls kann allerdings je nach Art des Schubverteilungsalgorithmus variieren.


Die Algorithmen selbst sind als fertig kompilierte Bibliotheksfunktionen (S-Function) angelegt. Während der automatischen Konfiguration der Simulation wird für das TAS-Modul eine Initialisierung durchgeführt und entsprechende Parameter für den Betrieb zur Verfügung gestellt. Da sich die benötigten Daten je nach verwendetem Algorithmus unterscheiden können, wird die Struktur namens *TAS\_params* mit jeweils unterschiedlichem Aufbau benutzt, um diese Informationen aufzunehmen.

Der Name der Skriptdatei, die für die Initialisierung des gewünschten TAS-Algorithmus zuständig ist, hat den Aufbau *init\_identifizier.m*. Wobei der *identifizier* als Kennwort für den ausgewählten Schubverteilungsalgorithmus steht (z.B. *pinv\_TAS*, *simplex\_TAS*, o.ä.). Da für einen TAS-Block immer das gleiche Kennwort benutzt wird, kann von der automatischen Konfiguration sowohl die Initialisierung ausgeführt werden, als auch die gewünschte TAS-Funktion aus der Bibliothek geladen werden.

Es ist noch zu beachten, dass die Initialisierung des Schubverteilungsalgorithmus erst dann erfolgen kann, wenn die Triebwerkskonfiguration geladen wurde und somit die Anzahl, Position und Ausrichtung der Triebwerke feststeht.

Momentan sind folgende Algorithmen implementiert:

- Pseudoinvers Moore-Penrose Matrix
- Pseudoinvers Dispatching Matrix
- Simplex Norm One
- Simplex Norm Infinity

	Simulationsumgebung zur Untersuchung von Algorithmen für das Thruster Actuation System	Doc.No.: INT-TAS-TN-ZAR-002 Issue: 1.0 Page: 11 of 25
---	--	---

Neben dem Ausgang für die Triebwerke, der den berechneten Schub enthält, existiert noch ein Ausgang für Analyseaufgaben. Hier können interne Zustände des Algorithmus, Fehlercodes oder Skalierungsfaktoren ausgegeben werden. Dies ist vor allem während der Entwicklung hilfreich, um Fehler beheben zu können.

### 3.3 Triebwerke

Ein weiterer essentieller Bestandteil der Simulation sind die Modelle zur Nachbildung der Triebwerke. Für ihre Implementierung wurden die Kenndaten und die Informationen über ihre Arbeitsweise aus dem Arbeitspaket 1100 übernommen.

Das Modul für die Triebwerke soll in erster Linie das dynamische Verhalten und die Rauschcharakteristik des Schubes wiedergeben. Auf der anderen Seite soll es aber auch die internen Zustände des Triebwerkes simulieren, anhand derer später eine Bewertung des Schubverteilungsalgorithmus stattfinden kann. In Abb. 5 ist dargestellt, dass sowohl ein Block für die Schubmodellierung vorhanden ist, als auch ein Element, das aus dem aktuellen Schub die internen Zustände nachbildet.

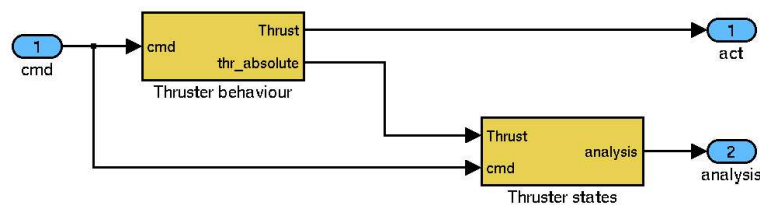


Abbildung 5: Grober Aufbau eines Triebwerkmodelles

#### 3.3.1 Schubmodellierung

Die Untersuchung verschiedener Triebwerkstypen und -technologien im Arbeitspaket 1100 [1] hat gezeigt, dass es mehrere Varianten einer optimalen Ansteuerung gibt. Die verschiedenen Triebwerke besitzen nicht nur unterschiedliche anwendungsbezogene Beschränkungen in Hinsicht auf den Schubbereich und die zugrunde liegende Dynamik. Auch die Art und Weise ihrer Konstruktion und des Funktionsprinzipes führen zu verschiedenen Definitionen von *Optimalität*.

Weiterführende Informationen hierzu sind im Arbeitspaket 2200 beschrieben, das sich mit der Erstellung der Bewertungsfunktion befasst.

Innerhalb der Simulationsstrecke werden die Modelle dazu benutzt, die Arbeitsweise der Schubverteilung zu verifizieren. Die TAS-Algorithmen sollten z.B. darauf vorbereitet sein, dass ein elektrisches Triebwerk eventuell nur langsam seinen Schub wechseln kann oder eventuell schon an der Grenze seines Arbeitsbereiches angelangt ist. Anhand des simulierten Schubes sind dann im schlimmsten Fall Differenzen zum kommandierten zu erkennen, so dass die Schubverteilung anders parametrisiert oder konzipiert werden sollte.

Es gibt zwei grundlegende Arten von Triebwerksmodellen. Die erste Kategorie ist sehr klein und umfasst nur die analytischen Modelle. Sie werden benutzt, um die grundlegende Funktionsweise eines neuen TAS-Algorithmus zu überprüfen. Neben dem *idealen* Triebwerk, das ein Schubkommando einfach nur durchleitet, gibt es auch ein *noise*-Modell,

das zu dem kommandierten Schub noch ein kleines Rauschen addiert. Das ideale Modell wird im fortgeschrittenen Entwicklungsstadium dazu benutzt, die erreichbare Genauigkeit der Schubverteilungsalgorithmen zu ermitteln, ohne das noch zusätzliche Eigenarten der Triebwerke das Ergebnis verfälschen.

Die zweite Modellgruppe bilden die Nachbildungen realer Triebwerke. Sie sind in den meisten Fällen ähnlich aufgebaut und setzen sich aus folgenden Elementen zusammen:

- Simulation der Ansterelektronik
- Simulation der Aktuatoren
- Beeinträchtigungen durch Rauschen

Im Bereich der Elektronikmodelle wird das kommandierte Schubsignal zum Beispiel auf eine festgelegte Schrittweite und innerhalb eines zulässigen Schubbereiches diskretisiert (siehe Abb. 6), um die digitale Steuerleitung zwischen dem On-Board Computer und dem Triebwerk zu simulieren.

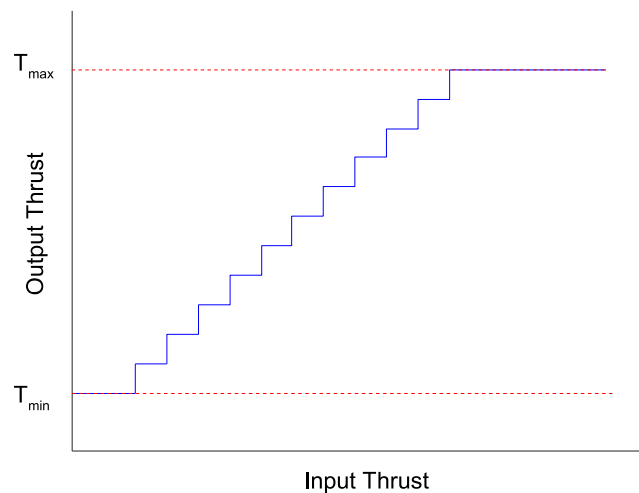


Abbildung 6: Beispiel einer Schubdiskretisierung

Für die Aktuatoren werden nicht lineare Kennlinien (siehe Abb. 7) mit Hilfe der vorhandenen Datenblätter generiert. Außerdem wird mit Verzögerungsgliedern die Trägheit der Spannungswandler und Gasflussregler nachgebildet (siehe Abb. 8).

Im Anschluss werden dann gemäß der gemessenen Rauschcharakteristik des Triebwerkes noch Störungen auf den Schub aufgebracht. Dies gilt vor allem für die Stärke, aber auch im kleineren Umfang für die Richtung (Axialität).



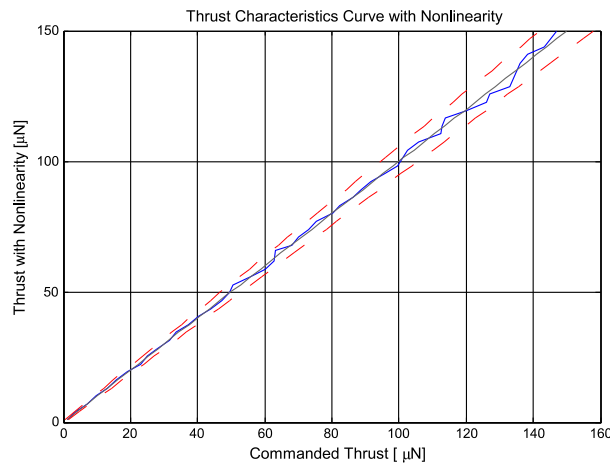


Abbildung 7: Nicht-lineare Kennlinie eines Triebwerkes

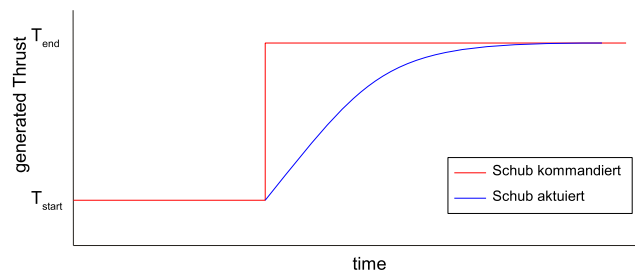


Abbildung 8: Verzögerung des Triebwerkes bei sprunghaften Schubänderungen

Es wurde bereits im Bericht zum Arbeitspaket 1100 angemerkt, dass nicht für jeden Triebwerkstyp eine gleichermaßen umfangreiche Dokumentation vorhanden ist. Die Bestimmung der Triebwerksparameter im Mikronewtonbereich bedarf teilweise aufwändiger Tests. Daher musste bei einigen Daten mit Schätzungen und Vergleichen zu ähnlichen Technologien gearbeitet werden.

Der Fokus liegt bei den implementierten Modellen vor allem beim verfügbaren Schubbereich, der Dynamik und dem zu erwartenden Rauschlevel.

Bisher sind folgende Triebwerksmodelle erstellt worden:

- FEEP
- Coldgas
- HEMP
- RIT
- Colloid

### 3.3.2 Zustandsmodellierung

Neben der reinen Modellierung des Schubverhaltens des Triebwerkes sind auch Informationen über die internen Zustände von Interesse und werden in einem eigenen Subsystem berechnet (siehe Abb. 9). Da sowohl elektrische Antriebe als auch Kaltgas-Systeme untersucht werden sollen, wurden folgende zu simulierende Zustände identifiziert:

- Schub in Newton
- Spannung in Volt
- Treibstoff-Massenstrom in kg/s
- Strom in Ampere
- Benutzungsgrad in 1/s (Useage)
- Effizienz in -

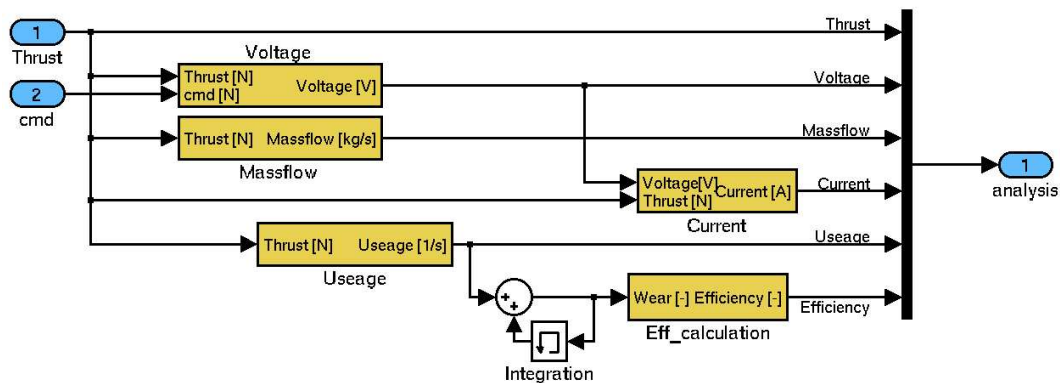


Abbildung 9: Berechnung der Triebwerkszustände

Die oben angegebenen Zustände zeigen die Betriebswerte des Triebwerkes. Die letzten beiden Einträge beschäftigen sich mit der Lebensdauer. Dies ist folgendermaßen zu verstehen.

Die Abnutzung bezieht sich auf den aktuellen Benutzungsgrad des Aggregates. Bei einer maximalen Benutzung (z.B. voller Schub) steigt dieser Wert auf  $1.0s^{-1}$ . Ein abgeschaltetes Triebwerk würde  $0s^{-1}$  ergeben, vorausgesetzt dass in diesem Fall keine weitere Alterung oder Degradation vorliegt. Der Grund für diese Zählweise ist zum einen eine nichtlineare Abnutzung bei einigen elektrischen Triebwerken (siehe Abb. 10). Große Schübe können zu überproportional größerer Schädigung des Materials führen. Die Kennlinie für das Schub/Abnutzungs-Verhältnis wäre also nichtlinear.

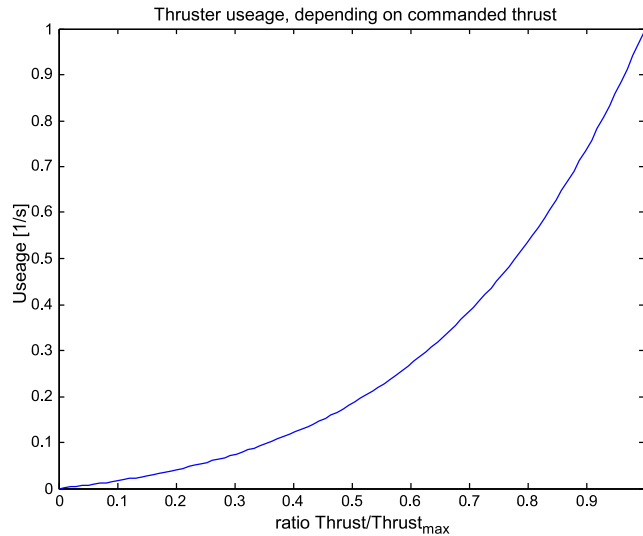


Abbildung 10: Abhängigkeit des Benutzungsgrades vom Schub

Auf der anderen Seite kann damit auch die integrale Abnutzung (Wear) aufsummiert werden. Sie stellt ein Äquivalent zu Betriebsstunden unter Vollast dar. Falls die Parametrisierung für die Berechnung des Benutzungsgrades einigermaßen realistisch ist, sollte auf diese Weise die Abnutzung eines Triebwerkes, das unter Vollast eine kurze Zeit gelaufen ist, und eines Triebwerkes das mit geringerem Schub eine längere Zeit gelaufen ist, ähnlich sein.

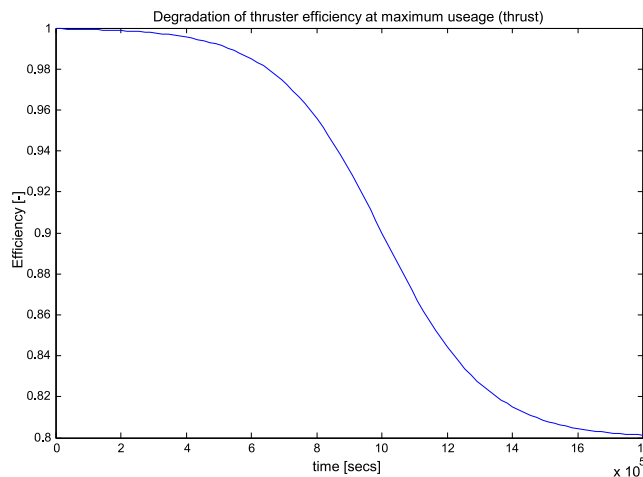


Abbildung 11: Abhängigkeit der Effizienz von der Abnutzung (Wear) bei vollem Schub

Diese Vorgehensweise zielt natürlich auf ein Element in der Bewertung der Ansteueralgorithmen hin. Dadurch, dass sich einige elektrische Triebwerke abnutzen, und so mit

fortlaufender Betriebsdauer eine höhere Ausfallwahrscheinlichkeit oder eine veränderte Effizienz aufweisen, kann es von Vorteil sein, dass man diese Abnutzung schon in der Schubverteilung berücksichtigt. Es könnte zum Beispiel versucht werden, möglichst alle Triebwerke eines Raumfahrzeuges gleichmäßig zu benutzen, statt immer nur einige wenige. So könnte verhindert werden, dass durch eine ungünstige Berechnung des Lösungsvektors für den Schub der Triebwerke, eines von ihnen praktisch ausgebrannt wird, während die anderen kaum benutzt wurden.

Der letzte Wert ist die Effizienz des Triebwerkes. Zum Beginn der Lebensdauer wird sie auf 1 gesetzt, und kann sich verringern, sobald Abnutzungserscheinungen eintreten (siehe Abb. 11). Es könnte zum Beispiel passieren, dass durch Erosion und Alterung im Beschleunigungssystem der Triebwerke, der produzierte Schub während der Lebensdauer sinkt.

Die Berechnung, oder besser Abschätzung, der Effizienz ist bisher nur extrem rudimentär implementiert, kann aber auch als Feed-Back für die Schubsimulation dienen.

Allgemein ist noch anzumerken, dass die simulierten Triebwerke ohne einen internen geschlossenen Regelkreis ausgelegt sind, der anhand von Schubmessungen die Nicht-Linearitäten der Spannungserzeugung oder Massenstromregelung wieder korrigiert.

Da die Eingangsgröße in das Triebwerksmodell der kommandierte Schub ist, müssen natürlich auch alle simulierten Zustände vom Schub abhängig sein. Aus der Literatur sind häufig die Abhängigkeiten des Schubes von den Zuständen wie etwa Spannung, Leistung und Massenstrom angegeben. Für die Triebwerksmodelle mussten im Vorfeld die inversen Abhängigkeiten erarbeitet werden. Die Zustände sind als Funktionen der Form  $V(T)$  oder  $\dot{m}(T)$  definiert, wobei  $T$  der Schub in Newton ist (siehe Abb. 12).

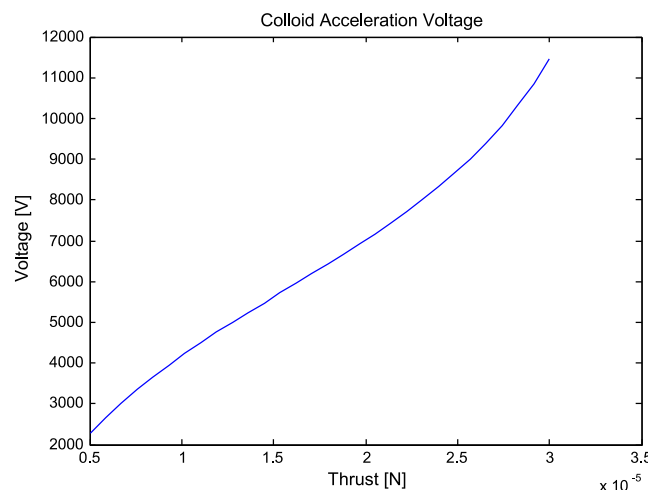


Abbildung 12: Beispiel für Schub/Spannungs-Zusammenhang

### 3.3.3 Initialisierung

Zu jedem Triebwerksmodell gehört ein Initialisierungsskript, welches die Betriebsparameter festlegt und in der Struktur *Thr\_params* ablegt. Dort sind neben allgemein gültigen Werten wie dem Schubbereich oder Charakteristiken zum dynamischen Verhalten auch Vektoren gespeichert, die von jedem Triebwerk einzeln ausgewertet werden, z.B. Noise-Seed.

Für die Initialisierung wird auch hier für jeden Triebwerkstyp ein Kennwort benutzt. Das dazu gehörende Initialisierungsskript trägt den Namen *init\_identifizier.m*.

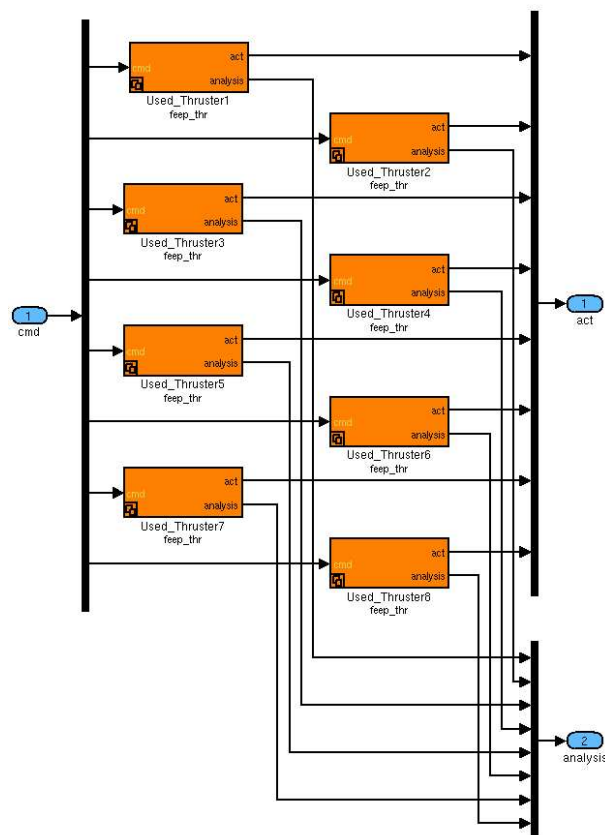


Abbildung 13: Platzhalter für Kopien des Triebwerksmodelles

Während der automatischen Konfiguration wird nach der Auswahl des richtigen Triebwerksmodells eine Anordnung von Platzhaltern für die entsprechende Anzahl von Triebwerken geladen (siehe Abb. 13). Diese Anordnung besteht aus so vielen Prototypen, wie Triebwerke an dem Raumfahrzeug vorhanden sind. Jeder dieser Prototypen wird dann mit einer Kopie des vorher ausgewählten Modells geladen. Damit stehen am Ende eine Reihe von vollständigen Modell-Kopien zur Verfügung, welche die einzelnen Triebwerke des Raumfahrzeuges unabhängig voneinander simulieren.

### 3.4 Triebwerks-Konfiguration

Die Konfiguration der Triebwerke eines Raumfahrzeuges ist nicht nur durch deren Anzahl, sondern auch durch die Position und Ausrichtung definiert. Diese Daten werden entweder parametrisch in der Form von Winkeln und Radien zur Verfügung gestellt, oder numerisch in der Form von Positionskoordinaten und Richtungsvektoren.

Innerhalb der Simulation übernimmt das Modul der Triebwerkskonfiguration die Aufgabe, den Schub, der von jedem Triebwerk im eigenen Koordinatensystem erzeugt und ausgegeben wird, auf das System des Raumfahrzeuges zu transformieren und die daraus resultierenden Kräfte und Momente zu bestimmen.

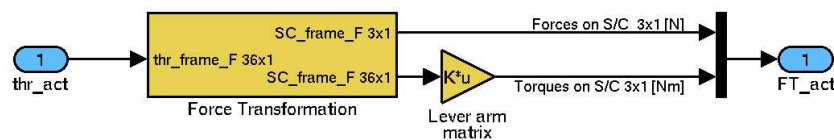


Abbildung 14: Aufbau des Schub-Transformationsmodul

Dies wird in zwei Abschnitten durchgeführt (siehe Abb. 14). Zuerst wird der Schubvektor jedes Triebwerkes mit einer Drehmatrix multipliziert, die ihn in das Koordinatensystem des Raumfahrzeuges transformiert. Die Ergebnisse aller Einheiten werden addiert und ergeben so die gesamte produzierte Kraft (siehe Abb. 15).

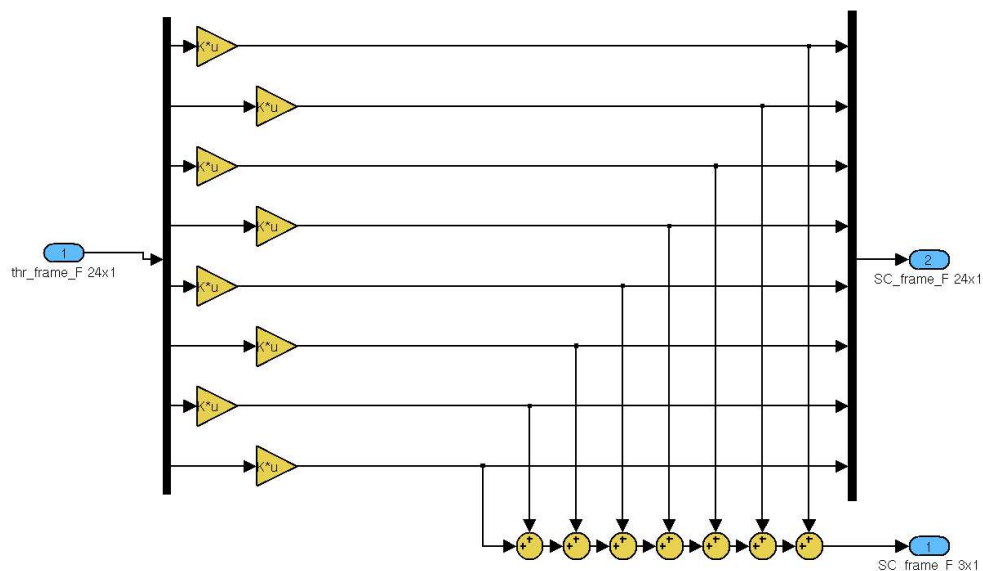


Abbildung 15: Aufbau des Schub-Transformationsmodul

Die einzelnen Ergebnisse der ersten Transformation werden allerdings auch noch mit der Hebelarmmatrix multipliziert, und ergeben so die produzierten Momente.



Die Anzahl der benötigten Matrizen hängt von der Anzahl der Triebwerke ab. Für jedes Aggregat muss eine 3x3 Matrix für die Richtungstransformation vorhanden sein, sowie eine weitere 3x3 Matrix für den Hebelarm. Die Dimension der zusammengesetzten Matrix ist dann  $6 \times (3 \times \text{Anzahl Triebwerke})$ . Sie wird als *thr\_config\_map* abgelegt. Innerhalb der Simulation werden dann die entsprechenden Elemente der Matrix für die Transformation oder die Momentenberechnung ausgelesen.

Hierbei ist noch zu beachten, dass die Berechnung in vorgefertigten Blöcken abläuft. Für jede unterschiedliche Anzahl von Triebwerken muss im Moment noch ein eigenes Konfigurationsmodul vorbereitet und abgespeichert werden.

Für die automatische Konfiguration der Simulation haben diese Module Namen nach folgendem Muster *nthr\_config* wobei *n* für die Anzahl der Triebwerke steht.

Das Initialisieren der Triebwerkskonfiguration wird am Anfang der Simulationsvorbereitungen durchgeführt. Dies ist darauf zurückzuführen, dass alle anderen Module die Anzahl der Triebwerke benötigen, um sich selbst zu konfigurieren. Die Auswahl an möglichen Konfigurationen bezieht sich dann auf unterschiedliche Raumfahrzeuge (LISA Pathfinder, LISA, GAIA) oder verschiedene geplante Triebwerks-Konfigurationen dieser Alternativen. Dem dazugehörigen Kennwort wird wieder ein *init\_* vorangestellt, um das passende Initialisierungsskript aufzurufen.

Die Initialisierung liefert als Ergebnis neben der vollständigen Matrix *thr\_config\_map* auch noch eine reduzierte Version mit dem Namen *FT\_Map* und die Anzahl *n\_thr* der verwendeten Triebwerke. Die reduzierte Form der Konfigurationsmatrix besitzt die Dimension  $6 \times (\text{Anzahl der Triebwerke})$  und ist etwas anders aufgebaut. Für jedes Triebwerk ist eine Spalte vorhanden. Multipliziert mit dem Schub des Triebwerkes werden direkt die dadurch realisierten Kräfte und Momente im KOS des Raumfahrzeuges berechnet. Mit ihr kann man allerdings keine Abweichungen der Schubrichtung von der Hauptachse des Triebwerkes modellieren, da sie nur eine Transformation der eindimensionalen Kraft ist.

Die *FT\_Map* ist allerdings für die Schubverteilungsalgorithmen interessant, da diese nur mit der Richtung der Hauptachse der Triebwerke arbeiten.

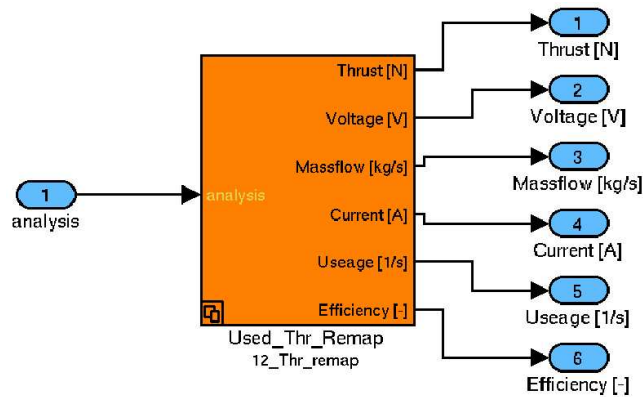


Abbildung 16: Sortiermodul für die Analyse der Triebwerkszustände

Die Anzahl der Triebwerke hat auch noch Auswirkungen auf ein austauschbares Modul, das für einen Teil der Auswertung der Triebwerkszustände zuständig ist. Es handelt sich hierbei um eine Sortierung der Signale, die von den Triebwerksmodellen kommen.

Für die Auswertung muss für jeden zu untersuchenden Zustand eine Signalleitung zusammengestellt werden, in der von allen Triebwerken die Daten dieses speziellen Zustandes übertragen werden. Da aber von den Triebwerken alle Zustände gleichzeitig geliefert werden, wird ein Sortiermodul benötigt, das einen bestimmten Zustandswert aus dem Signal jedes Triebwerkes extrahiert und mit den Werten der anderen Triebwerke kombiniert. Als Resultat wird dann jeweils ein Vektor ausgegeben, der zum Beispiel nur noch die Treibstoffmassenströme aller Triebwerke enthält (siehe Abb. 16) .

Dieses Sortiermodul ist auf die Anzahl der Triebwerke fest eingestellt, und muss daher für jede mögliche Anzahl von Triebwerken vorher erstellt werden. Da das Modul nur eine Sortierung der Zustandsdaten der Triebwerke vornimmt, benötigt es keine weitere Initialisierung.



## 4 Automatische Konfiguration

Dieser Abschnitt der Dokumentation für die Simulationsumgebung befasst sich mit der automatischen Konfiguration des Systems. Es hat sich im Laufe der Entwicklung herausgestellt, dass die Verwendung von unterschiedlichen konfigurierbaren Modulen zu einem größeren Aufwand bei der korrekten Initialisierung der Simulation führt. So führt die Auswahl einer anderen Triebwerkskonfiguration dazu, dass eine andere Anzahl von Aggregaten verwendet wird, was wiederum Auswirkungen auf den Schubverteilungsalgorithmus und die Anzahl der verwendeten Kopien des Triebwerkmodells hat. Das Zusammenstellen eines korrekten Initialisierungsskriptes, welches die notwendigen Parameter vor der Benutzung der Simulation einstellt, wird dadurch sehr zeitraubend.

In Hinblick auf die große Anzahl von Kombinationsmöglichkeiten und der sich daraus ergebenden Menge an vorgefertigten Skripten wurde beschlossen, das Laden und Initialisieren der einzelnen Module für die Simulationsumgebung als ein eigenes kleines Programm zu implementieren.

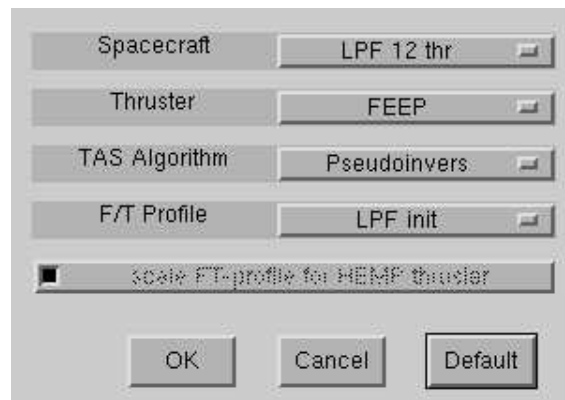


Abbildung 17: Grafische Benutzeroberfläche für die Automatische Konfiguration

Die Benutzeroberfläche (siehe Abb. 17) bietet die Möglichkeit, aus der Menge an vorhandenen Optionen die gewünschten herauszusuchen und mit diesen Vorgaben die Simulation starten zu lassen.

Der Ablauf der automatischen Konfiguration gliedert sich dabei in mehrere Abschnitte.

- Zusammenstellen der vorhandenen Optionen und dazu gehörenden Kennwörter
- Aufbau des grafischen Oberfläche und Auswahl der Module
- Ausführen der Initialisierungsskripte für die ausgewählten Module
- Selektion der gewünschten Module in vorgefertigten Bibliotheken
- Laden der Simulation mit Zugriff auf die Bibliotheken



Im ersten Abschnitt werden alle zur Verfügung stehenden Module ein Listen eingetragen und zwar sowohl mit ihrem Kennwort, als auch mit einem Klartext der später für den Benutzer sichtbar ist. Es gibt dadurch dann jeweils eine Liste für die Triebwerkskonfiguration *SC\_list*, für den Triebwerkstyp *thr\_list*, für den Schubverteilungsalgorithmus *tas\_list* und das zu verwendende FT-Profil *FT\_list*.

Diese Listen werden von der grafischen Benutzeroberfläche angezeigt und das ausgewählte Resultat wird intern gespeichert. Die Benutzung von Umgebungsvariablen sorgt dafür, dass bei einem erneuten Aufruf der GUI wieder die vorherigen Werte eingestellt sind. Über den Default-Button kann die Zusammenstellung für die Referenzmission (LISA Pathfinder, FEED Triebwerke, Pseudoinverses TAS, LPF init Profil) geladen werden. Eine Besonderheit gibt es noch für die HEMP Triebwerke. Da hier leider noch kein Modell für ein Mikronewtontriebwerk vorliegt, kann das ausgewählte FT-Profil um den Faktor 1000 skaliert werden, um in die Größenordnung von Millinewton zu gelangen.

Mit den Informationen über die Module werden die dazu gehörenden Initialisierungsdateien ausgeführt. Dies beginnt bei der Triebwerkskonfiguration. Dem Kennwort wird wie schon beschrieben ein *init\_* vorangestellt, und die Funktion mit dem entstandenen Namen aufgerufen. Dies liefert zum einen die Anzahl der vorhandenen Triebwerke *n\_thr* aber auch die Matrizen für die Schub-Transformation *FT\_Map* und *thr\_config\_map*.

Mit der bekannten Anzahl *n* der Triebwerke werden nun die Kennwörter für die Triebwerksprototypen *n\_Thruster\_array* und das korrekte Schub-Transformationsmodul *nthr\_config* zusammengesetzt.

Die Datei des ausgwählten Force/Torque-Profiles wird in den Speicher geladen und je nach ausgewähltem Triebwerk und GUI-Einstellung noch um den Faktor 1000 skaliert. Danach wird das Initialisierungsskript für den Triebwerkstyp ausgeführt, welches eine modellspezifische Struktur *Thr\_params* zurückgibt.

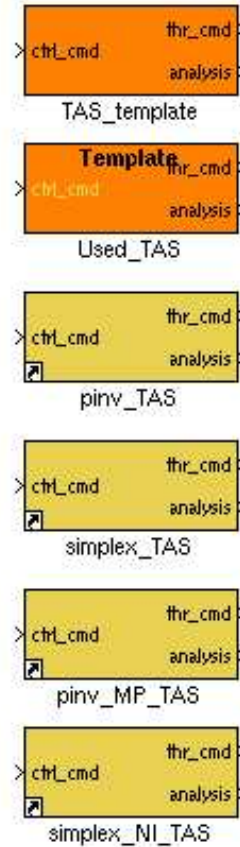


Abbildung 18: Beispiel für eine konfigurierbare Bibliothek

Nachdem alle nötigen Strukturen vorbereitet und Informationen zusammengetragen wurden, werden in verschiedenen Bibliotheken die Simulationsmodelle ausgewählt. So gibt es Bibliotheken wie zum Beispiel die *thrusters.mdl*, *TAS.mdl* und *thr\_configs.mdl*. Sie enthalten die eigentlichen Simulinkmodelle, bzw. Links zu den originalen Dateien. Außerdem besitzen sie für jedes konfigurierbare Modul ein Template, das die Möglichkeit bietet, an seiner Stelle eines der verfügbaren Elemente einzusetzen.

In der Bibliothek *TAS.mdl* (siehe Abb. 18) ist zum Beispiel solch ein Template zusammen mit den implementierten Schubverteilungsalgorithmen gespeichert. Diese Blöcke besitzen alle einen Namen, der ihr entsprechendes Kennwort enthält. Dadurch können sie während der automatischen Konfiguration im Template ausgewählt werden.

Dieser Vorgang wird außerdem mit den Triebwerkstypen durchgeführt, den Platzhaltern für die Triebwerksprototypen, dem Transformationsblock und dem Sortierblock in der Triebwerksanalyse. Jede der Bibliotheken wird geöffnet, auf die gewählten Elemente eingestellt und wieder gespeichert. Am Ende wird dann die Simulationsumgebung selbst geladen, die ihrerseits auf die aktualisierten Templates der Bibliotheken zurückgreift.



## Literatur

- [1] D. Bindel. Compilation of  $\mu$ -Propulsion Thrusters for Attitude and Orbit Control of Spacecraft. Technical Report INT-TAS-TN-ZAR-001, Center of Applied Space Technology and Microgravity (ZARM), May 2006.

	<p>Endbericht Algorithmen zur Triebwerksansteuerung Fkz: 50 JR 0484</p>	<p>Doc.No.: INT-TAS-RP-ZAR-001 Issue: 1.0 Page: 25 of 20</p>
---	---	--

## Anhang E

Technical Note zu den Ergebnissen des Arbeitspakets AP 2200



# Bewertungsfunktionen und Testsignale für Algorithmen des Thruster Actuation Systems

Project:	Document No.:
Thruster Actuation System	INT-TAS-TN-ZAR-003
ZARM - Center of Applied Space Technology and Microgravity	
Am Fallturm	Phone: +49-421-218-8136
D 28359 Bremen	Fax: +49-421-218-2521
Germany	E-Mail: bindel@zarm.uni-bremen.de

Doc. No.: INT-TAS-TN-ZAR-003

Issue: 1.0

Written:

Daniel Bindel

Date: 20. Oktober 2006

Approved:

Stephan Theil

Date: -

## Document Change Record

Issue	Date	Changed Pages / Changed Chapters	Remarks	Done
1.0	10.10.2006	all	Initial Version	✓



## Inhaltsverzeichnis

<b>1</b>	<b>Einleitung</b>	<b>4</b>
<b>2</b>	<b>Bewertungsfunktion</b>	<b>5</b>
2.1	Einfluss der Triebwerke . . . . .	6
2.2	Aufbau der Bewertungsfunktion . . . . .	7
2.3	Implementierung . . . . .	8
<b>3</b>	<b>Testsignale für Schubverteilungsalgorithmen</b>	<b>10</b>
3.1	Missionstypische Testsignale . . . . .	10
3.2	Künstliche Testsignale . . . . .	11
3.2.1	Erzeugung . . . . .	12
3.2.2	Kugelkoordinaten . . . . .	14
3.2.3	Gleichverteiltes kartesisches System . . . . .	15
3.2.4	Gleichverteiltes kartesisches System mit Grenzwert . . . . .	17
3.2.5	Normalverteiltes kartesisches System . . . . .	18
3.2.6	Anpassung an Randbedingung der Triebwerke . . . . .	19
3.2.7	Implementierung . . . . .	21





## 1 Einleitung

Dieser Bericht beschreibt das Arbeitspaket 2200 des DLR Fördervorhabens 50JR0484

### **Algorithmen und Optimierungsverfahren für die Ansteuerung von $\mu$ -Propulsion-Triebwerken zur Bahn- und Lageregelung von Raumfahrzeugen**

Der Inhalt dieses Arbeitspaketes ist die Ausarbeitung einer Bewertungsfunktion, die für den Vergleich mehrerer Schubverteilungsalgorithmen benötigt wird. Zu diesem Zweck sollen auch mehrere Testsignale definiert werden, um die Algorithmen unter verschiedenen Bedingungen untersuchen zu können.

Aufgrund der Ausrichtung des Projektes wurde der Fokus der Bewertungsfunktion darauf gelegt, eine möglichst optimale Ansteuerung der  $\mu$ -Propulsion-Triebwerke zu analysieren.

## 2 Bewertungsfunktion

Das Konzept einer Bewertungsfunktion, wie sie in dieser Untersuchung eingesetzt werden soll, ist der qualitative Vergleich von unterschiedlichen Schubverteilungsalgorithmen. Das Ergebnis einer Bewertung soll anschaulich zeigen können, welche verwendete Methode für die Triebwerksansteuerung besser geeignet ist.

Zu diesem Zweck wurde festgelegt, dass eine Bewertungsfunktion möglichst nur einen einzelnen numerischen Wert ausgeben soll, der später als *Benchmark* zu interpretieren ist. Da das Bewertungssystem mit sehr vielen Annahmen und Interpretationen arbeiten muss, sind die produzierten Ergebnisse relative Werte, die nur im direkten Vergleich zueinander eine Aussage ermöglichen.

Zu diesem Zweck ist es notwendig, einen Referenzfall mit einem definierten Eingangssignal und einem bestimmten Triebwerkstyp bzw. -konfiguration festzulegen, auf den sich alle anderen Bewertungsausgaben beziehen können. Diese Vorgehensweise ist auch notwendig, um mehrere Szenarien gegeneinander abzugrenzen. So können zum Beispiel für verschiedene Triebwerkstypen eigene Testkampagnen durchgeführt werden, um den für sie am besten geeigneten Schubverteilungsalgorithmus zu ermitteln.

Für die Triebwerksansteuerung ist es wichtig, dass die Arbeitsfähigkeit gewährleistet ist. Das heißt, dass die Summe der produzierten Kräfte und Momente auch dem Kommando entspricht, das als Eingang in den Test eingespeist wird. Diese Eigenschaft wird mit einem idealen Triebwerksmodell überprüft, da es keinerlei Modifikationen am kommandierten Schub vornimmt. Da während der Bewertungstests mit simulierten Triebwerksmodellen gearbeitet wird, sind Abweichungen durch das Schubrauschen kaum zu vermeiden.

Die zu untersuchenden Algorithmen zur Schubverteilung sollen im Hinblick auf wissenschaftliche Missionen, und die dort einsetzbaren  $\mu$ -Propulsion-Triebwerke, auf ihre Optimalität getestet werden. Daher ist es notwendig, vorher die Frage zu klären, wann solch eine Ansteuerung überhaupt optimal ist.

Allgemein wurden folgende Elemente für eine optimale Ansteuerung identifiziert:

- Berechnung einer Schublösung, die dem geforderten Reglerkommando entspricht
- Verlängerung der Missions durch Treibstoffersparnis
- Reduktion des Missionsrisikos durch Schonung der Triebwerke
- Berücksichtigung der Triebwerkseigenschaften bei der Berechnung der Schublösung

Der erste Punkt wird schon während der Entwicklung der Algorithmen sichergestellt. Jedoch können durch Trägheitseffekte im Triebwerk nicht immer sprunghafte Änderungen des Schubkommandos auch sofort umgesetzt werden. In solch einem Fall kann der geforderte Force/Torque-Vektor eventuell nicht mehr erzeugt werden. Dies schließt sich

jedoch auch an den vierten Punkt an, da der Schubverteilungsalgorithmus die Dynamik des Triebwerkes bei der Berechnung berücksichtigen kann.

Der sparsame Umgang mit Treibstoff ist nicht nur für Kaltgasysteme von Bedeutung, sondern auch für elektrische Antriebe von Bedeutung. Auf diese Weise kann entweder die Nutzlast des Raumfahrzeuges erhöht oder aber die Missionsdauer verlängert werden. Nach Untersuchungen im Arbeitspaket 2100 [2] sind die elektrischen Triebwerke meist weniger durch die Treibstoffmenge, sondern vielmehr durch die eigene Lebensdauer begrenzt.

Ein schonender Umgang mit den Triebwerken könnte sich in einer geringeren Abnutzung/Erosion und kleineren Ausfallwahrscheinlichkeit bemerkbar machen. Der Gewinn wäre eine erhöhte Sicherheit für die Mission.

## 2.1 Einfluss der Triebwerke

Die Kennzeichnung einer optimalen Ansteuerung ist für verschiedene Triebwerksarten [1] unterschiedlich definiert, da sich auch ihre Funktionsweisen voneinander unterscheiden. Zur Lösung dieses Problems werden aus dem aktuellen Schub die physikalische Zustände innerhalb der Triebwerksmodelle nachgebildet. Mit dem Wissen über die Funktionsweise und den Einfluss dieser Zustände auf das Triebwerk kann dann eine Bewertung vorgenommen werden.

Die intern simulierten Zustände sind folgende:

- Schub in Newton
- Spannung in Volt
- Treibstoff-Massenstrom in kg/s
- Strom in Ampere
- Benutzungsgrad in 1/s (Useage)
- Effizienz in -

Aus diesen Zustände können dann folgende Bewertungsgrößen berechnet werden:

$T_{step}$  - Schubsprung

$U_{step}$  - Spannungssprung

$U_{max}$  - maximale Spannung eines Triebwerkes

$\dot{m}$  - gesamter Treibstoffmassenstrom

$P_{el}$  - elektrische Leistung

$FT_{diff}$  - Differenz zwischen kommandiertem und aktuiertem FT-Profil

$Use$  - größte durchschnittliche Abnutzung eines Triebwerkes

Größen	Elektrisch	Kaltgas
$T_{step}$	hoch	hoch
$U_{step}$	hoch	niedrig
$U_{max}$	hoch	niedrig
$\dot{m}$	niedrig	hoch
$P_{el}$	mittel	niedrig
$FT_{diff}$	mittel	mittel
$U_{se}$	hoch	mittel

Tabelle 1: Einfluss der Bewertungsgrößen auf unterschiedliche Triebwerkstechnologien

Diese Größen wurden ausgewählt, da sie die bisher identifizierten, kritischen Eigenschaften der verschiedenen Triebwerkstypen abdecken. Bei Systemen mit einem niedrigen spezifischen Impuls liegt das zu untersuchende Interesse zum Beispiel beim verbrauchten Treibstoff, während bei einigen elektrischen und trägen Antrieben eher große Schubänderungen von Nachteil sind oder die Alterung des Aggregates.

Es ist daher zusätzlich zu diesen Bewertungsgrößen notwendig, geeignete Wichtungsfaktoren zu finden, um festzulegen wie stark die einzelnen Elemente in die Bewertungsfunktion einfließen sollen. Für die unterschiedlichen Triebwerkstypen wurden Tabellen erstellt, wie gravierend der Einfluss der Bewertungsgrößen auf ihre Arbeitsweise ist.

Eine grobe Übersicht für elektrische und Kaltgassysteme ist in Tabelle 1 dargestellt. Aus diesen Abschätzungen wurden im Anschluss numerische Wichtungsfaktoren für die implementierten Triebwerkstypen definiert.

## 2.2 Aufbau der Bewertungsfunktion

Es wurden zwei unterschiedliche Konzepte für die Bewertungsfunktion untersucht. Neben der bekannten additiven Methode (Formel 1) kam auch eine multiplikative Variante (Formel 2) zum Einsatz.

$$Benchmark_{add} = \frac{\sum Value_i \cdot Coeff_i \cdot Weight}{\sum Weight_i} \quad (1)$$

$$Benchmark_{mult} = \sqrt[\sum Weight_i]{\prod (Value_i \cdot Coeff_i)^{Weight_i}} \quad (2)$$

Zum Verständnis dieser Berechnungsmethoden müssen noch die spezifischen Koeffizienten eingeführt werden. Sie sind für jedes Triebwerk unterschiedlich und werden mit Hilfe der Referenzsimulation ermittelt. Ihre Benutzung ist auf die unterschiedlichen Größenordnungen der Bewertungsgrößen zurückzuführen. So werden Spannungen im Kilovolt-Bereich und Schubänderungen im  $\mu N$ -Bereich in der selben Berechnung benutzt. Die Koeffizienten für jede der Bewertungsgrößen sorgt dafür, dass sie in einen Bereich um 1.0 skaliert wird.

Größen	FEEP		Kaltgas	
	Koeffizient	Wichtung	Koeffizient	Wichtung
$T_{step}$	1/3.6e-6	3	1/2.83e-6	3
$U_{step}$	1/1600	4	1/0.115	1
$U_{max}$	1/6800	2	1/15.2	1
$\dot{m}$	1/3.5e-9	1	1/1e-7	4
$P_{el}$	1/6.5	2	1/24.17	1
$FT_{diff}$	1/2.35e-4	2	1/3.75e-5	2
$U_{se}$	1/0.029	3	1/0.13	1

Tabelle 2: Koeffizienten und Wichtungsfaktoren für zwei Triebwerkstypen

Zur Gewinnung der Koeffizienten wird das Triebwerksmodell in der Referenz-Simulation eingesetzt, und die einzelnen Bewertungsgrößen über die Laufzeit gemittelt. Die inversen Ergebnisse dieser Prozedur ergeben dann die Koeffizienten.

Der Unterschied zwischen den beiden Bewertungsmethoden ist die Intensität, wie sich Abweichungen der einzelnen Bewertungsgrößen auf das gesamte Ergebnis auswirken. Während bei der additiven Methode solche Effekte nur linear eingekoppelt werden, sind bei der multiplikativen Variante schon Auswirkungen in der dritten oder vierten Potenz möglich.

Nach mehreren Tests beider Berechnungsmethoden wurde die multiplikative Variante als geeignet eingestuft. Dies ist damit begründet, dass durch die hohe Anzahl der Bewertungsgrößen die linearen Wichtungsfaktoren kein deutlicher Indikator mehr sind. Die potenzierten Wichtungen zeigten hier klarere Ergebnisse.

Die Kombination aus Koeffizienten und Wichtungsfaktoren ist in Tabelle 2 beispielhaft für zwei Triebwerkstypen dargestellt.

## 2.3 Implementierung

Die Berechnung des Benchmark-Wertes erfolgt direkt innerhalb der Simulationsumgebung aus Arbeitspaket 2100. Auf diese Weise kann das Ergebnis der Bewertungsfunktion auch schon direkt angezeigt werden (siehe Abbildung 1).

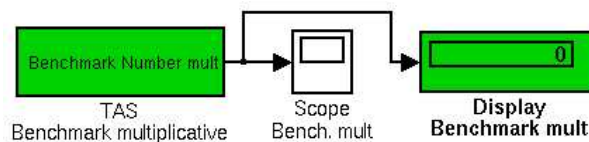


Abbildung 1: Ausgabe der Bewertungsfunktion

Für diese Berechnung, die parallel zur Simulation mitläuft, werden die Bewertungs-

größen mittels der Koeffizienten skaliert und anschließend mit den vorher definierten Wichtungsfaktoren potenziert (siehe Abbildung 2).

Es ist noch anzumerken, dass das Ergebnis der Bewertungsfunktion vor der Ausgabe über die Laufzeit gemittelt wird.

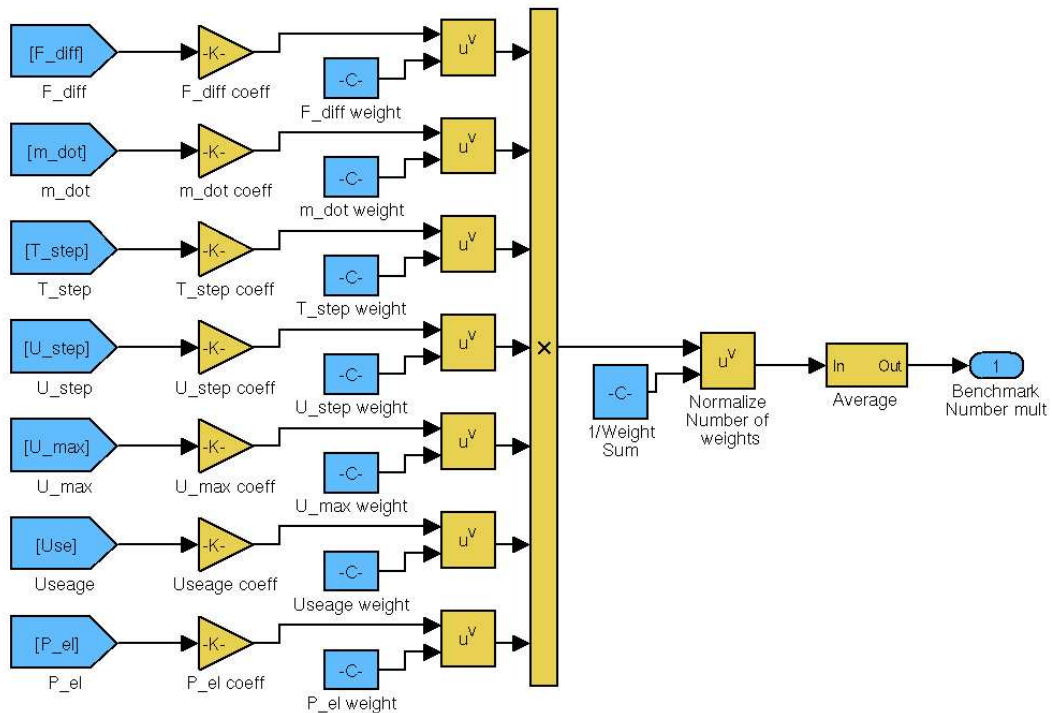


Abbildung 2: Berechnung der Bewertungsfunktion in MATLAB Simulink

### 3 Testsignale für Schubverteilungsalgorithmen

Der Vergleich von verschiedenen Schubverteilungsalgorithmen wird durchgeführt, indem man ihre Arbeitsweise in Testszenarios innerhalb einer Simulation analysiert.

Für diese Simulationen werden Eingangssignale benötigt, die auf der einen Seite ein möglichst realistisches Einsatzzenario abbilden sollen, oder aber für analytische Untersuchungen von Eigenschaften der Schubverteilungsmethoden dienen können.

Je nach Verwendungszweck wurden unterschiedliche Testsignale vorbereitet und gespeichert. Im folgenden werden sie als F/T-Profile bezeichnet, da sie gleichzeitig die geforderten Kräfte und Momente (Forces & Torques) enthalten.

#### 3.1 Missionstypische Testsignale

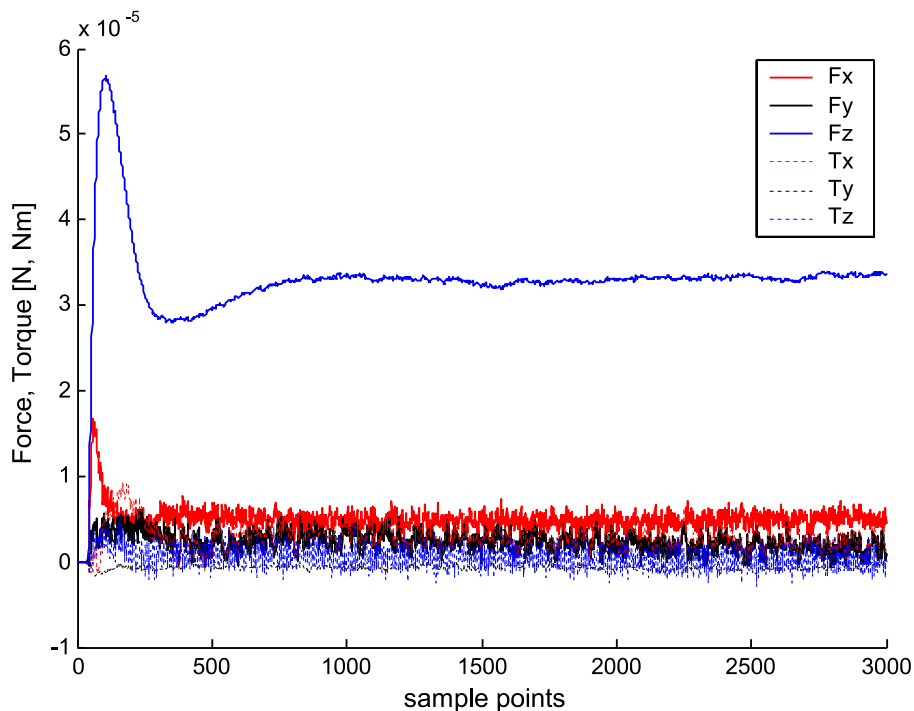



Abbildung 3: Beispiel für simuliertes FT-Profil (LISA Pathfinder)

Diese Klasse von FT-Profilen setzt auf existierenden oder geplanten Wissenschaftsmissionen auf. Leider liegen hier noch keine real gemessenen Daten von Missionen vor, die bereits eine sechsdimensionale Regelung benutzt haben. Daher wurde versucht, für geplante Missionen eine Abschätzung der zu erwartenden Reglerkommandos zu simulieren. Dieses Vorgehen ist recht aufwändig und beinhaltet ein Modell für die erwarteten Störungen im Zielorbit der Mission, für die Interaktion des Satelliten mit diesen Störungen

	Bewertungsfunktionen und Testsignale für Algorithmen des Thruster Actuation Systems	Doc.No.: INT-TAS-TN-ZAR-003 Issue: 1.0 Page: 11 of 22
---	---	---

und eine Annahme über die grobe Kontrollstrategie des Raumfahrzeuges. So unterscheiden sich zum Beispiel Drag-Free-Missionen wie etwa LISA Pathfinder von Astrometrie-Missionen wie GAIA dadurch, dass in einem Fall sowohl Lage und Position geregelt werden müssen, oder eben nur die Ausrichtung des Raumfahrzeuges.

Mit diesen Daten kann dann ein simuliertes Signal erzeugt werden (siehe Abb. 3). Dies wurde für die LISA Pathfinder Mission durchgeführt und steht in der Simulation als FT-Profil zur Verfügung. Weitere Missionen, die im Arbeitspaket 1200 beschrieben wurden, sind bisher noch nicht als Quelle für simulierte FT-Profile umgesetzt worden.

### 3.2 Künstliche Testsignale

Zur Untersuchung von allgemeinen Eigenschaften eines Schubverteilungsalgorithmus sind missionsspezifische FT-Profile nicht geeignet, da sie nur einen speziellen Einsatzzweck widerspiegeln. Für weitergehende Analysen, wie sich der Schubverteilungsalgorithmus unter verschiedensten Bedingungen verhält, benötigt man künstlich erzeugte Signale.

Bei der Verwendung von künstlichen Signalen werden die jeweils drei Komponenten der Kraft und des Momentes zu einem Vektor zusammengefasst, der sechs Dimensionen aufweist. Im Gegensatz zu simulierten missionsspezifischen FT-Profilen, die noch eine direkte Verbindung zu auftretenden Kräften und Momenten haben, sind die künstlichen Profile eher als abstrakte Daten anzusehen. Die sechs Komponenten des Signals beschreiben daher einen Vektor im sechsdimensionalen Raum. Dadurch sind Richtung und Länge festgelegt.

Der Vorteil dieser künstlichen Daten ist die Möglichkeit, praktisch alle Richtungen im 6-D Raum untersuchen zu können, unabhängig davon, ob diese Kommandos physikalisch auf einem Satelliten überhaupt auftreten würden. Das Ziel ist es vielmehr, kritische Konditionen identifizieren zu können und eventuelle Abhängigkeiten der Performance von der Vektor-Richtung zu finden.

Der Begriff der *Richtung* wird im weiteren Text daher auf die gesamten sechs Dimensionen des FT-Profiles bezogen, und nicht auf die drei Dimensionen der getrennten Kräfte und Momente.

Die Randbedingungen für künstliche FT-Profile sind folgende:

- Abdeckung von möglichst vielen unterschiedlichen Kommandorichtungen
- Berücksichtigung der triebwerksspezifischen Randbedingungen

Die zweite Randbedingung wurde eingeführt, da in der Simulationsumgebung aus AP 2100 auch Triebwerke mit einer trägen Dynamik zum Einsatz kommen können. Eine Abfolge von zeitlich nicht-korrelierten Kommandorichtungen könnte dann von der Schubverteilung nicht mehr auf diese Aggregate umgesetzt werden.



### 3.2.1 Erzeugung

Künstliche Signale ohne Bezug auf real auftretende Störkräfte und -momente können mit einfachen Noise-Generatoren erzeugt werden. Es müssen allerdings ein paar Eigenschaften beachtet werden.

Die Wahrscheinlichkeit der Richtungen sollte für alle sechs Dimensionen möglichst gleich verteilt sein. Es sollen keine Häufungen in bestimmten Raumwinkeln auftreten.

Es wurden mehrere Methoden zur gleichförmigen Richtungserzeugung entwickelt. Allerdings musste noch eine Möglichkeit zur Überprüfung der Gleichverteilungseigenschaft definiert werden. Dafür wurde eine Analogie zur Kugeloberfläche herangezogen.

Es wurde die Annahme zu Grunde gelegt, dass Richtungsvektoren, die mit einer gleichmäßigen Verteilung eine Kugeloberfläche durchstoßen, mit ihren Durchstoßpunkten eine gleichförmige Verteilung auf dieser Kugel abbilden. Das heißt, dass die Wahrscheinlichkeit von Durchstoßpunkten für jedes gleich große Flächenelement auf der Kugeloberfläche überall gleich ist.

Mit dieser Annahme wurde der Flächeninhalt von Flächenelementen auf einer Kugel als Maß für die Wahrscheinlichkeit von Durchstoßpunkten der Richtungsvektoren benutzt. Nach Gleichung 3 hängt der Flächeninhalt von Ringsegmenten bei gleichem Kugelradius nur von der Höhe  $h$  der Segmente ab.

$$A_P = A_M = 2 \cdot \pi \cdot r \cdot h \tag{3}$$

Dies gilt sowohl für Elemente an den Polen als auch in der Mitte der Kugel. In Abbildung 4 sind zwei solcher Ringsegmente dargestellt.

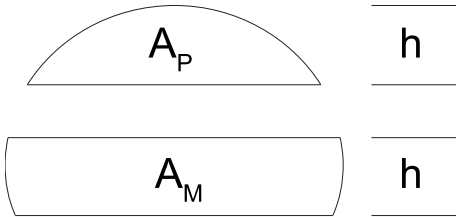


Abbildung 4: Ringsegmente einer Kugeloberfläche

Daraus folgt, dass bei einer Kugel für jeden gleich langen Abschnitt  $h$  der Flächeninhalt gleich ist. Dies gilt für jede Achse durch den Körper. Für die Verteilung der Richtungsvektoren bedeutet es, dass die Wahrscheinlichkeit der Durchstoßpunkte für jeden gleich langen Abschnitt  $h$  auf jeder Achse durch die Kugel gleich sein muss, wenn es sich um eine gleichmäßige Richtungsverteilung handelt.

Zur Überprüfung der unterschiedlichen Generatoren, die gleichverteilte Richtungsvektoren erzeugen sollen, wurde in einer Testumgebung eine große Menge an Richtungsvektoren erzeugt und anschließend mit statistischen Mitteln analysiert.

Für die Untersuchung wurde der dreidimensionalen Raum gewählt, aber die Ergebnisse sollten sich auch auf höhere Freiheitsgrade übertragen lassen. Für die Analyse wurden die produzierten Richtungsvektoren auf die Länge 1 normiert, um die Durchstoßpunkte mit der Kugel zu erhalten (siehe Abb. 5).

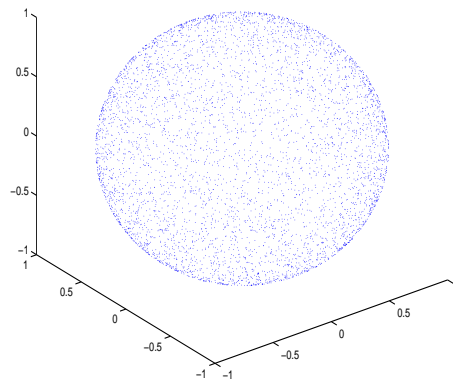


Abbildung 5: Gleichverteilte Durchstoßpunkte von Richtungsvektoren auf einer Kugel

Im Anschluss wurden Histogramme über die Punktverteilung entlang der X, Y und Z-Achse der Kugel erstellt. Nach der oben beschriebenen Annahme sollten die Histogramme bei einer gleichförmigen Punkteverteilung für jeden gleichgroßen Abschnitt auf den Achsen den gleichen Wert zeigen, also ein, im Rahmen der Statistik, konstantes Ergebnis.

### 3.2.2 Kugelkoordinaten

Dieses Modell zur Erzeugung der Richtungsvektoren arbeitet mit zwei Winkeln  $\phi$  und  $\theta$ , um die Raumrichtung zu definieren. Beide Winkelfunktionen werden in ihrem Wertebereich von  $0 - 2\pi$  und  $0 - \pi$  mit gleichförmig verteilten Zufallswerten aufgerufen. In den Abbildungen 6 und 7 ist aber zu erkennen, dass sich an den Polen um die Z-Achse eine Häufung von Punkten bildet.

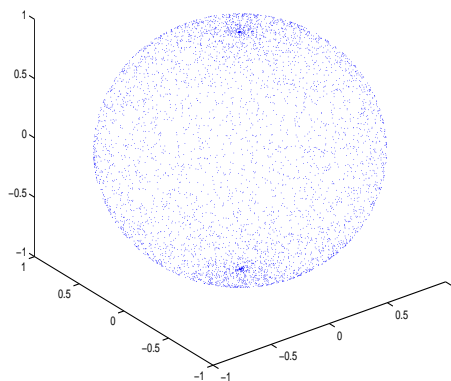


Abbildung 6: Punktverteilung bei gleichverteilten Kugelkoordinaten

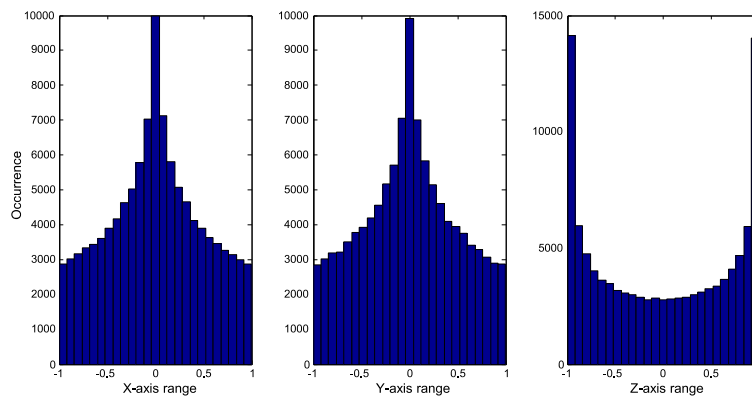


Abbildung 7: Histogramm bei gleichverteilten Kugelkoordinaten

### 3.2.3 Gleichverteiltes kartesisches System

Bei diesem Modell werden die Richtungsvektoren dadurch gebildet, dass jede der drei kartesischen Koordinaten im Bereich von  $-1$  bis  $1$  durch eine gleichverteilte Zufallszahl abgebildet wird. Das Ergebnis ist damit ein Würfelvolumen, in dessen Volumen die Wahrscheinlichkeit für einen Richtungsvektor überall gleich groß ist.

Die Abbildung 8 lässt vermuten, dass mit dieser Methode schon eine gleichförmige Richtungsverteilung erreicht werden kann, jedoch zeigt das Histogramm in Abbildung 9, dass sich in den Eckpunkten des Würfelvolumens Häufungen bilden.

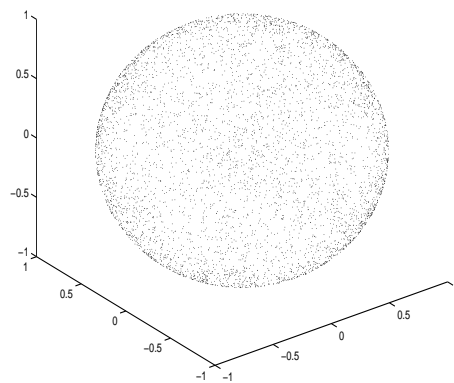


Abbildung 8: Punktverteilung bei gleichverteilten kartesischen Koordinaten

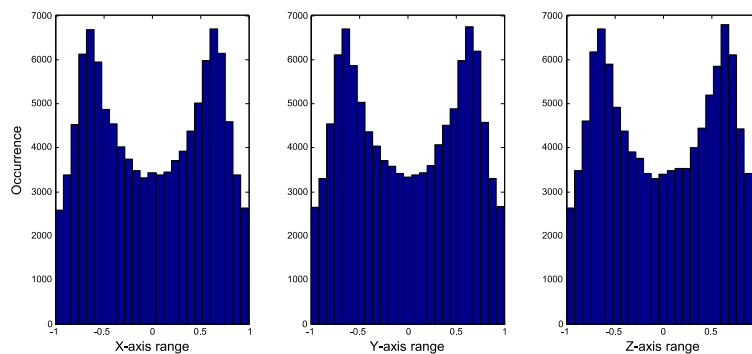


Abbildung 9: Histogramm bei gleichverteilten kartesischen Koordinaten

Der Grund dafür liegt im überschüssigen Volumen des Würfels, das über die Kugelkontur hinausgeht. In Abbildung 10 ist dies verdeutlicht. Hier ist ein Quadrant aus der Kugel ausgeschnitten. Es ist zu sehen, dass im Bereich um die Quadrant-Halbierende

die Würfecke über die Kugeloberfläche hinausragt. Da die Richtungsvektoren im gesamten Würfelvolumen gleichverteilt sind, werden auch die überschüssigen Anteile der Würfecke mit auf die Kugeloberfläche projiziert.

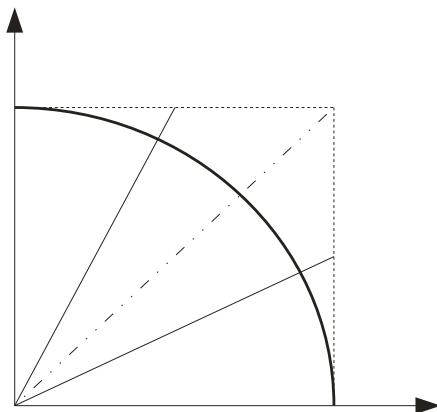


Abbildung 10: Quadrant-Ausschnitt aus Kugelkörper mit umgebendem Würfel

### 3.2.4 Gleichverteiltes kartesisches System mit Grenzwert

Im Gegensatz zum gleichverteilten kartesischen System wird bei diesem Richtungsgenerator nach der Vektorerstellung noch eine Abfrage eingefügt, ob der erzeugte Punkt innerhalb der Einheitskugel liegt. Andernfalls wird das Ergebnis verworfen und ein neues Koordinatentrippl erzeugt. Dadurch wird das umgebende Volumen des Würfels auf das einer Kugel reduziert. Es herrscht jedoch weiterhin eine Gleichverteilung der erzeugten Koordinaten innerhalb dieses Volumens.

Die Abbildungen 11 und 12 bestätigen, dass die daraus gewonnenen Richtungen die Bedingung zur Gleichverteilung erfüllen.

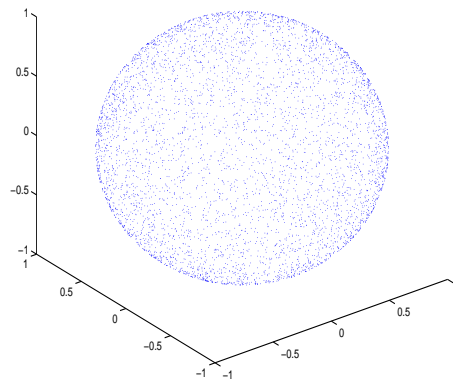


Abbildung 11: Punktverteilung bei abgeschnittenen kartesischen Koordinaten

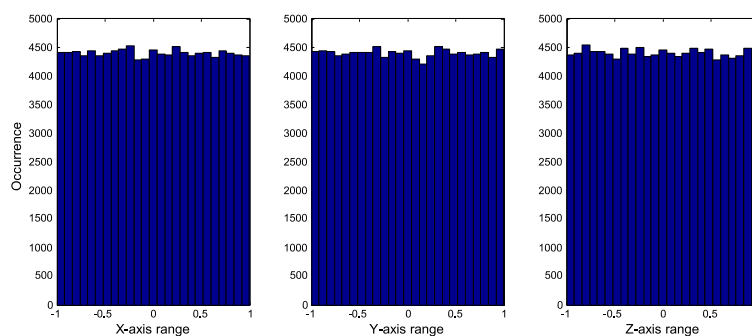


Abbildung 12: Histogramm bei abgeschnittenen kartesischen Koordinaten

### 3.2.5 Normalverteiltes kartesisches System

Bei diesem Modell werden die Richtungsvektoren dadurch gebildet, dass jede der drei Koordinaten durch eine normalverteilte Zufallszahl abgebildet wird. Das Ergebnis ist damit ein unbeschränktes Volumen, in dem die Wahrscheinlichkeit eines Richtungsvektors für jede seiner drei Koordinaten eine Gaußkurve bildet. Das heißt, dass im Bereich des Koordinatenursprungs sich die Punkte häufen und zum Rand hin immer mehr ausdünnen.

In den Abbildungen 11 und 12 ist zu erkennen, dass auch mit dieser Methode gleichverteilte Richtungsvektoren produzierbar sind.

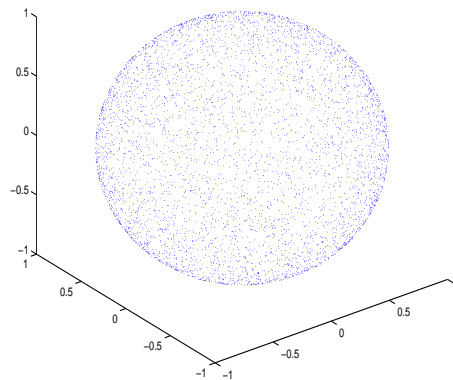


Abbildung 13: Punktverteilung bei normalverteilten kartesischen Koordinaten

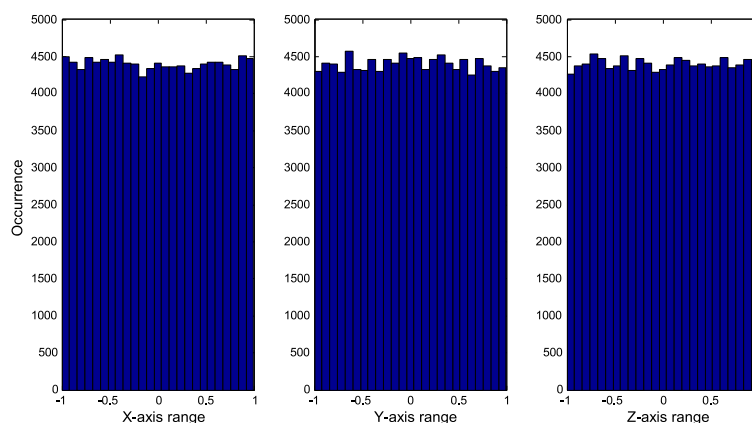


Abbildung 14: Histogram bei normalverteilten kartesischen Koordinaten

Für die Erzeugung der künstlichen FT-Profile wurde das normalverteilte, kartesische

System benutzt, da es zum einen eine Gleichverteilung der Richtung garantiert, und zum anderen ohne innere Abfragen und Schleifen auskommt.

### 3.2.6 Anpassung an Randbedingung der Triebwerke

Neben der Bedingung, dass eine möglichst gleichmäßige Verteilung der Kraft- und Momentenrichtungen vorliegen soll, muss auch auf die dynamischen Eigenschaften der Triebwerke geachtet werden. Aus diesem Grund ist es nicht möglich, das FT-Profil aus einer Reihe von zufälligen und zeitlich nicht korrelierten Kommandos zusammenzusetzen.

Es wurde daher eine *Random-Walk* Methode entwickelt, um die zufällig erzeugten Richtungen langsam ineinander überzuführen. Dies wird über ein dynamisches System zweiter Ordnung realisiert. Die Führungsgröße wird hierbei durch die zufälligen Richtungsvektoren implementiert, die ihrerseits mit einer sehr viel geringeren Frequenz produziert werden, als die Abtastrate des FT-Profiles. Übertragen auf den dreidimensionalen Fall ergibt sich eine Bahn auf einer Kugeloberfläche, wie sie in Abbildung 15 dargestellt ist.

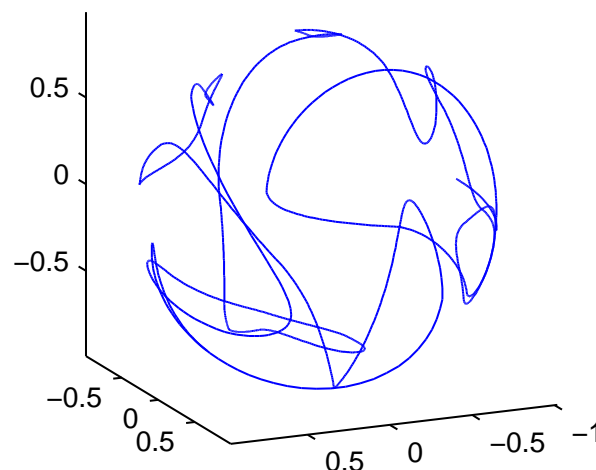


Abbildung 15: Bahn der Richtungsvorgabe auf Kugeloberfläche bei Random-Walk

Bei dieser Methode werden die drei Koordinaten der produzierten Zufallsvektoren unabhängig voneinander durch das System zweiter Ordnung verzögert. Im Anschluss werden die Koordinaten wieder auf die Länge von 1.0 normiert. Die Richtung wandert dadurch langsam auf der Kugeloberfläche von einem vorgegebenen Vektor zum nächsten. Das Random-Walking erfüllt also die Vorgabe, möglichst viele Richtungen für den Schubverteilungsalgorithmus zur Verfügung zu stellen, und berücksichtigt auch die möglichen Trägheiten der Triebwerke. Höherfrequente Störungen werden auch noch auf das Signal aufgebracht, jedoch haben sie eine wesentlich geringere Amplitude. Ein Beispiel für solch ein komplettes Kommandosignal ist in Abbildung 16 zu sehen.



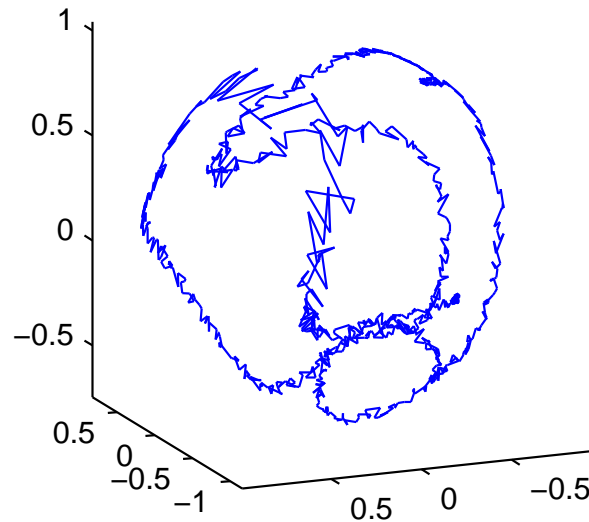


Abbildung 16: Richtungsvorgabe bei Random-Walk mit hochfrequentem Rauschen

Zu beachten ist bei der Erzeugung von künstlichen Signalen noch die Normierung auf die Länge 1. Je nach Verwendungszweck und des zu untersuchendes Triebwerk werden unterschiedliche Skalierungsfaktoren eingesetzt. Im Normalfall ist dies ein Wert von  $5 \cdot 10^{-5}$  für die  $\mu$ -Prolulsion-Triebwerke. Dies hat sich bei den Untersuchungen als brauchbare Einstellung erwiesen.

### 3.2.7 Implementierung

Der Generator für die künstlichen FT-Profile wurde wie die Simulationsumgebung in MATLAB Simulink implementiert. Wie in Abbildung 17 zu sehen ist, gibt es hoch- und niederfrequente Rauschgeneratoren, von denen die langsamen durch ein System zweiter Ordnung gefiltert werden. Vor der Ausgabe und Speicherung des Profils wird noch eine Normierung auf die Hypersphärenoberfläche und eine anschließende Skalierung durchgeführt.

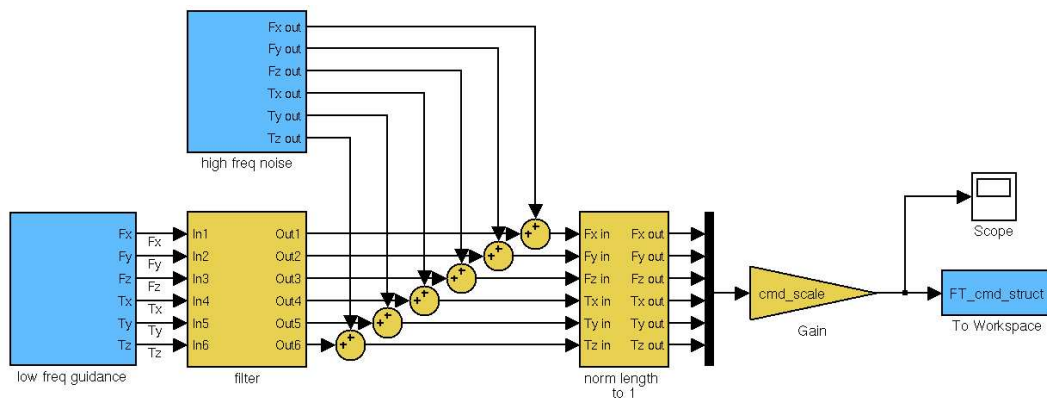



Abbildung 17: Generator für künstliche FT-Profile

Für eine spätere Version der Simulationsumgebung aus Arbeitspaket 2100 kann dieser Generator auch direkt als Ersatz für die FT-Profile eingesetzt werden, um Langzeitsimulationen durchzuführen. Für solche Einsatzszenarien könnten vorgefertigte und gespeicherte FT-Profile sonst zu umfangreich werden.

	Bewertungsfunktionen und Testsignale für Algorithmen des Thruster Actuation Systems	Doc.No.: INT-TAS-TN-ZAR-003 Issue: 1.0 Page: 22 of 22
---	---	---

## Literatur

- [1] D. Bindel. Compilation of  $\mu$ -Propulsion Thrusters for Attitude and Orbit Control of Spacecraft. Technical Report INT-TAS-TN-ZAR-001, Center of Applied Space Technology and Microgravity (ZARM), May 2006.
- [2] D. Bindel. Simulationsumgebung zur Untersuchung von Algorithmen für das Thruster Actuation System. Technical Report INT-TAS-TN-ZAR-002, Center of Applied Space Technology and Microgravity (ZARM), September 2006.

	<p>Endbericht Algorithmen zur Triebwerksansteuerung Fkz: 50 JR 0484</p>	<p>Doc.No.: INT-TAS-RP-ZAR-001 Issue: 1.0 Page: 26 of 20</p>
---	---	--

## Anhang F

Untersuchung einer Beispielmission MICROSCOPE mit Hilfe der in dem Vorhaben entwickelten Methoden



# TAS Analysis for MICROSCOPE

Project:	Document No.:
Thruster Actuation System	INT-TAS-TN-ZAR-005
ZARM - Center of Applied Space Technology and Microgravity	
Am Fallturm	Phone: +49-421-218-8136
D 28359 Bremen	Fax: +49-421-218-2521
Germany	E-Mail: bindel@zarm.uni-bremen.de

Doc. No.: INT-TAS-TN-ZAR-005

Issue: 1.0

Written:

Daniel Bindel

Date: September 6, 2007

Approved: -

Date: -

	TAS Analysis for MICROSCOPE	Doc.No.: INT-TAS-TN-ZAR-005 Issue: 1.0 Page: 2 of 18
---	-----------------------------	--

## Document Change Record

Issue	Date	Changed Pages / Changed Chapters	Remarks	Done
1.0	03.09.2006	all	Initial Version	✓



# Contents

- 1 Introduction** **4**
  
- 2 Control Authority** **5**
  - 2.1 Results . . . . . 5
  - 2.2 Conclusion . . . . . 6
  
- 3 Fuel Consumption** **12**
  - 3.1 Results . . . . . 13
  - 3.2 Comparison of Thruster commands . . . . . 17



## 1 Introduction

This report is a compilation of several investigations, that have been done for the Thruster Actuation System (TAS) of the MICROSCOPE spacecraft. The analyzed subjects are the Control Authority of the system (depending from different TAS methods) and the fuel consumption of the satellite. Here the question of the different fuel consumption of both tank clusters are interesting. That is, because a different drain of the fuel tanks could lead to an additional disturbance of the satellite main experiment sensor.

The analysis was carried out by using data from ONERA/CNES (configuration map, controller commands of one orbit, thruster commands of one orbit). The thruster commands of the different analyzed TAS algorithms where also compared to the original provided.



## 2 Control Authority

The control authority (CA) of a spacecraft defines the maximum forces and torques, that can be provided by the AOCS system. This includes the thrusters and any other actuators for forces and torques on the spacecraft and the TAS method to command them.

The following figures display the results of the CA analysis of the cold-gaz configuration of the spacecraft MICROSCOPE. The limitations for the thrusters where  $T_{min} = 0.5\mu N$  and  $T_{max} = 500\mu N$ . The following Thruster Actuation System algorithms have been used for the analysis:

- Direct Pseudoinverse algorithm (simple Moore Penrose pseudoinverse matrix)
- Nonlinear Iterative Pseudoinverse (NIP) algorithm (upper limit of propulsion system was bound to  $T_i \leq T_{max}$ ), low accuracy (see fig. 10)
- Linear Programming with minimization for vector Norm 1
- Linear Programming with minimization of tank drain difference (Norm MICRO)

### 2.1 Results

An interesting outcome of the analysis was the fact, that the choice of the thruster actuation algorithm has only a minor influence to the size of the control authority. The maximum values for all different methods are virtually the same (see table 1). Differences exist only in the outer shape of the Force-CA between the direct pseudoinverse algorithm and the iterative algorithms. The figures include cut planes through the major axes and an isometric view of the three-dimensional surface. This view is also illuminated, to show the differences of the shape, which are not visible in the 2D plots. The plot of the maximum torques (fig. 5) have been done only for the pseudoinverse algorithm, because the numerical results and the shape of the CA-surface are exactly the same for all of the TAS method.

Please keep in mind, that the control authority is a six-dimensional surface. So it is quite difficult to display it in one piece. The general convention is to plot the three-dimensional cut spaces for the maximum forces with no torques applied and the maximum torques with no forces applied. Of course there exist combinations between these special cases, because the control of a drag free satellite requires the simultaneous application of forces and torques.

The method to determine the control authority size is an iterative approach. A vector generator selects a six-dimensional direction and a length of that vector (see eq. 1), to test, if the TAS algorithm can accomplish that command with the available thrusters. The vector generator is increasing the  $cmd_{len}$  variable, until the resulting command

Axis	Pinv	NIP	LP Norm 1	LP Norm MICRO
+X force	1608	1602	1608	1608
-X force	-1608	-1602	-1608	-1608
+Y force	900	900	900	900
-Y force	-900	-900	-900	-900
+Z force	653	653	653	653
-Z force	-653	-653	-653	-653
+X torque	647	647	647	647
-X torque	-647	-647	-647	-647
+Y torque	539	539	539	539
-Y torque	-539	-539	-539	-539
+Z torque	798	798	798	798
-Z torque	-798	-798	-798	-798

Table 1: Maximum forces and torques in  $\mu N$  and  $\mu Nm$

vector is exceeding the control authority ( $FT_{act} < FT_{cmd}$ ). Then it is slowly decreased, until the difference between the commanded and actuated forces and torques are below a certain value (currently  $0.1\mu N$ ). The method of the control authority determination is therefore not mathematically proven accurate. But it works with virtually every thruster actuation algorithm, that is able to handle force/torque commands outside the control authority of the spacecraft and calculates sensible thruster commands.

$$cmd_{vec} = cmd_{len} \begin{bmatrix} dir_{Fx} \\ dir_{Fy} \\ dir_{Fz} \\ dir_{Tx} \\ dir_{Ty} \\ dir_{Tz} \end{bmatrix}; ||dir|| = 1.0 \quad (1)$$

## 2.2 Conclusion

The difference of the control authority for the MICROSCOPE configuration between the Nonlinear Iterative Pseudoinverse method and the Linear Programming is not recognizable. Though that behaviour is conform with the observations for these iterative algorithms. For a small number of thrusters, the results of the NIP and the Linear Programming are almost identical in terms of fuel consumption and the size of the control authority. But when the number of available thrusters is increased, the Linear Programming can gain some advantage against the NIP. A test with a theoretical 32 thruster spacecraft led to differences of 17% in the fuel consumption and a larger control authority.

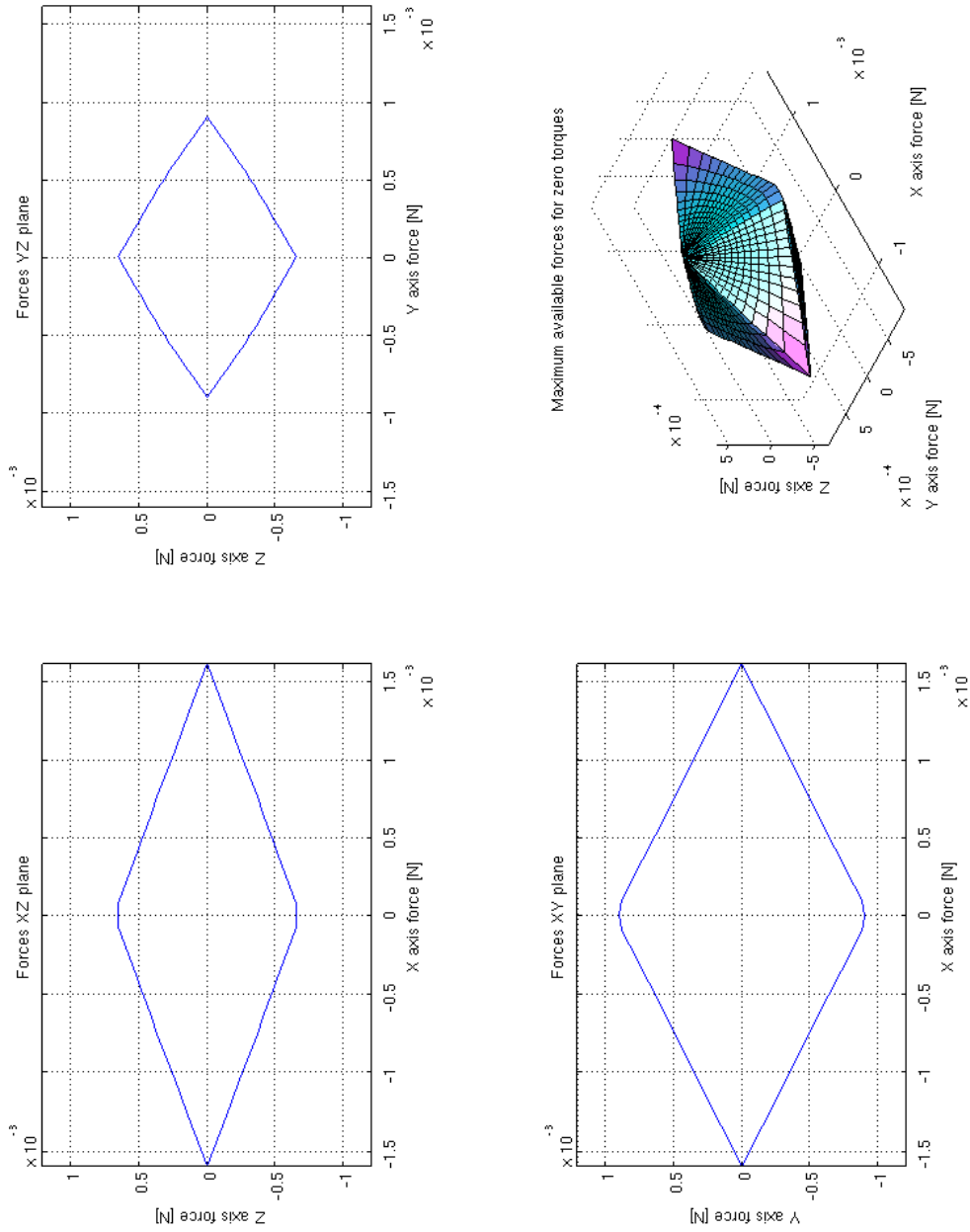


Figure 1: Control Authority, Forces, Direct Pseudoinverse

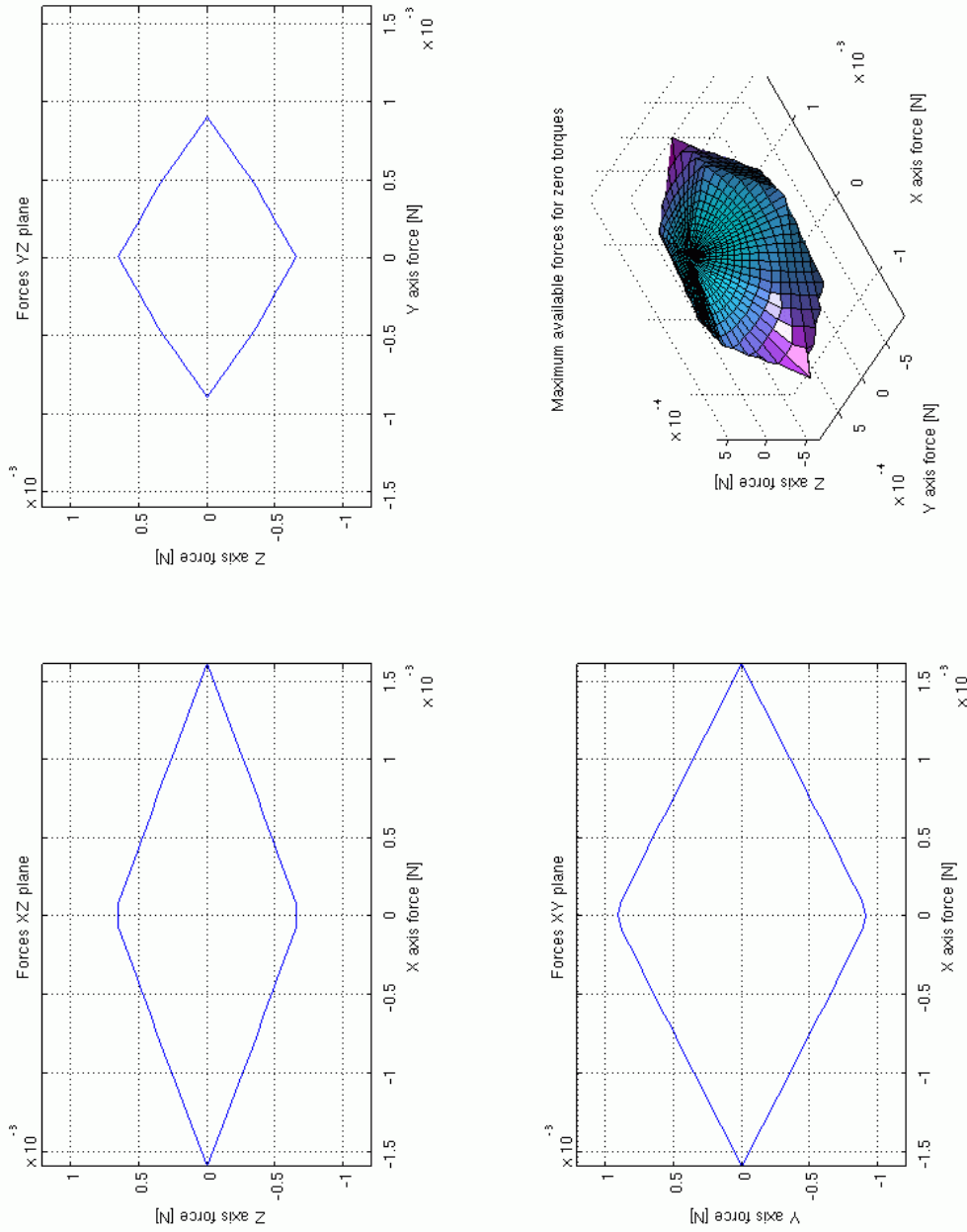


Figure 2: Control Authority, Forces, NIP

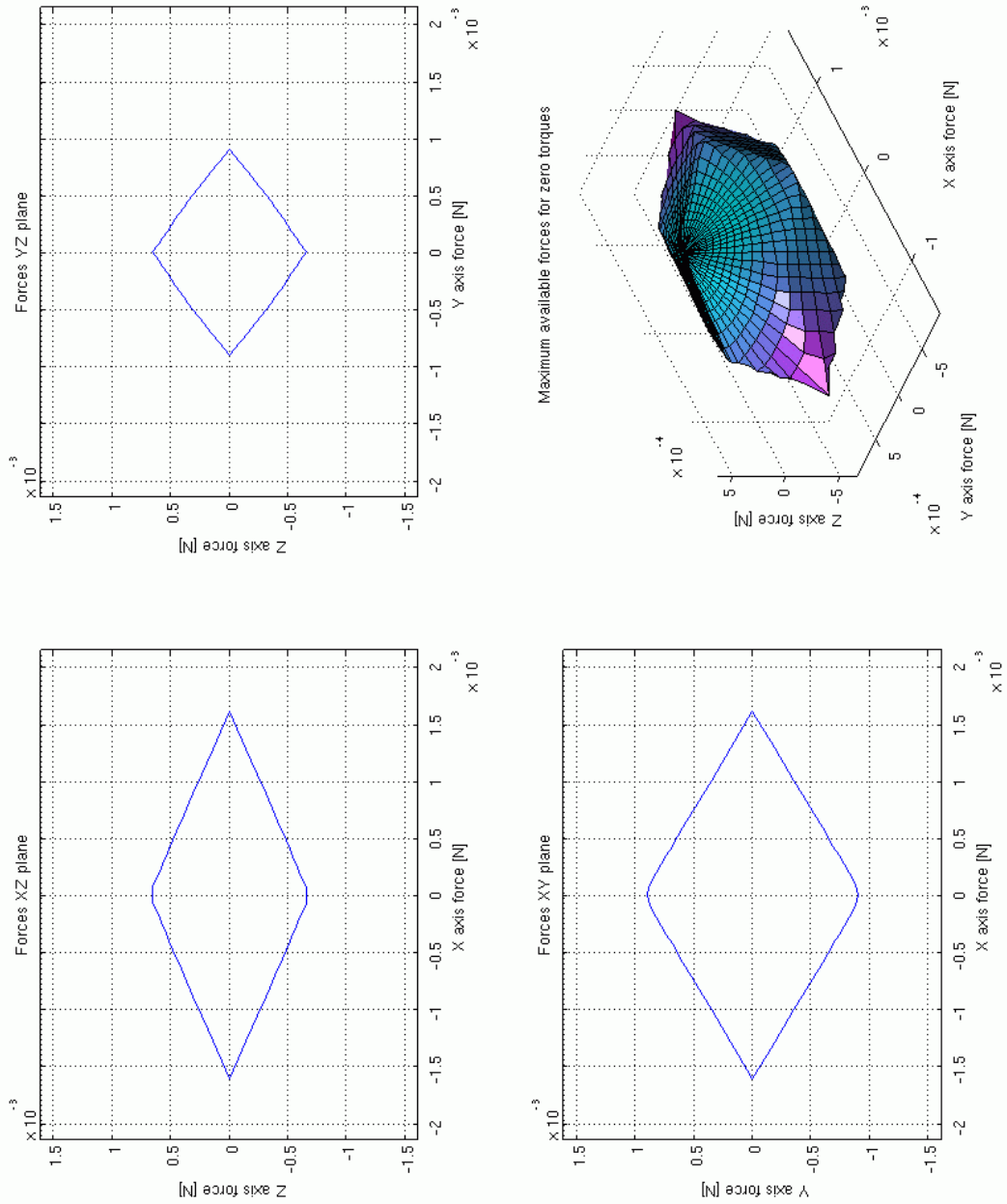


Figure 3: Control Authority, Forces, Linear Prog. Norm 1

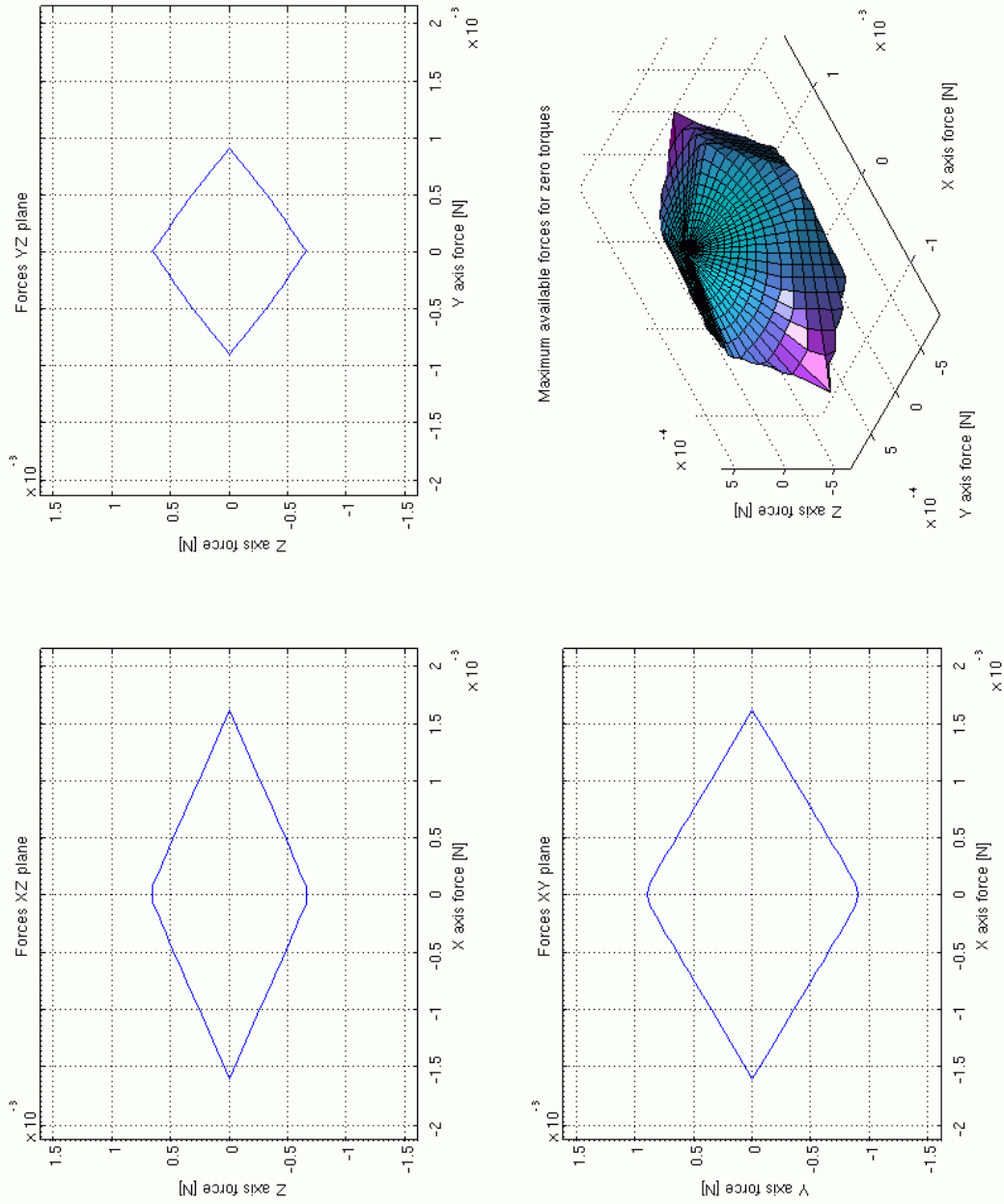


Figure 4: Control Authority, Forces, Linear Prog. Norm MICRO

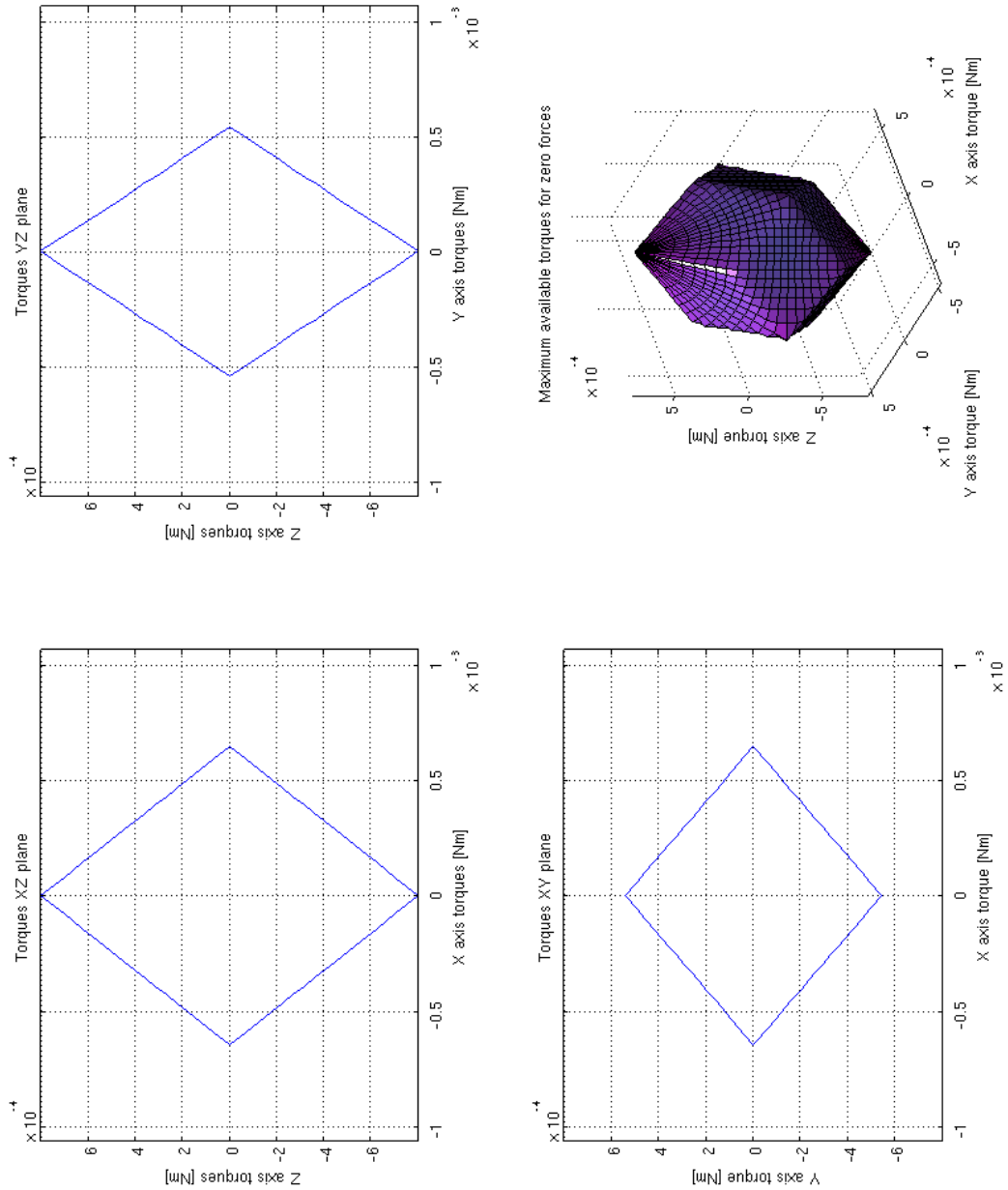


Figure 5: Control Authority, Torques, all algorithms

### 3 Fuel Consumption

The analysis of the fuel consumption for the MICROSCOPE spacecraft has been performed with an exemplary force/torque profile for one orbit as displayed in figure 6. The TAS methods, used for the fuel consumption analysis have been the same as for the control authority investigation.

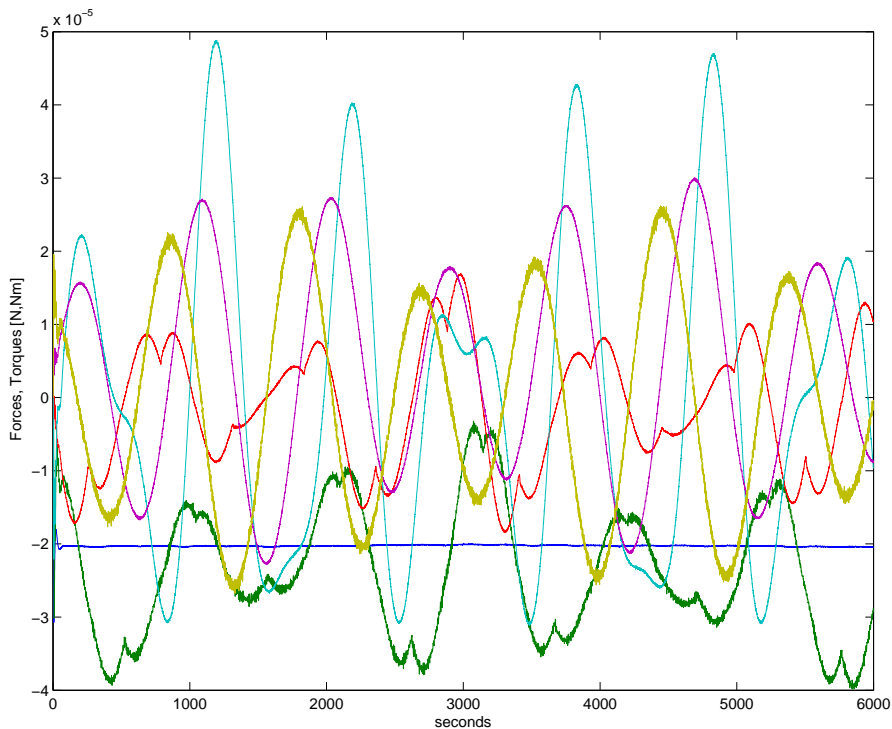


Figure 6: MICROSCOPE commanded forces and torques

The object of interest was the overall fuel consumption and the difference of the fuel drain between the two coldgas tank clusters.



### 3.1 Results

The results for the consumed massflow are displayed in table 2. It is obvious, that the direct Pseudoinverse method can not meet the optimal results of the Linear programming or the NIP algorithm in terms of total fuel efficiency. But an interesting point is the difference of the fuel drain from both tank clusters. The thrusters of the first tank are consuming 48.62 mg more gas in one orbit, than the thrusters of tank 2. This is also displayed in the figures 8 and 9.

tank	Pinv	NIP	LP Norm 1	LP Norm MICRO
total	1852	1471	1497	1497
tank2-tank1	-48.62	-48.62	-48.62	-48.62

Table 2: Consumed fuel in mg

After some investigations, the reason for this behaviour seems to be the commanded forces on the spacecraft Z axis. Figure 7 shows at least a correlation of the signal. The upper graph displays the accumulated impulse on  $F_z$  that is commanded by the AOCS controller. The lower graph shows the difference in the accumulated massflow of both tank clusters.

An explanation for this behaviour may be the configuration of the thrusters. Due to the package of both tanks on the positive and negative Z panel of the spacecraft, the thrusters are decoupled in the Z axis. Therefore, the thrusters of tank 1 can only provide forces in the negative Z direction and vice versa. The X and Y force axes on the other hand are coupled by both thruster packages, as are the torques on all three axes. The result of this configuration is, that any non-zero accumulated impulse on the Z axis is directly represented in a tank drain difference. So it seems impossible, to counter that problem with a smart thruster actuation algorithm.

$$\sum_0^{t_{end}} F_z \Delta t_{FT} = \Delta t_{FT} \sum_0^{t_{end}} F_z = \text{accumulated impulse} \quad (2)$$

$$F = \dot{m} I_{sp} g_0 \text{ with } F = \dot{m} c_e \text{ and } I_{sp} = \frac{c_e}{g_0} \quad (3)$$

$$\sum F_z \Delta t_{FT} = \sum \dot{m}_{diff} I_{sp} g_0 \Delta t_{\dot{m}} dir_z \quad (4)$$

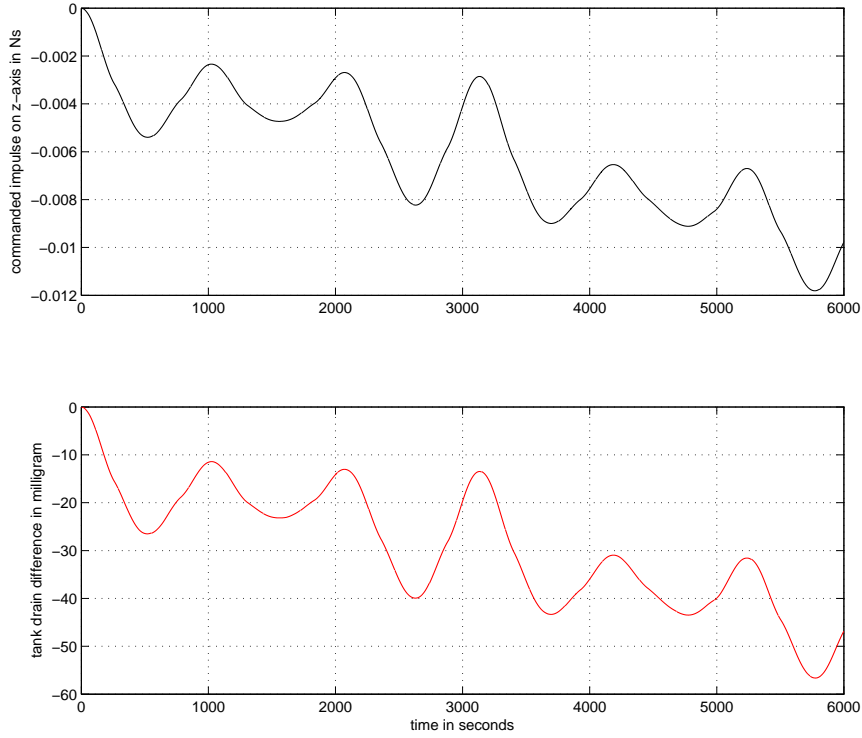


Figure 7: Accumulated commanded impulse on Z axis and difference tank drain

$$dir_z = 0.342 \text{ (from configuration map)}$$

$$\Delta t_{FT} = 0.25s$$

$$\Delta t_{\dot{m}} = 0.1s$$

$$\Delta t_{FT} \sum F_z = -9.785 \text{ mNs} \quad (5)$$

$$\Delta t_{\dot{m}} I_{sp} g_0 dir_z \sum \dot{m}_{diff} = -9.786 \text{ mNs} \quad (6)$$

The prove of the cohesion of the Z axis impulse and the massflow difference is displayed in the equations 2 to 6. Here the accumulated impulse on the Z axis (eq. 2) is expressed by a product of the massflow difference  $\dot{m}_{diff}$ , the specific impulse  $I_{sp}$ , the gravitational acceleration  $g_0$  and the force vector component  $dir_z$  which indicates, how much fraction of the thruster force is applied in Z direction (eq. 4). There are two different values for the time steps  $\Delta t_{FT}$  and  $\Delta t_{\dot{m}}$ , because the FT-profile was provided with 4Hz and the simulation was performed with 10Hz.

The results in equation 5 and 6 show, that the accumulated impulse on the Z axis is the dominant reason for the difference in the thruster fuel consumption.

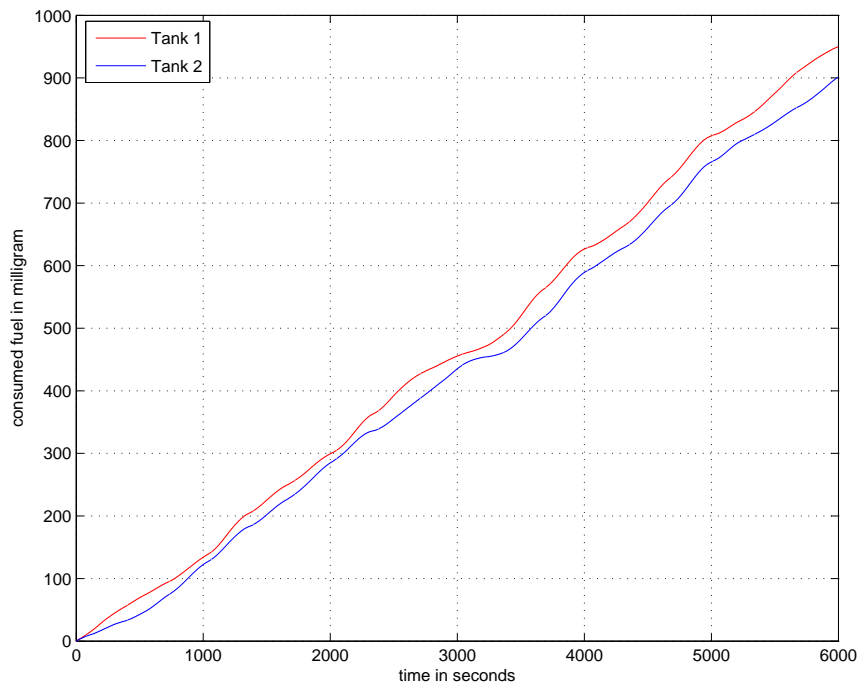


Figure 8: Fuel consumption of direct Pseudoinverse Method

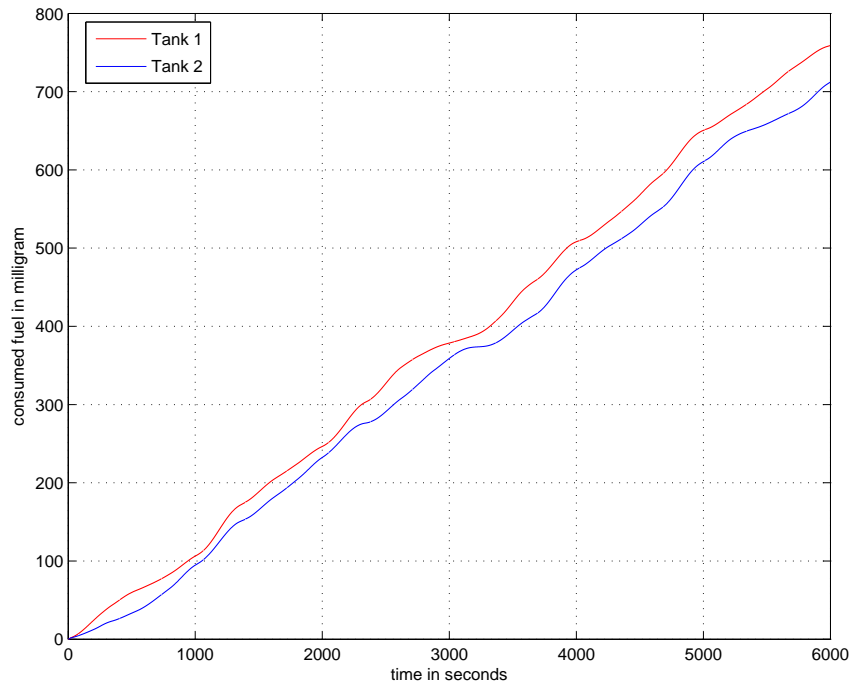


Figure 9: Fuel consumption of NIP algorithm

### 3.2 Comparison of Thruster commands

The thruster command outputs of the different TAS methods have been compared to the original thruster commands of the Nonlinear Iterative Pseudoinverse Decomposition (NIP deco) algorithm. A first issue for the interpretation of the command profile is the accuracy of the solution (difference between commanded and actuated forces and torques). In figure 10 the different methods are compared. Please note, that the own implementation of the standard NIP algorithm have been carried out with a low accuracy (convergence criterion set to  $5 \cdot 10^{-3}$ ) and high accuracy (convergence criterion set to  $1 \cdot 10^{-7}$ ) version.

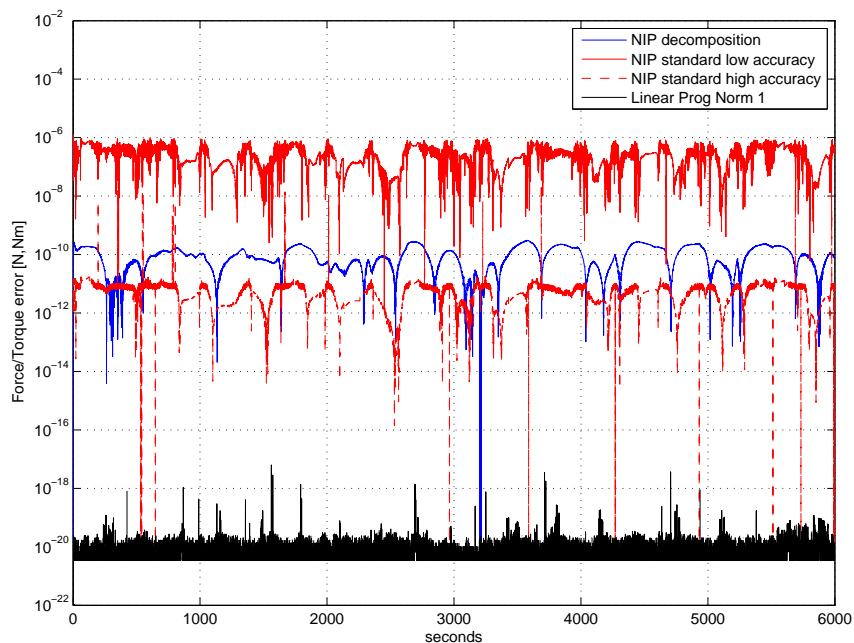


Figure 10: Accuracy of different TAS algorithms (length of error vector)

Table 3 displays the different results for the fuel consumption. If you compare these results to table 2, you will see, that these numbers are different. The reason for that fact is the different minimum thrust that was used for the analysis.

The thrust range of the coldgas thrusters have been characterized with  $T_{min} = 0.5\mu N$  and  $T_{max} = 500\mu N$ . Apparently, the delivered thrust command profile for the NIP deco algorithm indicates a minimum thrust of  $2.5\mu N$ . So the analysis of the thrust command comparison have been performed with that value.

The outcome of the different TAS methods are all in the range of  $1660mg$ . Please note, that the good result of the low accuracy NIP method corresponds to a higher error in

the force/torque calculation (fig. 10).

tank	NIP deco	NIP low accuracy	NIP high accuracy	LP Norm 1
total	1663	1635	1660	1660

Table 3: Consumed fuel in mg

The figures 11 and 12 display the difference between the thruster commands of the original NIP deco profile and the compared methods. The biggest differences are observed to the low accuracy version of the standard NIP implementation, while the high accuracy NIP and the Linear Programming produce a more equal result. In figure 12 only the difference between NIP deco and the Linear programming is displayed, because the thruster commands of the Linear Programming and the high accuracy NIP version are virtually the same.

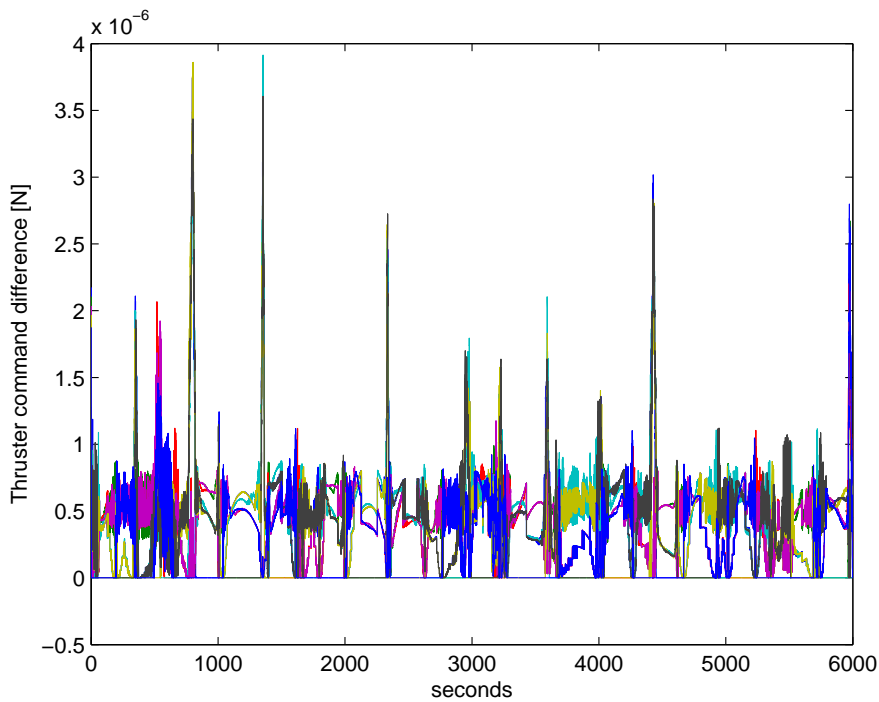


Figure 11: Thruster command difference between NIP deco and NIP low accuracy

It is an interesting fact, that the difference is always positive, so the NIP deco thruster commands are greater or equal to the solutions of the other algorithms. There are also some singular situations, where the difference is up to a few micro Newton, but that is perhaps based on the working method of the NIP Decomposition algorithm.

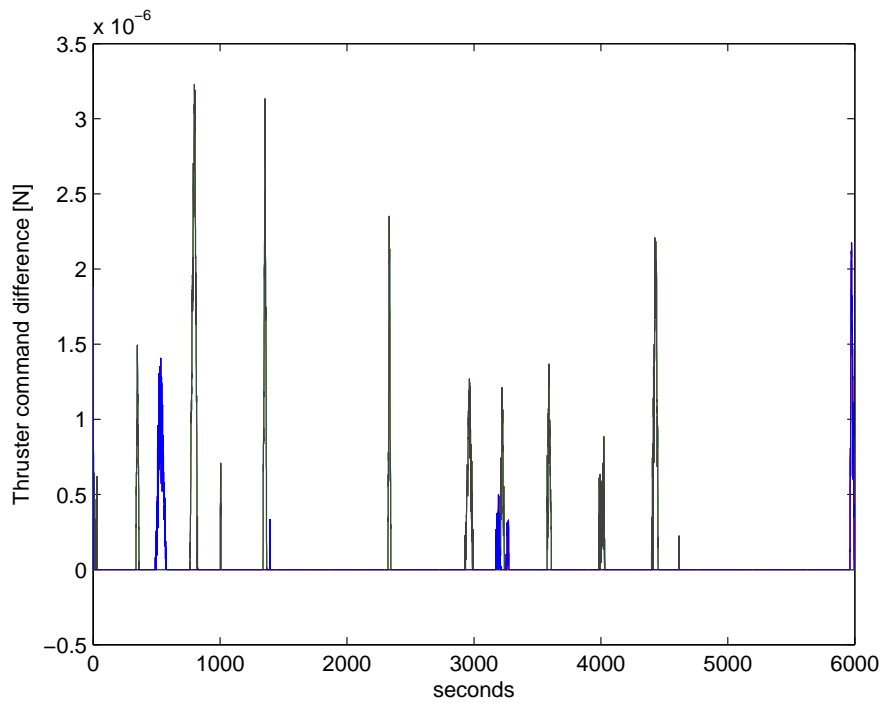


Figure 12: Thruster command difference between NIP deco and Linear Prog Norm 1

	<p>Endbericht Algorithmen zur Triebwerksansteuerung Fkz: 50 JR 0484</p>	<p>Doc.No.: INT-TAS-RP-ZAR-001 Issue: 1.0 Page: 27 of 20</p>
---	---	--

## Anhang G

Kurze Beschreibung zu einem zusätzlich entwickelten Werkzeug zur Auslegung des Triebwerkssystems auf Satelliten (CAAT)





CAAT  
Control Authority Analysis Tool  
Manual

Doc.No.: INT-TAS-TN-ZAR-004

Issue: 1.0

Page: 1 of 13

# CAAT

## Control Authority Analysis Tool

### Manual

Project:	Document No.:
Thruster Actuation System	INT-TAS-TN-ZAR-004
ZARM - Center of Applied Space Technology and Microgravity	
Am Fallturm	Phone: +49-421-218-8136
D 28359 Bremen	Fax: +49-421-218-4356
Germany	E-Mail: bindel@zarm.uni-bremen.de

Doc. No.: INT-TAS-TN-ZAR-004

Issue: 1.0


Written:

Daniel Bindel

Date: 2nd March 2007

Approved: -

Date: -

	<p>CAAT Control Authority Analysis Tool Manual</p>	<p>Doc.No.: INT-TAS-TN-ZAR-004 Issue: 1.0 Page: 2 of 13</p>
---	--	---

## Document Change Record

Issue	Date	Changed Pages / Changed Chapters	Remarks	Done
1.0	23.02.07	all	Initial Version	✓

# Contents

<b>1</b>	<b>Introduction</b>	<b>4</b>
1.1	Analysis features . . . . .	4
<b>2</b>	<b>Beginners Guide</b>	<b>5</b>
<b>3</b>	<b>Advanced Guide</b>	<b>7</b>
3.1	CA Database . . . . .	7
3.2	Custom Thruster Configuration . . . . .	8
3.3	Custom Thruster Model . . . . .	10
3.4	Custom Thruster Actuation System . . . . .	10
3.5	Working Principle . . . . .	12

# 1 Introduction

This document is a brief manual to the Control Authority Analysis Tool (CAAT), based on Matlab Simulink. It provides the basic information, to use this tool and calculate the CA of different thruster configurations. A second part will help the user to add his own thruster configuration to the system.

The underlying software of the CAAT was developed in the scope of a DLR founded project to research advanced Thruster Actuation Systems (TAS) for micropropulsion thrusters. The current analysis tool is a modified frontend of the Matlab Simulink libraries from the TAS test environment. So there are some parts in CAAT that are still compatible with the TAS test bench. The interface for the different TAS algorithms and thruster models are examples for this compatibility. An updated version of the original TAS test environment can be added to CAAT and is able to use shared information (model and library files).

That would enable the analysis of the fuel consumption or the noise level of the entire propulsion system in a working situation.

## 1.1 Analysis features

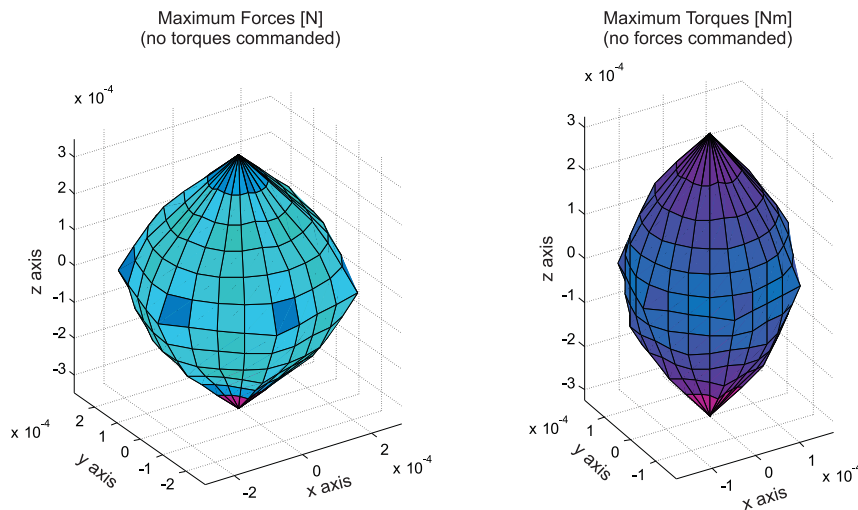


Figure 1: Control authority of LISA Pathfinder spacecraft (FEFP thruster)

The task of CAAT is of course the calculation of the control authority of a spacecraft. That are the maximum available forces and torques, that the propulsion system can provide. The Figure 1 depicts such a control authority for the exemplary LISA Pathfinder spacecraft.

There are three different elements, that influence the size and shape of the control authority. The biggest influence is the thruster type. A more powerful engine results in a larger control authority. The next element is the thruster configuration. It can be designed in a symmetrical way, to provide even forces and torques for every direction. But the thrusters may also be arranged in a way, that they are optimized for a certain bias or main-thrust direction. The number of thrusters is also very important. The last influencing element is the used TAS algorithm. In this version of CAAT, two different families of TAS methods are included. The first are direct solution algorithms (Pseudoinverse) and the other are iterative linear programming methods (Simplex). The results of them are quite different.

## 2 Beginners Guide

This is a short description, how to use CAAT to calculate the control authority for existing thruster configurations.

Start Matlab and enter the directory *m-files* in the CAAT package. Execute the script *ca\_init* and the main control window should appear as shown in Figure 2.

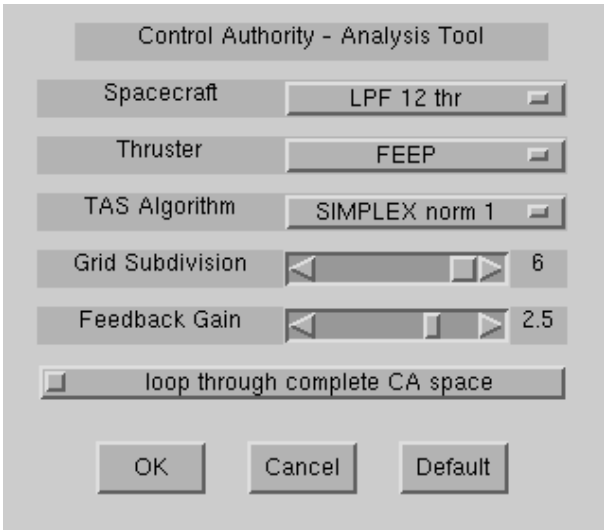


Figure 2: Main control window

Here you can choose different settings for the actual CA calculation.

- **Spacecraft:** Select one of the pre-defined thruster configurations. Currently there are two different configurations for the LISA Pathfinder, a preliminary LISA configuration and a exemplary config for a 32 thruster spacecraft (Hedgehog).

- **Thruster:** Choose between different engines. The pre-defined models range from FEEP to RIT. The only real difference is their maximum and minimum available thrust.
- **TAS Algorithm:** Select one of the Thruster Actuation algorithms. There are pre-compiled S-Functions for Pseudoinvers and Linear Programming methods.
- **Grid Subdivision:** This setting affects the resolution of the control authority grid. Smaller values result in fast calculation but very angular shapes, higher values take longer to compute but give smoother results.
- **Feedback Gain:** Controls the speed of convergence for each CA calculation. Most times, a high value is useable. But unusual thruster configurations may need lower values to converge. Anyway, the CA vector generator will decrease the feedback gain itself for every grid-point, if it can not find a convergence.
- **Complete CA space:** This is a switch, to enable the CA calculation for the entire six-dimensional force/torque space. For a first look, it should be switched *OFF* to keep the calculation time down. Then only the CA grid-points are calculated, where the forces and torques are zero (resulting in two plots at the end).

After choosing your preferred setup, click on *OK* and the simulation will automatically be configured and loaded. It should look like Figure 3.

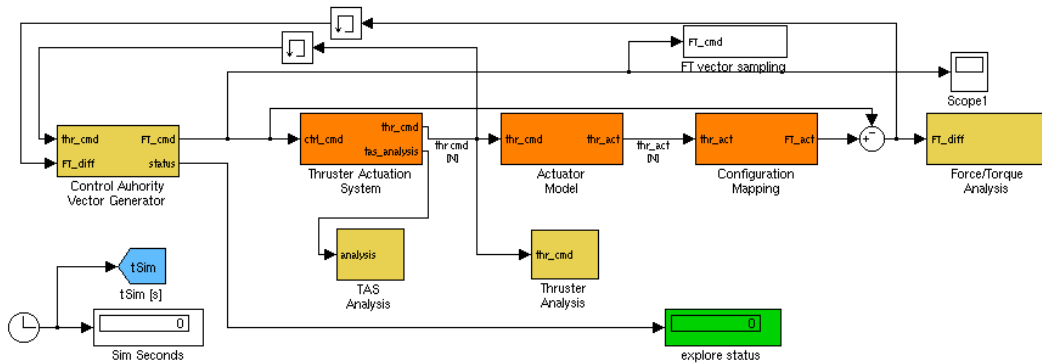



Figure 3: Simulation display

Now you just start the simulation as usual. The most interesting element is the *explore status* display. It shows the fraction of already calculated data. When it reaches 1.0 the CA computation is finished. The simulation will then stop automatical.

Execute the script *plot\_ca* to get the visual display of the control authority like Figure 1.

	CAAT Control Authority Analysis Tool Manual	Doc.No.: INT-TAS-TN-ZAR-004 Issue: 1.0 Page: 7 of 13
---	---	--

## 3 Advanced Guide

In this section the internal functions of CAAT are explained. This is useful, if you want to add your own thruster configuration to the system or change the display mode of the control authority.

### 3.1 CA Database

One of the most important elements of the analysis tool is the underlying database *db\_casize*. It is stored in the basic workspace of Matlab and contains the calculation results of the simulation.

Due to the six-dimensional nature of the control authority, this database is organized as a storage for sphere-coordinates. Imagine a six-dimensional hypersphere with five angles to define a direction and radius to define the distance of each surface point from the zero-origin. The database is a five-dimensional array to reflect the angles and the stored value is the calculated radius.

The number of elements in this array is defined by the *grid subdivision* setting *n* in the main GUI. There are  $4 \cdot n$  subdivisions for the first angle (*Force<sub>XY</sub>* plane, full circle) and  $2 \cdot n + 1$  subdivisions for every further angle (higher dimensions, half circle). So you can imagine that a high value of *n* will result in a large amount of memory usage.

The range of the angles is 0 to  $2\pi$  for the first angle and  $-\pi/2$  to  $\pi/2$  for all other angles. The database *db\_explore* works almost the same, but it does not contain the radius of the control authority, but zeros and ones. If CAAT has calculated the control authority for one specific point on the hypersphere surface, the value 1.0 is stored in the *db\_explore* database. Points, that not yet have been calculated contain a zero. By simply adding all elements in the database and dividing it by the number of entries, the *explore status* can be simply calculated.

The six-dimensional nature of the complete control authority is also problematic to display on a two-dimensional media or even to imagine. So there are virtual cutting planes used, to decrease the number of dimensions. To be exact, the *plot\_ca* script uses three-dimensional cutting spaces to display things, but it works just the same way, as if you would use a 2-D plane to get an intersection cut of a sphere.

The numbering scheme of the angles is done in a way, that there is always a discretized angle for the value *zero*. So we have sections in the complete CA space, where the vector direction  $F_x, F_y, F_z$  can have any value, and its components  $T_x, T_y, T_z$  are zero. This section describes the control authority for the case, when no torques are commanded to the propulsion subsystem and only the maximum available forces are required.

The other way around it is slightly more difficult. As the first angle *alpha* is a full circle in the *Force<sub>XY</sub>* plane, it can not set the values for x and y to zero at the same time. But if you choose the second angle *beta* in one of its singularities ( $-\pi/2$  or  $\pi/2$ ), the vector length in the *Force<sub>XY</sub>* plane becomes zero. This simple trick is used with the third



angle  $\gamma$ . By setting it to a singularity, it cuts down the components  $F_x, F_y, F_z$  of the direction vector to zero.

This trick with the  $\gamma$  angle is also necessary to reduce the number of angles for the *maximum torque* display. By cutting the CA space down to its three-dimensional section, where all forces are zero, the maximum available torques form a normal three-dimensional shape in sphere-coordinates (see right plot of Figure 1). So it is described with one full circle and one half circle. With  $\gamma$  being either  $-\pi/2$  or  $\pi/2$  you can combine it with the half circular angle  $\delta$  to a full circle, representing the azimuth  $Torque_{XY}$  plane, and  $\epsilon$  the elevation for the  $Torque_Z$  component.

This introduction into some aspects of the underlying mathematics is needed to understand the *Full CA space* switch in the main GUI at the beginning. If you set it to OFF, then CAAT will only calculate these points, that are later on displayed in the maximum force and maximum torque figure. But that is only a fraction of the full control authority. By activating the *Full CA* switch, you can command the analysis tool to compute the full six-dimensional hypersphere. But anyway, you will have to develop a sophisticated algorithm, to display the desired data. The minimum control authority would be an example to investigate the coupled force/torque behavior of a propulsion system.

With the full CA space you can compute for every force direction the minimum available torque margin and the other way around.

## 3.2 Custom Thruster Configuration

One main usage of CAAT is of course the investigation of different thruster configurations. So this subsection explains the way, how new thruster configurations can be added to the system. You will be able to analyse the control authority of your spacecraft design.

Basically a thruster configuration breaks down to a collection of numbers, giving the position and orientation of every thruster in respect to the center of mass, as seen in the following table. Remember, that all position data are given in meters, with respect to the center of mass. The direction data are elements of the unit-length vector, describing the thruster main axis.

thruster	$pos_x$	$pos_y$	$pos_z$	$x\_dir_x$	$x\_dir_y$	$x\_dir_z$
thr 01	0.638372	0.768405	0.591937	0.146689	-0.924034	-0.353049
...	...	...	...	...	...	...

Every thruster configuration has an init script to load this numeric data. You can find examples in the *spacecraft* folder of the CAAT package. Copy one of the existing init files and edit it to fit your needs.

Make sure, that you enter the correct number of thrusters  $n\_thr$ . Fill the array *thr\_raw\_config* with your data. Be careful with the *direction* data of the engines. The analysis tool



needs the force direction of the thruster. But some documentation provide only the thrust exhaust direction. You should negate the data in that case.

The script will itself calculate the necessary *FT\_Map* for the TAS algorithms. If you are using only the Linear Programming TAS algorithms you are almost finished with the config setup. But if you want to test also the Pseudoinverse control methods, you have to calculate the pseudoinverse matrices.

Go into the *tools* folder and locate the m-files *Precompute\_FT\_Pinvmat* and *Precompute\_FT\_Nullspace\_XXXthr*. There are some variations of the nullspace script. If your number of thrusters is different from the pre-defined scripts, change the existing m-files to your needs.

You will need the array *FT\_Map* in your Matlab workspace, in order to execute these files. So just run your previously created thruster-config file to get it.

The *Precompute* scripts will save their results automatically. The example files in the folder show you how to rename the produced files. The nullspace file with the *mp* element in its name belongs to the folder *algorithms/pinv\_mp/configs*. The other two files should be copied to *algorithms/pinv/configs*. The Moore-Penrose version of the Pseudoinverse matrix algorithm needs only a nullspace vector to operate and calculates the necessary pseudoinverse matrix during its initialization phase.

Related to the number of thrusters is also the internal thruster model array. It is located in the folder *m-files* in the library *thrusters.mdl*. There are already pre-defined thruster arrays for 8, 12 and 32 engines. If you want to add a thruster configuration with a different number of thrusters, then modify one of the existing Simulink subsystems and give it a proper name. afterwards you have to enable it in the template *Used\_Thr\_Array* in the same library. This is important for the automatic configuration of CAAT. The last step is the update of the *Thr\_Array\_Link* subsystem. Open it, and replace the existing *Used\_Thr\_Array* link with the current version of the template. That will enable the main model *ca.test.mdl* to use your new configuration.

All these previous steps have been preparations for the automatic configuration of CAAT. But you will have to tell the system, that there is a new thruster configuration to be used. This is done in the file *m-files/ca\_init* in the lines for *SC\_list* and *SC\_result*. The first list contains the strings, that are displayed in the main control GUI (Figure 2). The second list translates this into the internal identification strings for the auto-config. Just add the name of your configuration here. You should also make shure, that you have placed the init file for your thruster configuration in a folder that is in the Matlab search path. Otherwise there also exists the script *set\_paths* that you may update with an additional folder path.



### 3.3 Custom Thruster Model

Another way to customize the CAAT is the introduction of your own thruster model. For a simple CA analysis, it is sufficient to provide only the minimum and maximum thrust of the engines.

The CAAT needs only a simple init file to retrieve the necessary thruster parameter. In the directory *thruster* you will find several subfolders for every implemented thruster model. Each engine has its own init file. If you want to add an additional thruster model you have to provide the same interface for the autoconfig mechanism, as the existing models. These are the minimum and maximum thrust level  $T_{min}$  and  $T_{max}$ , the number of required seeds for random number generators ( $n_{seed}$ ), the maximum allowed thrust step for one simulation cycle ( $max\_delta$ ) and an additional custom structure to describe even more engine model parameters ( $Thr\_params$ ).

For the most simple model, set only the minimum and maximum thrust, leave  $n_{seed}$  to zero, set  $max\_delta$  to  $T_{max}$  and fill the structure  $Thr\_params$  with the fields  $T_{min}$ ,  $T_{max}$  and  $max\_delta$ .

The other parameter can be used by detailed Simulink thruster models in other simulations. It is possible, to describe the dynamic behavior and the noise properties of an engine type. But that is not part of the current CAAT version.

When you have created your own init file, make sure, that it can be found by Matlab. Update the *set\_paths* file, if necessary. Also check, if you have a proper name for your new thruster model. Include it in the name of the init script and the corresponding init function like *init\_feep\_thr* or *init\_colloid\_thr*.

The last modification has to be done in the *ca\_init* file. There are the entries *thr\_list* and *thr\_result*. The first list contains the strings that are displayed in the main control GUI, the second list is the internal identification string for the automatic configuration of CAAT. Make sure, that this internal string matches the name of your initialization file (for example *coldgas\_thr* and *init\_coldgas\_thr*).

### 3.4 Custom Thruster Actuation System

This is the most complex element, that can be customized in the CAAT software. The basic task for the TAS is the calculation of the correct thruster commands. The interfaces of the standardized TAS block are listed in the following table.

Name	Direction	Width	Unit
F_cmd	IN	6	N, Nm
thr_cmd	OUT	n_thr	N
analysis	OUT	2	-

The incoming command  $F\_cmd$  from the vector generator has six elements. It is composed by the values of  $F_x, F_y, F_z, T_x, T_y, T_z$  in exactly this order. The units of this input are SI standard (N and Nm).

The output  $thr\_cmd$  is passed to the thruster models. It has one element for each engine, and provides the thrust command in Newton.

The last output  $analysis$  is used to control the work of the TAS algorithm. It has two main channels, that can be internally multiplexed. Anyway, the CAAT simulation provides two Simulink viewing scopes to monitor the TAS analysis signal. The content of this output can range from error codes to scaling factors or iteration counters.

It is obvious, that a TAS algorithm can not work without a proper initialization and some parameters. So there is an initialization script for every TAS. A  $TAS\_init\_params$  structure is passed to the init file, and provides the minimum and maximum thrust level, the number of thrusters, as well as the force/torque map ( $FT\_Map$ ) and an identification string for the selected thruster configuration. The init script of the TAS algorithm may use this information and assembles a custom  $TAS\_params$  structure, that is passed afterwards to the Simulink S-Function. An example are the pseudoinverse TAS algorithms, that need pre-compiled data. These matrices are loaded by their init scripts.

To add a new TAS to the CAAT system, you will have to provide at least a Simulink model, containing a subsystem with one input and two outputs, as described in the table above. It is recommended to use an S-Function because of the complexity of a TAS. You also have to provide an initialization file, that takes the  $TAS\_init\_params$  structure as parameter and returns a custom  $TAS\_params$  structure for your TAS S-Function.

In the directory  $m-files$  is a file  $TAS.mdl$  that contains links to all available TAS blocks. Execute the script  $set\_paths$ , open this  $TAS.mdl$  file and your own TAS model. Drag your subsystem into the TAS library of CAAT and activate it in the  $Used\_TAS$  template (SubSystem parameters...). For safety, open the  $TAS\_template$  subsystem, and replace the original  $Used\_TAS$  link in it with the updated template. Save the TAS library.

In the last step, you have to add your new TAS algorithm to the main control GUI of CAAT. Open the file  $ca\_init$  and modify the lines for  $tas\_list$  and  $tas\_result$ . The first list will be displayed to the user in the gui, the second list contained the internal identification strings for the different TAS systems.

### 3.5 Working Principle

To complete this manual, a small description about the working principle of CAAT is also given. You can see the structure of the simulation in Figure 3. The main parts are the *Vector Generator*, the *TAS* and the *Actuator Model* (thruster parameter).

The vector generator contains the *db\_casize* database and decides, which force/torque command shall be issued to the Thruster Actuation System to test out the control authority. It uses the feedback of the current thruster commands and the difference between the commanded and actuated forces and torques.

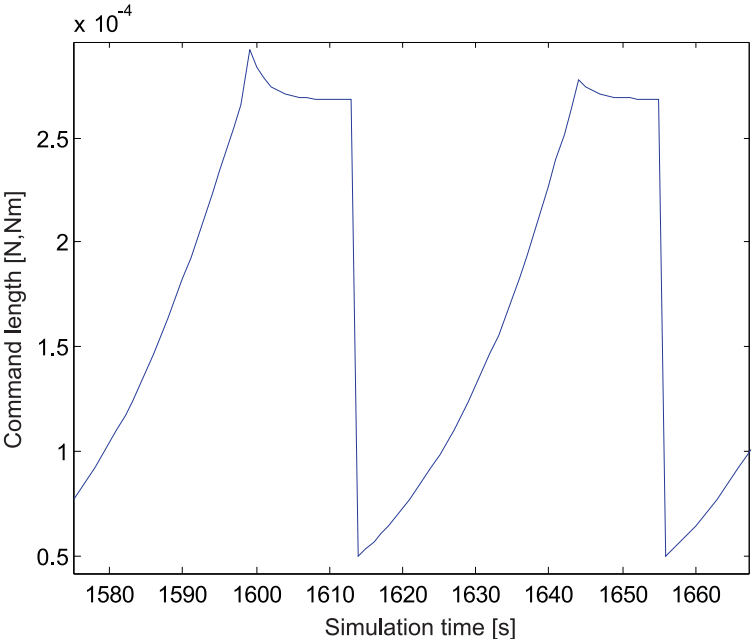



Figure 4: Typical shape of a force/torque command signal

The vector generator keeps track about the internal database and tests for every grid point of the six-dimensional hypersphere the size of the control authority (depending on the *Full CA* setting). In Figure 4 you can see the command signal to calculate two grid points.

The vector generator selects a new direction, by using the five discretized angles of the database, and starts with a small command length. The TAS and the thruster configuration can fulfill this command and the difference between the commanded and actuates forces and torques is in the range of the computational accuracy. The vector generator recognizes this fact and increases the *length* of the force/torque command. Where *length* is the radius of the six-dimensional direction vector. The vector generator uses the thruster commands to calculate the residual thrust margin of the engines. This margin is influencing the slope of the command length increase.

	CAAT Control Authority Analysis Tool Manual	Doc.No.: INT-TAS-TN-ZAR-004 Issue: 1.0 Page: 13 of 13
---	---	---

At some point, the force/torque command is so large, that the TAS and the propulsion system can not longer provide the commanded forces and torques. The difference signal of the commanded and actuated forces and torques is then used for a more fine decrease of the command length. In Figure 4 you can see, that in this second phase of the grid point convergence the command signal approaches a settling point - the final control authority.

The force/torque difference signal is almost linear to the spacecraft control authority violation. That means, that a command signal, 10% larger than the control authority, will result in a force/torque difference of almost 10% size of the commanded signal. This feature is founded in the working principle of the implemented TAS algorithms. If the thruster actuation method can not provide the commanded forces and torques, it will try to provide at least a force/torque vector in the same direction, but with a smaller length.

The control authority for one specific direction is found, when the force/torque difference is higher than the computational accuracy but within a defined threshold value ( $10^{-7}$ ). The vector generator stores the current command length in the database and selects a new direction for the next grid point.

It should be noted, that the CAAT system was created, to test micropropulsion thrusters with different thruster configurations. The applied gain factors are defined for this range of thrust. If you want to test more powerful engines, you might encounter strange control authority results. In the file *autoconfig\_simulation* two parameters are set in the *CA\_params* structure (*ft\_diff\_gain* and *thr\_diff\_gain*). Try to modify these two values and perhaps the *initlength* accordingly to your high-thrust engines. You can observe the result of the changes by plotting the variable *FT\_cmd\_len* in Matlab and comparing its shape to Figure 4.

	Endbericht Algorithmen zur Triebwerksansteuerung Fkz: 50 JR 0484	Doc.No.: INT-TAS-RP-ZAR-001 Issue: 1.0 Page: 28 of 20
---	--	---

## Anhang H

Veröffentlichung vorläufiger Ergebnisse des Vorhabens auf dem *56th International Astronautical Congress of the International Astronautical Federation* im Jahr 2005

# IAC-05-C1.P.10

## THRUSTER ACTUATION ALGORITHMS FOR SCIENTIFIC SPACE MISSIONS

**Daniel Bindel, Markus Schlotterer and Stephan Theil**

*Center of Applied Space Technology and Microgravity, University of Bremen, Am Fallturm,  
D-28359 Bremen, Germany, e-mail: bindel@zarm.uni-bremen.de*

### ABSTRACT

Research in fundamental physics or formation flying of multibody space telescopes require a very accurate attitude and position control system. Beside the type and amount of sensors and the design of the controller, the thruster actuation algorithm is an important part of the control system design for those spacecraft.

Typically the thrusters are arranged in a specific configuration so that every unit acts simultaneously on multiple degrees of freedom of the satellite. Therefore a thruster failure can be compensated by another unit - so the actuation system is underdetermined. The controller for the satellite attitude and position is providing force and torque commands to the actuation subsystem. Thus a thruster actuation algorithm has to drive the available thrusters in such a way that the required controller commands are accomplished.

The requirements for attitude and position accuracy of scientific space missions are very demanding and boosted the development of new types of thrusters that can act in the range of a few micro Newtons. Unfortunately the different types of thrusters induce different boundary conditions to the system design, so a general thrust distribution method is not feasible. This paper will outline the mathematical statement of these attributes and their influence on the thruster actuation algorithms.

Beside the various types of thrusters, the design of the thruster actuation algorithm can vary between different methods for the calculation of a valid thrust solution. This paper will point out the major vantages and drawbacks of the methods. This is important to optimize the quality of scientific benefit and the spacecraft lifetime.

### NOMENCLATURE

AOCS	Attitude and Orbit Control System
TAS	Thruster Actuation System
$T$	Thrust vector
$A$	Thruster configuration matrix
$F$	Vector of commanded forces and torques
$T_{min}$	Minimum thrust level
$T_{max}$	Maximum thrust level
$T_n$	Nullspace vector
$I$	Identity matrix
$n$	Number of spacecraft thrusters

### INTRODUCTION

The attitude and orbit control of a spacecraft requires an actuation system that is able to overcome disturbances by providing forces and torques. The needs for agility and accuracy of the actuator system depend on the mission type. It is obvious that satellites for scientific experiments have more stringent requirements on an accurate and undisturbed actuation system than commercial satellites. The design choice of possible components is crucial to achieve these requirements. This does not only include the

thruster technology or the geometrical configuration of the engines but also the thruster actuation system (TAS). The TAS algorithms, discussed in this paper, have been designed for continuous, proportional thrusters, due to the planned use of such engines on near future scientific missions.

### THRUSTER ACTUATION SYSTEM

The task of a thruster actuation system is to drive the available thrusters of a spacecraft in such a way, that the demanded forces and torques of the AOCS are achieved. In the past decades, the design of satellites and the configuration of their thrusters have allowed for very simple TAS algorithms. Most times it was possible to assign a thruster to exactly one force and one torque direction. By using complementary thruster pairs, every demanded combination of forces and torques could be achieved by simply routing the command to the dedicated thruster, i.e. for the x-axis (see Fig. (1)).

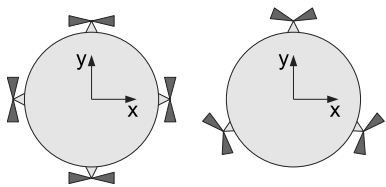


Figure 1: Example of trivial and complex thruster configuration for the 2-dimensional case

Unfortunately, in some cases the design of satellites, especially of scientific spacecraft, does not allow for a simple configuration of thrusters. The position of optics or sun shields as well as an unperturbed line of sight are limiting the choice of suitable thruster positions. As a result the installed thrusters are acting on several degrees of freedom simultaneously when they are fired. An appropriate algorithm is therefore needed to drive the thrusters with respect to their complex configuration.

By using the position and orientation of every thruster, a configuration map  $A$  can be created. Together with the thrust command vector  $T$  it calculates the generated forces and torques  $F$

$$F = AT . \quad (1)$$

The task to find the thrust vector  $T$ , when the desired force/torque vector  $F$  is provided, is not trivial, because  $A$  is not guaranteed to be invertible, because

it is not a square matrix. At least there is a band of different  $T$  vectors, that all solve Eq. (1) - the only difficult task is to find the optimal one.

### Boundary Conditions

The search for the thrust vector  $T$  is constricted when boundary conditions of the thrusters or the spacecraft are applied. The most basic constraint for the elements of  $T$  is given by the thrust range of the physical engines

$$T_{min} \leq T \leq T_{max} . \quad (2)$$

It should be noted, that the minimal thrust is not inevitable zero Newton. Most engines need at least a low value for a controlled thrust. Another restriction may be a limited fuel mass flow rate. In some cases the satellite can also trigger a boundary condition for the fuel supply. This may be imposed by pressure vents at the tank or due to storage of the fuel. Cryogenic missions like Gravity Probe B for example must slowly vaporize the stored helium to feed the thrusters and cool the experiment. In this case the thruster actuation system should drive the thruster in such a way, that the same amount of helium is consumed, as it is vaporized. This fact is expressed by the 1-norm. This is the sum of all absolute values of the solution vector  $T$

$$\|T\|_1 = \sum_i |T_i|, \quad \|T\|_1 \leq \dot{m}_{max} . \quad (3)$$

Furthermore the dynamic of the thruster can play an important role. It may be necessary to avoid large steps in the commanded thrust for the single thrusters and so one gets an extra condition

$$|\Delta T_i| \leq \Delta T_{max} . \quad (4)$$

### Optimization Criteria

Beside clear boundary conditions, the thruster actuation algorithm also needs criteria for the optimization. Because the thrust distribution problem is under-determined, an optimal solution vector  $T$  can be selected from a band of solutions.

There are different targets for the optimization that are connected to different technical attributes of the thrusters. For example it is important for the cold



gas thrusters, to use as few propellant as possible. The specific impulse of these engines is very low so the fuel consumption is enormous in comparison to electrical thrusters.

Therefore the 1-norm of the thrust vector  $T$  (for  $n$  thrusters) must be minimized to minimize the overall fuel consumption

$$\min_T \|T\|_1 = \min_T \left( \sum_i |T_i| \right). \quad (5)$$

If information about the degradation of the thrusters are available, it is possible to create a model for the worsening of the thruster efficiency. Due to erosion of electrodes or symptoms of abrasion there may be a degradation of the specific impulse  $I_{sp}$ , a higher power consumption or a higher failure risk.

A possible reduction of the degradation is a low usage of the thrusters. This can be done by minimizing the  $\infty$ -norm of the solution vector. The  $\infty$ -norm is the greatest absolute value of each vector element

$$\begin{aligned} \|T\|_\infty &= \max(|T_i|), \text{ so that} \\ \min_T(\|T\|_\infty) &= \min_T(\max(|T_i|)). \end{aligned} \quad (6)$$

Another procedure can be the minimization of the cumulative wear  $W$  of the thruster during its lifetime. For this task the thrust distribution algorithm should integrate the degradation of every single thruster. The result can be used to redistribute the thrust to other engines if one thruster has been wear down more than the others. Longterm tests with FEEP<sup>3</sup> engines have shown, that the degradation is not a linear function of the applied thrust. So a nonlinear function  $Use$  for the actual usage of the thruster should be established for calculating the wear

$$W_i = \int_{t_0}^t Use(T_i) dt. \quad (7)$$

$W_i$  can now be used as factor for optimizing the  $\infty$ -norm

$$\min_T(\|T(W)\|_\infty) = \min_T(\max(|W_i \cdot T_i|)). \quad (8)$$

This optimization criterion is especially important for the FEEP and colloid thrusters, because here the thrust is generated by very sharp needles or edges. An erosion of this surface leads to a considerably degradation of the engine. But also grid ion thrusters are affected by erosion due to high thrust.

## ALGORITHMS

The strategy to find a solution vector  $T$  for Eq. (1) can be divided into different approaches.

### Pseudoinverse Method

A basic method incorporates a so called *pseudo-inverse* matrix  $A^\dagger$  that meets the requirement

$$A \cdot A^\dagger = I. \quad (9)$$

Due to the fact, that the thruster configuration matrix  $A$  is not square, the pseudoinverse matrix  $A^\dagger$  is not explicit defined.

In 1983 Jeng-Heng Chen<sup>1</sup> proposed the basic type of a pseudoinverse algorithm. It invokes a Moore-Penrose solution in the form of

$$A^\dagger = A^T(AA^T)^{-1}. \quad (10)$$

It can be clearly seen, that this type of a direct solution will produce negative elements in the thrust vector  $T$ . So Chen also introduces the nullspace vector  $T_n$  that is added to the product of  $A$  and  $F$  and biases the result around a positive value that is most times the middle of the thrust range. As a part of the nullspace of matrix  $A$ , the positive vector  $T_n$  has the following feature

$$\begin{aligned} AT_n &= 0, \text{ so that} \\ T &= AF + T_n, \text{ with} \\ T, T_n &\geq 0. \end{aligned} \quad (11)$$

In 1992 Peter J. Wiktor<sup>7</sup> continued the work of Chen and concentrated on the performance of the system, made up by the thruster configuration and thruster actuation. He introduced the method of the minimum control authority plot, which is a tool for evaluating the various design options. He also identified three different types of thruster actuators (minimum power, minimum flow rate and minimum actuator force). This corresponds to three different vector norms, that can be minimized.

Beside the  $\infty$ -norm (see Eq. (6)) for the maximum actuator thrust and the 1-norm (see Eq. (5)) for the consumed flow rate there is also the 2-norm for the thruster power. The mathematical statement is

$$\|T\|_2 = \sqrt{\sum |T_i^2|}. \quad (12)$$

A TAS using the 2-norm as the criterion is the most simple algorithm, as it describes the "length" of the vector. So  $T$  is a linear function of  $A^\dagger$  and  $F$ . In this case the pseudoinverse  $A^\dagger$  can also be computed with a least square algorithm as long as it meets the criterion in Eq. (9).

Algorithms to compute a thrust solution  $T$  by using the 1-norm or  $\infty$ -norm are more complex, as they need a linear programming method. But this induces also a higher demand of computational resources and incorporates iterative algorithms. In comparison to the simple and straight forward architecture of the pseudoinverse method it was very unlikely to be implemented in a spacecraft on-board system.

In 1996 HaiPing Jin<sup>4</sup> suggested a nonlinear iterative pseudoinverse method. It was developed to overcome a drawback of the direct pseudoinverse controller in Eq. (11) which has a very small control authority. The nonlinear approach tries to lower the thrust vector  $T$  to a point, when it still meets the requirements in Eq. (1) but is as small as possible. The iteration is described as

$$T_p = A^\dagger F_c(k) + T_n \quad (13)$$

$$T = (T_p + |T_p|)/2 \quad (14)$$

$$F_c(k+1) = F_c(k) + (F - AT)K . \quad (15)$$

Here a preliminary thrust vector  $T_p$  and an intermediate force  $F_c$  are computed. For the first iteration  $F_c$  is the desired force  $F$ . When  $T_p$  contains any negative elements, the vector  $T$  will become smaller than  $T_p$  (Eq. (14)). The resulting error in Eq. (15) is then added to  $F_c$  and in the next iteration,  $T_p$  will be higher (Eq. (13)). To speed up the convergence, the gain factor  $K$  is used. Typically its value is about 2 or 3.

A new approach to the pseudoinverse topic was made 2004 by Denis Fertin<sup>2</sup> and Shufan Wu with the so called *Least square thruster dispatching* method. The idea is to split the demanded force/torque vector  $F$  into its positive and negative parts

$$\begin{aligned} F &= F_+ + F_- \\ &\text{with } F_+ > 0 \\ &\text{and } F_- < 0 . \end{aligned}$$

Negative thrust commands can now be eliminated by the use of two complementary pseudoinverse matrices  $A_{plus}$  and  $A_{minor}$  that consists of elements

greater or equal to zero and meet the requirements

$$A \cdot A_{plus} = I \quad (16)$$

$$A \cdot A_{minor} = -I . \quad (17)$$

The negative elements of  $F_+$  and the positive elements of  $F_-$  are replaced by zeros. The original Eq. (11) is now written as

$$T = A_{plus}F_+ - A_{minor}F_- . \quad (18)$$

Due to the fact, that  $A_{minor} > 0$  and  $F_- < 0$ , the second term of Eq. (18) is always negative and thus the result of the whole equation is always positive and a  $T_n$  no longer needed.

A least square algorithm is used to compute the matrices  $A_{plus}$  and  $A_{minor}$ . For every column  $i$  of the matrix  $A_{plus}$  a vector  $x$  has to be found so

$$\min_x (\|x_i\|_2) \quad (19)$$

$$\text{such that } -Ix_i \leq 0 \quad (20)$$

$$\text{and } Ax_i = \text{column}_i(I) . \quad (21)$$

The matrix  $A_{minor}$  is calculated by the same way, except that the constraint in Eq. (21) is interpreted as  $-Ax_i = \text{column}_i(I)$ , due to Eq. (17).

Since this method is not yet perfect, in 2004 Alexander Schleicher<sup>5</sup> developed a scaling law to fit the thrust vector  $T$  better to the constraint in Eq. (2). His approach includes again a nullspace vector and is written as

$$T = c_F(A_{plus}F_+ - A_{minor}F_-) + c_{Tn}T_n . \quad (22)$$

The problem of finding a thrust vector that meets the thrust limits then boils down to finding two scale factors  $c_F$  and  $c_{Tn}$  such that

$$\begin{aligned} \min(T) &= T_{min} \\ \max(T) &\leq T_{max} . \end{aligned}$$

Herein  $c_F$  should be as close to one as possible in order to minimize the difference between the force/torque demand of the control system and the forces and torques provided by the propulsion system. Furthermore  $c_{Tn}$  should be as close as possible to zero in order to avoid excessive thrust commands and fuel consumption. The algorithm to find  $c_F$  and  $c_{Tn}$  is not described here to keep this paper short. Hence this method can find a vector  $T$  that is at the  $T_{min}$  boundary and has the ability to compute a degraded solution for exceptionally high force/torque demands that exceed the control authority.

## Linear Programming

Beside the well developed pseudoinverse algorithms there also exists the idea of using a linear programming method to find a valid thrust solution  $T$  for the problem in Eq. (1).

One basic difference is at least the choice of a suitable cost function. While the pseudoinverse algorithms apply to the 2-norm of  $T$  (see Eq. (12)), a linear algorithm like SIMPLEX can only use the 1-norm (Eq. (5)). When the  $\infty$ -norm shall be used for the linear programming, the problem has to be defined in a special way

$$\begin{aligned} \min \quad & z \\ \text{subject to } T \quad & \leq z \\ \text{and } AT \quad & = F \\ z, T \quad & \geq 0. \end{aligned}$$

This way, the biggest element of  $T$  and thus the  $\infty$ -norm is minimized.

The advantages of the linear programming are the ability to minimize the 1-norm and so reducing the propellant consumption of the thruster system. This is crucial for cold-gas engines, as they have a very low specific impulse. On the other hand, some electric thrusters like FEEP or colloid should be actuated on a low thrust level to increase their lifetime. So the  $\infty$ -norm is a good approach to optimize the thrust vector  $T$ .

It is also possible to include some kind of wear-optimization into the cost function of a linear programming method, and thus consider characteristics of some thruster types.

Another benefit of the linear programming is the incorporation of boundary conditions like Eq. (2) or Eq. (4). A pseudoinverse algorithm is not able to meet this requirements, as the solution vector  $T$  is more or less a linear function of the desired force/torque vector  $F$ .

But a major advantage is the ability to use flexible thruster configurations. Assuming a thruster failure, the linear program can simply change the configuration matrix  $A$  and the corresponding equality constraints in the optimization algorithm. The pseudoinverse matrix  $A^+$  and all of its derivatives are precomputed, so an on-board modification is not feasible. All possible thruster configurations due to failures or other reason, have to be foreseen and precomputed.

The scenario of a thruster failure is not the only cause to take care of a flexible configuration. When the spacecraft is flying in close formation with other satellites, the plume contamination of the thrusters could prohibit the use of some spatial directions to avoid hitting partner objects with the engine exhaust. This concept of *safety sectors* could limit the available thrusters for a valid and safe thrust solution.

As an implementation of linear programming the D3 Group<sup>6</sup> presented in 2003 an algorithm called TMF\_Cone. It is a compromise between fast calculation and optimization. The basic idea is to precompute a variety of thrust solutions for different directions (so called *cones*) of the vector  $F$ . In the on-board computer the stored directions are then compared to the actual demanded vector  $F$  and the solution for the best fitting one is provided as start-solution to a parametric SIMPLEX algorithm to find the real thrust vector  $T$ .

Although the pseudoinverse approaches are still a valid design choice and well developed, the future of thruster actuation systems should incorporate linear programming methods. Not only the ability to include the thruster and system constraints directly into the linear program, but also the feature for on-board optimization are strong advantages. The drawbacks of iterative algorithms and high computational demands can be compensated by proper code-design and the increasing capability of on-board computers.

## SUMMARY

This paper gave an overview about the history and the state of the art of thruster actuation systems. As an introduction to the topic, the requirements of the thrusters and the spacecraft system have been described. It has been presented, how this constraints and requirements have to be specified to be compatible with the algorithms described.

The scope of this paper was to give only a small insight into the subject of thrust distribution. So the interested reader is advised to investigate the provided references.

## REFERENCES

- [1] Jeng-Heng Chen. *Helium Thruster Propulsion System for Precise Attitude Control and Drag Compensation of the Gravity Probe-B Satellite.*

- PhD thesis, Department of Aeronautics and Astronautics, Stanford University, December 1983.
- [2] Denis Fertin and Wu Shufan. Analysis of design of Lisa Pathfinder drag-free controllers. Memo TEC-ECN/DF/S2-21/10/2004, European Space Agency, December 2004.
- [3] A. Genovese, M. Tajmar, N. Buldrini, M. Scheerer, E. Semerad, and W. Steiger. Indium FEEP Multiemitter Development and Test Results. In *40th AIAA/ASME/SAE/ASEE Joint Propulsion Conference and Exhibit*, July 2004. AIAA-2004-3620.
- [4] HaiPing Jin. *Translation and Attitude Control for the QUICK-STEP Satellite*. PhD thesis, Department of Aeronautics and Astronautics of Stanford University, August 1996.
- [5] A. Schleicher. Thruster actuation algorithm design and analysis. Technical Report S2-ZAR-TN-2001, ZARM, July 2004.
- [6] Alexander Vankov and Vladimir Voloshinov. Spacecraft thruster management subsystem design and analysis software tool. Tech-Report D3-TMF-ABS-1\_1, D3 Group, December 2003.
- [7] Peter J. Wiktor. *The Design of a Propulsion System Using Vent Gas from a Liquid Helium Cryogenic System*. PhD thesis, Department of Aeronautics and Astronautics of Stanford University, June 1992.

	Endbericht Algorithmen zur Triebwerksansteuerung Fkz: 50 JR 0484	Doc.No.: INT-TAS-RP-ZAR-001 Issue: 1.0 Page: 29 of 20
---	--	---

## Anhang I

Veröffentlichung fortgeschrittener Ergebnisse des Vorhabens auf dem *30th ANNUAL AAS GUIDANCE AND CONTROL CONFERENCE* im Jahr 2007

# Six-Dimensional Thruster Actuation and Configuration Design for Spacecraft

Daniel Bindel

ZARM, Center of Applied Space Technology and Microgravity  
University of Bremen, Germany

February 1, 2007

The design of spacecraft for scientific missions includes the layout of a propulsion subsystem. The science goal usually limits the acceptable disturbances and thus the possible types of AOC actuators/thrusters. An ongoing investigation have been started to identify and develop suitable methods and algorithms to actuate these thrusters, regarding to six-dimensional controller commands (forces and torques). The algorithms should be capable to deal with complex thruster configurations and even engine failures.

During the work, a software test-bed for the different types of thruster actuation algorithms was implemented. It provides the opportunity to simulate various types of state of the art electrical thrusters with different configurations. So appropriate control methods can be analyzed and chosen for different thrusters and science missions. Additionally this tool is capable to support the design process of a spacecraft. It can calculate the exact control authority of the propulsion subsystem, depending on different types of thrusters, configurations and control algorithms. This is applicable for many near term science missions.

This paper will give an overview of current six-dimensional thruster control methods. It also outlines the advances that have been developed with respect to requirements of micro propulsion thrusters as well as onboard real-time restrictions. These new methods provide the opportunity to reduce the fuel consumption, extend the engine- and mission-lifetime and increase the failure tolerance for truster failures.

## INTRODUCTION

Before the different algorithms are explained in detail, a small task description of the thruster actuation system (TAS) will outline the requirements of this AOCS component. Due to the target missions and their proposed thrusters, some boundary conditions and optimization criteria for the TAS algorithms are introduced. This is necessary to evaluate the different methods later on.

The next section of this paper addresses the state of the art methods, used in several past and near term missions. They are based on the pseudoinverse approach. Although this methods bear some disadvantages, they are still considered as a first choice for a TAS, due to their simplicity.

Increasing on-board computational power and the advantages of optimization algorithms for the fuel consumption and mission lifetime make linear programming methods an interesting alternative. Unfortunately these methods have some inherent disadvantages and are thus not very often considered for real time applications in space. But nevertheless the research on these algorithms has revealed some solution for the drawbacks.

Looking over the edge of present and near term scientific space missions, there are also interesting concepts for spacecraft with massive-multiple thruster problems. Here solutions are needed for the control of thruster configurations with more than 20 or 30 different thrusters. Even if this is not yet implemented for science missions, other spacecraft like the european ATV are an example of applications for advanced thruster control. A section in this paper will reflect the results of a preselection algorithm, that reduces the complexity of the massive-multiple thruster problem.

The different TAS methods are presented with results of simulations from the LISA and LISA Pathfinder mission, to allow a comparison of their performance.

The last section is focussed on the potential useage of the developed simulation testbed to aid the spacecraft design process.

## THRUSTER ACTUATION SYSTEM

The task of a thruster actuation system is to drive the available thrusters of a spacecraft in such a way, that the demanded forces and torques of the AOCS controller are achieved.

The difficulty of this task is the problem, that the thrusters may not be aligned parallel to the axis of the satellite. As you can see in the left example of Figure 1 it is possible to route the demanded forces and torques to the engines, that are aligned with the corresponding axis.

Nethertheless, real spacecraft have some restrictions for placing their thrusters like plume contamination, mass-limitations or the position of optics or sun-shields. The position of the engines is most times a complex configuration like the right example of Figure 1. As a result the installed thrusters are acting on several degrees of freedom simultaneously when they are fired. An appropriate algorithm is therefore needed to drive the thrusters with respect to their complex configuration.

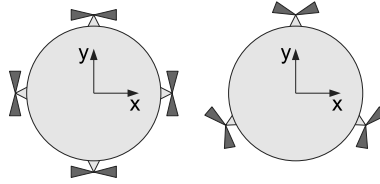


Figure 1: Example of trivial and complex thruster configuration for the 2-dimensional case

This leads to the basic equation Eq. (1) of the thruster actuation system. The demanded force and torque vector  $F$  is assumed here to be six-dimensional, so the TAS has to handle the three degrees of freedom for each translation and rotation. The configuration map  $A$  reflects the position and orientation of all spacecraft thrusters. It has the dimension  $6 \times n$  for  $n$  thrusters. By multiplying the thrust of each engine (vector  $T$ ) to the matrix, the forces and torques applied to the spacecraft are calculated.

$$F = AT . \quad (1)$$

Unfortunately, the desired thruster command vector  $T$  can not be achieved by simply inverting the matrix  $A$ , because it is not quadratic. Furthermore, the problem is underdefined, so there exist a large number of possible solution vectors  $T$  for the given problem. It is the task of the TAS to find one of them, if it exists.

This is illustrated in Figure 2. For a commanded force and torque vector  $F$  and a constant configuration map  $A$  exist more than one solution  $T$ , assuming that the control authority of the spacecraft is not exceeded. Some of these solutions represent vectors with optimal attributes, like least fuel or power consumption or least engine thrust. They are displayed as points  $T_{A,B,C}$  and depend from the given problem.

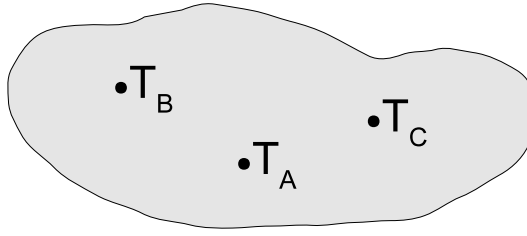


Figure 2: Range of possible solutions  $T$  for the given problem  $F=AT$

### Boundary Conditions

The solution range is further decreased, if additional boundary conditions are introduced. This is necessary, to adapt the final solution to the physical behavior of the engines. One example is the thrust range of the engines. They are not only characterized by their overall minimum and maximum thrust (see Eq. (2)), but can also be affected by dynamic effects. Some electrical engines incorporate a controlled gas or fluid feed, that has an influence on the generated thrust. The result is, that the thrusters may not be able, to increase or decrease their thrust output in a short time from minimum to maximum and the other way round. So it may be able to vary the thrust only in a certain range, depending on its previous thrust level (see Eq. (3)).

$$t_{min} \leq T_i \leq t_{max} \quad (2)$$

$$|\Delta T_i| \leq \Delta t_{max} \quad (3)$$

Another boundary condition can be the overall consumed propellant massflow rate. This can apply to systems with a single main tank and a limited massflow rate for all thrusters. Such a situation is rare, but it exists like the cryogenic missions Gravity Probe B, where the spacecraft produced its propellant by itself by boiling off the liquid helium. Eq. (4) describes this restriction.

$$\|T\|_1 = \sum_i |T_i|, \quad \|T\|_1 \leq \dot{m}_{max} \quad (4)$$

### Optimization Criteria

As explained in the previous section, the range of possible solutions contain many different combinations for the thrust vector  $T$ . By defining some criteria, an optimization method could find the best suitable vector from the band of all possible solutions.

To ensure a good handling of the real thrusters, the optimization should reflect a physical property of the engines. In this case, a reduction of the fuel consumption is the foremost aspect. Depending on the utilized thruster-technology, there are two different approaches.

Coldgas systems and a lot of electrical engines are using a single propellant reservoir. Additionally a lower thrust will lead to a lower fuel consumption. So by minimizing the sum of all thruster commands in the vector  $T$ , the massflow will also be minimized. In Eq. (5) this is displayed as a minimum of the the 1-Norm of the vector  $T$ .

$$\min_T \|T\|_1 = \min_T \sum_i |T_i| \quad (5)$$

Other types of engines like the FEEP have an own tank for every thruster. Here it is better, to reduce the thrust of each thruster, to preserve propellant. The Eq. (6) shows, how the Infinity-Norm of the vector  $T$  is minimized to find that optimal solution.

$$\begin{aligned} \|T\|_\infty &= \max(|T_i|), \text{ so that} \\ \min_T (\|T\|_\infty) &= \min_T (\max(|T_i|)) . \end{aligned} \quad (6)$$



The same procedure can be used, to apply a degradation-optimization. Primarily the electrical engines are affected with the wear of their components. It could be effective, to track down the engine degradation and to use this information in the optimization methods. The Eq. (7) proposes a way, to sum up the wear of an engine. A fundamental part is use usage  $Use$  that is dependant from the commanded thrust  $T$  of this thruster.

Integrated over the lifetime it will give an assumption about the cumulative wear  $W$  of that thruster. It tells, how much that particular engine have been degraded or worn out. In the second step, this information can be used, to improve the infinity norm optimization (see Eq. (8)). The system reduces the applied thrust for especially that thrusters, that have been used intensively in the past time.

Longterm tests with FEEP<sup>4</sup> engines have shown, that the degradation is not a linear function of the applied thrust. So a nonlinear function  $Use(T)$  for the actual usage of the thruster should be established for calculating the wear.

$$W_i = \int_{t_0}^t Use(T_i)dt \quad (7)$$

$$\min_T(\|T(W)\|_\infty) = \min_T(\max(|W_i \cdot T_i|)) \quad (8)$$

The optimization with respect to degradation is an interesting feature, that may help to enlarge the lifetime of FEEP and colloid thrusters. But grid ion thrusters are also affected by erosion due to intensive usage.

On the other hand, the power consumption of electrical engine can also be an issue of optimization, or at least a limiting factor of the power supply or the propulsion system. Here the vector norm 2 can be used, to express the consumed power, because it also involves the square value of the thrust (see Eq. (9)). Although, an optimization can also been done, without calculating the included square-root.

$$\min_T(\|T\|_2) = \min_T(\sqrt{\sum_i T_i^2}) \quad (9)$$

It should be noted, that all optimized solutions for the different vector norms of  $T$  are located inside the solution range. The Figure 2 depicts that fact.

## ALGORITHMS

There are different approaches, to find the desired thrust solution vector  $T$ . The state of the art methods are using a pseudoinverse matrix. A more complex attempt are linear programming methods. Both have their advantages and disadvantages.

### Pseudoinverse Method

The basic idea behind that algorithm is a so called *pseudo-inverse* matrix  $A^\dagger$  that meets the requirement of Eq. (10)

$$A \cdot A^\dagger = I \quad (10)$$

As described in the introduction, there does not exist a single inverse of the configuration matrix  $A$ . The  $A^\dagger$  must be calculated by a different way. Jeng-Heng Chen<sup>2</sup> introduced the Moore-Penrose (Eq. (11)) matrix to solve this problem.

$$A^\dagger = A^T(AA^T)^{-1} \quad (11)$$

The calculated pseudoinverse matrix has the features of Eq. (10), but a direct solution is not be able without the additional nullspace vector  $T_n$ . Eq. (12) shows the main feature of this vector, because it is a thrust solution, that does not apply any resulting force or torque to the spacecraft.

One of the main problems of the pseudoinvers approach is the fact, that a simple multiplication of the matrix  $A^\dagger$  and the vector  $F$  will lead to negative values in the solution vector  $T$ . That is impossible to realize, because the engines can produce only positive thrust. By adding a nullvector  $T_n$  of an appropriate size (Eq. (13)), the commanded thrusts will be shifted up, while the resulting forces and torques stay unaffected.

$$AT_n = 0, \text{ so that} \quad (12)$$

$$T = A^\dagger F + T_n, \text{ with} \quad (13)$$

$$T, T_n \geq 0.$$

In terms of fuel consumption or optimization, the nullspace vector  $T_n$  is very important. Like the standard problem Eq. (1) there exist a band of different solutions for the problem in Eq. (12) and with this an  $T_{n.min}$  and  $T_{n.max}$ . As a beginning, the final  $T_n$  can be computed from the average of these two vectors (Eq. (14)) and used as a fixed bias in Eq. (13)). It should be noted, that solving the Eq. (12) to retrieve the nullspace vectors is not done on board the spacecraft, but offline by using optimization algorithms (least squares method).

$$T_n = (T_{n.min} + T_{n.max})/2 \quad (14)$$

Here the pseudoinverse methods faces one its major disadvantages. It has no mechanism, to ensure a solution, where every thruster fits into its own thrust boundaries (Eq. (3)), but it can barely try to find a thrust vector  $T$  that meets the requirements of Eq. (2).

The pseudoinverse approach can not offer the variety of the complete six-dimensional solution space like in Figure 2, that solves the standard problem. It can only generate one fixed point solution, or a line at least, if the nullspace vector is seen as a variable. So  $T_n$  is one of the few ways, to influence the calculated pseudoinverse solution.

Beside the fixed bias as in Eq. (14) there is also a method, to scale the nullspace vector  $T_n$ , so that all elements of the thrust command vector  $T$  are above the global minimum thrust  $t_{min}$  of the engines.

$$T_{pc} = A^\dagger F \quad (15)$$

$$R_i = (t_{min} - (T_{pc})_i)/(T_n)_i \quad (16)$$

$$T_{n.dyn} = R_{max} T_n$$

$$T = T_{pc} + T_{n.dyn} \quad (17)$$

One way to do that, is a dynamic nullspace vector bias, that uses a preliminary thrust solution  $T_{pc}$  (Eq. (15)) and a ratio  $R_i$  (Eq. (16)) for every engine to retrieve the maxim of  $R_i$ . The dynamic nullspace vector  $T_{n.dyn}$  is then calculated with this ratio and the fixed nullspace vector  $T_n$ . Afterwards the final thrust command vector  $T$  is composed from the preliminary solution  $T_{pc}$  and the dynamic  $T_{n.dyn}$  (Eq. (17)).

Another approach to eliminate low thrust commands is an iterative process, that Hai Ping Jin<sup>5</sup> introduced in 1996.

$$T_p = A^\dagger F_c(k) + T_n \quad (18)$$

$$T = (T_p + |T_p|)/2 \quad (19)$$

$$F_c(k+1) = F_c(k) + (F_{cmd} - AT)K_i \quad (20)$$

$$F_c(0) = F_{cmd} \quad (21)$$

It is based on the calculation of a preliminary thrust vector  $T_p$  (Eq. (18)), and an intermediate force/torque vector  $F_c$  (Eq. (20)). The idea behind that system is, that Eq. (19) will change the thrust vector  $T$  unless, it has all positive values. The resulting force/torque error is applied with a gain factor  $K_i$  and fed back into the loop.

In this method the nullspace vector  $T_n$  stays unaffected and the intermediate force/torque vector  $F_c$  is changed, until the thrust vector  $T$  contains no more negative values, and the difference of commanded and

calculated forces and torques ( $F_{cmd} - AT$ ) is below a certain threshold value. To speed up the convergence, the gain factor  $K_i$  is used with values that are typically around 2 or 3.

One of the latest developments on the topic of the pseudoinvers thruster actuation systems was the introduction of the least squares thruster dispatching in 2004 by Denis Fertin<sup>3</sup> and Shu-Fan Wu. It is an approach, to avoid negative thruster commands from the first step of calculation by using two different and complementary pseudoinverse matrices  $A_{plus}$  and  $A_{minor}$ . The method also splits the commanded force/torque vector into its positive and negative components (Eq. (22)). The negative elements of  $F_+$  and the positive elements of  $F_-$  are replaced by zeros.

$$F = F_+ + F_- \quad \text{with } F_+ \geq 0 \text{ and } F_- \leq 0 \quad (22)$$

The two complementary pseudoinverse matrices are constructed in a way, that they meet the requirements of Eqs. (23) and (24) and consist only of elements greater or equal to zero.

$$A \cdot A_{plus} = I \quad (23)$$

$$A \cdot A_{minor} = -I \quad (24)$$

By redefining the original pseudoinverse equation to the new system (Eq. (25)) it is guaranteed, that the vector  $T$  is always positive. That is founded in the fact, that  $A_{minor} > 0$  and  $F_- < 0$ , so the second term of the new equation is always negative and thus the result of the whole equation is always positive.

$$T = A_{plus}F_+ - A_{minor}F_- \quad (25)$$

The composition of the rows  $x_i$  of matrix  $A_{plus}$  is done by using a least squares algorithm, that finds a solution for the requirements of Eqs. (26), (27) and (28).

$$\min_x (\|x_i\|_2) \quad (26)$$

$$\text{such that } -Ix_i \leq 0 \quad (27)$$

$$\text{and } Ax_i = \text{column}_i(I) \quad (28)$$

The matrix  $A_{minor}$  is calculated by the same way, except that the constraint in Eq. (28) is interpreted as  $-Ax_i = \text{column}_i(I)$ , due to Eq. (24).

Unfortunately, this least squares thruster dispatching can only guarantee thrust commands above or equal zero. For a solution, that meets at least the requirements of minimum thrust as described in Eq. (2) there is again a nullspace vector application necessary.

In 2004 Alexander Schleicher<sup>6</sup> introduced a scaling method (Eq. (29)), to bring the smallest element in the thrust command vector  $T$  to exactly the minimum thrust  $t_{min}$ .

$$T = c_F(A_{plus}F_+ - A_{minor}F_-) + c_{Tn}T_n \quad (29)$$

Here it can be seen, that there are two scale factors  $c_F$  and  $c_{Tn}$  to influence the nullspace vector and the commanded force/torque vector. The requirements that have to be met are displayed in Eqs. (30) and (31). The factor  $c_F$  should be as close as possible to 1.0, to avoid large differences between the commanded and actuated force and torque vector  $F$ . Furthermore  $c_{Tn}$  should be as close as possible to zero in order to avoid excessive thrust commands and fuel consumption.

$$\min(T) = t_{min} \quad (30)$$

$$\max(T) \leq t_{max} \quad (31)$$

The big advantage of this algorithm is the ability, to scale down the demanded force/torque vector, if the control authority of the propulsion system is exceeded.

The biggest advantage of the pseudoinverse algorithms is the simplicity of their construction. The solution is found basically by multiplying matrices and vectors. Beside the iterative approach of Jin, this involves no iterative loops. The big disadvantage is, that the possible six-dimensional space of solutions is reduced to only a small band of vectors. Thus, there is no real optimization of the final solution possible. But anyway, the scaling methods are quite effective in reducing the fuel consumption. There is still the problem, that the algorithm might violate the thrust requirement of Eq. (3). For this reason, the AOCs controller has to be tuned to a point, where it commands no big variations of the force/torque vector  $F$  to the TAS.

## Linear Programming

As depicted in Figure 1, the range of possible solutions for the original problem  $F = AT$  is very large. Due to the linearity of the system of equations it is obvious that a linear programming method could be used, to find a proper solution  $T$ .

In the analysis of this topic, the Simplex algorithm was chosen as a linear optimizer to solve the set of equations and restraints. The advantage is, that such a method is able, to apply some optimizations. So there will be first an introduction to the problem definition for this numeric system.

The optimization for the vector norm 1 (Eq. (5)) is the most simple method, because the objective function  $z$  of the optimizer is simply the sum of all elements in the vector  $T$  (Eq. (32)). One of the features of the simplex algorithm is the fact, that its output is by definition positive.

But anyway it is possible, to apply restrictions to the thrust range for each thruster (Eq. (34)) separately to meet the requirements for thrust variations and the maximum thrust range in one step. Overall, this method requires six equalities in the form of Eq. (33) to fulfill the basic task, and two times the number of thrusters as inequalities, to incorporate the thrust range restrictions.

$$\min_T(z) = \min_T \sum T_i \quad (32)$$

$$\text{subject to } AT = F \quad (33)$$

$$\text{and } t_{min.i} \leq T_i \leq t_{max.i} \quad (34)$$

The search for a solution, that represents an optimal infinity norm (Eq. (6)) of the vector  $T$  is more complex. The objective function in Eq. (35) is reduced to  $z$ , so the algorithm will try to minimize it. Due to the additional inequalities in Eq. (36) every thruster will be kept below this value  $z$ . By this way, the result is a thrust vector  $T$  with a minimized maximum element.

$$\min z \quad (35)$$

$$\text{subject to } T_i \leq z \quad (36)$$

$$\text{and } AT = F \quad (37)$$

$$\text{and } t_{min.i} \leq T_i \leq t_{max.i} \quad (38)$$

The implemented linear optimizer Simplex has also some special features that have to be considered. The major difficulty is the correct setup of the linear program with its equalities and inequalities. The setup must also be able to handle the characteristics of the optimizer. The numeric optimizer is not able to handle an infeasible problem. That situation will occur, if the commanded force/torque vector  $F$  exceeds the control authority. On the other hand, the algorithm has the ability, to find the global optimal solution in a finite amount of iterations, if such a solution exists.

So one of the most important components for a correct linear program setup is an enhancement to pass only feasible problems to the Simplex method. This is necessary, to guarantee a valid and robust thruster command vector  $T$  in the realtime environment onboard the spacecraft for every AOCs loop.

Two different failure cases have been identified, where a solution of the commanded vector  $F$  is not feasible with the given thrust restrictions of the engines.

The first situation is an exceeding of the control authority. The propulsion system is not able, to provide a thrust or torque vector of such a big length, as it is demanded from the AOCs controller. One possible

solution is to scale down the commanded vector  $F$  until it is again feasible to be solved. A scale gain factor  $s$  is used to do so.

In Eq. (39) the extension of the original TAS problem is described. For  $s$  being zero, the equation represents the original commanded force/torque vector  $F$ . For any value between 0 and 1 of  $s$ , the vector  $F$  is scaled down until it is 0. By assuming, that the propulsion system is able to provide a state, where no forces and torques are acting on the spacecraft, this scale gain will lead to a linear program, feasible to solve within the current control authority.

$$\begin{aligned} AT &= F - sF \\ AT + sF &= F \\ \text{with } 0 &\leq s \leq 1 \end{aligned} \quad (39)$$

Due to the physical properties of the proposed electrical engines, the dynamic behavior must also be considered. Assuming a continuous working state of the propulsion system, it may not be able to reach a nullvector. A restriction of the feasible thrust variation (Eq. (3)) can prevent this. So a further extension of the main TAS equation is necessary.

For this purpose, the difference gain  $t$  is introduced. It uses the difference vector  $F_{diff}$  (Eq. (40)) of the commanded  $F$  and the previously actuated  $F_{old}$ , to make the linear program robust against oversized command variations. In Eq. (41) this is shown as an equality constraint for the TAS problem. In Eq. (42) the combined scale extensions are inserted into the linear program.

$$F_{diff} = F - F_{old} \quad (40)$$

$$\begin{aligned} AT &= F - tF_{diff} \\ AT + tF_{diff} &= F \end{aligned} \quad (41)$$

$$\text{with } 0 \leq t \leq 1$$

$$AT + sF + tF_{diff} = F \quad (42)$$

To use the proposed scale and difference gains in a linear program for the optimization algorithm, additional inequalities for the range of  $s$  and  $t$  must be introduced and the objective function must be updated. For the norm 1 optimizer this is done in Eq. (43) and for the infinity norm optimizer in Eq. (44). The value of the scaling weights  $\sigma$  and  $\phi$  should be at least three orders of magnitude higher than the maximum thrust of the engines. Simulations have shown, that this penalty values have almost no influence to the calculated thrust command solution. Comparing results from non-enhanced linear programs and robust variations indicate differences in the range of ten orders of magnitude lower than the commanded and actuated vector  $F$ .

$$\min_T (\sum T_i + \sigma s + \phi t) \quad (43)$$

$$\min_T (z + \sigma s + \phi t) \quad (44)$$

$$\sigma = \phi \approx 1000 \cdot t_{max}$$

Another modification for the linear programming algorithm is the *Thrust Window (Twin)* preprocessor. Due to the working principle of the optimizer, strange situation can occur, when the thrust commands of successive AOCS loops are changing a lot. In this case, the thruster configuration might be ill-conditioned. As a result the optimizer switches between two very different optimal solutions of  $T$  for only small variations in the force/torque vector  $F$ . In Figure 3 this is displayed in the left graph. The thruster command is alternating between two thrust levels. The range of the alternations is restricted by the allowed thrust step  $\Delta t_{max}$ .

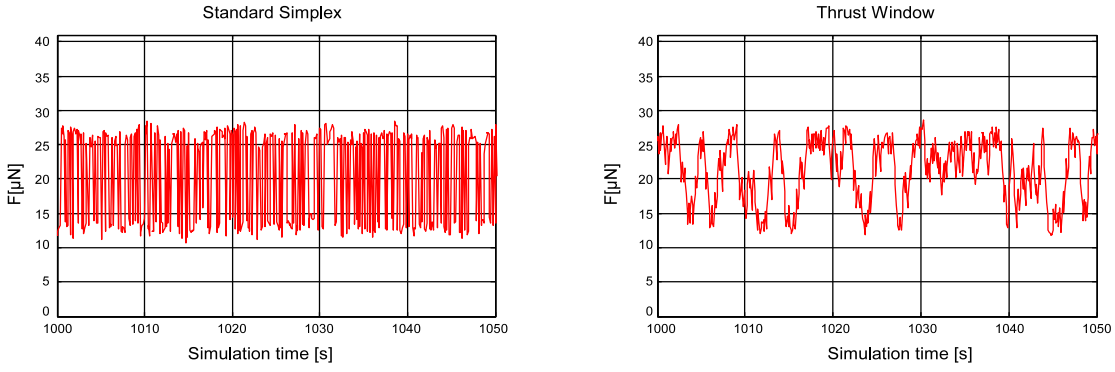


Figure 3: Commands for a LISA thruster with standard Simplex and Twin modification

The idea of the Twin algorithm is to set the allowed thrust step to a value, that is coupled with the variation  $F_{diff}$  of the force/torque vector  $F$ . Here the assumption is used, that a small variation in the force/torque command vector  $F$  can not lead to large variations in the thrust command vector  $T$ . So it is not necessary, to allow the optimizer the full range  $\Delta t_{max}$  for thrust variations.

The 1-norm of the difference vector ( $\Delta cmd\_size$ ) and two empiric parameters  $Twin_{scale}$  and  $Twin_{min}$  are used, to calculate a smaller step size, that still allows a proper solution of the linear program (Eqs. (45) through (48)). The  $Twin$  parameters have been chosen after several AOCS simulations of the spacecraft and should be checked for every new thruster configuration.

The right graph of Figure 3 displays the effect of the Twin algorithm for a LISA simulation. For this example, the value of  $Twin_{scale}$  was 0.5 and the value of  $Twin_{min}$  was  $3 \mu N$ . The maximum allowed thrust step  $\Delta t_{max}$  was  $30 \mu N$  for each AOCS loop. It should be noted, that the problems with the large thrust jitter occurred only with the norm-1 optimization. The infinity norm optimizer did not produced such a strange output.

$$\Delta cmd\_size = |F_{diff}|_1 \quad (45)$$

$$\Delta t = Twin_{scale} \cdot \Delta cmd\_size \quad (46)$$

$$\text{if } \Delta t < Twin_{min} \text{ then } \Delta t = Twin_{min} \quad (47)$$

$$\text{if } \Delta t > \Delta t_{max} \text{ then } \Delta t = \Delta t_{max} \quad (48)$$

### Algorithm comparison

Comparing the different algorithms must be done by considering their different attributes and performances. One fact for the comparison is the overall fuel consumption of the propulsion system. The proposed FEED engine configuration of LISA Pathfinder and a random profile of force/torque commands have been used, to retrieve the massflow performance. Another point of interest is the maximum workload, that a single thruster has to produce. This information is given as an average impulse in  $Ns/day$ .

The Figure 4 displays the required massflow of the different TAS algorithms. It is obvious, that the linear programming Simplex with the norm-1 optimization has the lowest value, because it is designed to find the global minimum. Another interesting fact is the behavior of the pseudoinverse methods. Although the Least Squares Thruster Dispatching algorithm (Pinv LSQ) is equipped with optimized pseudoinverse matrices, it has no big advantage against the Moore-Penrose derivate (Pinv MP). The reason for this observation is the effective nullspace vector scaling method of Alexander Schleicher, that was implemented in both algorithms. Their only difference is the way, how the pseudoinverse matrix is calculated.

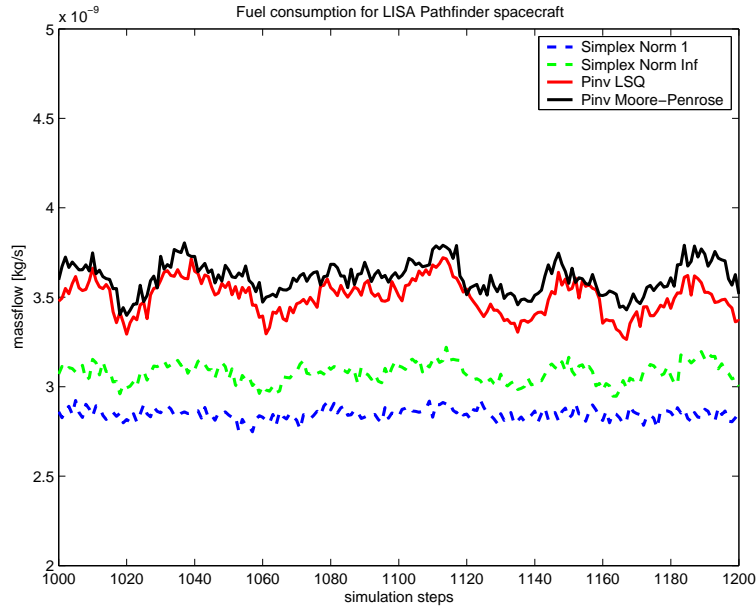


Figure 4: Fuel consumption of different TAS algorithms

Beside the simulated performance there are other features of the different methods, that should be considered. An important topic is the numeric computation effort. The pseudoinverse algorithms are the least complex examples. They only need one or two multiplications of vectors with matrices and some simple scaling laws. The linear programming optimizer on the other hand has the disadvantage of handling a big matrix, constituted of several inequality and equality constraints. Its working principle will cause the algorithm, to investigate a long search for a feasible vector  $T$  first, followed by a rather fast optimization of that solution. The infinity norm optimization takes 50 % more effort to compute, than the norm-1 derivate, because it needs more inequalities in the setup of the linear program.

Another advantage of the linear programming methods is their ability, to use every possible thruster configuration without pre-calculated data. The pseudoinverse methods rely on optimized matrices, that are computed on ground. In a case of an engine failure, the AOCs must wait, until the ground control can upload a new matrix, or it must be equipped with a set of matrices that cover every possible thruster configuration for a failure case.

<u>Algorithm</u>	<u>Overall Impulse</u>	<u>Maximum Single Impulse</u>
Pinv LSQ	10.2	1.31
Pinv MP	10.3	1.31
Simplex Norm 1	8.7	1.38
Simplex Norm Inf	9.3	1.25

Table 1: AVERAGE IMPULSE FOR DIFFERENT TAS ALGORITHMS, LISA PATHFINDER [NS/DAY]

The table 1 displays the average values of the overall generated impulse and the maximum single engine impulse. The results can be anticipated, as the optimization algorithms have reached the best performance. It must be noted, that this simulation was done with a realistic profile of forces and torques, that the spacecraft will experience during its mission. If there are random profiles are tested, the infinity norm optimizer may show a drawback for the maximum single impulse. This is due to the current implementation. The algorithm does not yet memorize the beforehand generated impulse of every thruster and calculates an optimal solution for only the present linear program. For a profile with very different force/torque profiles, it can not assure an optimal result over all integrated AOCs cycles.

## MASSIVE MULTIPLE THRUSTER PROBLEMS

The algorithms, that have been outlined in the previous sections are considered for spacecraft with a limited number of thrusters. The thruster configurations of these satellites are optimized for the forces and torques, that will occur during their mission. But future developments or special applications can demand a much higher number of engines onboard a spacecraft. Highly agile vehicles may have the need for a more versatile thruster configuration. An example can be the european ATV. For the analysis of the TAS algorithms for a large number of thrusters, a test satellite layout named *Hedgehog* had been designed. In Figure 5 the shape and thruster configuration of this vehicle can be seen. It incorporates 32 different thrusters, arranged in 8 clusters.

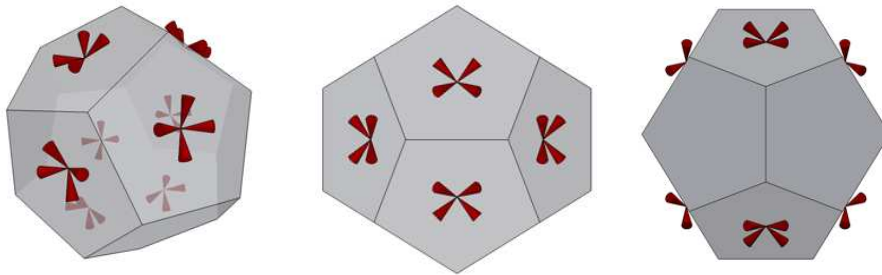


Figure 5: Perspective, top and side view of the Hedgehog test spacecraft

The topic of massive multiple thruster problems was already analyzed by the D3 Group<sup>1,7</sup> proposing a method in 2003 and 2005 to find solutions vectors for pulsed thruster systems like the ATV.

It is possible, to use standard TAS algorithms for the calculation of a proper thrust command vector  $T$ . But due to the large number of engines it would be more profitable, to use only the thrusters of the spacecraft for the computation, that give the best contribution in solving the commanded force/torque vector  $F$ .

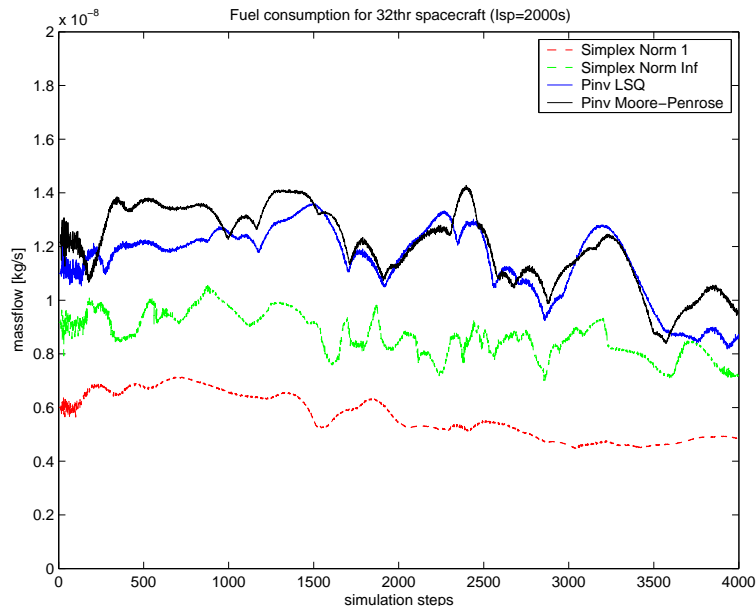


Figure 6: Fuel consumption of different TAS algorithms (32 thrusters)

In Figure 6 an overview of the propellant massflow consumption for the different standard algorithms and a random force/torque profile is displayed. The large difference between the pseudoinverse algorithms



and the norm-1 optimized solution is based in the working principle of the PinvLSQ and PinvMP method. While the linear optimizer is commanding most of the thrusters to  $t_{min}$  and utilizes only a few engines to overcome the commanded force/torque vector  $F$ , the pseudoinverse algorithms are acting simultaneously on all thrusters. The more thrusters a vehicle offers for the propulsion system, the more the difference in the fuel consumption will occur between the pseudoinverse and linear programming methods.

Unfortunately, there is a problem, that prevents the usage of an unmodified Simplex algorithm for this kind of TAS task. The complexity of the setup for the linear programming increases with every thruster, that is involved in the computation. Therefore an *Engine Preselection (EPre)* algorithm should select a suitable set of thrusters, that is then passed to the optimizer for the main calculation. The forces and torques of the residual thrusters are treated as additional disturbance in the system. The Eq. (49) displays the modified basic equation of the TAS problem. The vector  $T_{sel}$  contains the thrust commands for the selected set of thrusters, while the vector  $T_{res}$  contains the current minimum thrusts for the residual thrusters.

$$A_{sel}T_{sel} + A_{res}T_{res} = F \quad (49)$$

The idea is, that the commanded force/torque vector  $F$  is after all only a six-dimensional vector, providing a direction and a length. By using the actuated force and torques of each thruster in a vector, one is able to compute a scalar product from the normalized vectors. Therefore the enclosed angle between this two vectors can be retrieved. The collection of all thrusters, that fire in the same direction as the vector  $F$  demands is then the set of selected thrusters.

The algorithm for this EPre method is displayed shortly in Eqs. (50) through (60). It consists of an initialization part, a loop that is executed until enough thrusters have been found and an update section that handles the necessary actions after a thruster selection.

The initialization part simply sums up the residual force, that would be applied to the spacecraft, if all thrusters are commanded to their current minimum allowed thrust. The six-dimensional vector  $F_{min.i}$  is the force/torque vector for each thruster  $i$ , firing on its  $t_{min.i}$  thrust.

The main loop is evaluated, until enough thrusters have been selected. It searches through all unselected thrusters and calculates the scalar product (Eq. (56)) of their normed force/torque direction (Eq. (55)) and the normed force/torque vector  $F_{norm}$ . Please note, that the vector  $F_{norm}$  consists of the commanded vector  $F$  and the forces and torques from the residual thrusters, except the analyzed one (Eqs. (53) and (54)).

After searching through all unselected thrusters, the maximum value of the scalar products is found (Eq. (58)). If the value is greater or equal to a certain threshold value  $dir_{thres}$ , then the corresponding thruster is added to the list of selected engines (Eq. (59)). An update of the vector  $F_{res}$  removes the selected thruster from the residual thrusters (Eq. (60)). For the tests with the Hedgehog spacecraft configuration, a threshold value of  $dir_{thres} = -0.15$  led to good results.

Initialization of EPre algorithm:

$$F_{min.i} = A_i \cdot t_{min.i} \quad (50)$$

$$F_{res} = \sum F_{min.i} \quad (51)$$

$$(52)$$

Loop over all unselected thrusters indexed as  $i$ :

$$F_{norm} = F - (F_{res} - F_{min.i}) \quad (53)$$

$$F_{norm} = F_{norm}/|F_{norm}|_2 \quad (54)$$

$$F_{vec.i} = A_i/|A_i|_2 \quad (55)$$

$$dir_i = F_{vec.i} \cdot F_{norm} \quad (56)$$

$$(57)$$

Selection the best suitable thruster:

$$i_{sel} = \max(dir_i) \quad (58)$$

$$\text{if } dir_{i_{sel}} \geq dir_{thres} \text{ then } selectlist[i_{sel}] = true \quad (59)$$

$$F_{res} = F_{res} - F_{min.i_{sel}} \quad (60)$$

When using the EPre preprocessor for the exemplary Hedgehog configuration, the number of utilized thrusters could be reduced considerably (Figure 7). This leads to a decrease of the necessary iterations for the optimization algorithm. In Figure 8 the original norm-1 and infinity-norm optimizer and a norm-1 optimizer with the EPre preprocessor are compared.

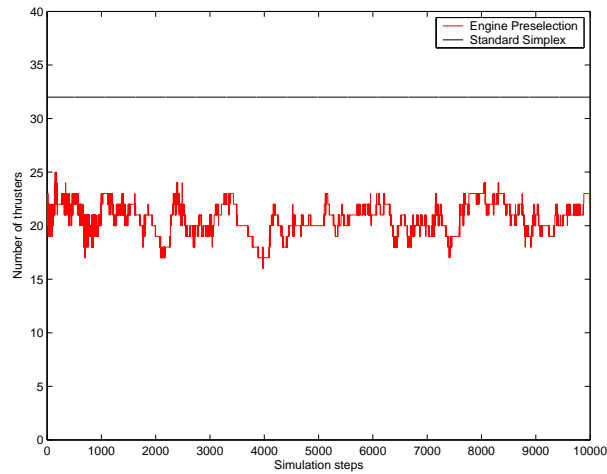


Figure 7: Number of thrusters, used for linear programming

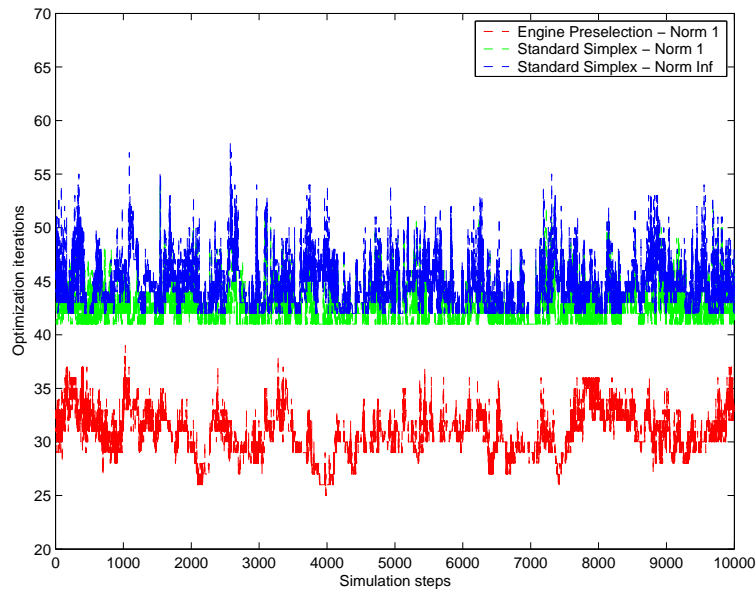


Figure 8: Amount of necessary iterations for different algorithms

The main advantage of the EPre method is the ability, to handle thruster configurations without the need of a precomputed database. It is also able to handle the thruster dynamics of electrical thrusters, that can not change their thrust level very fast. A drawback is the robustness of the approach. By using scalar products, the thruster selection is more or less a rough estimation. It can not guarantee, that the engines are able to provide a sufficient control authority for the commanded forces and torques. Further analysis have to be done on this topic, to evaluate the behavior of the EPre method under extreme conditions.

## CONTROL AUTHORITY

The design process of the different thruster actuation algorithms and the performance testing required a simulation environment. For the analysis, a MATLAB Simulink model have been created for this purpose.

The Figure 9 displays the layout if this system. The input is a stream of command vectors  $F$ , that is fed into the TAS algorithm. That input can be a set of flight recorded data, a sample of a simulated mission or it may be a set of random generated vectors  $F$ .

The TAS block calculates the thrust command vector  $T$  and passes it to a thruster model. Here, some thrust noises and dynamic effects are applied to the commanded thrust. This model is also able to estimate information about the consumed propellant massflow, the electrical power or the required voltages of the thrusters. These data can be analyzed afterwards, to evaluate the performance of the TAS algorithm.

The simulated thruster output  $T_{act}$  is transformed with the configuration block, that simply contains the configuration matrix  $A$ . So the actuated forces and torques  $F_{act}$  are simulated. The difference between the commanded and actuated forces and torques is then analyzed and evaluated.

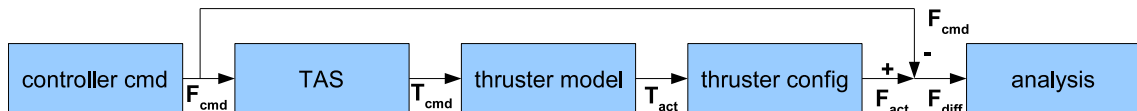


Figure 9: Layout of testbed for TAS simulations

The simulation testbed was designed, to test various combinations of TAS algorithms, thrusters and spacecraft. In Figure 10 the user interface for choosing the different simulation parameters is displayed. The testbed also features autoconfiguration methods. So selecting a certain spacecraft will result in a correct setup of the TAS algorithm and the proper thruster configuration.

The choice between different engine types allows the comparison of the outcome of this spacecraft design. The different thruster models have been parameterized to simulate the noise shape, dynamic, fuel consumption and other characteristics as best as possible. So the user is able, to check, which thruster type would fit best to the selected spacecraft and force/torque profile  $F$ .

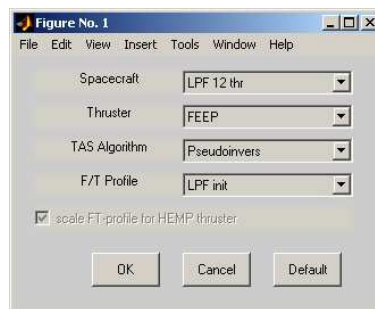


Figure 10: Control interface of TAS simulation testbed

The main advantage of such a testbed is of course the ability, to check, how the thruster actuation system and a thruster configuration will perform for a proposed mission. So, this tools can aid the design process of a spacecraft to find the best combination of engine type, thruster actuation algorithm and thruster configuration.

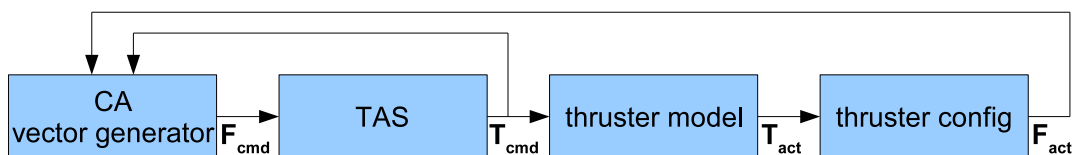


Figure 11: Layout of control authority simulation

With a small modification, the TAS simulation testbed is also able, to calculate the control authority (CA) of the spacecraft. The Figure 11 displays, that the force/torque input has been exchanged by a vector generator. This block has an internal database, representing a discretized version of the six-dimensional spacecraft control authority. The vector generator tests the maximum output of the propulsion system for every direction.

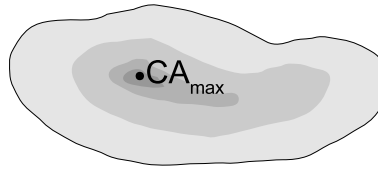


Figure 12: Reduction of space for possible solutions while approaching the control authority

The figure 12 depicts the working principle of the vector generator. In a first iteration, a vector with the desired direction and small length is commanded to the propulsion system. The TAS can select a suitable thrust command vector  $T$  from a large solution space. In the next iteration the vector generator increases the vector-length of the command. The space of the possible solutions (displayed as different shades of gray) becomes smaller with every iteration until only one point is left. This is then the control authority for the analyzed six-dimensional direction.

A feedback of the current thruster commands helps the vector generator, to estimate the remaining control authority for every iteration. The commanded vectors  $F$  in the next iterations is increased, until the propulsion system can no longer produce the desired output. At this point the vector generator decreases the command signal to a point, where the commanded and actuated forces and torques are almost equal. The range of possible solutions has collapsed to the solution  $CA_{max}$  that provides the strongest force/torque output in this particular direction.

One of the problems of the vector generator is the fact, that the estimation of the control authority is no linear problem. The feedback of the thruster commands is only an estimation, how many margin is still left in the system. If one thruster is reaching its maximum thrust level, then the TAS might be able to find another thrust solution, that has an even higher force/torque output. The vector generator has therefore a fast increase of the command vector length in the first step of the CA calculation.

The error feedback of the commanded and actuated force/torque vector  $F$  is a more linear indicator, how much the control authority in the analyzed direction has been violated. Due to this linearity, the vector generator can decrease the command length very accurately until the real control authority value has been found.

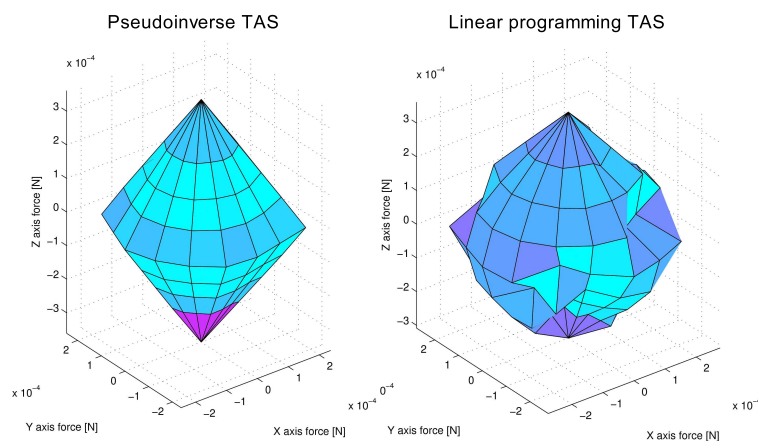


Figure 13: Maximum force Control Authority for LISA Pathfinder, 12 FEFP thruster configuration

After looping through all six-dimensional directions of the control authority, the internal database of the vector generator is completed. The result can be read out and transformed to three-dimensional surfaces.

Figure 13 shows the maximum forces that can be actuated with the proposed thruster configuration and FEEP engines. It is important to note, that the size of the control authority is influenced by the implemented TAS algorithm. The linear programming methods achieve a higher CA, than the simple pseudoinverse algorithms. In the figure that fact is displayed by the rounder shape of the CA, generated by Simplex (right plot), rather than the pseudoinverse algorithm (left plot). The bulges of the linear programming result result from the low resolution of the discretization.

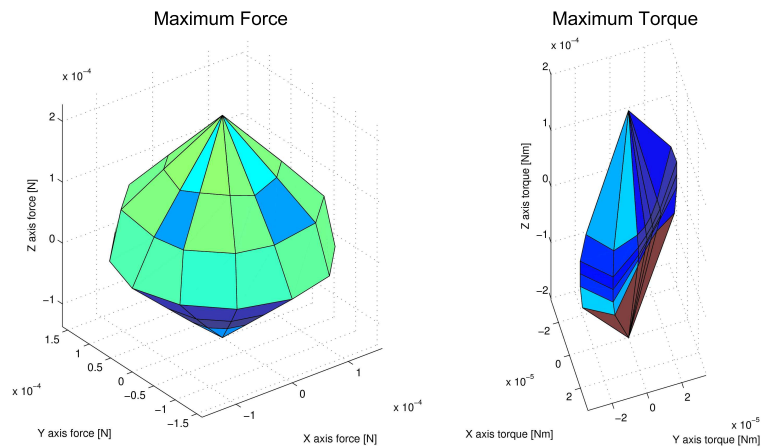


Figure 14: Maximum Force and Torque Control Authority for LISA Pathfinder, 8 Colloid thruster configuration

As a comparison the control authority results of the LISA Pathfinder thruster configuration, proposed for the Colloid engines is displayed in Figure 14. The right plot shows the surface of the maximum torque control authority, that is shaped like a thin blade. It is obvious that this configuration has a major drawback in this for this property. A fact, that if founded in the use of only two clusters. So there is almost no control momentum around the connection axis of these two clusters. The right plot shows the surface of the maximum torque control authority, that is shaped like a thin blade.

## CONCLUSION

The paper outlined the different algorithms for a thruster actuation system. It focussed on the special properties of electrical engines. Beside the state of the art algorithms with a pseudoinverse approach, a series of modifications for the linear programming Simplex have been introduced, to enable its implementation in a real-time environment onboard a spacecraft. The performance of the linear optimization methods in terms of fuel consumption is very encouraging to consider such methods for future missions.

An overview of the simulation testbed points out the potential use of such a tool for the spacecraft design process.

## References

- [1] F. Ankersen, S. Wu, A. Aleshin, A. Vankov, and V. Volochinov. Optimization of spacecraft thruster management function. *Journal of Guidance, Control and Dynamics*, 28(6):1283–1290, 2005.
- [2] Jeng-Heng Chen. *Helium Thruster Propulsion System for Precise Attitude Control and Drag Compensation of the Gravity Probe-B Satellite*. PhD thesis, Department of Aeronautics and Astronautics, Stanford University, December 1983.
- [3] Denis Fertin and Wu Shufan. Analysis of design of Lisa Pathfinder drag-free controllers. Memo TEC-ECN/DF/S2-21/10/2004, European Space Agency, December 2004.

- [4] A. Genovese, M. Tajmar, N. Buldrini, M. Scheerer, E. Semerad, and W. Steiger. Indium FEEP Multiemitter Development and Test Results. In *40th AIAA/ASME/SAE/ASEE Joint Propulsion Conference and Exhibit*, July 2004. AIAA-2004-3620.
- [5] HaiPing Jin. *Translation and Attitude Control for the QUICK-STEP Satellite*. PhD thesis, Department of Aeronautics and Astronautics of Stanford University, August 1996.
- [6] A. Schleicher. Thruster actuation algorithm design and analysis. Technical Report S2-ZAR-TN-2001, ZARM, July 2004.
- [7] Alexander Vankov and Vladimir Voloshinov. Spacecraft thruster management subsystem design and analysis software tool. Tech-Report D3-TMF-ABS-1\_1, D3 Group, December 2003.